DOCTORAL THESIS

Polychromatic Adaptive Optics to evaluate the impact of manipulated optics on vision

Óptica adaptativa policromática para evaluar el impacto de la óptica manipulada en visión

Memoria presentada para optar al grado de Doctor en Física por la Universidad Complutense de Madrid por:

María Viñas Peña

Dirigida por:

Susana Marcos Celestino

Laboratorio de Óptica Visual y Biofotónica
Instituto de Óptica "Daza de Valdés"
Consejo Superior Investigaciones Científicas

Departamento de Óptica
Facultad de Ciencias Físicas
Universidad Complutense de Madrid

Madrid, December 2015

Instituto de Óptica "Daza de Valdés" 2015
Cover design: María Viñas & Daniel Cortés

A mis monsters, y a la reinita.
Ellos saben por qué

"A scientist in his laboratory is not only a technician: he is also a child placed before natural phenomena which impress him like a fairy tale."

Marie Curie.
Cited in Madame Curie: A Biography (1937) by Eve Curie Labouisse

Acknowledgements

The moment that for a long time seemed so far away has arrived faster and more abruptly than expected. Now it seems odd that the moments lived in the Lab and the results of the work of all these years can be summarized in only one manuscript.

First of all, no doubt, thank you **Susana** for all these years in the lab. The opportunity to develop this long-term project has been an amazing challenge, where I have felt your support all the way ahead. Your ability to compile the crazy experimental results in one single coherent idea, to push me harder looking for the best response of the system (and my own), to support me in all the new projects I have wanted to participate in, to give me the freedom and the responsibility to lead the AOII project, in summary, to rely on me during these years… That has been the first engine of this thesis project.

I remember that when I first arrived to the Viobio Lab I barely knew what Adaptive Optics (AO) was, and I am sure that I was not Lab material at all. Thank you **Lucie** for teaching me almost everything I know about AO and about working in the AO lab. One of the most terrifying moments during my PhD was the discovery of the breakdown of the deformable mirror and subsequent dismantle and rebuilt of the AOI. However what I learnt from that experience has helped me infinitely through the life of the AOII. Thank you for being a constant support these years, both

professional and personal. I missed the crazy hours in the lab aligning the system and the coffees or beers in between.

I do not know how many times I have called the 07 office and said: **Carlos**, we have a problem…Like the Apollo XIII help call to Houston. Every time I had enjoyed the discussions trying to solve a tricky experimental problem coming from one of the multiple sections and devices of the AOII or trying to find some sense in the avalanche of results coming from those experiments, or deciding about the design of a logo!! I have learnt a lot from you. Thank you for all the support and the advice and for making me put the brakes on sometimes.

This project would not have come to a successful end without the incredible support of **Daniel Pascual**. He has helped me through all the stages of the setting up of the system, and together we have learnt a lot…mainly to hate the supercontinuum laser source!! Moreover I have survived to all the scary jokes in the lab, which almost kill me of a heart attack!! You were right, I have cried but I have survived. I could not have done it without you!! The other Dani, **Daniel Cortes**, has been the wizard after the programming of the system, finding a way to make everything work and not crash!! Thank you for "Call me maybe", that helped me a lot. And thank you for sending the messages I could not send.

Big thanks to **Aishu**, for being so brave and confident and put her eye, where anybody else wanted. We finally survived to the programming of the psychophysical experiments! The Pluto would not be working nicely right now without the hard work of **Veronica** and all the time she spent in the darkness looking at millions of different colors interference fringes. We will never forget that the position of a polarizer can change everything. We made it!! The patience of **Luis** from the Workshop of the Institute of Optics cannot be forgotten. He managed to understand and improve my hand-made designs for the pieces he had to fabricate for the AOII system.

Of course, the experimental setup is worth nothing without the incredible patience and cooperation of all the **subjects participating in the experiments**. Thank you for not running away when you understood that a laser was going to impact your retina, that you had to bite a dental impression for several hours, and that you had to perform the same task again and again…I would like to thank all the people in the lab during these years, the veterans (**Nandor**, **Mengchan**, **Andres**, **Judith**, **Sabine**, **De Gracia**, **Lamela**, **Miriam, Bustos**,…) and the new ones (**Edu**, **Clara**, **James**, **Aida**, **Rocío, Álvaro, Vyas, Hrebesh**,..)! I have learnt a lot with you! Enormous thanks to **Eloy**, **Jose Luis**, **Chary** and **Encarnita**, for fighting the bureaucracy and do not lose their smile. In summary,

thanks to all, who help me developing this project. It would not have been possible without you!!

I cannot forget to thank **Prof. Jim Schwiegerling**, who helped me a lot during my short-stay at his lab in the College of Optical Sciences at the University of Arizona from the very first day when a hurricane surprised me! He improved the optical designs we had proposed and provided very interesting feedback for the future visual testing in our lab. Thank you **Eddie** for manufacturing the lenses! Everybody there was so nice: **Yusuke**, **Jackie** and our Grand Canyon trip, **Prof. Frieden** and his stories about the University of Arizona, NYC, and everything! Thank you all!

In these years in the lab I have found amazing people. **Pablo Pérez**, who makes me smile when circumstances are not very funny. Thank you for helping me in the lab, for teaching me so many things, for the long hours in the lab (and in the pubs) discussing about this and that, discussing about the "silent people", travelling everywhere... **Alberto**, who had all the patience in the world to explain me all the things I constantly asked him in our office while he tried to listen his music. Today I have almost forgotten the heat in the office when you forbid us to switch on the air conditioner (in august... in Madrid!!). Old warm times!! The oldies from the 303 office… **Enrique** I miss you! **Lourdes**, who was at the Institute of Optics only during my first month there, but who has helped me a lot during these years!! Thank you for those Skype calls!! Malaysia, Australia, what's next?

I will always remember the Italian mafia, **Giorgio** and **Roberta**!! Wonderful barbecues no matter the weather!! **Andres** and his "fast piti", which was so fast that ended before we arrived!!Thank you for the crazy and funny times, when I first arrived to the Institute. I miss them! I still remember the coffee break where Sol@CSIC started…and the extremely hard hiking at Huesca… Those were exciting times! I love discussing stuff with **Mario**. I know we will never agree…but I do like the process. I cannot forget the GPL guys! **Jan**, **Dani Puerto** and **Ramón**! And the rest of the crazy PhD and postdoc guys of the IO: **Nuño**, **JL**, **Giuseppe**…I have enjoyed this time with all of you! A big hug to all **IOSA** people! We have worked hard and we have achieved great things. I have really enjoyed my time organizing things and travelling with you!

Thank you for all the coffee breaks and "fast pitis" at the door of the Institute. What would have been our mornings without the guiri version or without the weird/crazy/absurd philosophical discussions after lunch?? Nice sharing these moments with you guys! Thank you all for the beers at "el gallego" or at "Galaika"

or everywhere! You have supported me during these years. I enjoyed the shared moments and I hope we will share much more.

I cannot forget my friends (**Marina, Cresy, Irune, Concha, Alberto**…), who have helped me through the years in this and other adventures, with whom I have shared so many special moments. To **Carlos González** for all his help.

To my **family**, that has constantly supported me in the good and bad moments. It was not always easy. You have encouraged me since I was a child to achieve all my goals. To my grandfather **Agapito**, I wish you were here. To my new family, **Antonio**, who gives me joy every day and supports me in all the crazy ideas I have. To all of you, I have to thank a lot.

María Viñas Peña
Office 303, Institute of Optics, CSIC,
Madrid, 2015

Funding

The research developed during this thesis would have not been possible without the funding received from the following public and private institutions:

- Spanish Government (MICINN). FPU predoctoral fellowship to Maria Viñas
- Spanish National Research Council (CSIC). JAE predoctoral fellowship to Maria Viñas
- Essilor International. Collaborative agreement. PI: Prof. Susana Marcos
- MICINN grants: FIS2008-02065, FIS2011-25637 to Prof. Susana Marcos
- EURHORCs-ESF EURYI-05-102-ES (The European Young Investigator Awards) & ERC-2011-AdG-294099 (European Research Council) to Prof. Susana Marcos
- PhysIOL Collaborative agreement. PI: Prof. Susana Marcos

Keywords


hydrophobic
Zernikepolynomials
astigmatism
reflectometric
HartmannShack
doublepass
visualperformance
opticalquality
wavefrontsensing
aging
multifocal
SLM
VIS
optics
psychophysics
visualquality
coma
hydrophilic
monochromatic
TCA
vision
Badal
radial
convolution
adaptiveoptics
angular
longitudinal
modelling
eye
perceptuallearning
wavefront
LCA
aberrations
retina
pupil
wavelengths
presbyopia
AO
phakic
visualfunction
vivo
laser
timecourse
phasemodulator
IOLs
transverse
simulation
accommodation
PSF
RMS
NIR
interaction
cataract
subjective
chromatic
objective
visualperception
lasersafety
supercontinuum
ophthalmic
perceivedneutralpoint
neuraladaptation
polychromatic
visualprocess
retinalimagequalitymetrics
wavefrontsensor
opticalqualitymetrics
pseudophakic
phasepattern
spatiallightmodulator

Summary of the thesis

Background

The eye is an optical instrument that project scenes of the visual world onto the retina. However the human eye is far from being a perfect optical system, and, as a consequence, the images projected on the retina are blurred by ocular aberrations, as well as diffraction and scattering. Therefore in the last years, multiple technologies based on wavefront sensing and Adaptive Optics (AO) have been developed for the measurement and correction of ocular aberrations. As a result important knowledge has been gained on the contribution of the different components of the eye to the degradation of image quality. However the processes underlying neural adaptation to ocular aberrations are not yet well understood. Understanding the effects of a particular low order aberration, astigmatism, is particularly attractive to investigate adaptive processes in the visual system due to the inherent oriented nature of the blur that it produces.

Typically, the impact of ocular aberrations on vision is studied using wavefront sensors with monochromatic, generally infrared, light. However, the retinal image quality is degraded by the presence of both monochromatic and polychromatic aberrations in the ocular optics. The study of the impact of retinal image quality on vision should therefore consider both the aberrations in the visible light, as well as the effect of chromatic aberrations. In addition optical and structural properties of the eye change with age and with certain ocular conditions and treatments, altering the natural aberrations, as well as the interactions between monochromatic and chromatic aberrations, and consequently the visual function.

The understanding of the interactions of these aberrations and their effect upon correction is essential to explore the limits of human spatial vision, and to design and optimize new alternatives of correction of Presbyopia/Myopia and more complex individualized refractive corrections.

In this thesis we have used AO techniques to study the effect of specific monochromatic aberrations and their combinations on vision, to test neural adaptation to those aberrations and their correction, to measure chromatic aberrations of the eye in normal and pseudophakic eyes, and to test vision with simulated multifocal solutions for Presbyopia.

Methods

Two different custom developed AO systems have been used: (1) the Viobio Lab AO I system was built in previous projects and has been used in different studies in the lab prior to this thesis. (2) The Viobio Lab AO II system has been specifically designed and built during this project. This AO system has been built to extend the capabilities as visual simulator of current AO systems. In particular, incorporating a supercontinuum laser source and a Spatial Light modulator, has allowed us to perform psychophysical experiments to investigate the optical and visual quality in polychromatic conditions, as well as to evaluate the impact of manipulated optics, including multifocal corrections, on vision.

Results & Discussion

In this thesis, the developed AO visual simulators have been used to provide deeper insights in the neural adaptation to natural astigmatism. In addition, the developed technologies have allowed to investigate whether the perception of astigmatic oriented blur is biased by the native astigmatism of the subjects, and to study the time course of the after-effects following spectacle correction of astigmatism in habitually non-corrected astigmats. They have also allowed investigating the extent what prior adaptation to astigmatism affects visual performance, whether this effect is axis-dependent, and the time-scale of potential changes in visual performance following astigmatism correction.

Chromatic aberration of the human eye has been also investigated during this thesis. The visual world is polychromatic and the study of the impact of retinal image quality on vision should consider the aberrations in the visible light, as well as the effect of chromatic aberrations. Measurements of the Longitudinal Chromatic Aberration (LCA) of the human eye have been performed using wavefront sensing, double-pass retinal images, and psychophysical methods in a wide spectral range (450-950 nm), with control of subjects' natural aberrations. This study has provided insights for the reported differences on the measured LCA with different techniques. Chromatic aberration has been quantified in both phakic and pseudophakic eyes.

Finally, AO technology has allowed the simulation of new optical solutions to optically correct for Presbyopia, the age-related loss of the accommodative amplitude of the human eye, and to explore the effect of multifocal simultaneous vision corrections with different designs on vision, in the presence and absence of natural aberrations.

Resumen de la tesis en castellano

Introducción

El ojo es un instrumento óptico que proyecta escenas del mundo visual en la retina. Sin embargo, el ojo humano está muy lejos de ser un sistema óptico perfecto, y, por lo tanto, las imágenes que se proyectan en la retina están emborronadas debido a las aberraciones oculares, así como por los fenómenos de difracción y dispersión oculares.

En los últimos años, se han desarrollado un gran número de técnicas basadas en Óptica Adaptativa (AO) para la medida y corrección de las aberraciones oculares. Como consecuencia, se ha alcanzado un profundo conocimiento acerca de la contribución de los diferentes componentes del ojo a la degradación de la calidad de las imágenes. A pesar de estos esfuerzos, los procesos subyacentes a la adaptación neuronal a las aberraciones oculares no son entendidos completamente. Entender el efecto de una aberración de bajo orden específica, como puede ser el astigmatismo, es muy interesante para investigar dichos procesos de adaptación neuronal debido a la orientación del emborronamiento que causa en las imágenes retinianas.

Normalmente, el impacto de las aberraciones oculares en la visión se estudia mediante sensores de frente de onda que utilizan luz monocromática, generalmente infrarroja. Sin embargo, la calidad de la imagen retiniana es degradada por la presencia de aberraciones monocromáticas y policromáticas, y por tanto, el estudio de su impacto en la calidad de la imagen retiniana debería considerar ambas aberraciones. Además, las propiedades ópticas y estructurales del ojo cambian con la edad y con algunos tratamientos y condiciones oculares,

alterando el patrón de aberraciones natural del sujeto, así como con las interacciones entre las aberraciones monocromáticas y cromáticas, alterando por tanto la función visual. La comprensión de las interacciones entre las diferentes aberraciones monocromáticas y el efecto de la corrección de las mismas es esencial para explorar los límites de la función visual, y para el diseño y optimización de nuevas alternativas para la corrección de la presbicia/miopía, así como otras correcciones refractivas más complejas y personalizadas.

En esta tesis, se han utilizado técnicas de Óptica Adaptativa (AO) para estudiar el efecto de aberraciones monocromáticas específicas, de combinaciones de las mismas y de su corrección en la función visual; para medir la aberración cromática del ojo en sujetos fáquicos y pseudofáquicos; y, para evaluar el impacto de nuevas correcciones multifocales para Presbicia en la función visual.

Métodos

Para ello, se han utilizado dos sistemas de Óptica Adaptativa diseñados y desarrollados en el laboratorio: (1) el sistema Viobio Lab AO I, construido en proyectos anteriores, y (2) el sistema Viobio Lab AO II que ha sido diseñado y desarrollado específicamente durante este proyecto de tesis. Este sistema AO se ha construido para extender las capacidades como simuladores visuales de los sistemas AO disponibles, mediante la incorporación de una fuente láser de supercontinuo y un modulador espacial de fase, que han permitido la realización de experimentos psicofísicos para investigar la calidad óptica y visual en condiciones policromáticas, así como la evaluación del impacto en la visión de óptica manipulada.

Resultados y Discusión

En esta tesis, los sistemas de AO desarrollados se han utilizado para obtener un mayor conocimiento de los mecanismos de adaptación neuronal al astigmatismo, prestando especial atención a si la percepción del emborronamiento astigmático depende del astigmatismo natural de los sujetos, y a la evolución temporal de los cambios de adaptación neuronal tras la corrección del astigmatismo natural de los sujetos con gafas. También han permitido investigar el alcance de dicha adaptación neuronal en la función visual, si dicho alcance depende de la orientación del astigmatismo, y, la evolución temporal de posibles recalibraciones del sistema visual tras la corrección de dicho astigmatismo.

Las aberraciones cromáticas del ojo humano también han sido objeto de estudio durante esta tesis. El mundo visual es policromático y, a la hora de estudiar el impacto de la calidad de la imagen retiniana en la visión, se deberían considerar las aberraciones en el visible, así como el efecto de las aberraciones cromáticas en la calidad de imagen retiniana. Se han realizado medidas de la aberración cromática longitudinal (LCA) del ojo humano utilizando un sensor de frente de onda, un sistema de imagen de retina de doble paso, y métodos psicofísicos en un amplio

rango espectral (450-950 nm), con control de las aberraciones naturales del sujeto. Esto ha aportado información significativa a la hora de explicar las diferencias en los valores de LCA obtenidos utilizando diferentes técnicas de medida. Las aberraciones cromáticas se han cuantificado en ojos fáquicos y pseudofáquicos.

Por último, mediante técnicas de AO, se han evaluado nuevas soluciones para corregir ópticamente la presbicia, la pérdida de la amplitud de acomodación del ojo humano debida a la edad. Se ha explorado el efecto de las correcciones de visión simultánea multifocales con diferentes diseños, en presencia y ausencia de aberraciones naturales.

Contents

Chapter 2. Methods 71

List of commonly used abbreviations

Optical terms
LCA = Longitudinal Chromatic Aberration
TCA = Transverse Chromatic Aberration
IR = Infrared
NIR = Near Infrared
VIS = Visible
DoF = Depth-of-Focus
LOAs = Low Order Aberrations
HOAs = High Order Aberrations
SA = Spherical aberration
FT = Fourier Transform
FFT= Fast Fourier Transform
RMS = Root Mean Square wavefront error
PSF = Point Spread Function
MTF = Modulation Transfer Function
PTF = Phase Transfer Function
CSF = Contrast Sensitivity Function
OTF = Optical Transfer Function
SR = Strehl Ratio
VSOTF = Visual Strehl Ratio

Techniques & Instruments
HS = Hartmann-Shack
IM = Interaction matrix
CM = Command matrix

CL = Closed-loop
LRT = Laser Ray Tracing
OCT = Optical Coherence Tomography
AO = Adaptive Optics
AOVS = Adaptive Optics visual simulators
AOSLO = Adaptive Optics Scanning Laser Ophthalmoscope
2AFC = Two-alternative forced choice procedure
8AFC = Eight-alternative forced choice procedure
QUEST = Quick Estimate by Sequential Testing
SLD = Superluminiscent Diode
SCLS = Supercontinuum laser source
LC = Liquid crystal
LCoS = Liquid crystal on silicon
LCD = Liquid crystal display
CCD = Charge-coupled device
CMOS = Complementary metal oxide semiconductor
SLM = Spatial Light Modulator
DMD = Digital Micro Mirror
AOTF = Acousto-optic Tunable Filter
AOI = Viobio lab AOI system
AOII = Viobio Lab AOII system

Ophthalmic & Clinical terms
D = Diopters
Cyl = Cylinder
Sph = Spherical error
IOL = Intraocular Lens
A-IOL = Accommodating-IOL
ALs = Achromatizing lenses
KC = Keratoconic eyes
WTR = With-the-rule astigmatism
ATR = Against-the-rule astigmatism

Variables
W(x, y) = Wave aberration in Cartesian coordinates
Z_n^m = Zernike polynomial in Cartesian coordinates
C_n^m = Zernike coefficient (order, n; frequency, m).
$\mathrm{R_e}(\lambda) =$ Chromatic difference of refraction
$\mathrm{t}(\lambda) =$ Chromatic difference of position
CDM = chromatic difference of magnification
MPE = Maximum Permissible Exposure
MPHc = Maximum permissible exposure per pulse
MPΦ = Maximum permissible radiant power

1

Introduction

"To suppose that the eye, with all its inimitable contrivances for adjusting the focus to different distances, for admitting different amounts of light, and for the correction of spherical and chromatic aberration, could have been formed by natural selection seems, I freely confess, absurd in the highest possible degree. Yet reason tells me, that if numerous gradations from a perfect and complex eye to one very imperfect and simple, each grade being useful to its possessor, can be shown to exist; if further, the eye does vary ever so slightly, and the variations be inherited, which is certainly the case; and if any variation or modification in the organ be ever useful to an animal under changing conditions of life, then the difficulty of believing that a perfect and complex eye could be formed by natural selection, though insuperable by our imagination, can hardly be considered real."

Charles Darwin. On the origin of species. VI. Difficulties of the Theory. Organs of Extreme Perfection and Complication (1859)

The eye is an optical instrument that projects scenes of the visual world onto the retina. However the human eye is far from being a perfect optical system, and, as a consequence, the images projected on the retina are blurred by diffraction, scattering and ocular aberrations. Ocular aberrations blur the retinal image, reducing image contrast, limiting spatial frequencies available for further stages of the visual processing, and affecting considerably the visual function.

In the last years, multiple technologies have been developed for the measurement and correction of ocular aberrations and important knowledge has been gained on the contribution of the different components of the eye to the degradation of image quality. Its understanding and correction is essential to explore the limits of human spatial vision, and to design and optimize new alternatives of correction of Presbyopia/myopia and more complex individualized refractive corrections. However, the effects of the ocular aberrations on vision are not yet well understood.

1.1 Motivation

Since the Adaptive Optics (AO) technique was first applied to the eye [1], its use to measure, correct or induce ocular aberrations has increased dramatically, and it has even made its way into the clinic. Wavefront sensing and Adaptive Optics have been applied to the understanding of the optical quality of the eye, and its change with refractive error, accommodation, aging in the normal eye, diseases (i.e. keratoconus) and treatment (refractive surgery, cataract surgery, contact lenses, intrastromal rings, etc...). Several studies have investigated the effect of ocular aberrations on visual function and to what extent visual performance increases when correcting higher order aberrations and mechanisms of neural adaptation to those aberrations. In fact the processes underlying neural adaptation to ocular aberrations are not yet well understood. Astigmatism is particularly attractive to investigate adaptive processes in the visual system due to the inherent oriented nature of the blur that it produces.

So far, the impact of ocular aberrations on vision is studied using wavefront sensors with monochromatic, generally infrared, light. However, the retinal image quality is degraded by the presence of both monochromatic and polychromatic aberrations in the ocular optics. The study of the impact of retinal image quality on vision should therefore consider the aberrations in the visible light, as well as the effect of chromatic aberrations.

In addition, optical and structural properties of the eye change with age and with certain ocular conditions and treatments, altering the natural aberrations and, the interactions between monochromatic and chromatic aberrations, and therefore the visual function. Correcting the high order aberrations or inducing certain combinations of aberrations allows improving the design of customized optical

solutions (i.e. intraocular lenses, contact lenses, custom refractive surgery, multifocal solutions for Presbyopia). However this manipulation of the optics of the eye is made monochromatically, although the improvement in the visual function should work for a polychromatic world.

In this thesis, we have developed a custom polychromatic Adaptive Optics system combined with psychophysical channels, which allowed to study the effect of specific monochromatic aberrations and their combinations on vision, to test neural adaptation to those aberrations and their correction, to measure chromatic aberrations of normal and pseudophakic eyes, and to test vision with simulated multifocal solutions for Presbyopia. This *Chapter* presents a brief review of current knowledge on the measurement and impact of monochromatic and chromatic aberrations on visual function, as well as a brief review of the state-of-the-art of Adaptive Optics and solutions for Presbyopia.

"The light transports what we see into the eye and the eye transports it to the entire human. The outside world mirrors itself in the human body."

Johann Wolfgang von Goethe. Zur Farbenlehre (1810)

1.2 The visual process

Vision is a very complex process, where the visual system transforms light stimuli into information that is processed by the brain. Besides, the visual system is able to adjust extraordinarily to changes in the environment (illumination, color, contrast), as well as to changes within the eye (aging, pathologies, treatments or refractive errors), adapting continuously to maintain a match between visual coding and visual environment. Despite its importance and the search since ancient times for insights on how vision works, the visual process is not fully understood. The nature of the visual processing has been studied over history, from Greek times (400 B.C.) up to the beginning of the XVII century, when the fundamental advances on the nature of the ocular anatomy, the optics of the eye and the visual function were made, until now. Great names in the history of Science were fascinated by the function of the human visual system: Aristotle, Ptolemy, Seneca, Alhazen, Galen, Leonardo da Vinci…among others. All of them studied the eye and contributed with different theories to explain such a complex organ. The formalization of the concept that vision begins with the formation of an image on the retina set the earliest foundations for understanding the basis of reduced retinal image quality and reduced visual performance.

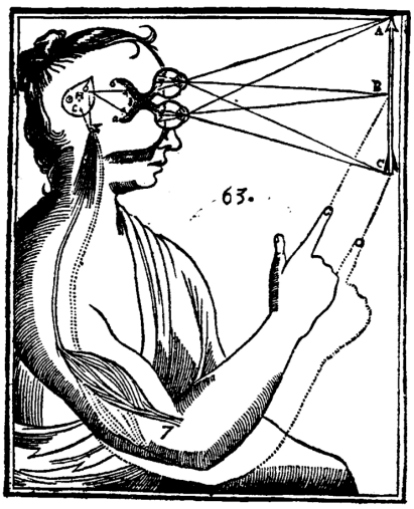

Figure 1.1 The visual process according to Descartes theory, exposed in his work "The World (Treatise on the light)" (circa 1629-1633) [2].

It was Johannes Kepler, who finally synthesized these previous theories on anatomy, optics and vision, proposed a full ray tracing model of the eye and offered the first theory of retinal image: "Therefore vision occurs through a picture of the visible things on the white, concave surface of the retina" [3]. Later on, René Descartes provided a deeper insight in the eye's optics and the visual processes, and offered an explanation of the phenomena of reflection and refraction [4]. Helmholtz, aware of the fact that the optics of the eye were far from perfect, also recognized that the eye was so adapted to its function that its limits were set to its defects [5]. Since Helmholtz's times, technology has advanced to the point of introducing ocular aberrations in the process of diagnosis, treatment of pathologies and design of new ophthalmic designs. Moreover it has also helped to provide insights on the neural processing stage; however most of the mechanisms underlying neural processing remain unknown.

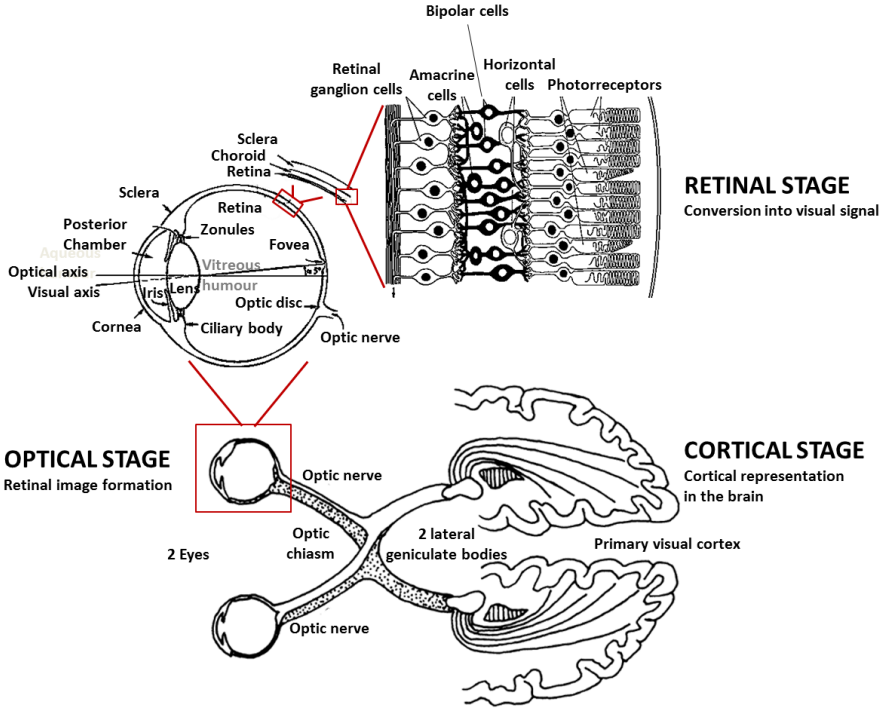

Figure 1.2 The 3 stages of the visual process. Image shows a drawing of a section of the human eye (optical stage), an enlargement of the layered retinal structure (retinal stage) and the visual pathway, from the retina to the primary visual cortex via the lateral geniculate bodies (cortical stage). Adapted from Atchison & Smith (2000), and Keating (2002).

Such a complex process is done in 3 different stages: optical, retinal and cortical (Figure 1.2). Light coming from an object is first focused by the eye's optics (mainly the cornea and the crystalline lens) to form an image on the retina. In the retina,

photoreceptors sample the light distribution, and then the light is absorbed and converted into chemical and electrical signals (visual signals) by the retinal layers. These signals exit the eye via the optic nerve and are transformed into cortical representations in the brain. The following sections describe the eye's optics, the retina and the neural process onto the brain.

1.2.1 The optics of the human eye

The image formation in the eye can be compared to man-made optical systems like a camera, which has a dark interior chamber to avoid stray light, a variable aperture to let in more or less light, and an adjustable focus in order to image objects at different distances. The optical system of the eye has those 3 elements, and it is mainly formed by the cornea and the crystalline lens, which project the images on the retina throught a limiting aperture, the pupil, defined by the iris. However there are some differences between both optical systems, which have their origin in the eye's biological basis. The optical system of the eye responds to its environment, grows, ages and sufferes from diseases, in an attempt to provide the best image under different circumstances.

A simplified diagram of the human eye is shown in Figure 1.2 (optical stage) [6, 7]. The cornea, the most powerful refractive surface of the eye, is the curved transparent front surface of the eye covered by the tear film of the eye, which maintains the optical qualities of the cornea. This surface is followed by a chamber filled with aqueous humor and nearby is the iris, which has an opening at its center, the pupil. The iris contracts or expands the pupil in response to the external illumination, controlling the amount of light entering the eye and impacting on the retinal image quality through the influence of diffraction. Behind the iris and the aqueous humor chamber lies the crystalline lens, a transparent biconvex-like-shape high protein material surrounded by fibers, connecting it to the ciliary muscle. Contracting the muscle results in changes in the focusing power of the eye, providing the eye with the ability to focus near and far objects (accommodation). The lens is placed before a dark chamber filled with the vitreous humor (transparent gelatinous substance), whose far limit is the retina. The averaged axial length of the human eye is approximately 24 mm, its refractive power is around 60 D thanks to the contribution of the cornea and the crystalline lens. The cornea contributes about two-thirds of the refractive power for the relaxed eye, approximately 42 D, while the crystalline lens is the responsible for the remaining refraction of the eye, approximately 14 D [7].

1.2.2 The neurosensory retina

The retina is a neural structure located at the eye fundus, a light sensitive tissue directly connected to the brain through the optical nerve, which is involved in the signal transduction, and conversion of the light into neural signal.

Optically, the position of the retina in the unaccommodated eye, in relation to the focused image projected by the cornea and the lens determines the refractive state of the eye. If the retina is in front of the image, the eye will be hyperopic, and conversely, if it is behind the image, the eye will be myopic.

Histologically, it is composed of several cellular and pigmented layers and a nerve fiber layer that faces the vitreous body and forms the optical nerve. A scheme of the main components of the layered retinal structure is shown in Figure 1.2 (retinal stage). The light reaches the retina at the inner limiting membrane, goes through the highly transparent layers in between and reaches the photoreceptors layer, which samples the image projected on the retina. The photoreceptors are the light sensitive cells and are in contact with the retinal pigment epithelium. There are two kinds of photoreceptors: rods, which are sensitive to low-level light, and the cones, which are wavelength sensitive and are classified as L, M and S depending on whether they are sensitive to long (peak at 588 nm), medium (peak at 531 nm) or short (peak at 420 nm) wavelengths of the visible spectrum, respectively. Cone directionality in the retina makes human observers considerably more sensitive to light coming through the center of the pupil than they are to the off-center rays, the so called Stiles-Crawford effect [8], which is due to the directionality of the human cones that acts like waveguides [9] and are tuned typically towards the center of the pupil becoming more sensitive to light entering near the center of the pupil than in peripheral regions [10]. The area of higher resolution in the retina is the fovea (a 1.5 mm wide zone, located at about 5 degrees from the optical axis), where cones predominate (no rods exist at its center). The fovea presents an area where the optical aberrations do not change significantly, the *isoplanatic patch*. On the other hand, there are no rods or cones at the place where the optic nerve leaves the retina, so this area is blind [6, 7]. The retinal pigment epithelium, is in contact with the choroid and has a high content of melanin granules, and subsequently presents a strong absorption and scattering.

The nature of fundus reflections has important implications in the optics of the eye. A classic source of controversy is the fact that there seem to be a consistent discrepancy between psychophysical and double-pass-based measurements of Longitudinal Chromatic Aberration (LCA) of the human eye, with the objective values underestimating the psychophysical values. The lower estimates of LCA from reflectometric double-pass techniques [11, 12] have been hypothesized to arise from the wavelength-dependence of the reflectivity of the different retinal layers [13]. It has been suggested that most of the light contributing to the core of double-pass aerial images likely comes from the light captured and guided back from the photoreceptors [14, 15]. The halo appearing in the double pass images is likely produced by effects other than aberrations, such as retinal stray light scattered at the choroid [16]. Retinal scattering increases for longer wavelengths due to their deeper penetration within the retina and the choroid [17]. The relative contribution of the directional component coming from the photoreceptors, the

diffuse component coming from other retinal layers, choroid and optically turbid media, and a specular component, from smooth boundaries of optical media (such as the inner limiting membrane or corneal surface), is wavelength-dependent [18]. Photoreceptor alignment reflectometry demonstrates a high directional component in green light, which is highly reduced in IR [19]. The directional component will be highly concentrated around the central peak of the aerial image, whereas diffuse or (defocused) specular components will yield little contribution to the peak, and lead to potential differences in the plane identified as in focus. The implications of the different reflectivities of the retinal layers in the quantification of the LCA are further discussed in *Chapters 5* and *6*.

Following optical projection of the image on the retina, neural factors that limit the finest resolvable detail, contribute to the degradation. Neural factors affecting spatial visual perception include neural sampling by the photoreceptors, both spatial and spectral, due to their size, spacing and directionality, and spatial and temporal summation of quanta due to the quantum nature of light [20]. The photoreceptor mosaic samples discretely the continuous distribution of light in the retinal image. Therefore, the visual system is susceptible to sampling artifacts, or aliasing. The Nyquist limit (critical frequency expressed in c/deg) in the eye is estimated at around 60 c/deg. When the spatial frequency of a retinal image is above the Nyquist limit, under-sampling occurs that yields to a misrepresentation of the signal projected onto the retina, called aliasing. Other additional factors have been pointed out to preclude aliasing in the fovea such as irregularities in the mosaic, low pass filtering by individual photoreceptors and fixation instability might produce high temporal frequencies that effectively blur the high spatial frequencies [20].

1.2.3 The visual cortex

The visual process cannot be studied considering the optics in complete isolation from the neural components since they play a fundamental role in processing information. The cortical stage (Figure 1.2) starts when the neural impulses leave the retina via the optic nerve and travel to the optic chiasm, where the nerve fibers from the nasal side of the fovea in each eye cross over to the opposite side of the brain, while the fibers receiving input from temporal retina remain on the same side of the brain. From there they follow to the lateral geniculate nucleus of the thalamus, and finally end in a large area in the occipital cortex called primary visual cortex (area V1). The information is processed in the visual cortex, having influence in the processing of shapes, orientations, color, movement, size, noise reduction, edge filtering, color separation, image compression, motion analysis, pattern and object recognition, as well as other processing processes that occur in the brain.

"Now it is not too much to say that if an optician wanted to sell me an instrument with all these defects I should think myself quite justified in blaming his carelessness in the strongest terms and giving him back the instrument."

Hermann von Helmholtz, Popular scientific lectures (1885)

1.3 The optical quality of the eye

The human eye is far from being a perfect optical system. The images projected on the retina are blurred by diffraction, scattering and ocular aberrations. Diffraction effects are associated with limited aperture size and thus predominate for small pupil sizes. Scattering occurs at the cornea [21] and more prominently in the lens [22], and increases with age (due to changes in the crystalline lens) and other conditions such as corneal scars and refractive surgery [23]. Ocular aberrations blur the retinal image, reducing image contrast, limiting spatial frequencies available for further stages of the visual processing. Its understanding and correction has been led by the study of refractive errors, since the most important refractive anomalies in the eye are defocus and astigmatism (low order aberrations, LOAs). However, the eye suffers from other high order aberrations (HOAs). Figure 1.3 shows a schematic representation of the impact of ocular aberrations on the retinal image quality in (a) an aberration-free eye and (b) an aberrated eye.

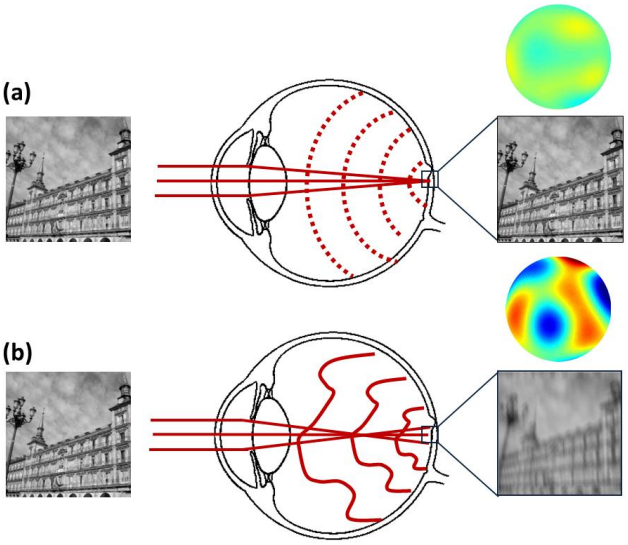

Figure 1.3 Schematic representation of the monochromatic wave aberrations and its impact on retinal image quality in (a) an aberration-free eye and (b) an aberrated eye.

The following sections describe ocular aberrations, mono- and chromatic, the different methods to their quantification, their magnitudes in the eye, and the optical quality metrics used in this thesis.

1.3.1 Optical aberrations

Optical aberrations in the human eye have been noted and measured since at least the time of Scheiner (1619), who invented a disk with a central and a peripheral pinhole that was placed in front of the eye of a subject, so that an imperfect eye would form two retinal images when looking at a distant point light source. Thomas Young observed for the first time astigmatism and spherical aberration in the human eye and reported it in his publication *"On the mechanism of the eye"* (1801). Young used an optometer to measure refraction and accommodation, and discovered his own astigmatism. He considered the different possible origins of accommodation and confirmed that it was due to change in shape of the lens rather than to change in shape of the cornea or an increase in axial length. He also studied the biometric parameters of the eye, peripheral refraction, longitudinal chromatic aberration, depth-of-focus and instrument myopia [24]. Young's works were completed and expanded by Helmholtz in his *"Treatise on physiological optics"* (1855), which was a revolution in the field of ophthalmology [25]. He invented the ophthalmoscope, provided empirical theories on depth perception, color vision, and motion perception, and formed a theory of accommodation that went unchallenged until the final decade of the 20th century. Around the same time, in 1894, Tscherning built what he called "an aberroscope" to measure human eye aberrations, consisting on a grid superimposed on a 5-D lens so that the image of the grid was shadowed on the subject's retina when viewing a distant point light source through the "aberroscope". Aberrations were estimated from the distortions of the grid [26]. Later on, Seidel developed his theory of geometric aberrations, where he decomposed the first order monochromatic aberrations into five primary aberrations [27].

Aberrometric techniques were fast developed since 1900, when Hartmann used Scheiner's idea to measure aberrations in mirrors and lenses, using an opaque screen perforated with numerous holes, which is commonly referred to as wavefront sensor [26]. In 1971 Shack and Platt improved Hartmann's screen by using an array of microlenses instead of the perforations to analyze the wavefront coming out of the optical system to study. The array of microlenses is called a Hartmann-Shack (HS) wavefront sensor, and it is composed of a number of microlenses with the same focal length, arranged in a known geometry. In this technique [1] a point source is created in the object space, at the fovea. Light from the eye reaching each lenslet is brought to a focus in the focal plane of the lens array. When an aberrated wavefront is measured, the image spot produced by each lenslet shifts with respect to the corresponding point in the reference a distance proportional to the local phase distortion. This technique, which has been

used throughout this thesis, will be more extensively described in *Chapter 2, Section 2.2.2*.

Some years later, the Ray Tracing technique (LRT) was applied to measure ocular aberrations [28]. In this technique collimated laser pencils are sequentially delivered through different pupil positions, so that each pencil is deviated an angle proportional to the local wave aberration, and impacts at a foveal location away from that of the reference central ray (transverse aberration). The joint plot of the impacts corresponding to the rays entering through different pupil locations is a spot diagram. A psychophysical version of the ray tracing is the Spatially Resolved Refractometer (SRR), where the ray aberration at each pupil point is computed as the angle that the subject has to tilt the incoming beam in order to visualize the ray centered on the retina [29].

Today, most used aberrometers can be classified in two groups. First ones measure the ray aberration on the retina or image space (i.e. LRT, SRR or Tscherning's type aberrometers), while the others measure aberrations in the object space (i.e. Hartmann-Shack technique). In the last decades, with the development of rapid and reliable aberrometers, the accurate measurement of ocular aberrations has become easier, and different studies have reported that ocular aberrations vary widely in the population, in range and in distribution [30-32].

The optical performance of the eye is described in terms of wave aberration *W(x, y)*, which describes the distortions of a certain wavefront (surface containing points with the same phase and orthogonal to the propagation axis) in the pupil plane as it goes through the optical system. The wave aberration of a general optical system is a complex surface that is typically described mathematically as a combination of simpler polynomials. In a perfect aberration-free system, the wavefront would be perfectly spherical-shaped and the image of a point source through a circular pupil would be only limited by diffraction, thus the image of a point source will be a point [7, 33]. The presence of aberrations induces deviations in the wavefront from the ideal spherical shape. The wave aberration map *W(x, y) (in cartesian coordinates)*, represents therefore the difference between a perfect spherical wave (reference sphere) and the aberrated wavefront at the exit pupil [34] and can be represented in a wave aberration map as shown in Figure 1.4. Moreover, depending on the requirements of the system, optical aberrations can be represented as: wave aberration (departure of the wavefront from the ideal wavefront, as measured at the exit pupil), transverse aberration (departure of a ray from its ideal position at the image plane), or longitudinal aberration (departure of the intersection of a ray with the optical axis from its ideal position) [7]. The following sections detail how monochromatic wave aberrations are described mathematically as a combination of simpler polynomials.

Moreover, ocular aberrations can be divided in chromatic and monochromatic (geometrical) aberrations. The following sections describe both types of ocular aberrations, the methods for their estimation and the retinal quality metrics related.

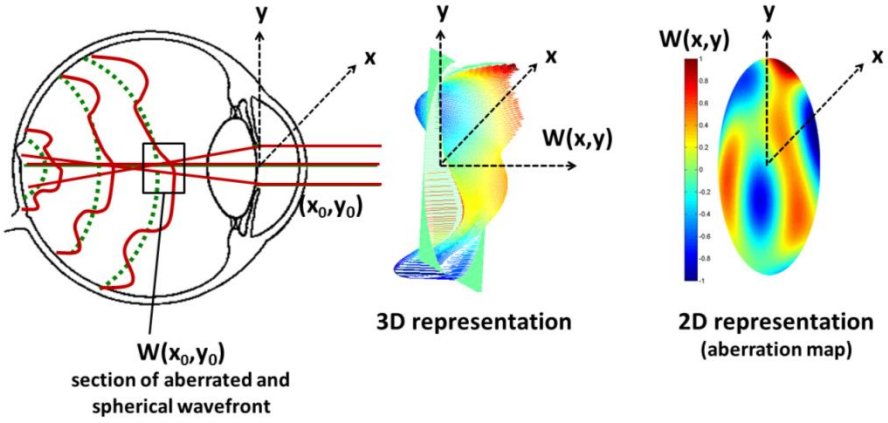

Figure 1.4 Schematic representation of the wave aberration. Wave aberration values (distances between the distorted aberrated wavefront and the spherical reference) can be represented as z-coordinate referred to the pupil plane (three-dimensional representation) or can be represented as a color map (Aberration map). Adapted from Llorente (2009).

1.3.2 Monochromatic wave aberrations. Zernike polynomials

Monochromatic wave aberrations arise from the geometry, irregularities, tilts and decentrations of the components of the optical system. They increase with the diameter of the exit pupil considered, and depend on wavelength [7, 27].

The monochromatic wave aberration of a general optical system is a complex surface that is typically described mathematically as a combination of simpler polynomials. For ocular aberrations, the Zernike polynomial expansion, originally described by Frits Zernike (1934) to describe the diffracted wavefront in phase contrast imaging [35], has become the standard representation [15, 36] due to their properties.

The Zernike polynomials are a set of functions that are orthogonal over the unit circle and are useful for describing the shape of an aberrated wavefront in the pupil of an optical system [35]. A wave aberration can be described as a sum of Zernike polynomial functions weighted by the so-called Zernike coefficients, which indicate the magnitude of each particular aberration present. The spatial frequency of Zernike modes increases with their order.

The standard mathematical definition of the Zernike polynomials, as well as the convention regarding sign, normalization and ordering, used in this thesis is the one recommended by the Optical Society of America (OSA) [15]. According to that, a wavefront phase map can be represented as a weighted summation of Zernike polynomials (in polar coordinates) as follows:

$$W(\rho,\theta) = \sum_{i=0}^{\infty} c_n^m Z_n^m(\rho,\theta) \qquad (1.1),$$

where $\mathbf{c_n^m}$ are the corresponding Zernike coefficients, and $\mathbf{Z_n^m}$ is the Zernike polynomial of order n and frequency m, and has the general form given by:

$$Z_n^m(\rho,\theta) = \begin{cases} N_n^m R_n^{|m|}(\rho)\cos(m\theta); & for\ m \geq 0 \\ -N_n^m R_n^{|m|}(\rho) sin(m\theta); & for\ m < 0 \end{cases} \qquad (1.2),$$

where $\mathbf{R_n^{|m|}(\rho)}$ is given by

$$\mathrm{R_n^{|m|}}(\rho) = \sum_{s=0}^{(n-|m|)/2} \frac{(-1)^s (n-s)!}{s![0.5(n+|m|)-s]![0.5(n-|m|)-s]!} \rho^{n-2s} \qquad (1.3),$$

and the normalization factor $\boldsymbol{N_n^{|m|}}$ is

$$\mathrm{N_n^{|m|}} = \left(\frac{2(n+1)}{1+\delta_{m0}}\right)^{1/2} \qquad (1.4),$$

where **n** = 0, 1, 2,…, and where **m** = -n, -n+2, -n+4, …n, and $\boldsymbol{\delta_{m0}}$ is the Kronecker delta (ie. $\delta_{m0} = 1$ for m = 0, $\delta_{m0} = 0$ otherwise). Tip and tilt are considered during the alignment of the setup, but otherwise not included. Figure 1.5 shows the Zernike polynomials up to 6th order with the corresponding notation.

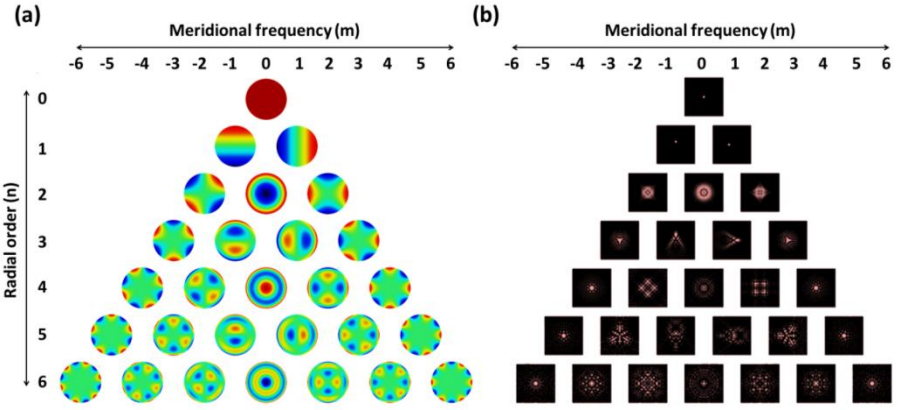

Figure 1.5 Representation of (a) the Zernike base functions up to 6th order and (b) the corresponding point spread function (PSF) for a 1 µm Zernike coefficient and 6 mm pupil size. Each row in the pyramid corresponds to a radial order of the polynomial, and each column to a meridional frequency. Positive and negative frequencies indicate harmonics in cosine and sine phase, respectively. Negative frequency astigmatism and n-foil terms are usually denominated "oblique" astigmatism or n-foil. Positive and negative frequency coma terms are usually denominated as horizontal or vertical coma, respectively.

Second order Zernike coefficients can be converted to a sphero-cylindrical prescription in power vector notation using [37, 38]

$$M = \frac{-c_2^0 4\sqrt{3}}{r^2}; \qquad J_0 = \frac{-c_2^2 2\sqrt{6}}{r^2}; \qquad J_{45} = \frac{-c_2^{-2} 2\sqrt{6}}{r^2}; \tag{1.5}$$

where $\boldsymbol{c_n^m}$ is the Zernike coefficient of meridional frequency **m**, and **r** is the pupil radius. The power vector notation is easily transposed into conventional minus-cylinder or plus-cylinder formats used by clinicians [38].

There are different approaches to measure objectively the monochromatic wavefront aberrations at the pupil; however the most used aberrometric technique is the Hartmann-Shack wavefront sensor, where the method of estimation of the wave aberration is based on local sampling of the pupil and measurement of the local wave aberration slope. The wave aberration is reconstructed by integrating the slopes of an array of beams intersecting the eye's entrance pupil. In ocular aberrometry, modal reconstruction is widely used. It is based on the expansion of the derivatives of wave aberration as a linear combination of the derivatives of Zernike polynomial expansion, and subsequent least-squares fit of the expansion coefficients to the measured gradients. It is used because is superior to zonal estimation in terms of noise propagation, particularly when only a fixed number of modes are of interest, and it is computationally easier and faster [33]. *Chapter 2 Section 2.2.2 (B)* describes the performance of a HS wavefront sensor in an AO system environment.

1.3.3 Chromatic aberration of the human eye

Over 300 years ago, Newton (1670) described a simple experiment to demonstrate the presence of chromatic aberration in the human eye [39]. He held an opaque card near the eye so that only the rays of light passing close to one edge of the pupil were allowed to enter the eye. This maneuver isolated incident light rays which strike the refracting surfaces of the eye obliquely and thus are strongly refracted. Because the indices of refraction of the ocular media vary inversely with wavelength, blue rays are refracted more than red rays. One consequence of chromatic dispersion, as Newton described, is that the edge of a white object is not seen distinctly, but tinged with color.

Chromatic aberrations are a consequence of the dispersion (variation of refractive index with wavelength) of the refractive media of an optical system [7]. There are two types of chromatic aberrations: the longitudinal chromatic aberration (LCA) and the transverse chromatic aberration (TCA). Examples of the impact of both aberrations in an image are shown in Figure 1.6. The following sections describe chromatic aberrations, their magnitude and the different estimation methods.

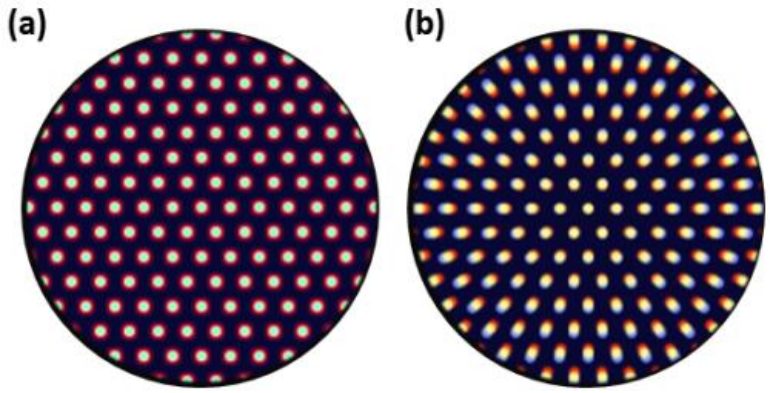

Figure 1.6 Images suffering from (a) Longitudinal Chromatic Aberration (LCA) and (b) Transverse Chromatic aberration (TCA). Reproduced from http://www.handprint.com/ASTRO/ae4.html#terms

A. Longitudinal chromatic aberrations of the human eye (LCA)

Chromatic effects in the eye arise from the wavelength-dependence on the refractive index of the ocular media (chromatic dispersion), affecting diffraction, scattering and aberrations [40-42]. In particular, chromatic dispersion causes short wavelengths to focus in front of long wavelengths, producing a chromatic difference of focus between the shorter and longer wavelengths, known as Longitudinal or axial Chromatic Aberration (LCA) [43]. As a rule, refractive indices decrease with increase in wavelength, so the eye has lower power as wavelength increases.

The LCA of the eye can be quantified in different ways: estimating the chromatic difference of power, which is the variation in power with wavelength [41], or as chromatic difference of refraction, which is the vergence of the source for which the source is focused at the retina for a range of wavelengths. For any level of ametropia and accommodation, chromatic difference of refraction is the difference between the vergences of the retinal conjugates for a wavelength **ʎ** and a reference wavelength **ʎ'** [7, 44].

Figure 1.7 shows a general schematic eye and the retinal conjugates (**P** and **P'**) for wavelengths **ʎ** and **ʎ'**. These conjugates are at distances **l(ʎ)** and **l(ʎ')** from the eye, and their corresponding vergences are **L(ʎ)** and **L(ʎ')**. The chromatic difference of refraction is calculated as

$$R_e(\lambda) = L(\lambda) - L(\lambda') \qquad (1.6).$$

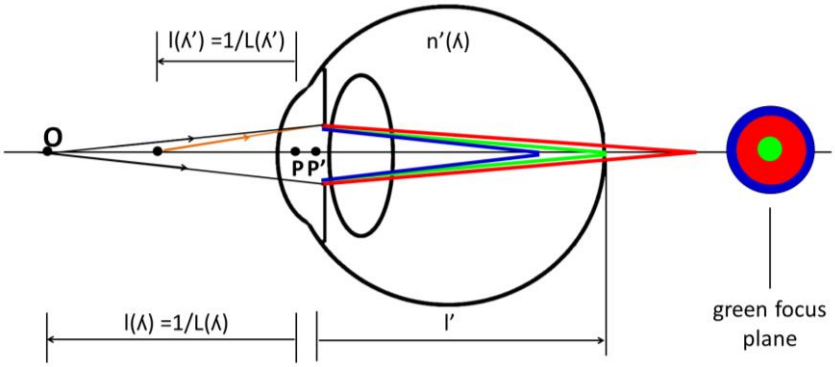

Figure 1.7 Longitudinal Chromatic Aberration in the eye. Rays of longer wavelength (i.e. red) are focused behind the retina and shorter wavelength rays (i.e. blue) are focused in front of the retina. As a consequence, the image of a point in the green focus plane is a focused on green, with halos in red and blue. Modified from Atchison & Smith (2000).

B. Transverse chromatic aberration of the human eye (TCA)

Optical irregularities, misalignments between the ocular components and the off-axis position of the fovea result in a transversal shift of focus for different wavelengths, known as Transverse Chromatic Aberration (TCA) [45-48]. Because of LCA, the different wavelength images of the point are defocused by different amounts relative to the retina. Also, because the power of the eye is lower for long wavelengths than for short wavelengths, longer wavelength rays are deviated less than shorter wavelengths rays, and meet the retina further from the optical axis.

Similarly to the LCA, the TCA can be expressed in two different ways. First by the chromatic difference of position, which is an angular measurement, and second by the chromatic difference of magnification (CMD), which is the wavelength dependent variation in image size of extended objects [41]. Figure 1.8 shows how two rays, one of wavelength **ʎ** and the other of the reference wavelength **ʎ'**, originate from different positions in object space but pass through the same point in the pupil and intersect at the retina. It can be seen that the chromatic difference of position associated with a height **h** of the rays relative to the nodal ray is given by

$$t(\lambda) = b - a \qquad (1.7)$$

where **a** and **b** are the angles subtended by the two rays with the nodal ray in object space. From *Equation 1.6* a linear relationship between the TCA given by **t(ʎ)**, *the* chromatic difference of position, and the LCA given by $\mathbf{R_E(\lambda)}$, the chromatic difference of refraction, can be easily established

$$t(\lambda) \approx hR_E(\lambda) \qquad (1.8).$$

The TCA of most interest is that associated with foveal vision. In this case, the nodal ray becomes the visual axis, and the pupil location of interest is that representative of the light beam.

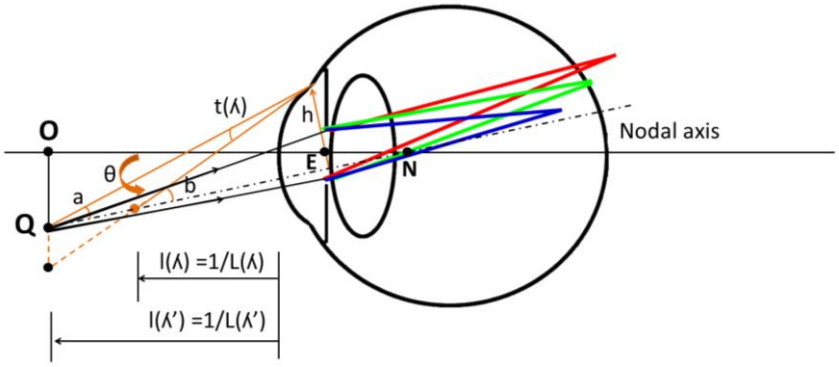

Figure 1.8 Transverse Chromatic Aberration of an eye, that is a centered optical system (including pupils), and for an off-axis object point at Q. The object point is on the optical axis. Adapted from Atchison & Smith (2000).

TCA can be theoretically estimated from the wavelength dependent variation in image size of extended objects referred as chromatic difference of magnification (CDM), which is the TCA in angular terms, **t(λ)**, divided by the angular size of the object

$$CDM = t(\lambda)/\theta \qquad (1.9),$$

where **θ** is the angular size of the object subtended at the eye's nodal point (**N**). The chromatic difference of magnification (CDM) can be related directly to the chromatic difference of refraction $\mathbf{R_E(\lambda)}$.

$$\theta \approx h/EN \qquad (1.10),$$

where **EN** is the distance between the entrance pupil at **E** and the front nodal point at **N**, and **h** is the displacement of the entrance pupil from the visual axis in Figure 1.8. From here the relationship between the chromatic difference of magnification (CDM) and the chromatic difference of refraction $\mathbf{R_E(\lambda)}$ is calculated with

$$CDM = R_E(\lambda)EN \qquad (1.11).$$

1.3.4 Estimation of the chromatic aberration of the human eye

Since the demonstration by Young (1802) and Helmholtz (1885) of the variation of power of the human eye across the visible spectrum, chromatic aberration has been measured using different methods and in different spectral ranges.

1.3.4.1. Methods

LCA has been measured using different psychophysical techniques (i.e. stigmatoscope [43, 49], Badal optometer [50], Vernier alignment [51], or the spatially resolved refractometry [10]) and across different spectral ranges [7, 25]. LCA has also been measured objectively by means of reflectometric techniques, such as double-pass retinal images of a slit [14] or of a point source [18] at different wavelengths. The most frequently used objective (Double pass technique and wavefront sensing) and subjective (Best focus method, laser speckle, Vernier method) techniques to measure chromatic aberration are described below.

A. Subjective

Best focus method. A target with fine detail, illuminated by light of various wavelengths is blurred with pure defocus and the observer has to subjectively choose the best focus for each condition. Target can be blurred by different methods: (1) axially shifting the target, (2) using trial lenses of different powers in the spectacle plane, while the target remains fixed and (3) using a Badal optometer keeping the image angular subtend constant, so that that the chromatic difference of refraction is linearly related to the position of the target [52]. This is the method used in the polychromatic AO system to measure subjectively the LCA, as described in *Chapters 5* and *6*.

Laser speckle. When viewing a laser reflected diffusely from a rotating drum, a speckle pattern is seen that moves in the same or opposite direction to the drum rotation. When an eye is focused at the drum, the pattern appears merely to 'boil'. Lasers of different wavelengths are used, and focus is achieved for each wavelength by moving the drum or using auxiliary trial lenses [50, 53].

Vernier method. Two narrow test targets of different wavelengths are imaged on the fovea, but light from them is restricted to pass only through a small aperture in front of the eye, which can be displaced across the pupil perpendicularly to the length of the target [51]. There is one position in the pupil for which the targets are both aligned and appear aligned, the 'foveal achromatic axis', which is usually referred as the visual axis. One of the targets can be displaced perpendicularly to its length. For chosen aperture positions relative to the visual axis, this is done so that the targets appear again to be aligned. $\mathbf{R_E(\lambda)}$ can be estimated from the aperture displacement, the target displacement, the target distance from the eye and the target distance from where the test wavelength ray intersects the axis [7]. This method allows to measure both LCA and TCA [47].

B. Objective

Double pass technique. The image of a narrow illuminated slit [14] or of a point source [18] is formed on the fundus, which reflects a portion of the light. An aerial

image forms outside the eye. Correcting trial lenses can be used to minimize the width of this image for various wavelengths [14]. A double-pass-technique-like method is used to measure LCA with the polychromatic AO system, as described in *Chapter 5*.

Wavefront sensing. Wave aberrations are measured as a function of wavelength, and LCA is estimated from the Zernike defocus term for other wave aberration-derived metrics for best focus [10, 17]. *Chapter 5* and *6* present results of measurements performed with this technique to obtain the LCA in the visible and near infrared ranges.

1.3.4.2. Modelling chromatic aberration

Classically, the eye's variation of focal power with wavelength was modeled by a reduced schematic eye (Emsley's reduce eye model) that consisted of a volume of water encased within a single, spherical refracting surface. In this model, the chromatic aberration of the reduced eye was attributed solely to the variation of the refractive index of water with wavelength. By including a pupil in the model the reduced eye also accounted for two forms of transverse aberration: chromatic difference of magnification and chromatic difference of position [47]. This reduced eye model accounted well for the major features of ocular chromatic aberration in human eyes, however experimental measurements showed some discrepancies and new eye models were developed [54, 55].

Thibos et al. (1992) proposed a new reduced-eye model of ocular-aberration in humans (Indiana chromatic eye model), where the parameters of the eye model were obtained by fitting experimental data for a range of wavelengths between 400 nm and 700 nm and using Cornu's expression for the dependence of the index of refraction with wavelength. The chromatic difference of refraction is given (in Diopters) by

$$R_E(\lambda) = 1.68524 - \frac{633.46}{(\lambda - 214.102)} \qquad (1.12)$$

where the reference wavelength is 589 nm and the wavelength λ is in nm. *Equation 1.12* agrees well with experimental data in the literature for visible wavelengths up to 760 nm. However Cornu's equation typically fails beyond the visible and other expressions should be used. Validity of Indiana chromatic eye model in comparison with visible and near infrared light LCA measurements is studied in *Chapters 5* and *6*.

1.3.4.3. Magnitude of chromatic aberration

It is fairly accepted that LCA is rather constant across the population, almost invariant in small and moderate angles across the visual field [18], and fairly

constant with age [11, 51, 56], although some studies have reported an age-dependent decrease of LCA [57, 58].

Compared with LCA, there have been relatively few studies of TCA associated with foveal vision [10, 46, 47, 59, 60]. The mean TCA obtained from those studies, although the wavelength range of measurement must be taken into account, is about half the 1.05 min. arc predicted for schematic eyes (486-656 nm) with centered pupils and the fovea 5 degrees to the optical axis. However, some studies also suggested that the variability of the TCA in the population could be associated to geometrical factors beyond surface alignment [48].

Psychophysical LCA has been reported in many studies, with values spanning from 3.20 D in a 365-750 nm range [49] to 1.33 D in a 450-650 nm range [10]. Reports of reflectometric LCA span from 1.40 D (460-700 nm) [14] to 1.00 D (458-632 nm) [18]. More recently, chromatic difference of focus between two wavelengths has been obtained from objective wavefront sensing (Hartmann-Shack and Laser Ray tracing) with a value of 0.72 D (532-787 nm) [17] and 0.40 D in the NIR (700-900 nm) [12, 61]. Some of these studies are presented in Figure 1.9, reproduced from Thibos et al (1992), where published measurements (up to that date) of ocular chromatic aberration are compared with the traditional water-eye model and with the Indiana chromatic-eye model.

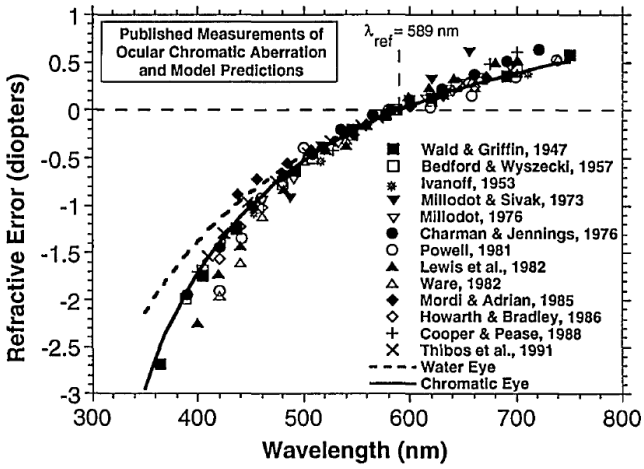

Figure 1.9 Comparison of published measurements of ocular chromatic aberration with the traditional water-eye model and with the Indiana chromatic-eye model. Published results were put on a common basis by translating data points vertically until the refractive error was zero at the reference wavelength (589 nm). Reproduced from Thibos et al. (1992).

Despite the differences in the chromatic ranges and studies, there seems to be a consistent discrepancy between psychophysical and double-pass-based

measurements of LCA, with the objective values underestimating the psychophysical values. These differences between objective and psychophysical LCA were observed in measurements on the same subjects where the discrepancies mostly occurred in the shorter wavelength range [14]. A later study compared the objective best focus (from double-pass aerial images) with the subjective best focus of a point source, and showed that objective data were slightly lower that subjective at the fovea and for 6-mm pupil [18]. The differences across studies in the measurement techniques and spectral ranges pose uncertainty on the actual magnitude of the differences between psychophysical and reflectometric LCA, and limits the assessment of the different hypotheses.

Chapters 5 and *6* present the first evaluation of the change of HOAs with wavelength using objective aberration in the visible spectrum, as well as objective and subjective measurements of the LCA in the same subjects at different wavelengths in visible light. Hypothesis stated by previous authors as a potential cause of discrepancy between subjective and reflectometric techniques [44, 55] are discussed thanks to new data provided by the measurements with the polychromatic AO system.

1.3.5 Optical quality metrics

Several optical quality functions can be obtained from wave aberration using Fourier optics computations. There are two main types of metrics to define image quality: pupil plane metrics and image plane metrics. The following sections describe the optical quality metrics used in this thesis.

A. Root Mean Square wavefront error (RMS)

A standard global pupil plane metric to evaluate the optical quality is the Root Mean Square wavefront error (RMS), which measures the deviation of the wavefront from a perfect plane wave. RMS is defined as the root square of the sum of the squares of the optical path differences as measured from a best-fit reference spherical wavefront over the total wavefront area and it is computed directly from the Zernike coefficients

$$RMS = \sqrt{\sum_{n.m} c_n^{m2}} \qquad (1.13),$$

where $\boldsymbol{c_n^m}$ is the Zernike coefficient corresponding to the order **n** and frequency **m**. Moreover, the Zernike terms are normalized so that the coefficient of a particular term or mode is the RMS contribution of that term. The calculation of RMS error can be done either individually or grouped arbitrarily (coma, trefoil and spherical, among others). Tip and tilt are often removed as they merely represent a shift in the image which is of no consequence to its quality.

B. Retinal image quality metrics

Retinal image quality metrics, computed from wave aberration, include the combined effects of diffraction and aberrations, but not scattering. In this thesis the optical quality is typically described using retinal image quality based metrics, which have been shown to correlate better with visual function [62]. Retinal image quality based metrics used in this thesis are the Point Spread Function (PSF), the Optical Transfer Function (OTF), the Modulation Transfer function (MTF), the Strehl Ratio (SR) and the Visual Strehl Ratio (VSOTF).

Point Spread Function (PSF)

The Point Spread Function (PSF) is the image of a point object through the optical system. The pupil function, P(x, y), defines how light is transmitted by the eye's optics,

$$P(x,y) = A(x,y)\, exp(i\frac{2\pi}{\lambda}W(x,y)) \qquad (1.14),$$

where **P(x, y)** is the pupil function, **A(x, y)** is an apodization function (when the waveguide nature of cones is considered) [9, 37] and **W(x, y)** is the wave aberration (in Cartesian coordinates). **P(x, y)** is zero outside the pupil. The PSF is calculated as the squared magnitude of the inverse Fourier transform of the pupil function [20, 36],

$$PSF(x,y) = K\left|FT\left[A(x,y)\, exp(i\frac{2\pi}{\lambda}W(x,y))\right]_{f_x=\frac{x}{z},f_y=\frac{y}{z}}\right|^2 = K\left|FT[P(x,y)]_{f_x=\frac{x}{z},f_y=\frac{y}{z}}\right|^2 \qquad (1.15),$$

where **FT** is the Fourier transform operator, **K** is a constant and **z** is the distance from the pupil to the image (eye length). The PSF for a diffraction-limited optical system is the Airy disk. The presence of ocular aberrations causes the light to spread out over an area and the corresponding PSF is broader than the aberration-free PSF for the same pupil size.

Optical Transfer Function (OTF)

The OTF is a complex function that measures the loss of contrast in the image of a sinusoidal target, as well as any phase shifts. It is the autocorrelation of the pupil function, or equivalently, the Fourier transform of the PSF

$$OTF = FT(PSF) \qquad (1.16).$$

Modulation Transfer Function (MTF) & Phase Transfer Function (PTF)

The modulus of the OTF is the Modulation Transfer Function (MTF), which represents the decrease in the contrast as a function of the spatial frequency.

$$MTF = |OTF| \qquad (1.17).$$

The phase of the OTF is the Phase Transfer Function (PTF). The PTF produces phase shifts, and it is associated with the presence of asymmetrical aberrations, such as coma and astigmatism. Figure 1.6 shows an example of the representation of the RMS, PSF and MTF profiles obtained from a wave aberration defined by its Zernike coefficients.

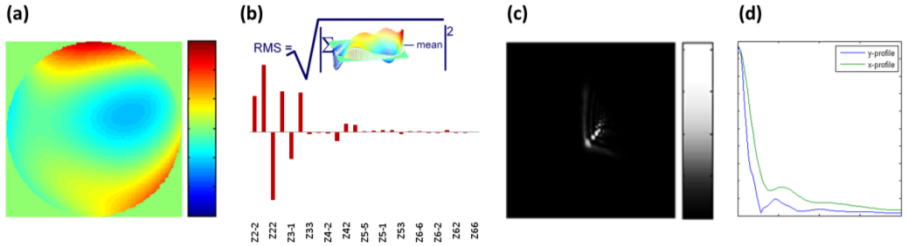

Figure 1.10 Representation of (a) Aberration map from a certain subject's wave aberration, (b) Zernike coefficients from which the RMS is computed from, (c) Point Spread Function (PSF) from those coefficients and (d) Profiles of the Modulation Transfer Function (MTF) from those same coefficients.

Aberrations affect the retinal image by reducing its contrast (MTF) or translating the image sideways to produce a spatial phase shift with spatial frequency (PTF). Together, the MTF and PTF comprise the eye's optical transfer function (OTF) [36]. The optical system of the eye works as a filter that lowers the contrast and changes the relative position of each grating in the object spectrum as it forms a degraded retinal image. A high quality OTF in the eye is therefore indicated by high MTF values and low PTF values, and most of the scalar metrics of image quality in the frequency domain are based on these two attributes of the OTF.

Strehl ratio (SR)

The Strehl Ratio (SR) is a scalar metric that describes the quality of the PSF in the eye, describes the reduction in the peak power of the point image [36]. In the spatial domain, it can be calculated directly from the PSF, as the maximum value of the PSF in the presence of aberrations, normalized by the maximum of the diffraction limited PSF for the same pupil size. The SR ranges from 0 to 1, with 1 defining a perfect optical system.

$$SR_{SPATIAL} = \frac{\max(PSF)}{\max(PSF_{DL})} \qquad (1.18),$$

In the frequency domain, the SR is computed as the volume under the MTF of an aberrated system normalized by the diffraction-limited MTF, for the same pupil diameter.

$$SR_{FREQUENCY} = \frac{\int_{-\infty}^{\infty}\int_{-\infty}^{\infty} MTF\,(f_x,f_y)df_xdf_y}{\int_{-\infty}^{\infty}\int_{-\infty}^{\infty} MTF_{DL}(f_x,f_y)df_xdf_y} \qquad (1.19),$$

where **MTF** is the MTF of the aberrated wavefront, while the $\mathbf{MTF_{DL}}$ is the diffraction-limited MTF. Strehl ratio computed by the MTF method is equivalent to

the SR for a hypothetical PSF that is well-centered with even symmetry computed as the inverse Fourier trans-form of MTF (which implicitly assumes. PTF=0). Thus, in general, $SR_{FREQUENCY}$ is only an approximation of the actual SR computed in the spatial domain ($SR_{SPATIAL}$)[37]. The residual RMS wavefront error is often the number quoted to represent the spatial performance of an AO system. An approximation of the SR based on the RMS wavefront error is given by [63]

$$SR = \exp[-(2\pi\sigma)^2] \quad \textit{(1.20),}$$

where **σ** is the RMS wavefront error in waves. In order to reach a SR of 0.8 and therefore to consider the system to be diffraction limited and fulfill the Marechal criterion [35]

$$RMS < \frac{\lambda}{14} \quad \textit{(1.21).}$$

For a wavelength of 550nm this is equal to a residual RMS of 0.04 mm [63].

Visual Strehl (VSOTF)

As the SR includes in the calculation regions of the MTF with spatial frequencies beyond those relevant to the visual system, a new metric was introduced to adapt the definition to visual optics (Visual Strehl) [64]. Visual Strehl has been reported as an optimized metric to predict the visual performance of the eye from the aberrations of that eye [65], since it holds the highest correlation variance against subjective acuity testing in a clinical setting. The VSOTF, from which VS is calculated, is computed in the frequency domain, where the OTF is weighted by the neural contrast sensitivity function (CSF_N) [36]

$$VSOTF = \frac{\int_{-\infty}^{\infty}\int_{-\infty}^{\infty} CSF_N \,.OTF(f_x,f_y)df_x df_y}{\int_{-\infty}^{\infty}\int_{-\infty}^{\infty} CSF_N.OTF_{DL}(f_x,f_y)df_x df_y} \quad \textit{(1.22).}$$

where **CSF_N** is the neural contrast sensitivity function, **OTF_{DL}** is the OTF limited by diffraction, **OTF** is the OTF of the aberrated system, and **(fx, fy)** are the spatial frequency coordinates.

C. Representing retinal image by PSF convolution

The simulation of the retinal image as the convolution of the original image with the PSF of the subject's eye [66] has been largely used in visual optics since 1955, when Flamant (1955) pioneered the application of the Fourier theory of optics with convolution of a slit target with the eye's Line Spread Function [20]. It has been used to study light distribution in the image formed by the living human eye [67], to simulate and study the effects of Seidel aberrations (primary defocus, spherical aberration, astigmatism, and coma) [68], to compute the Foveal point-spread functions from experimental wave-aberration data for individual emmetropic subjects [69] or to study how post-receptoral neural processing of the retinal image affects the processing of blurred retinal images [70].

More recently, Peli and Lang (2001) presented filtered images to bilaterally implanted patients with monofocal/multifocal intraocular lenses (IOLs), to simulate the appearance of images through the multifocal IOL, and Applegate et al. (2003) used an image-convolution based approach to evaluate the effects of individual aberration terms on visual acuity [71]. Legras et al. (2004) used convolved images to simulate the degradation produced by defocus, astigmatism and spherical aberration to evaluate the minimum amounts of these aberrations that produced just-noticeable differences to subjects [72]. Sawides et al. used convolved images in experiments investigating the adaptation to blur produced by HOAs [73, 74] or to astigmatic blur [75]. In this thesis the simulation of retinal astigmatic blur has been performed using this technique as shown in *Chapter 3*.

D. Polychromatic image quality metrics

Chromatic aberration, both LCA and TCA, are responsible of reducing polychromatic image quality, although the actual relative extent of this degradation depends on several factors, including pupil size and location, retinal eccentricity, and wavelength spectrum of the source [41]. In fact polychromatic and monochromatic image quality will differ [10, 41, 76], due to the fact that diffraction and higher-order aberrations also vary with wavelength [10].

The wavefront aberration function is a monochromatic concept, therefore when a source emits polychromatic light, the wavefront aberration maps for each wavelength are treated separately because light of different wavelengths is mutually incoherent and they do not interfere. For this reason, the definition of metrics of wavefront quality does not generalize easily to handle polychromatic light.

The most frequently used approach to evaluate the impact of chromatic aberration on retinal image quality involves the computation of the polychromatic PSF. Van Meeteren used representative average levels of both chromatic and monochromatic aberrations (assumed to be independent of wavelength) derived from the literature to compute optical transfer functions (OTFs) for the average human eye for equal-energy white light [77, 78]. Marcos et al. (1999) measured LCA and TCA, as well as monochromatic aberrations at six wavelengths for individual eyes. They interpolated the monochromatic aberration data from individual subjects at every 10 nm, from which monochromatic point-spread functions (PSFs) were computed, weighted, shifted by the TCA and combined to generate the polychromatic PSF of an individual eye [10]. Thibos et al. (2004) proposed to compute the value of a given metric for each wavelength in a polychromatic source and then form a weighted average of the results,

$$Metric_{poly} = \int V(\lambda) Metric(\lambda) d\lambda \qquad (1.23).$$

where the weighting function **V(ʎ)** is the luminous efficiency function that describes how visual sensitivity to monochromatic light varies with wavelength ʎ [37]. They also proposed that polychromatic metrics of image quality for point objects are computed similarly than for monochromatic images.

"For the eye has every possible defect that can be found in an optical instrument, and even some which are peculiar to itself; but they are all so counteracted, that the inexactness of the image which results from their presence very little exceeds, under ordinary conditions of illumination, the limits which are set to the delicacy of sensation by the dimensions of the retinal cones. But as soon as we make our observations under somewhat changed conditions, we become aware of the chromatic aberration, the astigmatism, the blind spots, the venous shadows, the imperfect transparency of the media, and all the other defects of which I have spoken. The adaptation of the eye to its function is, therefore, most complete, and is seen in the very limits which are set to its defects."

Hermann von Helmholtz, Popular scientific lectures (1885)

1.4 Monochromatic visual quality of the eye

The impact of optical aberrations on visual performance or, alternatively, the benefits of correcting ocular aberrations on vision are important questions in visual optics. The understanding of the optical and neural contributions to visual function allows predicting the limits to spatial vision and to predict the visual consequences of optical interventions.

AO technology, in combination with a psychophysical channel, is an excellent tool to explore those questions and to explore the effects of manipulated optics on vision. The design, operation, calibration and performance of AO systems are described in detail in *Chapter 1, Section 1.8*. Such systems allow performing visual tasks while viewing visual stimuli through an optical system containing adaptive optics elements, which can effectively correct or manipulate the ocular aberrations. In the following sections relevant studies making use of AO techniques to explore the impact of ocular aberrations on vision are summarized.

1.4.1 Impact of monochromatic aberrations on visual performance

The question of whether inducing changes in the optics of the eye has an impact on visual performance is more relevant when considering the possibility of altering high-order aberrations (HOAs) (with lenses or surgery) of individual subjects. So far few studies have addressed the changes in visual performance with correction of HOAs.

Early experiments controlling monochromatic wave aberrations provided compelling evidence that correction of HOAs results in improved visual performance. Liang et al. (1997), in the first systematic study using AO in vision

science, reported an improvement in contrast sensitivity of the eye in monochromatic light, better than that obtained with the best conventional spectacle correction [79]. Figure 1.11 shows contrast-sensitivity measurements for two observers before (filled symbols) and after (open symbols) AO correction. At 55 cycles per degree, with AO correction, the observers required approximately 40% contrast on average to detect the grating. At another spatial frequency, 27.5 cycles per degree, contrast sensitivity was improved by close to a factor of 6 by AO correction. Yoon and Williams (2002) found a significant improvement in logMAR Visual Acuity (VA), by a factor of 1.2, when correcting monochromatic aberrations, and by a factor of 1.6, when correcting both monochromatic and chromatic aberrations [76].

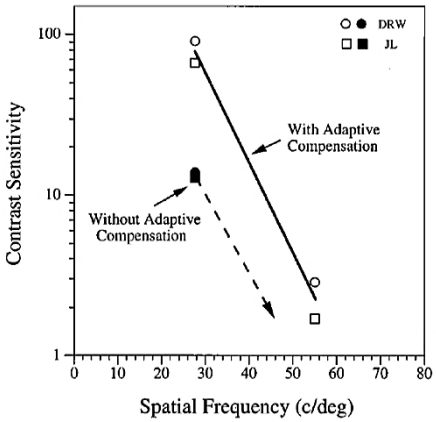

Figure 1.11 Contrast-sensitivity measurements for two eyes for a horizontal grating of 27.5 and 55 c/deg with and without AO correction. Reproduced from Liang et al. (1997).

Subsequent studies have confirmed that contrast sensitivity and visual acuity are improved by aberration correction [80-82]. Marcos et al. (2008) showed that correcting aberrations results in an overall improvement in visual acuity under a range of conditions (different polarities and a wide range of luminances), by a factor of 1.29 on average across luminances. This improvement was relatively higher in eyes with significant amounts of aberrations (Figure 1.12) [83]. Other everyday tasks such as face recognition were shown to improve after aberration correction [84] as well as modest improvements in visual performance in the periphery, where optics are not generally expected be the limiting factor for spatial resolution [85].

Despite the expected direct improvement of the contrast sensitivity function (CSF), by improvement of the modulation transfer function (MTF) upon correction of optical aberrations, the relationship between the improvement in the MTF and the corresponding improvement in the CSF is not fully understood. Elliot et al. (2009)

compared the improvement in the CSF and MTF for different age groups with correction of optical aberrations and found that although the CSF values were lower for older observers they did benefit more from the AO correction than younger observers [82]. They found optical benefits of up to a factor of 2 for a spatial frequency of 18 c/deg, slightly lower than the visual benefit that they found in the CSF (factor of 2.5 for the same spatial frequency of 18 c/deg).

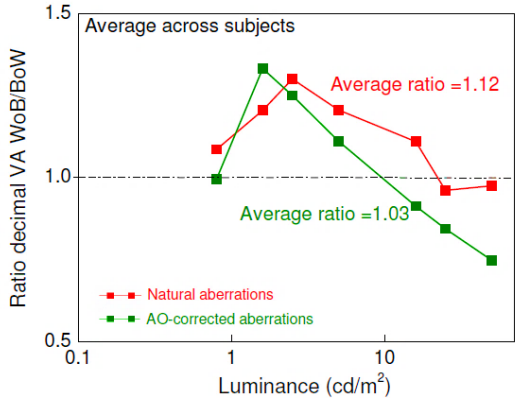

Figure 1.12 Decimal VA ratios (WoB target/BoW target) as a function of luminance (in a linear-log scale), with natural and AO aberration correction, for dilated pupils (6mm). Reproduced from Marcos et al. (2008).

De Gracia et al. (2011) measured the contrast sensitivity function (CSF) in monochromatic and polychromatic conditions under natural aberrations and after AO correction for a wide range of angles and frequencies. They found that the CSF increased on average by 1.35 times (only for the mid and high spatial frequencies) and was lower (0.93 times) for polychromatic light. The consistently higher benefit of correcting aberrations in the MTF than in the CSF (factor of 5) suggests a significant role for the neural transfer function in the limit of contrast perception [86].

The role of ocular aberrations on the accommodative response has been also investigated. Chen et al. (2006) suggested that some subjects can use monochromatic higher-order aberrations to guide accommodation [87]. Fernandez and Artal (2005) found that the response time of accommodation was reduced when removing odd-order aberrations [88]. Gambra et al. (2009) studied the effects of different aberrations on the accuracy of the static accommodative response to a stimulus, and quantified the extent to what reduced depth of focus resulting from corrected aberrations may compromise vision out of focus in subjects during accommodation [89].

The correction of high order aberrations has a different impact depending on the refractive profile of the subject. Rossi et al. (2007) found lower benefit in measured

VA for myopes than emmetropes when correcting their HOAs using an Adaptive Optics Scanning Laser Ophthalmoscope [90].

In general, AO-correction of high order aberrations of the eye has positive effects on visual performance. However debates arise on the overall benefit for correction of high order aberrations. One aspect under discussion is the fact that the largest benefit from aberration correction is achieved for large pupils, but those are only realized in dim light conditions at which retinal factors limit the benefit [83, 91]. Another potential adverse consequence of aberration correction is the increased possibility of aliasing. At the fovea, the cone spacing is about 0.5 minutes of arc which, from a simplistic sampling point of view, provides a maximum sampling frequency of 60 cycles per degree. Using high contrast interference fringes, Williams (1985) showed that aliasing is in fact perceived and, owing to the size of the cone aperture, can persist for spatial frequencies as high as 200 cycles per degree [92]. Optical imperfections of the eye effectively mitigate against this aliasing for foveal vision.

1.4.2 Interaction between monochromatic wave aberrations

The idea of increasing visual performance in certain conditions by using different combinations of aberrations has been also explored. Applegate et al. (2003) studied the interaction of aberrations that could increase visual performance, specifically of combinations of defocus and spherical aberrations as well as astigmatism and secondary astigmatism. Induction of these combinations of aberrations reduced VA compared to naive conditions, but some particular combinations of aberrations produced significantly better performance than one aberration alone [71]. McLellan et al. (2006) showed that the actual combination of HOA found in eyes produced typically better Modulation Transfer Function (MTF) than most combinations of equal amounts of aberrations and random signs [93].

Along these lines, de Gracia at al. (2011) found, first computationally and then experimentally, that the combination of coma with astigmatism improved decimal VA over VA with astigmatism alone when all the rest of aberrations were AO-corrected, although the actual response was dependent on refractive profile of the subjects (non-astigmats habitually-corrected astigmats and habitually-non-corrected astigmats) [94, 95]. Legras and Rouger (2008) showed the subjective effect of blur with side-by-side comparison of images blurred with high order aberrations or partially corrected spherical aberrations (SA), coma and trefoil, and reported that the subjective quality of vision of a subject with typical aberrations could be improved by either a partial (50%) or a full correction of both SA and coma, this gain being comparable to 1/8D of defocus blur [96].

The effect of interactions between astigmatism and coma on vision is further explored in *Chapter 4*.

"Proposition I. Theorem I. Lights which differ in Colour, differ also in Degrees of Refrangibility.
[…] Wherefore in both Cases the Light which comes from the blue half of the Paper through the Prism to the Eye, does in like Circumstances suffer a greater Refraction than the Light which comes from the red half, and by consequence is more refrangible."

Isaac Newton. Opticks or a Treatise of the Reflections, Refractions, Inflections and Colours of Light. 4th Edition (1730)

1.5 Polychromatic visual quality of the eye

The retinal image quality is degraded by the presence of monochromatic and polychromatic aberrations in the ocular optics. However, ocular aberrations are measured using wavefront sensors with monochromatic, generally infrared, light. Nevertheless, the visual world is polychromatic and the study of the impact on vision should consider the aberrations in the visible light, as well as the effect of chromatic aberrations. The following sections describe the impact of chromatic aberrations on visual function and the different methods for their compensation.

1.5.1 Impact of chromatic aberration on visual function

Chromatic aberrations impact retinal image quality and, therefore visual quality. The presence of chromatic aberrations impacts positively some visual functions. For example the LCA helps the accommodation system respond correctly when there is defocus blur, however, an issue related to LCA is the wavelength at which a white target is in focus at various levels of accommodation [7].

Chromatic aberration also impacts clinical refractions, which are invariably performed using white light. Thibos et al. proposed that monochromatic methods for an objective refraction could be extended into the polychromatic domain with the aid of an optical model of the eye's ocular chromatic aberration (Indiana eye model) [55] to determine the focus shift associated with referencing measurements taken at habitual near infrared wavelength to a visible wavelength in focus.

Figure 1.13 shows the variation of refractive error with wavelength calculated using that eye model. As illustrated there, when an eye views through a spherical lens, the LCA curve shifts vertically. Positive lenses change the eye–lens system in the myopic direction, which corresponds to a negative refractive error clinically, hence the curve shifts downward. Conversely, negative lenses shift the LCA curve upward. This shifting of the curve changes the balance between the state of focus and the

relative luminance of each wavelength component of polychromatic light. Shifting the curve upward reduces the amount of defocus in the shorter wavelength but increases the amount of defocus in the longer wavelengths. In white light, the optimum PSF occurs for an additional spherical lens of power - 0.25 D. However the eye is no longer well focused for 555 nm but for 515 nm [36].

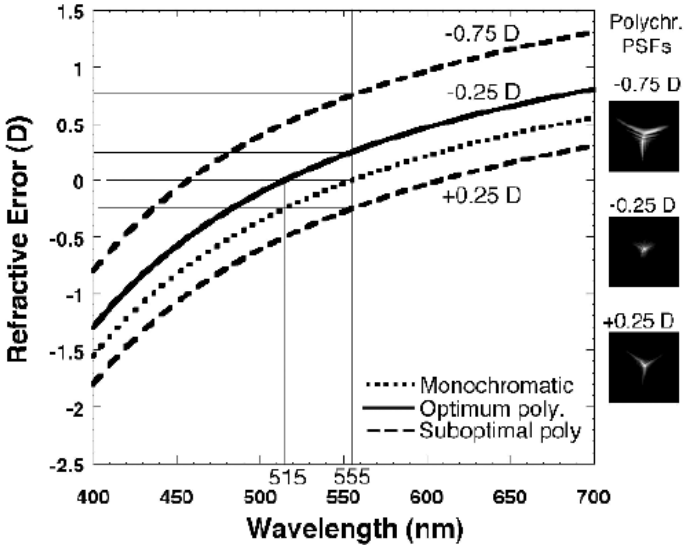

Figure 1.13 Polychromatic refraction shifts the LCA function vertically. If the eye is emmetropic at 555 nm, then the same eye will appear to be myopic when viewing through a positive lens and the wavelength in focus will shift to a longer wavelength. Conversely, the eye will appear to be hyperopic when viewing through a negative lens and the wavelength in focus will shift to a relatively short wavelength. Thus the lens value (−0.25 D in this example) that optimizes retinal image quality for polychromatic light corresponds to a unique wavelength in focus (515 nm) when the eye is well focused for polychromatic light emitted by a distant object. Reproduced from Porter et al. (2006).

Chromatic aberration is also an important factor in the optical performance of the pseudophakic eyes in polychromatic light. In recent years, monofocal IOL designs have improved not only to restore transparency or to correct refractive errors (sphere and cylinder), but also to reduce the spherical aberration of the eye [97-101] However the replacement of the lens also modifies the chromatic dispersion properties of the eye, as this is affected by the refractive index wavelength-dependency of the IOL material. Therefore, the optical performance will be determined by both the IOL design and the IOL material. Results of *in vivo* objective and subjective measurements of the LCA in pseudophakic patients bilaterally implanted with monofocal aspheric hydrophobic and hydrophilic IOLs are presented in *Chapter 6*.

1.5.2 Interactions between monochromatic and chromatic aberrations

In polychromatic light, the retinal image quality is affected by interactions between monochromatic and chromatic aberrations. It has been suggested that monochromatic aberrations play a protective role against chromatic aberrations [102], which may explain why achromatizing lenses [52, 61] aimed at correcting LCA in the eye do not noticeably improve visual performance, unless both chromatic and monochromatic aberrations are corrected [13].

Few studies have developed computational methods for characterizing the optical quality of the eye that incorporate both types of aberrations and explain the complex interactions between monochromatic and chromatic aberrations in forming the retinal image. Marcos *et al.* (2002) measured both, LCA and TCA, as well as monochromatic aberrations at six wavelengths for individual eyes. They interpolated the monochromatic aberration data at every 10 nm, from which monochromatic point-spread functions (PSFs) were computed and summed to generate the polychromatic PSF of an individual eye [102]. The MTF associated with a specific spectral sensitivity function (i.e. the S-cone fundamental) was computed from a weighted PSF, in which the weights represented the relative sensitivity at each wavelength. The polychromatic PSF must also take into account each individual's TCA, which shifts the position of each monochromatic PSF on the retina.

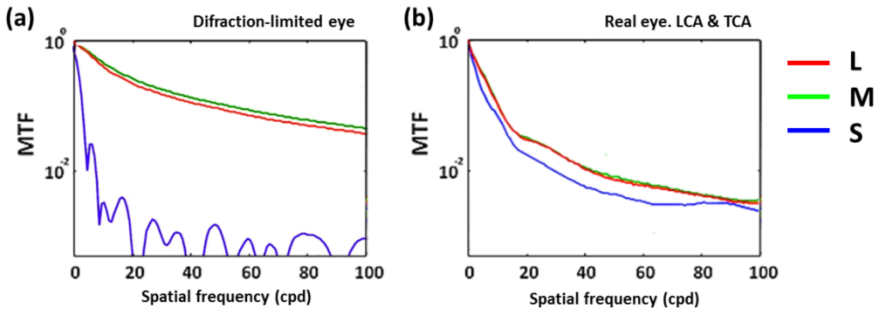

Figure 1.14 Polychromatic MTFs computed with a 6-mm pupil for L cones (red line), M cones (green line) and S cones (blue line) for theoretical model eye with LCA only (a) and one subject (b) with measured LCA, TCA and wave aberrations. RMS wavefront error (at 530 nm) for the subject was 1.83 µm. The TCA magnitude was 0.30 arcmin nm^{-1}. Similar results were found with a 4-mm pupil. Adapted from McLellan et al. (2002).

Figure 1.14 (a) shows the MTFs for the L-cone, M-cone and S-cone fundamentals in equal-energy white light for the model eye with LCA alone and with optimal resolution at 550 nm. The S-cone MTF lies well below those of L and M cones, because of the image blur caused by LCA at short wavelengths. The individual

peaks in the S-cone function represent spatial frequency ranges of alternating contrast reversal, in which light and dark are exchanged. Figure 1.14 (b) shows MTF computed for each cone class for one of the subjects of the study, incorporating LCA, TCA and monochromatic wave aberrations at a series of wavelengths. Differently to the diffraction-limited eye model, the potential image quality for the S-cones approaches that of L and M cones for all subjects.

Ravikumar et al. (2008) employed a model of ocular chromatic aberration based on population average levels of LCA to examine the impact of different levels of monochromatic aberrations and TCA and to compute the polychromatic image quality of the human eye from a single measure of monochromatic aberrations [77].

1.5.3 Chromatic aberration compensation and correction

Some attempts to achromatize the human eye using refractive elements with different lens designs in the visible range for visual application have been accomplished. These achromatizing lenses (ALs) intended to enhance vision, by introducing the opposite LCA found in the human eye. A first design consisted in a symmetrical triplet was exploited in different studies [43, 103-105], reporting some subjective gain in vision with polychromatic stimulus, however all these designs suffered from a rapid increase in TCA off-axis, which is an important limitation when testing the lenses with extended polychromatic objects. Powell (1981) proposed a more complex design compounded by a triplet and a doublet air-space, which performed well over a 14-deg field of view [106]. Zhang *et al.* (1991) determined that 0.4 mm of misalignment of an achromatizing lens relative to the eye would cancel any benefit the lens would give to spatial vision [107].

More recently, Artal et al. (2010) explored the visual effect of the combined correction of spherical aberration (SA) and LCA in IOLs using an AO system and a diffractive element respectively [108]. They showed that the visual improvement provided by the correction of SA was higher than that from correcting LCA, while the combined correction of LCA and SA provided the best visual performance and suggested that an aspheric achromatic IOL may provide some visual benefit when compared to standard IOLs. Other diffractive IOLs designs have been proposed to compensate for the chromatic aberration of the eye.

Retinal imaging may also benefit from the correction of the eye's chromatic aberration. The development of modern ophthalmoscopes, using infrared light, and new ophthalmic imaging modalities using polychromatic light sources (i.e. optical coherence tomography (OCT)), inspired new methods to correct the LCA to further improve the quality of the retinal images, especially when large pupils and broad spectral bandwidths are used. Fernandez et al. (2006) investigated the correction

of the ocular LCA in the NIR using a new design achromatizing lens for retinal imaging purposes with no induction of any other parasitic aberrations.

"In fact, the difficulty of seeing things upright by means of upright retinal images seems to consist solely in the resistance offered by the long-established previous experience. There is certainly no peculiar inherent difficulty arising from the new conditions themselves. If no previous experience had been stored up to stand in opposition to the new perceptions, it would be absurd to suppose that the visual perceptions in such a case would seem inverted."

George M. Stratton. Some preliminary experiments on vision without inversion of the retinal image. Psychological review (1897)

1.6 Visual perception and adaptation

The subjective image quality of the human eye is affected by both optical blur and neural factors that limit the eye resolution, as well as by the observer's visual experience. However the visual system is able to adapt to changes in the environment, as well as to recalibrations to changes within the observer.

To study neural plasticity after experimental modification, Stratton (1896) first studied the effect of presenting an inverted image to the retina and reported that after removing the reversing lenses (8 days), it took several hours for his vision to return to normal [109]. This neural plasticity of the visual system combines two fundamental mechanisms: a neural adaptation process that recalibrates the internal norm to maintain a match between visual coding and visual environment, and perceptual learning that refers to the performance after a training task. The following sections describe both mechanisms, present astigmatism as an example of both mechanisms in the eye, and highlight different psychophysical paradigms that have been used to evaluate them.

1.6.1 Neural adaptation

Visual adaptation describes the processes by which the visual system alters its operating properties in response to changes in the environment, thus having important consequences in perceptual experience [110]. It is well known that the visual coding is a dynamic process, adapting continuously to changes in the visual context (for instance, changes in the contrast, luminance, blur or color in the visual scene), or changes in the observer him/herself (for example by disease, treatment, aging, or a new spectacle prescription) [111]. Adaptation is therefore related to the adjustment of the visual system to changes in the environment, as well as to recalibrations to changes within the observer, which allow maintaining a match between visual coding and visual environment throughout the life span. These

adaptation processes can occur over very a wide range of time-scales going from over millisecond to minutes [112, 113] to life-spans [111].

Among the most straightforward ways to modify the appearance of the visual world to investigate the processes underlying visual adaptation is image blurring. This can be achieved by lenses, or by computer simulations of image blurring/sharpening. The advent of Adaptive Optics has actually allowed modifying the high order aberrations of the eye, therefore allowing high control over the amount and specific form of the blur of the retinal image of the subjects[79, 83, 114]. Short-term adaptation adjusts the visual system to temporary changes, as for example changes in light illumination levels or in the blur perceived in natural scenes. Short-term adaptation to blur was first reported by Webster et al. (2002) in a seminal paper, where they showed that subjects can adapt to blur produced by computed generated Gaussian blur. After viewing a blurry or sharpened image, a physically focused image appeared too sharp or too blurry, respectively. Thus the point of subjective focus shifted toward the adapting image (Figure 1.15). These effects are consistent with a re-normalization of perception, so that the currently viewed stimulus becomes the new prototype for proper image focus [115]. These aftereffects occur and can be selective for different types of stimuli, for luminance or chromatic blur [116], spatial or temporal blur [117], and different depth planes [118].

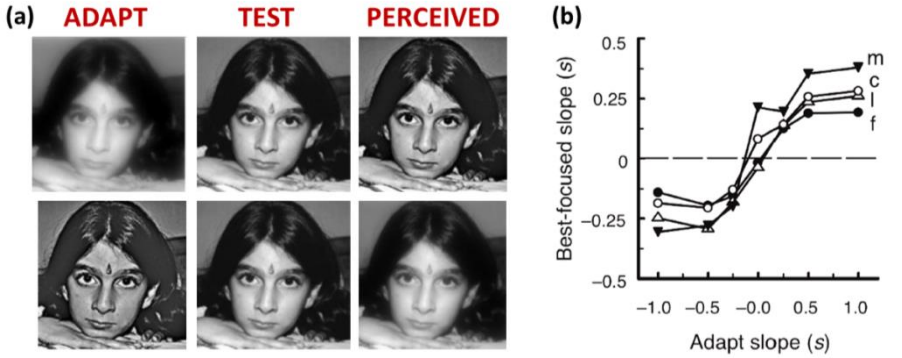

Figure 1.15 (a) Blur adaptation process: Viewing a blurred image (positive slope) causes the correctly focused image to appear too sharp and viewing a sharpened image (negative slope) leads to the opposite after-effect (b) Slope of the image amplitude spectrum that appeared best-focused after adapting to images with different spectral slopes, testing 4 different images: face (f), leaves (l), check board (c) and meadow (m). Adapted from Webster et al. (2002).

Long-term adaptation adjusts the visual system to changes in the environment or within the observer. If observers are exposed to and thus adapted to different environments, their vision will be normalized in different ways and their subjective visual experience may differ, while if observers are exposed and adapted to common properties in the environment, their vision will be adjusted toward

common states, and may develop common features in their visual response. How the world looks depends on the recent and long-term visual experience [20]. An example is the visual degradation produced by an ocular disorder (myopia, keratoconus, cataract), which constrains the observer to continuously adapt to their vision. It is well known that the visual system changes over time. Werner and Schefrin (1993) studied how the visual system is calibrated for some longer term estimate of the environment by measuring the locus of the achromatic point. They found no significant changes as a function of age in subjects who did not suffer from ocular disease, suggesting that partial compensation for age-related changes in visual mechanisms occurs in a way that preserves constancy of the achromatic locus across the life-span [119].

Eye's adaptation to its native aberrations

Adaptation to spatial blur is especially interesting in the eye since ocular aberrations produce a spatial blur of the retinal images, reducing the visual quality. However, observers do not have the impression of image degradation, perhaps due to the presence of a mechanism such that the visual system may be compensated for the eye's imperfections. Blur is an important factor of image quality and the visual system makes intuitive blur judgments inherent to each subject.

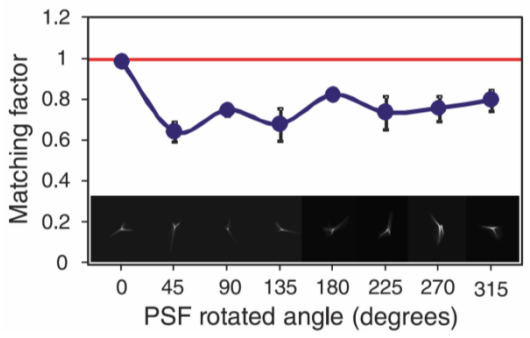

Figure 1.16 Blur matching as a function of PSF orientation. The lower images illustrate the range of PSF orientations that were tested in the experiment with the leftmost PSF being its native orientation. The matching factor (y-axis) is the amount that that magnitude of the aberrations had to be changed from the initial magnitude to generate a degree of blur that appeared equivalent to the blur produced by the subject's native PSF orientation. All rotated PSFs appeared blurrier than the native PSF and the subject had to reduce their magnitude to make a subjective blur match. Adapted from Artal et al. (2004).

Artal et al. (2004) showed that a stimuli seen through an individual's natural aberrations always appear sharper than when seen through a rotated version of the same aberrations, even though the magnitude of the blur is the same and the same spatial frequency content is present in both images [114]. Subjects were asked to view a scene and compare the scene blurred by their native PSF to a similar scene blurred by their rotated PSF. In order to make a subjective blur match, the subjects had to reduce the magnitude of the aberrations in the rotated PSF

condition to match that of the native PSF condition. Figure 1.16 shows that the aberrations to generate an unfamiliar PSF need to be reduced by over 20% to make the blur appear similar to one generated by the native PSF. They suggested that these results may be a consequence of neural adaptation to the specific degradation produced by someone's HOAs.

Sabesan and Yoon (2010) studied potential effects of adaptation in eyes with keratoconus, a disease of the cornea where local thinning gives rise to an irregular shape and severe aberrations [120]. They measured high and low contrast Visual Acuity (VA) in four keratoconic (KC) eyes, wearing their own prescribed soft toric contact lenses over a 6-mm pupil, and in three emmetropic eyes, where an AO system was used to correct the natural ocular aberrations and to induce the aberration of the KC eye during vision testing. KC eyes showed significantly better high and low contrast VA than normal eyes with KC aberrations (Figure 1.17). In KC eyes, the neural visual system appears to compensate for long-term visual experience with an asymmetrically blurred retinal image, resulting in improved visual performance.

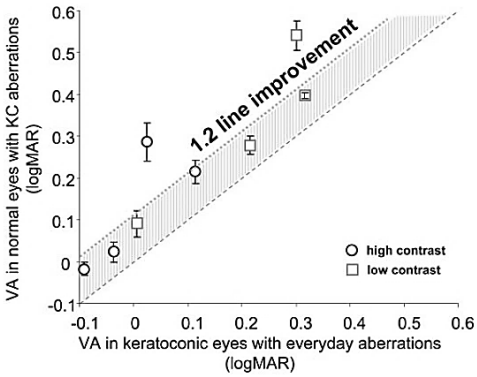

Figure 1.17 Comparison of visual performance between KC eyes and normal eyes with KC aberrations. Each data point represents the average of three normal eyes for each KC eye. Dashed line: equal acuity line; shaded region: average 1.2-line improvement in VA in KC eyes. Reproduced from Sabesan & Yoon (2010).

Chen et al. (2007) showed that an image that appears the sharpest to the subject is not necessarily the one that is generated with a full AO correction. Subjects selected an image that was blurred by some remaining aberration as the sharpest image, rather than the diffraction-limited image [121].

Interestingly, there is increasing evidence that observers appear to be adapted to the blur level produced by their high order aberrations, as the level of blur that produces no after-effects matches the native blur level in subjects[73, 74, 122].

However, the role of orientation of the specific form of blur remains to be elucidated.

Adaptation to modified aberrations

Some studies have reported relatively fast improvements in visual performance upon adaptation of blur. Mon-Williams et al. reported an increase in visual acuity (VA) in subjects after exposure to spherical blur [123]. Pesudovs observed that patients with increased aberrations following refractive surgery, progressively improved VA in the course of 10 weeks after the procedure [124].

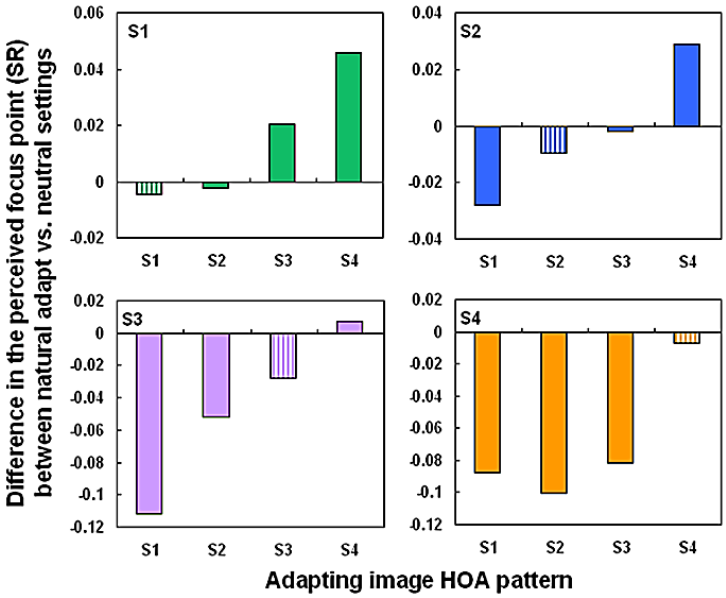

Figure 1.18 Testing scaled high order aberrations patterns. Difference in the perceived focus level (in terms of Strehl Ratio) between natural adaptation and the subject's neutral settings, when the subjects adapted to their own aberrations (striped bars) or to the aberrations for each remaining subject (solid bars). Reproduced from Sawides et al. (2011).

Recent studies have shown that subjects can adapt to the blur produced by defocus as well as high order aberrations (scaled versions of their own aberrations, or other subjects' aberrations) [73, 74]. These short-term after-effects appeared in both perceived blur and visual acuity, following exposure to blur introduced optically or by filtering images [115, 123, 125].

More recently, Sawides et al. (2011) found that an observer's focus settings remain largely unaffected when adapting to their own aberrations, but were significantly biased toward higher or lower blur levels when adapted to the aberrations from observers with more or less optical blur respectively. Furthermore, the finding that aftereffects were weakest near the level of the observer's natural blur (Figure 1.18,

S1 and S4) further suggests that the individual's subjective neutral point corresponded to the long-term adapted state induced by their optics. This in turn suggests that the blur level that appears correctly focused to an observer is not merely a learned criterion. The results provide strong evidence that spatial vision is calibrated for the specific blur levels present in each individual's retinal image and that this adaptation at least partly reflects how spatial sensitivity is normalized in the neural coding of blur [74].

1.6.2 Perceptual learning

Perceptual learning refers to the phenomenon where practice or training in perceptual tasks often substantially improves perceptual performance. Its specificity in what is learned is highly specific to the stimulus and the task factors, such as retinal location, spatial frequency, orientation, background texture or visual field position [126]. Perceptual learning operates in a very specific manner, which depends on stimulus and task, whereas adaptation is thought to reflect a recalibration of the visual system to handle a change in the visual world.

An interesting debate is the relationship between adaptation and perceptual learning [111]. Adaptation is typically characterized by an immediate shift in perceptual appearance of a scene after a typically brief exposure to a modified visual experience. On the other hand, perceptual learning is normally characterized by a longer time course [127], leading to changes not only in visual appearance, but also on visual performance [128]. However, the line between adaptation and perceptual learning is blurred by the fact that learning can actually produce changes in the appearance of visual scenes [129], and some adaptation processes can actually operate at long time-scales, can show persistent after-effects, and in fact exhibit some forms of learning [130].

An example of the latter is a study of Yehezkel et al. (2010), where they investigated whether adaptation was affected by previous experience with the adapting stimulus and examined whether adaptation becomes more effective with experience [130]. Efficient adaptation processes may reduce biases in perception, both when the adapting stimulus is applied and removed, the latter by reducing the duration of after-effects. In their study, they induced an artificial one-dimensional visual blur by using a cylindrical lens of 1D mounted in front of one eye of the observers for an adaptation period of 4 h in two sessions, (in two different days) and probed the underlying mechanism and the time course of the adaptation effect. The obtained learning effect suggested learning of adaptation to the induced blur rather than learning of the task per se (Figure 1.19).

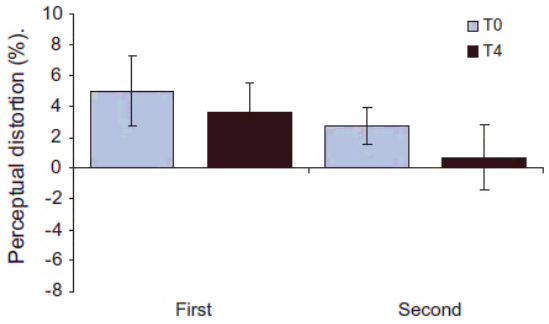

Figure 1.19 The learning effect: Comparison of the first two sessions shows a continuous decrease in distortion, from 5 ± 2 % at time T0 of the first session to 0.68 ± 2 % at time T4 of the second session. Reproduced from Yehezkel et al. (2010).

Perceptual learning involvement in perceptual adaptation to the correction of natural astigmatism is further discussed in *Chapter 3*.

1.6.3 An example: astigmatism, perceptual and adaptational effects

Astigmatism is one of the most frequent aberrations in the human eye: occurs in 85% of the population [131], and can be easily corrected (or induced) by cylindrical lenses. Uncorrected astigmatism has a high impact on vision, even when relatively low amounts of astigmatism are present [131-134]. Also, numerous studies have shown that large amounts of astigmatism left uncorrected in childhood may lead to meridional visual deficits, so called meridional amblyopia, although those are not found in all visual tasks [135, 136].

Astigmatism (as well as other high order aberrations (HOA) like coma) is increased in certain pathologies (i.e. keratoconus)[137], induced in several surgical procedures (i.e. keratoplasty, cataract surgery)[138] or with ophthalmic lenses [139]. Astigmatism is particularly attractive to investigate adaptive processes in the visual system, due to the inherent oriented nature of the retinal blur that it produces. Besides, adaptation to astigmatism, and in particular, to a newly prescribed correction of astigmatism, is relevant clinically, where the optometrist or the surgeon faces the decision of astigmatism correction by spectacles, contact lenses, intraocular lenses or corneal surgery. However, the extent to which astigmatic subjects are adapted to their own astigmatism, recalibrate upon its correction and the extent to what these perceptual changes affect visual performance is not well known

Astigmatism is a meridian-dependent type of refractive error, where refractive surfaces have two principal meridians, with the curvature of the surface ranging from a minimum on one of these meridians to a maximum on the other, caused by a lack of symmetry on the optical surfaces of the cornea and the crystalline lens [7,

140]. Astigmatism has a great impact on the quality of retinal image and subsequently in vision. In an emmetropic eye or with spherical ametropia (Figure 1. 21 (a), top), rays diverging from a point on the axis are converged to a conjugate image point provided that the paraxial approximation is taken into account. In an eye with regular astigmatism (Figure 1. 21 (a), bottom), the image of a point object is not a point because of the different refractive powers corresponding to each of the principal meridians. In this case, the image of a point object is generally an ellipse. In this particular case, the vertical meridian (y) has the greatest optical power and a focal line F'_y. This means that parallel rays contained in a vertical plane will be converged onto a point located on this focal line, while parallel rays contained in a horizontal plane will be converged onto a point located on the focal line F'_z. At any other distance other than that of the two focal lines, the cross-section of the refracted pencil is generally an ellipse. Precisely at the dioptric midpoint between the two focal lines, the cross-section of the pencil is circular and is called the disc of least confusion (DLC). The region between these two focal lines is known as the conoid of Sturm or Sturm's interval. The characteristics of the blurred ellipse depend on the pupil diameter and on the type of astigmatism [140].

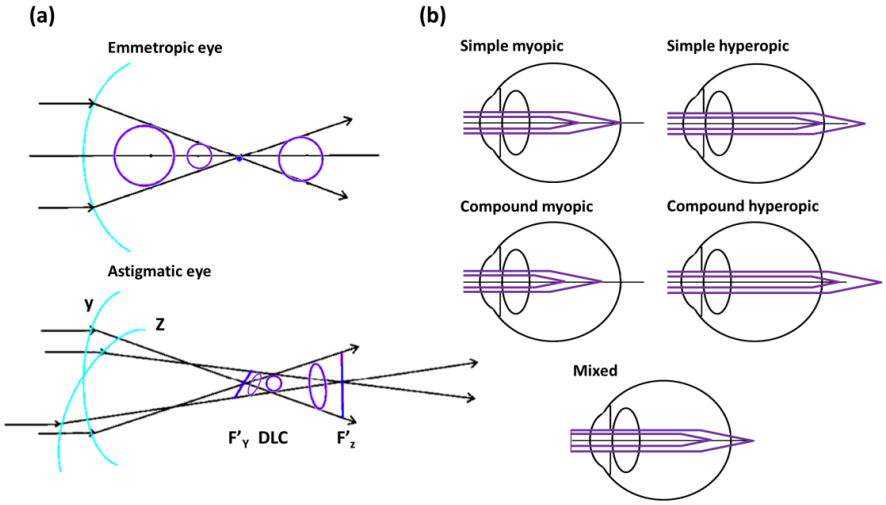

Figure 1.20 (a) Schematic diagram of image formation in an emmetropic eye or an eye with spherical ametropia (top) and in an eye with astigmatic refractive error (bottom). The principal meridians (y, z), the first and second focal lines (F'y, F'z), and the disc of least confusion (DLC) are shown. (b) Types of astigmatism related to the associate spherical refractive errors: simple myopic, simple hyperopic, compound hyperopic, compound hyperopic and mixed. Adapted from Vilaseca et al. (2012).

There are different types of astigmatism which can be classified according to several different factors: to the associate spherical refractive errors, the axis direction and the regularity of the surfaces. Figure 1.20 (b) shows the types of astigmatism related to the associated spherical refractive errors:

Myopic astigmatism. The eye is too powerful for its length in one principal meridian for simple myopic astigmatism, and in both principal meridians for compound myopic astigmatism.
Hyperopic astigmatism. The eye is too weak for its length in one principal meridian for simple hypermetropic astigmatism, and in both principal meridians for compound hyperopic astigmatism.
Mixed astigmatism. The eye is too powerful for its length in one principal meridian (myopic astigmatism), and too weak for its length in the other principal meridian (hyperopic astigmatism).

According to the axis direction, astigmatism can be classified in With-the-rule (WTR, the flattest meridian is 90 ± 30 degrees, nearer the horizontal), Against-the-rule (ATR, the flattest meridian is 0 ± 30 degrees, nearer the vertical) and Oblique (the principal meridians are 45 ± 15 degrees). WTR astigmatism produces vertically oriented retinal blur and ATR horizontally oriented retinal blur. Astigmatism can also be classified according to the regularity of the surfaces in Regular (the principal meridians are perpendicular to each other) and Irregular (the principal meridians are not perpendicular to each other).

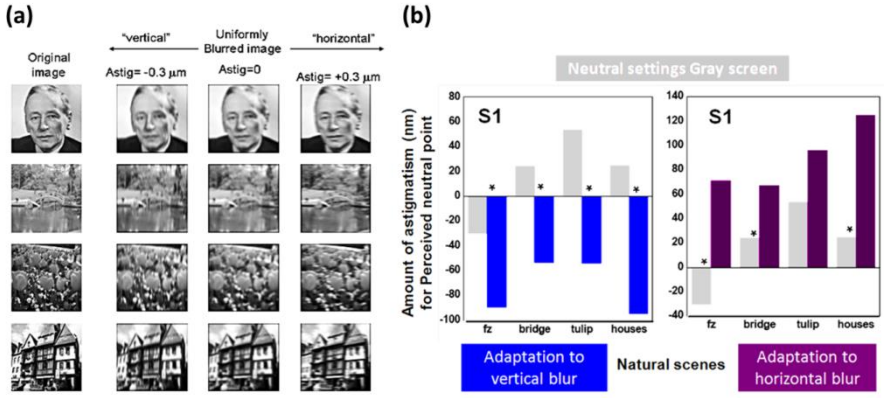

Figure 1.21 (a) Images from the stimulus arrays formed by varying different combinations of astigmatism and defocus (keeping a constant blur strength B = 0.76 D). Astig stands for Zernike coefficientC_2^{-2}. Original images were convolved with the PSF of wavefronts containing the LOAs of astigmatism and defocus. A negative astigmatism at 0/90 deg produces blur with a vertical orientation bias; a positive astigmatism produces a horizontal bias. Equivalent blur from defocus only produces isotropic blurring. (b) Stimulus levels that appeared isotropic before or after adapting to the same image with negative (blue) or positive (purple) astigmatism tested on three subjects for individual images of natural scenes. The vertical axis represents the amount of astigmatism (in nm; negative for vertical and positive for horizontal) that makes the image appear isotropically blurred for the observer. Error bars represent standard deviation across measurements; *indicates significant differences ($p < 0.05$) before vs. after adaptation. Adapted from Sawides et al. (2010).

Perceptually, it has been shown that the perception of focus can be strongly affected by brief periods of exposure to a blurred stimulus [115]. These short-term

after-effects appeared in both perceived blur and visual acuity, following exposure to blur introduced optically or by filtering images [115, 123, 125]. There is also evidence that with longer exposures to blur (by lenses, surgically-induced, or resulting from a corneal condition) [123, 141-143] adaptation may lead to improvements in visual acuity, perhaps by some form of perceptual learning. Moreover, Sawides et al. (2010) showed that after brief exposures to images blurred with vertical or horizontal astigmatism the perception of neutral point was shifted towards those images (Figure 1.21). Indicating that adaptation can be selective to the orientation of the blur inherent to natural astigmatism [75].

Prior adaptation to astigmatism also has an impact on visual performance. A previous study from De Gracia et al. (2011) measured VA under induction of astigmatism in subjects with different refractive profiles and found that VA under induction of astigmatism in non-corrected astigmats was less impaired than in non-astigmatic subjects, suggesting that non-corrected astigmats were adapted to their natural astigmatism (Figure 1.22) [94]. Impact of astigmatism and its correction in visual perception and performance is further discussed in *Chapters 3* and *4*.

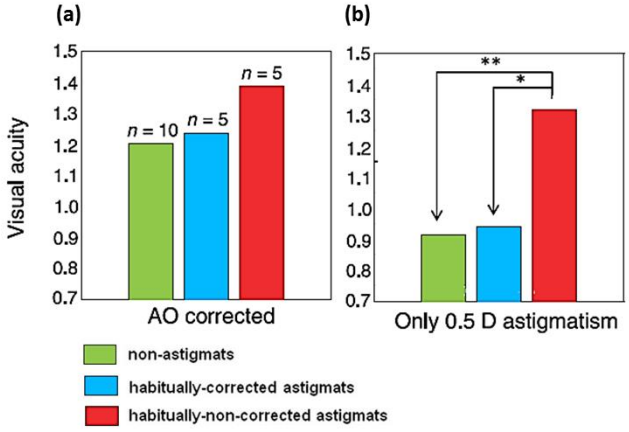

Figure 1.22 Decimal VA for the 3 groups of the experiment, non-astigmats habitually-corrected astigmats and habitually-non-corrected astigmats when (a) natural aberrations are AO-corrected and (b) after induction of 0.5 D x 45deg of astigmatism. Data are averaged across subjects in each group; **p<0.001 and *p<0.05. Adapted from de Gracia et al. (2011).

1.6.4 Psychophysical methods to measure visual function

Psychophysical methods allows evaluating the subjective image quality of the human eye, which is affected by both optical blur and neural factors that limit the eye resolution as well as by the observer's visual experience. In psychophysical studies visual perception and performance are evaluated by measuring an observer's performance on a visual task (visual acuity, contrast sensitivity, detection, identification and recognition task, judgment of blur). Classical

psychophysical methods used in vision sciences are those that measure a threshold, quantified in terms of the finest size of detail in a scene that can just be resolved by the eye measured with different targets such as lines, bars, grating, letters and the contrast sensitivity threshold at which one observer can detect a sinusoidal grating or Gabor patches of different spatial frequencies.

In general, there are two kinds of decision tasks: adjustments, where the observers have to adjust the stimulus accordingly to the task asked for, and judgments, where the observers have to classify the stimulus of percept [144]. The judgment decision tasks differ from the adjustment decision tasks primarily in the number of alternative stimuli that may be presented on a given trial and the number of alternative responses that the observer is allowed. Among them, the alternative forced choice procedure, and the rating scale are the methods used in this thesis.

In the two-alternative forced choice procedure (2AFC), two separate stimuli (blank/nonblank) are presented in random order, sequentially or side by side and the observer is forced to choose between alternative choices, whether the nonblank stimulus was first or second (or on the left or right). In a 2AFC, there is already a 50% chance of a correct response and the starting threshold is commonly considered as 75% (half way between 50 and 100%). For a 4AFC, threshold is considered to be at 62.5% (half way between 25% and 100 %).

In the rating scale task, the observer is asked to rate the likelihood that a blank or nonblank stimulus was presented. There must be blank and nonblank stimulus alternatives, and there may be any number of alternative ratings. The end points of the rating scale are “stimulus definitely blank” and “stimulus definitely nonblank” with intermediate degrees of confidence in between.

Most judgment experiments usually require many trials. An uninterrupted sequence of trials is called a run. A powerful method of sequencing the trials within a run to measure threshold in a limited number of trials is the use of the observer’s previous responses to calculate the next stimulus size and estimate the threshold with algorithm such as QUEST (Quick Estimate by Sequential Testing) [145]. At the end of the procedure, the trial size is considered the best estimate of the subject’s threshold.

Different psychophysical paradigms used in this thesis are further explained in *Chapter 2, Section 2.4* and the corresponding *Chapters* describing each particular study.

"It has been observed that the central part of the crystalline becomes rigid by age, and this is sufficient to account for presbyopia without any diminution of the humour; although I do not deny the existence of this diminution, as a concomitance circumstance."

Thomas Young & Richard Brocklesby, Observations on Vision. Philosophical Transactions of the Royal Society of London (1793)

1.7 The aging process: Accommodation and Presbyopia

The human visual system has the ability to change its power to bring objects of interest at different distances into focus, thus having an essential contribution on visual function. This mechanism is called accommodation. As a consequence of the aging process, the accommodation capacity of human eye declines with age with the consequent limitations to perform near-vision tasks.

Limitations of near vision with aging have been widely studied through history. Aristotle referred to his fellow sufferers as "presbyters", a Greek reference to old men and the origin of the name Presbyopia. Alhazen (Ibn al-Haitam) in the 11th century described the role of the crystalline lens and the problems that older people experience with near vision. In the Middle Ages "reading stones" become of common use by monks to assist in reading and illuminating manuscripts, and finally glass lenses were developed by Roger Bacon, who used parts of glass spheres as magnifying glasses and recommended then to be used for helping people in reading tasks. Examples of these first glasses are shown in Figure 1.23.

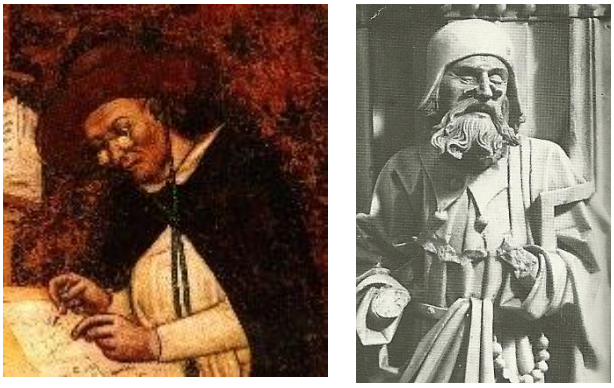

Figure 1.23 (a) Detail of a portrait of the Dominican Cardinal Hugh of Saint-Cher painted by Tommaso da Modena (1352), one of the first representations of the use of glasses for Presbyopia. (b) Tomb of Don Alfonso in the Carthusian Monastery of Miraflores (Burgos, Spain) by Gil de Siloé (1489-1493), one of the first representations of glasses in Spanish art [146].

In the 19th century, Thomas Young was the first to quantify the loss of accommodation with age. Young, Frans Cornelis Donders and Marius Hans Erik Tscherning published their classical theories of accommodation and Presbyopia. Today, the understanding of the mechanism of accommodation during relaxed accommodation is based on Helmholtz's (1909) theory.

In the following sections accommodation process, Presbyopia and current state-of-the-art of solutions for Presbyopia are further described.

1.7.1 Accommodation, Presbyopia and Cataract

Accommodation is the dioptric change in power of the eye to provide a sharp retinal image for all distances, and it is also often described as being linked with convergence and pupil constriction (so-called accommodation triad). With the focus of the eye at its far point, the zonules connecting the lens and ciliary body pull on the lens and flatten it. During accommodation, i.e. when changing focus from far to near vision, the ciliary muscle contracts, thus reducing the tension on the zonules (Figure 1.24). Because of the elastic properties of the capsule of the lens, the lens adopts a more rounded shape. Thus, both the lens and the eye increase in refractive power [7]. In addition to the dioptric changes due to curvature variations, a modification in the refractive index gradient is also found. These changes overall contribute an extra 10-15 D of refraction in the young adult eye, diminishing to <2 D by middle age [147].

The accommodative response is the actual amount of accommodation produced by the lens for a given stimulus, and it is limited by the depth-of-focus and the inability to detect small amounts of blur. At far distance, the system usually over-accommodates, while at near underaccommodates, creating a lag of accommodation [6].

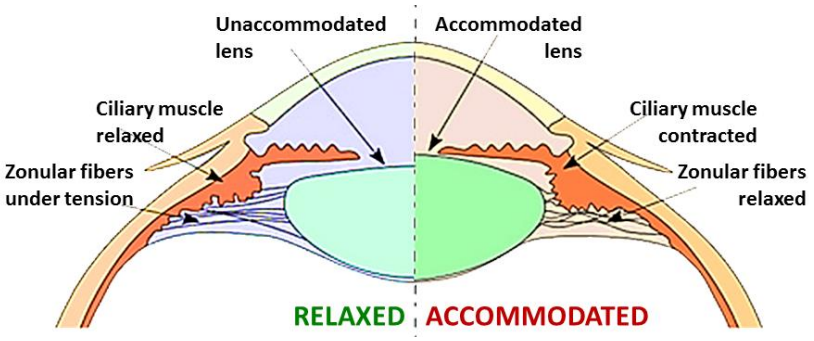

Figure 1.24 Schematic representation of the accommodation process of the eye. Reproduced from Parel et al. (2006).

The aging process of the eye has considerable impact on the crystalline lens resulting from biochemical and biophysical changes, which affects visual function. Presbyopia, the consequence of a progressive loss of lens elasticity, accompanied by a fall in the rate and amplitude of accommodation, and Cataract, loss of lens transparency, are the two most important consequences.

Presbyopia
Presbyopia is an age-related loss of the accommodative amplitude of the human eye [148], in which the lens fiber and capsule of the crystalline lose their elasticity, while the size and shape of the crystalline lens increase resulting in a gradually decrease in amplitude and speed of accommodation. The basis of Presbyopia development is crystalline lens hardening, the lens becoming too stiff to respond by bulging when tension is removed.

Age-related cataract
Age-related cataract is caused by the opacification of the crystalline lens, although also involves genetic and environmental factors. Protein aggregation is the single most important factor in cataract formation. A cascade of pathologic alterations develops an increase of the proteolytic enzyme activity, a rupture in cell membrane, a loss of low molecular weight proteins and an increase in water content [147]. There are several distinct forms of age-related cataract, whose morphologies imply different etiologies of different lens regions. Nuclear cataracts are the most common age-related cataract

1.7.2 Presbyopia solutions: state-of-the-art

Correction of Presbyopia consists of placing the image of a near object into the retina by using external (spectacles or contact lenses) or surgical (corneal procedures or IOL implantation) solutions. Current available solutions aim to optically correct for Presbyopia, and restore some near-vision functionality, although none of them is able to restore the full dynamic capability of the young eye. However there are multiple solutions that attempt to provide functionality for both near and far vision. Table 1.1 summarizes main current solutions to correct for Presbyopia [149, 150], which involve either the provision of additional optical power for near vision, using external optics or by surgical modification of the powers of the optical components of the eye, or surgical intervention designed to restore or enhance the accommodative ability of a presbyopic eye. The purely optical correction may either be passive, in that a fixed correcting power is provided, or active, where the power can be varied in either a stepwise or continuous fashion.

These solutions are based on different principles: alternating vision, monovision and simultaneous vision. Alternating vision solutions are bifocal or progressive spectacle lenses, where changes in gaze or head position allow selection of the

zone of the spectacle used to view near or far objects [151, 152]. In monovision solutions one eye is corrected for distance vision and the other for near vision, typically in the form of corneal inlays, intraocular lenses or laser refractive surgery [153].

Strategy	Method	Solution	Design
A To provide additional optical power for far, intermediate and near vision	External optics	Spectacles	Single-vision Bifocal, Trifocal Progressive
		Contact lenses	Monovision/simultaneous vision bifocal, multifocal Alternating vision
	Surgical modification of the eye's optical components	Corneal surgery (surface)	Monovision/simultaneous bifocal/multifocal
		Corneal surgery (inlay)	Pinhole/simultaneous bifocal/multifocal
		Phakic IOL	Monovision Simultaneous bifocal/multifocal
B To restore or enhance the accommodative ability	Surgical intervention	IOLs/lens /ciliary body	Simultaneous bifocal/multifocal IOLs Accommodating IOLs Lens/scleral treatments

Table 1.1 Main current solutions for Presbyopia. Adapted from Charman et al. (2014).

An increasingly popular treatment for Presbyopia relies on simultaneous vision solutions, where the eye is simultaneously corrected for both distance and near vision [154, 155]. Simultaneous vision represents a new visual experience in which a sharp image is superimposed to a blurred replica of the same image, thus reducing the overall contrast.

Figure 1.26 summarizes current presbyopic contact lens designs. Almost all refractive simultaneous-vision designs involve different powers being associated with different circular or annular regions of the lens. Thus their overall on-eye performance depends on which portions of the lens are used in forming the foveal image. Of particular interest are the proportions of the overall light contributing to

the distance and near images: these depend upon the relative areas of the two or more corrections within the pupil. In general, it seems reasonable that in a bifocal lens approximately equal amounts of light should contribute to the distance and near images, although this may not be the case in modified monovision when different lenses are worn on the two eyes.

In simultaneous-image bifocal designs, some areas of the lens have a power corresponding to the required distance correction and the rest of the optical zone provides the near correction (Figure 1.25). The dimensions of the zones are such that the area of the entrance pupil of the eye is partially covered by both distance and near corrections. It has long been recognized that the limitation of this approach is that during vision of both distant and near objects the in-focus image formed by rays passing through the 'correct' part of the optical zone is superimposed on the out-of-focus image due to the 'wrong' part [149]. The result of this superposition of in- and out-of-focus images is that the contrast of smaller details in the desired in-focus image is degraded by the light from the out-of-focus image. Fortunately high-contrast acuity is relatively robust against contrast loss, but difficulty may be experienced when tasks involving low object contrasts are involved [149].

Effects with aspheric or other multifocal designs are more complex but the end result is always that unwanted light which has passed through those regions of the lens with the 'wrong' power degrades the in-focus image formed by the appropriate parts of the lens, and lowers the contrast of smaller details to an extent which depends upon the relative areas of the two corrections within the effective pupil.

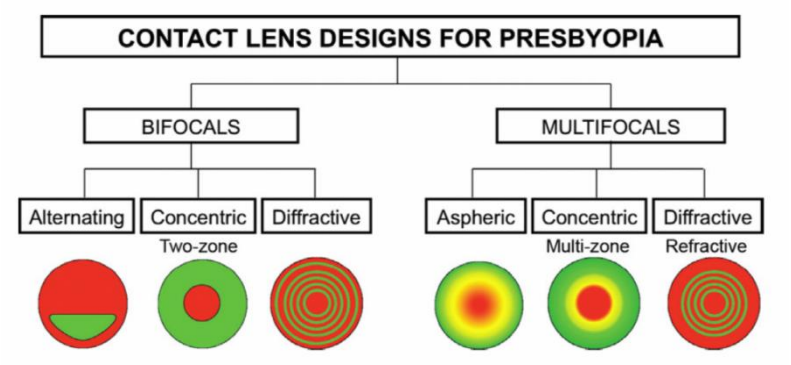

Figure 1.25 Current presbyopic contact lens designs. The red, green and yellow areas represent areas for distance, near and intermediate vision respectively. Reproduced from Charman et al. (2014).

Multifocal simultaneous vision corrections are increasingly used solutions to correct for Presbyopia, aiming at expanding the depth of focus (DoF) of the eye (i.e.

by increasing the optical aberrations of the eye or by using different combinations of optical aberrations) or at producing multiple foci (multifocal corrections) (Figure 1.26). With any multifocal solution the quality of the retinal image will result from the interaction of the lens power profile, the pupil diameter, the amount of residual ocular accommodation available, and the ocular spherical aberration. An interesting question is whether, after extended periods of simultaneous vision, adaptation occurs to the low contrast images, resulting in improvements in acuity and contrast sensitivity [156].

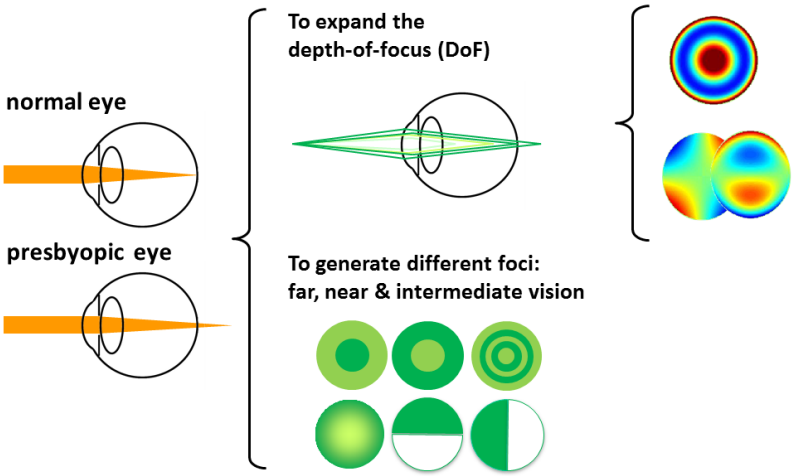

Figure 1.26 Multifocal simultaneous vision corrections. First type looks for expanding the DoF by increasing spherical aberration or using different combinations of optical aberrations. Second type aim at producing different foci for far, near and intermediate vision using different optical designs geometry.

Clinically deployable AO systems also have the potential to show the patient the range of optical correction options. The effect of multifocal simultaneous vision corrections on vision is further explored in *Chapter 7*.

1.7.3 Intraocular lenses

The replacement of the opacified crystalline lens by an intraocular optical element was performed for the first time by Sir H. Ridley in 1949. Cataract surgery with intraocular lens (IOL) implantation has become a routine surgical procedure and several IOLs materials and designs are currently available.

Traditional IOLs are monofocal (spherical, aspherical), which only correct defocus for far vision. Early monofocal IOLs were simply intended to create near-emmetropia after cataract removal. However, it was observed that some patients could achieve satisfactory standards of vision at both distance and near without spectacle wear [157], which probably arises (monocularly) as a result of increased

DoF associated with unusually small pupils, small amounts of residual myopic astigmatism and HOAs [150, 158, 159]. It is also possible that adaptation to slightly blurred imagery plays some role [114, 123, 160]. In recent years, monofocal IOL designs have improved not only to restore transparency or to correct refractive errors (sphere and cylinder), but also to reduce the spherical aberration of the eye [97-101]. Other current designs include toric, aspheric, multifocal and accommodative IOLs. Toric and aspheric IOL designs aim at compensating the astigmatism and spherical aberration of the cornea respectively, while multifocal and accommodative IOLs offer the possibility of seeing well at more than one distance [147].

The designs of most bifocal and multifocal IOLs are similar to those of simultaneous vision contact lenses (Figure 1.26). Several designs are refractive with both a central circular area and a series of concentric annular zones providing near and distance foci or, less often, a gradual change of power with zonal radius. Many state-of-the-art multifocal IOLs are diffractive designs, in which the phase profile across the lens is modified by a series of annular diffractive zones to produce distance and near foci [150]. The major problems with multifocal IOLs are the same as those of multifocal contact lenses: a loss in image contrast at medium and high spatial frequencies and, for most of the refractive but not the diffractive designs, a pupil-dependence in visual performance. The loss of contrast is caused by the out-of-focus image formed by the 'wrong' portion of the lens being superimposed on the in-focus image due to the 'correct' portion of the lens, and results are pupil-dependent since the pupil affects the area of the IOL used by the image–forming rays. The impact on the retinal image of different multifocal designs has been briefly studied [161, 162], however multifocal optical designs implications should be further studied.

In addition to monochromatic aberrations, the replacement of the lens also modifies the chromatic dispersion properties of the eye, as this is affected by the refractive index wavelength-dependency of the IOL material. Therefore, the optical performance of the pseudophakic in polychromatic light will be affected by both the IOL design and the IOL material. The dispersion properties of the IOL are defined by the Abbe number (ranging in most of designs from 35 to 60). The higher the Abbe number, the lower the LCA. The impact of the chromatic aberrations in the pseudophakic eye has been acknowledged [163-165]. There are even proposals for IOL (diffractive) designs aiming at correcting the ocular LCA [108, 166]. Most reports of LCA and polychromatic optical quality in pseudophakic eyes are based on computational predictions on eye models and the IOL material Abbe number [163, 166, 167]. There are very few studies reporting *in vivo* measurements of LCA of pseudophakic eyes. Chromatic aberration in pseudophakic patients is studied in *Chapter* 6, where the results of i*n vivo* LCA measurements in pseudophakic patients bilaterally implanted with monofocal aspheric hydrophobic and hydrophilic IOLs are presented.

"Even when corrected with the best spectacles or contact lenses, normal human eyes still suffer from monochromatic aberrations that blur vision when the pupil is large. We have successfully corrected these aberrations using adaptive optics, providing normal eyes with supernormal optical quality."

Liang et al., Supernormal vision and high-resolution retinal imaging through adaptive optics. Journal of the Optical Society of America (1997)

1.8 The technique: Adaptive Optics

The link between astronomy and the eye, apparent in Kepler's scientific contributions and Lipperhey's telescope, is a recurring theme in the history of vision science, culminating in the recent translation of Adaptive Optics (AO) from astronomy to vision science. When light passes through inhomogeneous media (i.e. atmosphere, ocular media), aberrations are introduced to the light's wavefront. The idea of AO was first introduced to correct these aberrations in real time, to give a better resolution of the sky to ground-based telescopes.

An early attempt to obtain subjective information about the eye's most important aberrations was performed by Scheiner (1619), an astronomer with interests in physiological optics, who constructed what was arguably the first wavefront sensor for the eye. Scheiner's wavefront sensor evaluated the light passing through only two locations in the eye's entrance pupil, when held close to the eye, the perceived image was doubled if the eye was defocused and single only if the eye was in focus [168]. However it was Babcock in 1953, who proposed, a solution to the problem of imaging objects in space through the atmospheric turbulence and introduced the idea of an adaptive optical element capable of correcting the time-varying aberrations caused by the atmospheric turbulence. Due to the technical complexity of measuring atmospheric aberrations and fabricating and controlling wavefront correctors, the first successful AO system in astronomy was only developed in 1977 by Hardy et al. [169]. Today, the major ground-based telescopes worldwide are provided with AO systems, which can collect high resolution images comparable to those obtained with space telescopes.

AO was first applied to the eye in the 1990's, when Liang et al. (1994) developed a new ocular aberrometer based on Hartman-Shack wavefront sensing, applied previously in astronomy, which largely exceeded in spatial resolution and temporal acquisition prior ocular aberroscopes [1]. The use of an Adaptive Optics system to measure, correct or induce low and high order aberrations with increasing applications in Vision correction and retinal imaging.

In the following sections the basic principles of Adaptive Optics technique are described, as well as different monochromatic and polychromatic AO systems used for ophthalmic applications.

1.8.1 Basic principles

Adaptive Optics corrections in the eye comprise three steps, represented in Figure 1.27:

(1) Wavefront sensing. Light reflected off the retina reaches the wavefront sensor that measures any residual distortion in the wavefront.

(2) AO control. The centroid positions are obtained from the wavefront sensor data and processed by a calculator to determine the appropriate voltages applied to the wavefront corrector to modify its shape.

(3) Wavefront correction. The deformable mirror modifies its shape according to the information provided and reflects the light back to the sensor.

Most AO systems operate in closed-loop, which means the wavefront sensor is placed so that it can measure the effectiveness of the wavefront correction. The three steps are repeated in a loop that compensates in real time the aberrations of visual optics and micro-fluctuations of accommodation.

Both the wavefront sensor and the wavefront corrector are placed in pupil conjugated planes and communicate by means of an adaptive optics control computer. In these systems the same correction used to correct light emerging from the eye can be used to correct the light going into the eye. As illustrated in Figure 1.27, the wavefront sensor records a flat wavefront if the mirror is shaped correctly. The scheme, shown in Figure 1.27, includes both imaging and stimulus delivery, and applies to both conventional and scanning laser systems.

A. Wavefront sensor

Hartmann-Shack (HS) wavefront sensor is the most suitable sensor in current AO systems. A typical HS wavefront sensor consists of a matrix of microlenses (lenslet array) of the same focal length, and a CDD camera at the focal of the lenslet. When an ideal perfect spherical wavefront passes through the HS wavefront sensor, each microlens focusses at the focal on the CCD camera, forming a regular array of spots (reference spots). But, when a distorted wavefront is sampled, the corresponding lenslet focuses a spot in a position laterally shifted with respect to the reference. The local slope of the wavefront at the corresponding lenslet positions are obtained from the shift of each spot with respect to the reference spot. Wave aberrations are calculated from the local slopes acquisition.

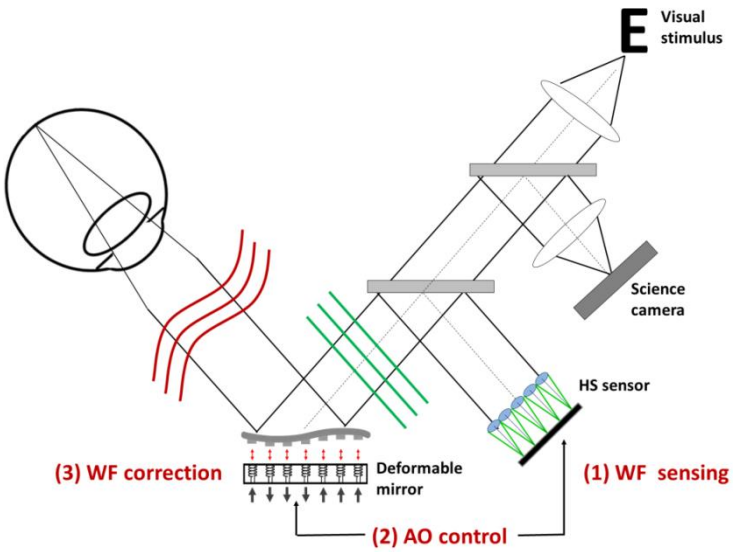

Figure 1.27 Basic layout of an AO system for imaging and vision testing comprising the 3 steps of the process: (1) WF sensing, (2) AO control and (3) WF correction. Adapted from Roorda (2011).

B. Phase modulator and wavefront corrector

There are different strategies to alter the phase profile of the incident wavefront: using deformable mirrors, that change the physical length over which the wavefront propagates or using liquid crystal devices that change the refractive index of the medium through which the wavefront propagates. Both types of devices are implemented in the AO system developed during this thesis, as described in *Chapter 2*.

Magnetic Deformable Mirrors.
In this work, we used a magnetic deformable continuous surface membrane mirror (fully described in *Section 2.2.2 of Chapter 2*). The common principle of deformable mirror is the use of multiple actuators located at the rear of the reflective surface. Depending on the voltage applied to each actuator, it pushes or pulls the surface, allowing controlling the exact shape of the mirror by a computer. The actuators of the magnetic deformable mirror are composed by a magnet, located behind the reflective membrane, and a coil. When applying a voltage to the coils, an electromagnetic field is created pushing or pulling the magnets and so the surface changes locally allowing the control of the mirror shape.

Phase modulators
Frequently used types of phase modulators are electro-optic modulators based on Pockels cells, and liquid crystal modulators. The latter is the one implemented in the AO system to modify the optical phase: a liquid crystal on silicon (LCoS) active

matrix reflective mode phase-only liquid crystal display (LCD). A LCoS display allows modifying the phase of a wavefront by applying different voltages to the different pixels of the device, modifying the refractive index and subsequently the optical path. As a consequence, a phase difference is created between the different pixels, where each level of phase is linked to a different level of gray. There are two approaches using LCOS devices, amplitude modulation and phase modulation. In this thesis we used a spatial light modulator operating in reflection, and modulating the phase (described in *Section 2.2.2* of *Chapter 2*).

The architecture of a phase-only LCoS device is shown in Figure 1.28 (a) and consists of a transparent top substrate with transparent ITO electrodes, alignment layers, LC material, spacers (a gap supported by a single layer of spacers to control the thickness of the LC layer), aluminum reflective electrodes (pixel arrays) and a functional CMOS silicon backplane, which consists of the electronic circuitry that is buried underneath pixel arrays to provide a high 'fill factor' [170]. The pixels are aluminum mirrors deposited on the surface of the silicon backplane. The incident light is transmitted through the LC layer with almost zero absorption. The integration of high-performance driving circuitry allows the applied voltage to be changed on each pixel, thereby controlling the phase retardation of the incident wavefront across the device. In a phase-only LCoS device, the phase delay is accomplished by electrically adjusting the optical refractive index along the light path, which is possible because of the non-zero birefringence of the LC materials in use, as shown in Figure 1.28 (a).

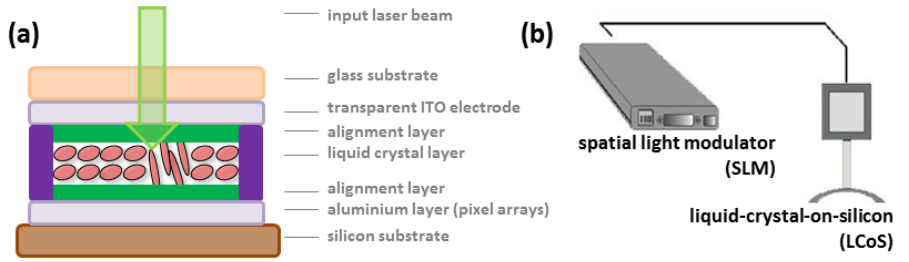

Figure 1.28 Illustration of (a) the structure of a phase-only LCOS device, consisting of transparent top substrate with transparent ITO electrodes, alignment layers, LC material, spacers (a gap supported by a single layer of spacers to control the thickness of the LC layer), aluminum reflective electrodes (pixel arrays) and a functional CMOS silicon backplane (CMOS: complementary metal oxide semiconductor; ITO: indium tin oxide; LC: liquid crystal; LCOS: liquid crystal on silicon) (Adapted from Zhang, 2014) [170] and (b) the spatial light modulator used to control the liquid crystal on silicon (LCOS) active matrix reflective mode phase only LCD.

C. AO control

The control algorithm converts the wave aberrations measurement made by the wavefront sensor into a set of actuators commands that are applied to the wavefront corrector to satisfy a suitable system performance criterion, such as

minimizing the residual wave aberrations or presenting other wave aberrations to the eye. When a unit voltage is applied to one actuator on the deformable mirror the surface deformation produced by this activated actuator is called the actuator's influence function.

A detailed description of the wavefront sensor, both wavefront corrector devices and the AO control algorithm, and their performance is shown in *Chapter 2 Section 2.2.2*.

1.8.2 Monochromatic and Polychromatic AO systems for ophthalmic applications

In the 1990's, an Adaptive Optics system was first applied to the eye by using a new ocular aberrometer based on Hartman-Shack wavefront sensing, which largely exceeded in spatial resolution and temporal acquisition prior ocular aberroscopes [79]. Since then different system designs have rapidly evolved incorporating new technologies.

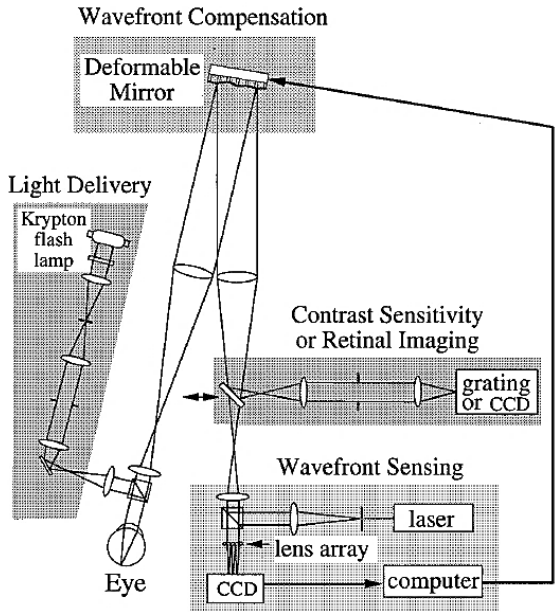

Figure 1.29 AO system. The system allowed for wavefront sensing and adaptive compensation, as well as for observations of point sources, retinal imaging and contrast sensitivity measurements. For wavefront sensing and adaptive compensation the eye focused a collimated laser beam onto the retina. The light reflected from the retina formed an aberrated wave front at the pupil. The distorted wave front is measured by a Hartmann–Shack wave-front sensor. A deformable mirror, conjugate with the pupil, compensated for the eye's wave aberration. After compensation was achieved, psychophysical or retinal imaging experiments were performed with a 6-mm pupil. Reproduced from Liang et al. (1997).

The first AO device used in the eye was a segmented mirror, which proved capable of correcting astigmatism and of increasing the quality of retinal images [1]. Shortly after the first closed-loop AO system, which was able to correct higher order aberrations in the eye, a high-resolution retinal imaging AO system was developed and provide normal eye with supernormal optical quality [79]. The system (Figure 1.29) produced an improvement of contrast sensitivity of the eye in monochromatic light, higher than that obtained with the best conventional spectacle correction and obtained higher contrast images of the cones mosaic.

Real time correction of the wave aberration became possible with the development of automated wavefront sensing by Hofer et al. [2001], which allowed dynamic measurement of the ocular aberrations and closed-loop correction with a bandwidth of 1-2 Hz [171]. This section presents a review of some of the AO systems built for different applications for visual testing and retinal imaging.

A. Adaptive Optics in ophthalmic imaging

AO improves the capabilities of any ophthalmic instrument where the optics of the eye are involved, from fundus cameras to phoropters. Retinal imaging techniques have also benefited from the incorporation of AO. To increase the resolution of retinal imaging is one of the broad lines of research where the application of AO has spread. AO now allows the routine examination of single cells in the eye, such as photoreceptors and leukocytes, providing a microscopic view of the retina that could previously only be obtained in excised tissue. The ability to see these structures in vivo provides the opportunity to non-invasively monitor normal retinal function, the progression of retinal disease, and the efficacy of therapies for disease at a microscopic spatial scale as well as to improve certain surgical techniques.

The first AO retinal imaging systems were flood illuminated designs. In 1996, Miller et al. (1996) obtained the first *in vivo* images of the cone receptors using a high resolution flood illuminated fundus camera (coupled with a precise second-order refraction) [172]. The introduction of a full AO system by Liang and Williams (1997) further enhanced the contrast and quality of the cone images [79] (Figure 1.30). Since then many other AO systems have been built using improved AO components to image a variety of retinal structure and function in both normal and diseased eyes. Adaptive Optics in combination with a scanning laser ophthalmoscope (SLO) [173] represented a major advance in ophthalmoscopy because offered a new and unique imaging modality for the living human eye, conferring several advantages, which included improved efficiency in light collection and real-time imaging. These instruments allowed visualizing photoreceptors, nerve fibers and flow of white blood cells in retinal capillaries.

More recently, Roorda et al. (2002) constructed the first close-loop AOSLO, to correct high-order aberrations and provide real-time, microscopic views of the living human retina with unprecedented optical quality (Figure 1.30). Newer systems have pushed the performance even further allowing for the use of dual deformable mirrors, increased fields of view and the ability to visualize the rod photoreceptors [174]. Furthermore, AO in combination with OCT [175] has allowed to increase lateral resolution, to reduce speckle, and to enhance sensitivity from conventional flood illumination Ophthalmoscopes and Scanning Laser Ophthalmoscopes.

B. Adaptive Optics for Vision testing

The use of Adaptive Optics for correcting aberrations in the human eye opened the possibility of evaluating the effect of neural factors since the optical effects are compensated for. Examples of custom-design AO systems devices to study visual function are those of Murcia Lab , Rochester lab [176], QUT lab [177], and Viobio Lab [83]. These systems incorporate a HS wavefront sensor and a membrane deformable mirror to measure and correct for ocular aberrations respectively. Rochester and Viobio Labs uses a an electromagnetic deformable mirror (52 actuators, 15-mm effective diameter, 50 µm stroke, MIRAO, Imagine Eyes, France), while QUT Lab a deformable micro-electromechanical system mirror (12 × 12 array of actuators, 4.4 mm diameter on side, Boston Micromachines Corporation µDMS-Multi). An interesting system is the KTH Lab AO system [178], built to correct the peripheral aberrations of the subjects while performing different psychophysical experiments, but with similar AO elements than Rochester and Viobio Labs'.

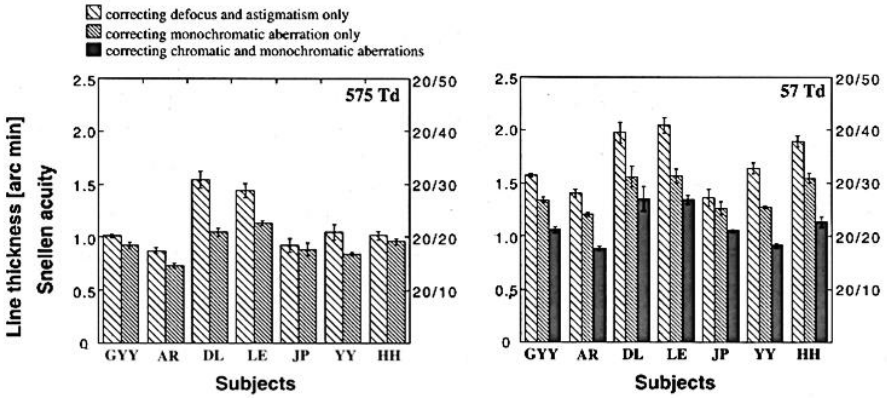

Figure 1.30 Visual acuity (line thickness of the letter E target) measurements at two retinal illuminance levels, 575 (~ 20 cd/m^2) and 57 Td (~ 2 cd/m^2) when correcting various aberrations. The estimated Snellen acuity is also shown on the other vertical axis. The pupil size was 6-mm in diameter and the eyes were under cycloplegia. The error bars represent 6 one standard error. Reproduced from Yoon & Williams (2002).

Using these systems, several studies have investigated the effect of AO on visual function and to which extent visual performance increases at correcting higher order aberrations. Visual acuity and contract sensitivity [76, 81, 83, 108, 179], as well as everyday tasks [84], are significantly improved after AO correction of natural aberrations (Figure 1.30). This improvement in visual acuity and contrast sensitivity following AO correction of aberrations is shown also in subjects with different refractive profiles [90, 94]. Adaptive optics can be used to investigate the role of ocular aberrations on the accommodative response [89] or the effect of manipulating the aberrations on depth of focus, particularly in presbyopic patients. These results spurred the development of customized vision corrections based on the possibility to incorporate the correction of the high order aberrations of the subjects. Improvements in subjective and objective refraction [37, 38], wavefront-guided refractive surgery [23] and diagnostics techniques have been shown in other studies.

Optical and neural factors involved in the visual function have been also studied using AO systems to explore the limits of the visual improvement to optical improvements in retinal image quality [86, 125], as well as the contributions of optical and neural factors to age-related losses in spatial vision [82]. Moreover Adaptive Optics has allowed the possibility of undertaking psychophysical experiments without the retinal blur produced by optical aberrations allows exploring neural adaptation [73, 74, 114, 120, 121].

Induction of aberrations in combination with vision testing is easily done with AO systems and can be used to probe aberration types and magnitudes that optimize depth of field at minimal cost to the best vision performance. More recently, AO systems have made their way into the clinic with systems that combine wavefront aberrometry, autokeratometry and accommodation assessment (irx3^{TM}, Imagine Eyes, France) or that allows the patient to experience standard optical solutions before their implementation (AOneye, Voptica, Spain).

C. Adaptive Optics for visual simulation of optical corrections

The use of an Adaptive Optics system to manipulate ocular aberrations in order to perform visual testing through a modified optics can be of interest both to study the visual system, as seen in the previous sections, and to design new ophthalmic optical elements, as well as to save several steps in current procedures of ophthalmic optical design and eventually lead to improved optical solutions. One of the most promising applications of the Adaptive Optics Visual Simulators (AOVS) is the development of new ophthalmic optical elements, where the use of an AOVS for non-invasive preliminary testing of new phase profile designs has many advantages when the phase profiles are designed to be implemented in permanent elements, as intra-ocular lenses or refractive surgery profiles. A related application

of AOVS is their use to present a patient the effects of a given correction prior to surgery, particularly important when a non-reversible treatment is intended.

Recently AOVS have been improved by introducing liquid crystal programmable phase modulator (PPM) as active elements to correct and induce more sophisticated aberrations patterns [180]. These systems are an excellent tool for the design of advanced ophthalmic optical elements (i.e. in the development of multifocal phase profiles that could be implemented in contact lenses or intraocular lenses), or to test whether a new ophthalmic design meets the design specifications. Figure 1.31 shows two examples of bifocal and trifocal phase maps tested using a phase modulator and the Strehl Ratio obtained experimentally for those multifocal designs.

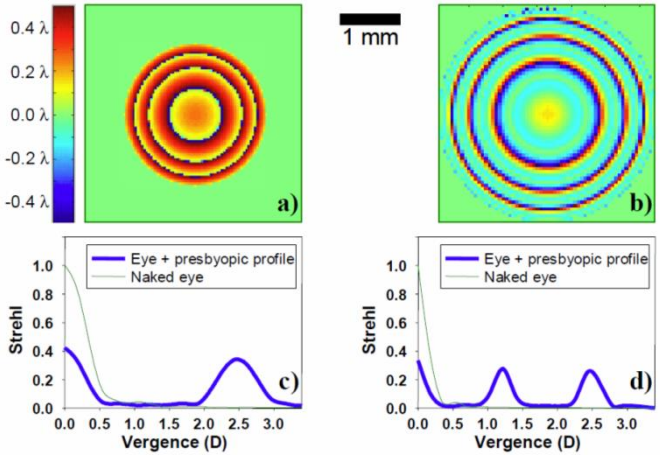

Figure 1.31 Multifocal profiles: (a) bifocal profile over a 2.4-mm pupil. (b) trifocal profile over a 3.6-mm pupil (Upper row). Correspoding experimental Strehl ratio (symbols) obtained from the recorded PSF images and theoretical calculations (lines) (Lower row). Reproduced from Manzanera et al. (2007).

In recent years, AOVS systems have been improved by introducing binocular adaptive optics visual analyzers (BAOVA), which offer the possibility to study binocular vision under carefully controlled optical conditions. An example of this design is the Binocular AO visual simulator designed by Fernandez et al. (2009) [181]. The instrument allows for measuring and manipulating ocular aberrations of the two eyes simultaneously, while the subject performs visual testing under binocular vision. An important feature of the apparatus consists on the use of a single correcting device and wavefront sensor. Aberrations are controlled by means of a liquid-crystal-on-silicon spatial light modulator (SLM), where the two pupils of the subject are projected. Aberrations from the two eyes are measured with a single Hartmann–Shack sensor.

In *Chapter 2,* the design and development of a polychromatic Adaptive Optics Visual Simulator incorporating a deformable mirror and a spatial phase modulator is described in detail.

1.9 Open questions

Adaptive Optics technology has allowed a deeper understanding of the impact of ocular aberrations on visual function, increasing knowledge on the spatial limits of vision and the development of corneal laser ablation algorithms, intraocular lenses, contact lenses, aiming at customized corrections or at increasing depth of focus by manipulating aberrations.

The retinal image quality is degraded by the presence of monochromatic and polychromatic aberrations in the ocular optics, and the study of the impact of retinal image quality on vision should consider the aberrations in the visible light, as well as the effect of chromatic aberrations. However, so far, the impact of ocular aberrations on vision is studied using wavefront sensors with monochromatic, generally infrared, light.

The studies of this thesis use polychromatic Adaptive Optics to evaluate the impact of manipulated optics on vision, and address the following questions:

1. **Are subjects adapted to their natural astigmatism and its correction?** In particular, is the perception of oriented blur biased by the native astigmatism of the subject? Which is the time course of the after-effects following spectacle correction of astigmatism in habitually non-corrected astigmats? Is the impact of astigmatism on VA greatly dependent on the orientation of the induced astigmatism, even in non-astigmats? Does prior experience to astigmatism play a role on Visual Acuity?

2. **What is the magnitude of the Longitudinal Chromatic Aberration of the human eye in visible and near infrared?** Which is the impact of chromatic aberrations on the optical quality in the presence and absence of monochromatic wave aberrations? What is the reason for the differences between objective and subjective measurements of the LCA of the eye? How does the LCA in pseudophakic eyes implanted with different material IOLs compare to phakic eyes?

3. **Do new multiple multifocal designs increase the multifocal benefit in presbyopic patients?** Are angular designs perceived better than radial designs? Which is the effect of multifocal simultaneous vision corrections on vision, in the presence and absence of natural aberrations?

1.10 Goals of this thesis

The main purpose of the thesis is to design and develop a custom-made polychromatic Adaptive Optics system to study the impact of astigmatism on visual function, to quantify the LCA in normal and pseudophakic eyes and to test vision with new multifocal designs for Presbyopia.

The specific goals are:

- To explore the effects of astigmatic blur in visual perception and performance, and the extent to which subjects are adapted to their own natural astigmatism and the capability to adapt to its correction.

- To develop a polychromatic adaptive optics system with extended capabilities as visual simulator, to measure, correct/induce aberrations, combined with psychophysical paradigms to study visual performance and visual perception in a polychromatic environment. To calibrate and validate the system. To develop psychophysical routines to evaluate the monochromatic and polychromatic visual function.

- To quantify the longitudinal chromatic aberration (LCA) of the human eye in normal and pseudophakic eyes using subjective and objective techniques in a wider spectral range than previously explored. To study the relationship between optical and visual quality in polychromatic conditions their impact on visual function in the presence and absence of monochromatic wave aberrations.

- To test vision with new multifocal designs for Presbyopia.

1.11 Hypothesis

The hypotheses of this thesis are:

- Non-corrected astigmats are adapted to their astigmatism, and astigmatic correction significantly changes their perception of their perceived neutral point, even after a brief period of adaptation**.**

- The impact of astigmatism on Visual Acuity is greatly dependent on the orientation of the induced astigmatism.

- The presence of natural aberrations is not the cause for the discrepancies between objective and subjective measurements of the Longitudinal Chromatic Aberration of the human eye.

- Different material IOLs produce changes in the ocular LCA of pseudophakic patients.

- Multifocal simultaneous vision solutions with radial and angular designs increase the depth-of-focus in presbyopic patients.

- Aberrations play a role in perceived visual quality across different multifocal patterns, however this is secondary to the effect of the multifocal pattern.

1.12 Structure of this thesis

The body of this thesis is structured as follows:

Chapter 1 presents the background and motivation of the thesis.

Chapter 2 presents a description of the methods used throughout this thesis and common to the different studies. In particular, it includes a description of the developed Adaptive Optics system to measure and correct subject's aberrations, including its calibrations, validation and developed control software.

In **Chapter 3**, we investigate whether the perception of oriented blur is biased by the native astigmatism, and studied the time course of the after-effects following spectacle correction of astigmatism in habitually non-corrected astigmats. We tested potential shifts of the perceptual judgments of blur orientation in 21 subjects. Longitudinal measurements (up to 6 months) were performed in three groups of subjects: non-astigmats and corrected and uncorrected astigmats. Uncorrected astigmats were provided with proper astigmatic correction immediately after the first session.

In **Chapter 4**, we investigate the extent to what prior adaptation to astigmatism affects visual performance, whether this effect is axis-dependent, and the time-scale of potential changes in visual performance following astigmatism correction. Also, whether the effect of possible positive interactions of aberrations might be altered after recalibration to correction of astigmatism. Visual acuity was measured in 25 subjects (astigmats and non-astigmats, corrected and uncorrected) under induction of astigmatism at different orientations and combinations of astigmatism and coma, while controlling subject aberrations. 14 different conditions were measured, using an 8-Alternative Forced Choice procedure with tumbling E letters and a QUEST algorithm. Longitudinal measurements were performed up to 6 months. Uncorrected astigmats were provided with proper astigmatic correction after the first session.

In **Chapter 5**, we present LCA measured in subjects using wavefront sensing, double-pass retinal images, and psychophysical methods with a custom-developed polychromatic Adaptive Optics system in a wide spectral range (450-950 nm), with control of subjects' natural aberrations.

In **Chapter 6**, we present measurements of the LCA in vivo using psychophysical and wavefront sensing methods in patients bilaterally implanted with monofocal IOLs of similar aspheric design but different materials. Measurements were performed using psychophysical (480-700 nm), and wavefront sensing (480-950

nm), methods, using a custom-developed Adaptive Optics system. Chromatic difference of focus curves were obtained from best focus data at each wavelength in each experiment, and the LCA was obtained from the slope of linear regressions to those curves.

In **Chapter 7**, we further explore the effect of multifocal simultaneous vision corrections on vision, in the presence and absence of natural aberrations using a polychromatic Adaptive Optics simulator, and to evaluate the multifocal performance with them. Visual quality with six radial and angularly segmented multiple zone multifocal phase patterns was evaluated optically and psychophysically, by means of simulations of Visual Strehl-based-metrics and measurements of the relative perceived visual quality, respectively.

Chapter 8 presents a summary of the major findings of this work, and their implications for the state-of-the-art, as well as the scientific activities developed during this thesis.

2

Methods

"Experiment adds to knowledge. Credulity leads to error."

Anonymous. Arabic Proverb

This *Chapter* describes the experimental techniques used in this thesis, specifically two different Adaptive Optics (AO) systems. The Viobio Lab AO I system was built in previous projects and has been used in prior studies, including the effect of correcting the aberrations on visual performance, on the perception of natural images, and on face recognition, as well as the influence of the correction and induction of aberrations on accommodative lag [83, 84, 89]. The system has been also intensively used in studies of neural adaptation to blur produced by low and high order aberrations, their correction and the internal code for blur in every subject [73, 74, 95].

The Viobio Lab AO II system was specifically designed and built during this thesis. This AO system has been built to extend the capabilities as visual simulator of current AO systems by incorporating a supercontinuum laser source (SCLS) and a Spatial Light modulator (SLM), to perform psychophysical experiments to investigate the optical and visual quality in polychromatic conditions, as well as to evaluate the impact of manipulated optics on vision. In this *Chapter* the implementation of the optical system and the different components, its calibration and validation, as well as control routines of the system are described. General experimental protocols for both AO systems are described in this *Chapter*, although particular implementations and developments for each specific study will be presented in the corresponding *Chapter*.

The author of this thesis has designed and implemented the AO system, calibrated and validated the system, in collaboration with Daniel Pascual, Carlos Dorronsoro and Susana Marcos. The first design of the system was performed in collaboration with Lucie Sawides, Carlos Dorronsoro and Susana Marcos. Veronica Gonzalez participated in the calibration of the Spatial Light Modulator (SLM). The author also participated in the development of the routines to control the AO system, which were programmed by Daniel Cortes. The author performed the psychophysical routines for longitudinal chromatic aberration measurements, perception of natural images and perception of best focus.

A first description of the experimental system was presented at the congress of the Association for Research in Vision and Ophthalmology ARVO2014 (May 2014), celebrated in Orlando, USA. The current version of the system was presented at ARVO2015 (May 2015), celebrated in Denver, USA. The system has been described in different publications [182, 183].

2.1. Custom monochromatic Adaptive Optics system for visual psychophysics

2.1.1 General description of the Viobio Lab AO I system

A scheme of the Viobio Lab AO I system is shown in Figure 2.1. The setup was designed to study the visual performance of the eyes in the presence /absence of aberrations and has been described in previous publications [83, 84, 89]. The main components of the system are a Hartmann-Shack wavefront sensor (32x32 microlenses, 3.6 mm effective diameter; HASO 32 OEM, Imagine Eyes, France), and an electromagnetic deformable mirror (52 actuators, a 15-mm effective diameter, a 50 mm stroke, MIRAO, Imagine Eyes, France), which integrate the AO-control Channel (see green line in Figure 2.1). Both devices are placed in conjugate pupil planes of the system by means of different relay lenses. This means that two points are said to be conjugate points if one is the image of the other, and in the case of 2 planes the intensity distribution across one plane must be an image of the intensity distribution across the other plane [66].

Illumination comes from a Super Luminescent Diode (Superlum, Ireland) coupled to an optical fiber (red line in Figure 2.1) emitting at 827 nm. A motorized Badal system compensates for spherical error. A pupil monitoring Channel (yellow line in Figure 2.1), consisting of a CCD camera (TELI, Toshiba, Japan) conjugate to the pupil, is inserted in the system by means of a plate beam-splitter and is collinear with the optical axis of the imaging Channel.

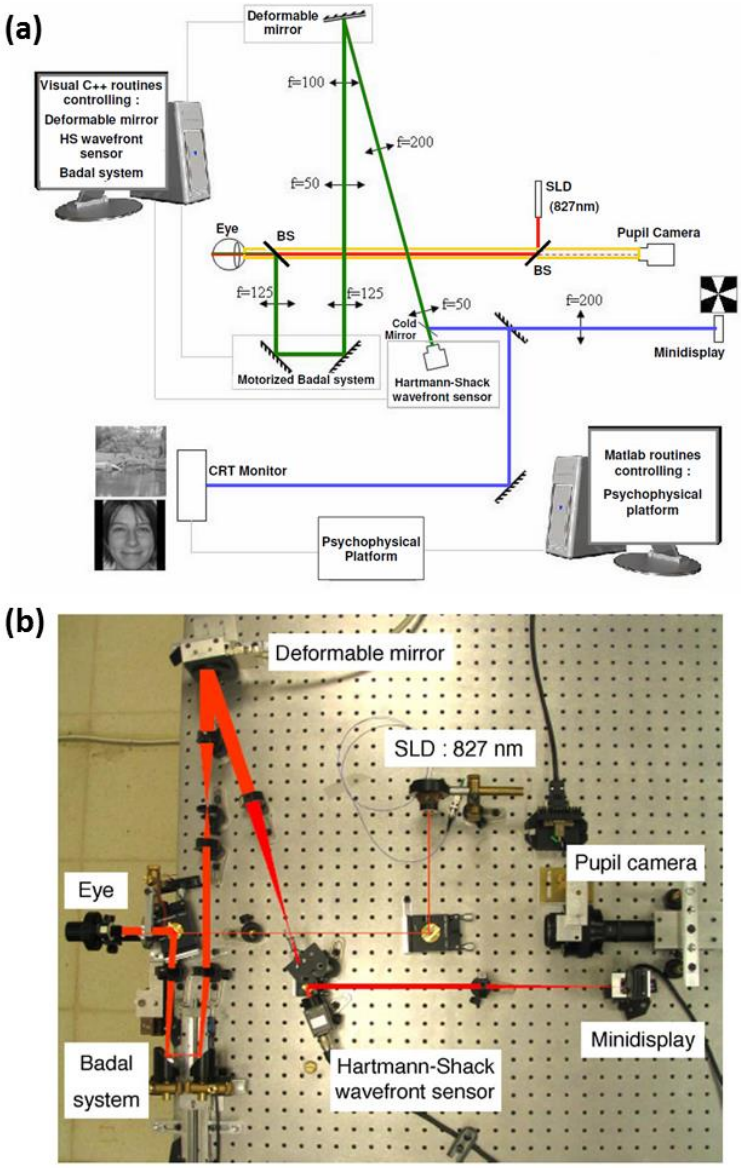

Figure 2.1 (a) Schematic diagram of the VioBio Lab AO I system from Sawides thesis manuscript [20], that shows the five channels of the setup: illumination Channel with a 827 nm SLD source (red); AO-control Channel with the Hartmann-Shack wavefront sensor and the deformable mirror (green); Psychophysical Channels, one provided with a minidisplay, the other with a CRT monitor (blue); Pupil monitoring Channel (yellow). (b) Image of the Viobio Lab AO I system reproduced from Marcos et al. (2008).

All optoelectronic components of the system, Hartmann-Shack system, deformable mirror and closed-loop correction, are controlled with custom software in C++. The state of the mirror that compensates the aberrations of the subject is found in a closed-loop operation, and continuous measurements of the subjects' aberrations throughout the psychophysical test ensure proper correction.

Typically, measurements are performed for 6-mm pupils (limited by an artificial pupil, AR-PP), under natural viewing conditions. Visual stimuli are presented through two different psychophysical channels (blue lines in Figure 2.1) - one provided with a minidisplay (12x9 mm SVGA OLED, LiteEye 400, LiteEye systems, USA), and the other with a CRT monitor (Mitsubishi Diamond Pro 2070, Mitsubishi, Japan). Both channels go through the Badal and AO mirror correction. The stimulus display is controlled by the psychophysical platform ViSaGe (Cambridge Research System, United Kingdom). This system has been used in the work presented in *Chapters 3* and *4* of this thesis.

2.1.2 Custom software for the VioBio Lab AO I system

Figure 2.2 shows the custom-made software used to control the AO system, which was built in previous studies [83, 89, 95]. The system is controlled using custom routines written in Visual Basic, Visual C++ (with the use of DLL libraries) and Matlab. Two different synchronized computers are used, one to control the AO system (deformable mirror and HS wavefront sensor) and the motorized Badal system, and the other to control the ViSaGe psychophysical platform and CRT monitor.

The Interface program allows measurement, correction induction of ocular aberrations, monitoring the pupil, automatized displacement with the motorized Badal system, communication and synchronization of the control computers and data saving. Outlined in red are functions of the software customized specifically for this thesis. These new routines focus on the induction of astigmatism and/or coma in different amounts and orientations used in the work presented in *Chapters* 3 and 4 of this thesis.

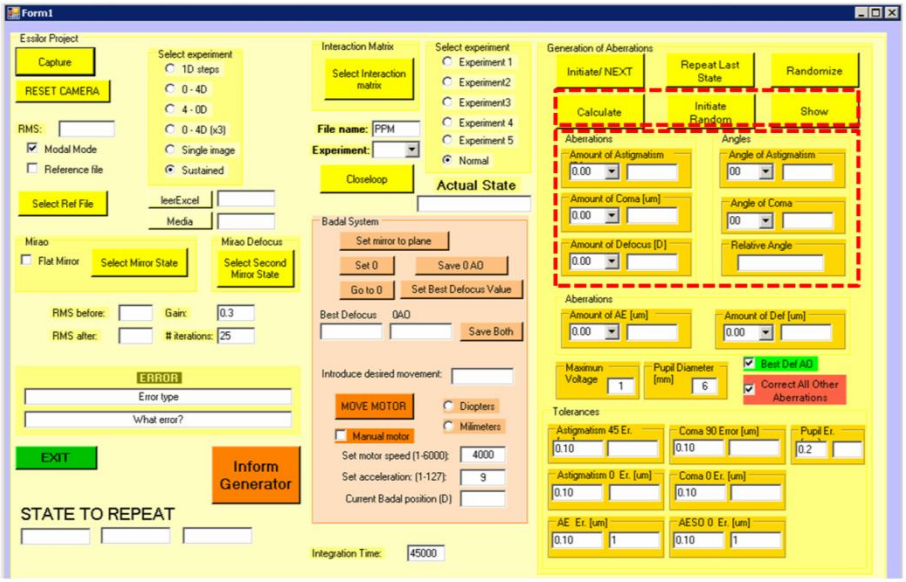

Figure 2.2 Custom-made software to control the VioBio lab AO I system. Outlined in red are features customized specifically for the studies shown in *Chapters 3* and *4*.

2.2. Custom development of a polychromatic AO system for visual psychophysics

2.2.1 General description of the polychromatic AO system as visual simulator

During this thesis, a polychromatic Adaptive Optics system has been developed to study the optical and visual quality in polychromatic conditions, as well as to evaluate the impact of manipulated optics on vision. The instrument allows control of the aberrations of the subject, while performing psychophysical settings of best focus and/or visual perception/performance tasks, acquisition of double-pass retinal images or wavefront aberration measurements at different wavelengths.

The initial design of the system is shown in Figure 2.3 (a), as well as (b) and (c) two pictures of the current configuration of the setup during one of the experiments.

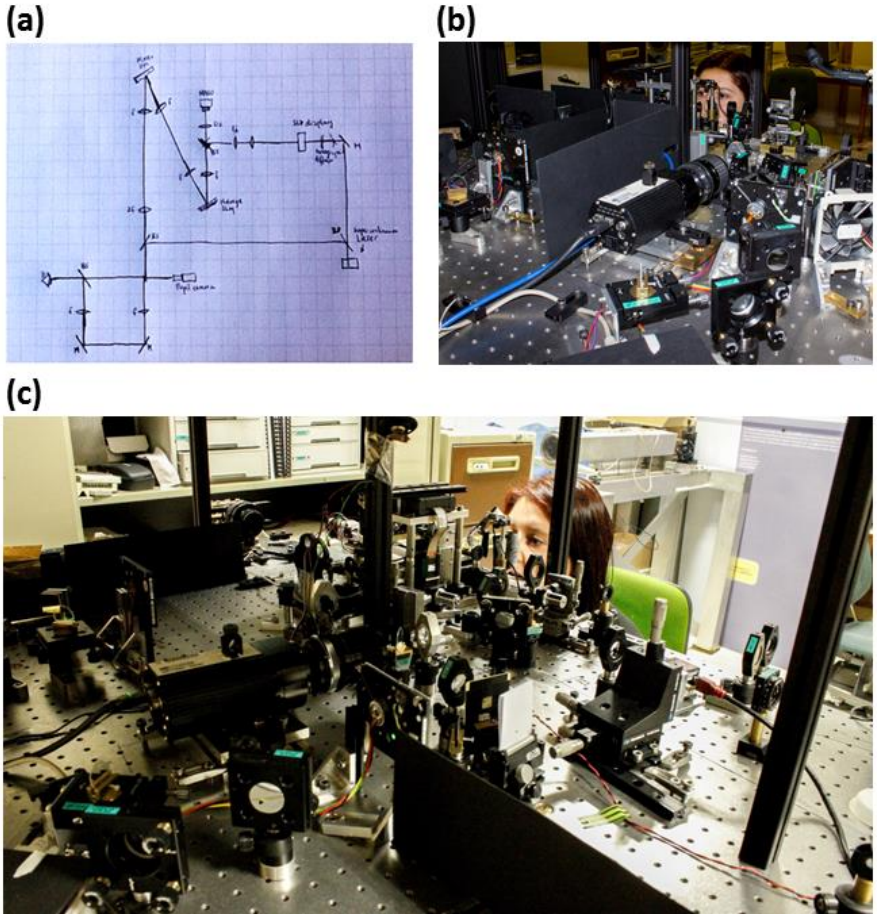

Figure 2.3 (a) Schematic setup AO II first draft (January 2012) (b) and (c) Pictures of the Viobio Lab AOII system in its current configuration (May 2015), while performing one of the experiments.

The current system (shown in a schematic diagram in Figure 2.4) is formed by 6 different channels: the **illumination Channel**, with light coming from the supercontinuum laser source (SCLS) (red line); **the AO-Channel**, whose main components are the Hartmann-Shack wavefront sensor and the deformable mirror (green line); the **SLM-Channel**, which incorporates the Spatial Light Modulator (SLM) to the system (yellow line); the **retinal imaging Channel** (pink line), which captures retinal aerial images; the **pupil monitoring Channel** (purple line); and the **psychophysical Channel,** monochromatically illuminated with light coming from the SCLS and provided with a Digital Micro Mirror (DMD) device (blue line). The system is mounted on an optical bench, whose physical dimensions are 900 x 1800 x 58 mm.

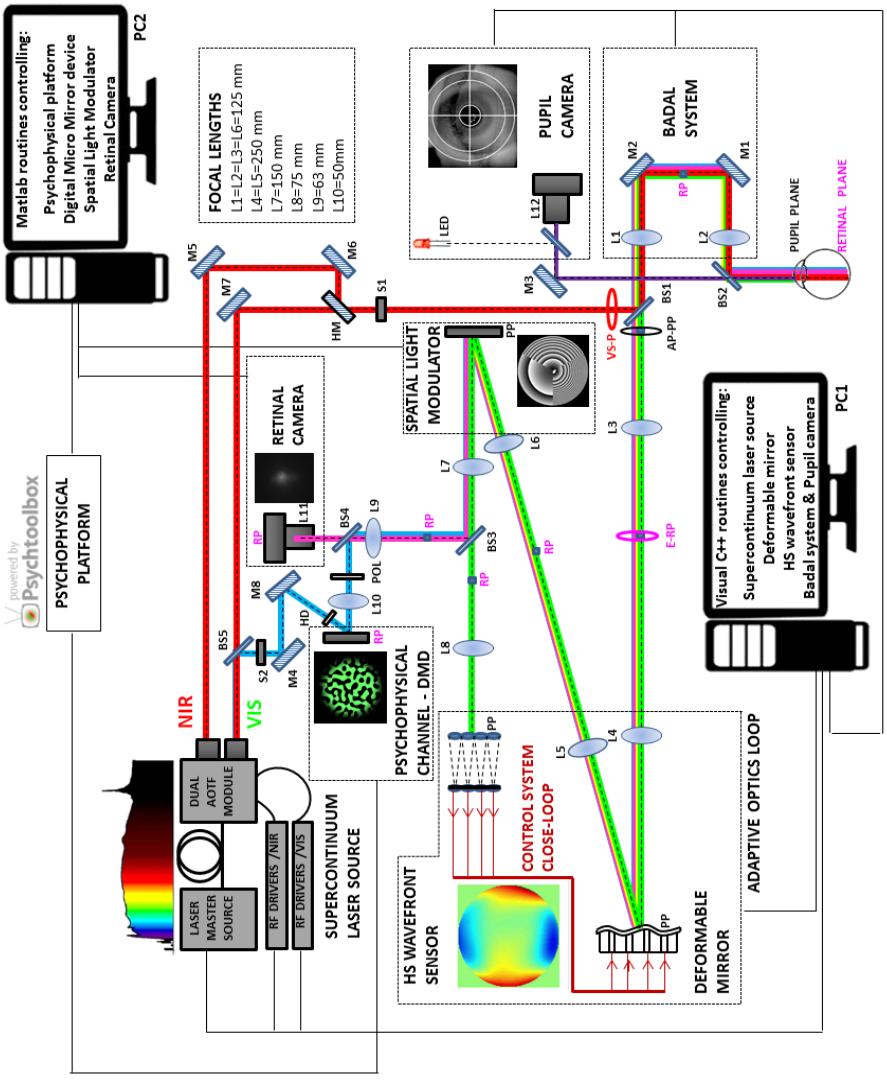

Figure 2.4 Schematic diagram of the VioBio Lab AO II system with the different channels in its final configuration (May, 2015): the illumination Channel (red line), the AO-Channel (green line); the SLM-Channel (yellow line); the retinal imaging Channel (pink line); the pupil monitoring Channel (purple line), and the psychophysical Channel (blue line). NIR: near infrared light; VIS: visible light; RP: retinal plane; PP: pupil plane; BS: beam splitter; S: shutter; L: lens; M: mirror; HM: hot mirror; POL: polarizer; E-RP: retinal pinhole; AP-PP: artificial pupil; VS-P: variable size pupil;

2.2.2 System functional modules

A. The illumination Channel: the supercontinuum laser source

A supercontinuum laser source (SCLS, SC400 femtopower 1060 supercontinuum laser source, Fianium Ltd, United Kingdom) is used as the light source of the system. The SCLS delivers a supercontinuum spectrum, spanning from below 450 nm to beyond 1100 nm (in our system configuration), and consists of three main sub-systems (Figure 2.5) (1) Master source: a passively mode locked low power fiber laser based on a core-pumped, Yb-doped-fiber, whose main characteristics are 4.16 W power, 40 MHz fixed repetition rate, 400 fs pulse duration and 50nJ of max pulse energy. (2) A high power fiber amplifier: based on a double-clad-Yb-doped-fiber, pumped by a high power, multi-emitter laser diode pump module. (3) A high nonlinearity supercontinuum generator, which comprises a long highly-nonlinear optical fiber, so that the pulses experience large spectral broadening within the nonlinear fiber, covering the spectrum from 380 to 1200 nm. The output optics are free space and the collimator optics are mounted at the end of a 1.5 m-long, armored cable.

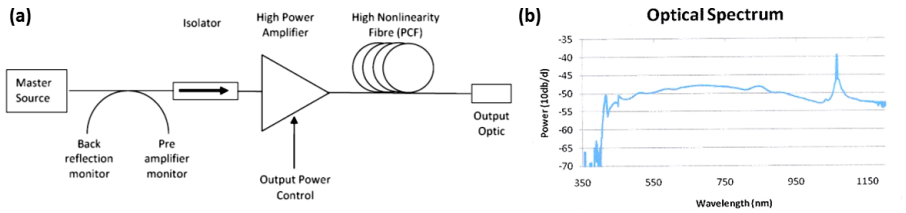

Figure 2.5 (a) Scheme of the main subsystems of the supercontinuum fiber laser source: master source; high power fiber amplifier; and a high nonlinearity supercontinuum generator. (b) Spectrum generated by the SCLS, spanned from below 400 nm up to 1200 nm.

A dual Acousto-optic Tunable Filter (AOTF) module (Gooch & Housego, United Kingdom), composed of two single-AOTF modules, is coupled to the SCLS. Each single-AOTF module is composed by an 8-channel AOTF and a Radio Frequency (RF) driver system, which provides up to 8 separate wavelength channels, all of them tunable in wavelength and intensity. The dual AOTF module enables delivery of either the entire supercontinuum spectrum or the electronically filtered spectrum and it is used to automatically select the desired wavelengths. This dual system allows two independently filtered fiber-outputs, one for visible light (VIS) and the other for near infrared (NIR), with a spectral bandwidth of approximately 5nm (2-4nm (VIS); 3-6nm (NIR)). Output is a collimated beam coupled to a 2 independent multimode fibers.

Both the main source and the RF drivers are software-controlled. Figure 2.6 shows the software provided from the manufacturer to select the preferred wavelength and the spectral characterization of the most used wavelengths of both channels. Typical used wavelengths are: VIS-channel: 455, 488, 500, 532, 555, 570, 633 & 700 nm and NIR-channel: 730, 780, 810, 827, 850, 880, 950 & 1020 nm.

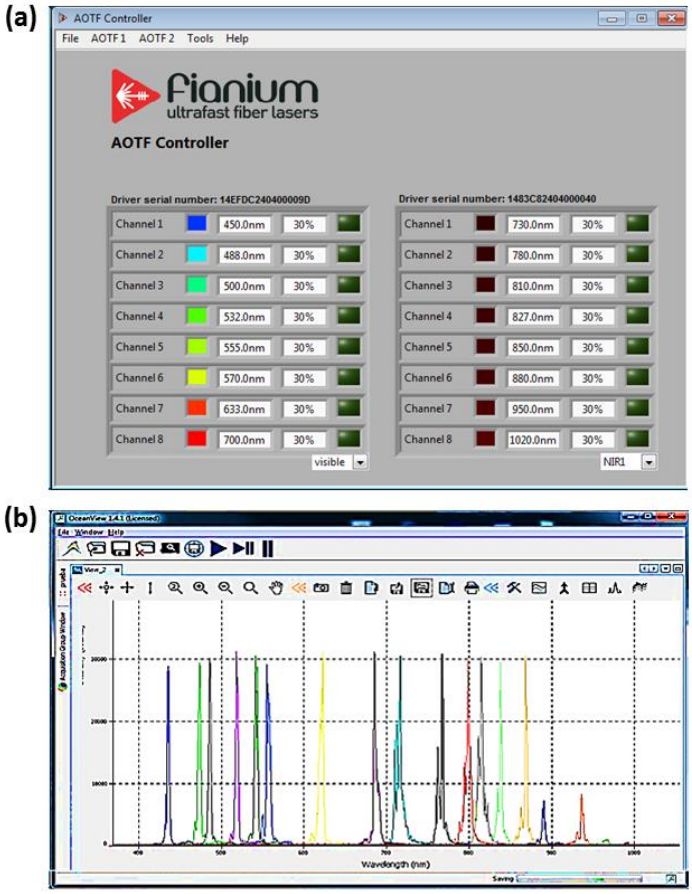

Figure 2.6 (a) Software to control the dual Acousto-optic Tunable Filter, that allows selecting the preferred wavelength. (b) Spectral characterization of the most used wavelengths of both channels measured with a spectrometer.

Illumination coming from the two independent fiber-channels of the SCLS enters the system collinearly by means of a hot mirror (HM). The beam is collimated and enters the eye with a diameter of around 2 mm for NIR channel and 3 mm for VIS channel. A variable-size pupil (VS-P) allows modifying the beam size and position of the beam entering the eye. The beam is slightly (1mm) off-centered with respect to the pupil center to avoid a corneal reflection in the Hartmann-Shack images. The

laser power measured at the corneal plane ranges between 0.5 and 50 µW, which is at least one order of magnitude below the ANSI standards safety limits at all tested wavelengths [184-186]. Laser safety calculations are explained in *Chapter 2 Section 2.2.3.2.*

B. The Adaptive Optics Channel

The Hartmann-Shack wavefront sensor and the electromagnetic deformable mirror are the principal components of the AO Channel. Both devices are placed in conjugated pupil planes of the system by means of different relay lenses.

The deformable mirror is conjugated to the pupil by a pair of relay lenses of 125 mm and 250 mm focal lengths (L3 and L4). The microlenses array of the HS-wavefront sensor is conjugated to the pupil with 2 relay lenses of 250 mm and 125 mm (L5 and L6), and 150 mm and 75 mm focal lengths (L7 and L8). The focal lengths are set to allow a measurement pupil diameter of 7mm (effective diameters are 3.65 mm for the wavefront sensor and 15mm for the deformable mirror), thus a x2 magnification is achieved from the subject's pupil to the deformable mirror and a x0.5 magnification from the subject's pupil to the microlenses array plane. Light from the SCLS passes through the Badal system and enters the eye. The reflected light off the retina passes through the Badal system and the deformable mirror and is focused on the CCD camera of the Hartmann-Shack wavefront sensor.

The Hartmann-Shack wavefront sensor

The Hartmann-Shack wavefront sensor (HASO 32 OEM, Imagine Eyes, France) consists of a microlens array of 40 x 32 microlenses of the same focal length and a CCD camera at the focal of the lenslet. The effective diameter of the sensor is 3.65 mm (aperture dimension: 4.8 x 3.6 mm^2) and the spatial resolution is ~110 µm. The microlens matrix is conjugated to the pupil with an x0.5 magnification factor from the pupil of the system to the microlens array. The working spectral range of the sensor is 350 - 1100 nm, while the sensor is centered at 1062 nm. A variable size artificial pupil (AR-PP), placed in pupil conjugate plane, ensures constant pupil diameter in the measurements.

Figure 2.7 illustrates the Hartmann-Shack measurement principle for an aberration-free wavefront (a) and for an aberrated wavefront (b). When a wavefront (aberrated or flat) passes through the Hartmann-Shack wavefront sensor, the beam is broken down into "multiple elementary beams" using the matrix of microlenses, each microlens focuses a portion of the incident wavefront at its focal on the CCD camera, forming an array of spots. These secondary beams are focused on the detector of the CCD camera. An analysis of the information is then performed to determine the phase and intensity of the beam, where the first derivative of the phase is what is measured.

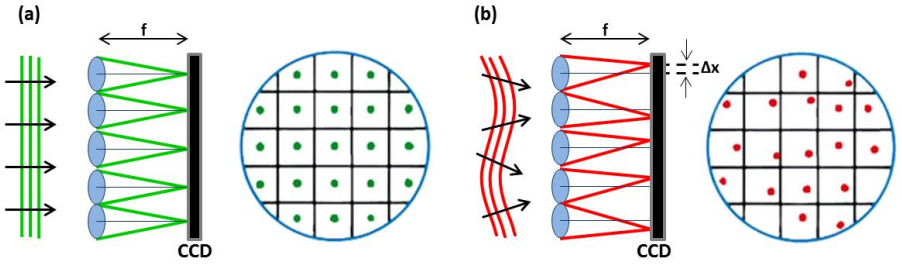

Figure 2.7 Illustration of the Hartmann-Shack wavefront sensor centroid calculus for an aberration-free wavefront (a) and an aberrated wavefront (b).

The array of spots serves to set the origin of coordinates for each subaperture on the focal plane. If the wavefront is flat, the spots will be equidistant from each other, while if the wavefront is aberrated the spots will be displaced from the focus of each microlens and the local tilt at each subaperture will determine the position of each spot centroid at the focal plane.

The array of spots is casted on the detector and finally computer software calculates the centroid of each spot and its position with respect to the calibration array spots (from the reference). Geometric rays are perpendicular to the wavefront. Therefore, if the wavefront is locally approximated by a tilted plane, the displacement of each aberrated spot with respect to the reference spot is proportional to the local slope of the wavefront. The wavefront aberration can be then reconstructed from the first derivatives of the wave aberration using

$$\left.\frac{\partial W(x,y)}{\partial x}\right|_{x=xi,y=yi} = \frac{\Delta xi}{f}; \qquad \left.\frac{\partial W(x,y)}{\partial y}\right|_{x=xi,y=yi} = \frac{\Delta yi}{f}; \qquad (2.1),$$

where **i** is the lenslet considered, **f** the focal length of the lenslet, **Δxi** and **Δyi** the displacements of the aberrated spots measured behind the considered lenslet on the CCD camera, $\left.\frac{\partial \mathbf{W(x,y)}}{\partial \mathbf{x}}\right|_{\mathbf{x=xi,y=yi}}$ and $\left.\frac{\partial W(x,y)}{\partial y}\right|_{x=xi,y=yi}$ the average partial derivatives of the wavefront aberration over the lenslet area. As for the intensity of the beam, it is directly proportional to the amplitude of each focal spot on the camera's sensor.

The deformable mirror

The magnetic deformable mirror (MIRAO52, Imagine Eyes, France) incorporated in the AO system is composed by a high quality reflecting membrane (silver coated >98% for 830 nm wavelength) and 52 miniature actuators assembled in a rigid aluminum housing, whose scheme is shown in Figure 2.8. The actuators of the magnetic deformable mirror are composed by a magnet, located behind the reflective membrane, and a coil. Voltages are applied to coils which produce a magnetic field. This attracts or repels magnets attached to the mirror surface

depending on the sign of the voltage [20, 63]. The mirror has a stroke (maximum generated wavefront amplitude) of ±50 µm peak-to-valley, while the interactuators distance is 2mm and the mirror effective diameter is 15 mm.

In the optical system, the deformable mirror is conjugated to the pupil with a x2 magnification factor from the pupil of the system to the mirror. The angle of the incident and reflected beam is 10 degrees, to ensure proper performance of the deformable mirror. The performance of this mirror had been extensively evaluated in previous works [20, 83, 187].

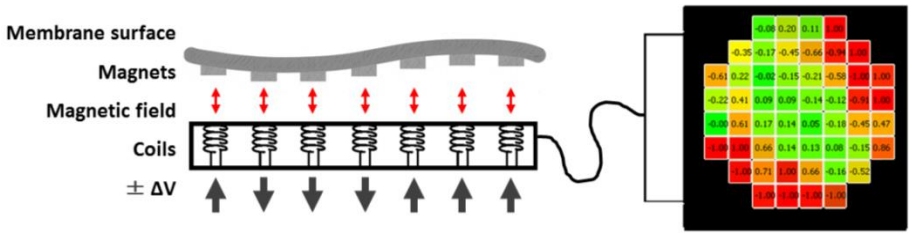

Figure 2.8 Schematic representation of the continuous surface magnetic deformable mirror (Adapted from Hampson, 2008) [63] and corresponding 52 actuators in the MIRAO52 (imagine eyes, France).

C. The Spatial Light Modulator (SLM) Channel

A spatial light modulator (SLM) (PLUTO-VIS; Holoeye Photonics AG, Germany) is used to control a liquid crystal on silicon (LCoS) active matrix reflective mode phase-only liquid crystal display (LCD). A LCoS display allows modifying the phase of a wavefront by applying different voltages to the different pixels of the device, modifying the refractive index and subsequently the optical path. As a consequence, a phase difference is created between the different pixels, where each level of phase is linked to a different level of gray.

In our system a Pluto SLM platform is used to control the LCoS device, where the signal is addressed via a standard DVI signal by the PC2's graphics card and the LCoS display works like an extended monitor, where all phase function are addressed via DVI (Figure 1.28 (b). The LCoS is an active matrix reflective mode phase-only LCD (1920 X 1080 pixels resolution; 0.7" diagonal; Pixel pitch: 8.0 µm; Image frame rate: 60 Hz; max. resolution: 62.5 lines/mm; 8 bits). The LCoS is optimized for visible light (420-700 nm) and an absorption filter is placed in front of the LCoS to block residual UV irradiation coming from the device. In our system's specific configuration and after calibration (see *Section 2.2.3.3*) a maximum phase shift of 2π is achieved for each wavelength used.

A linear polarizer is placed in the path of the SLM (POL) at the calibrated polarization angle to ensure the maximum efficiency. 256 gray levels are used for a phase pattern, where each of the gray level is associated to a different phase shift achieved when different voltages are applied to each pixel of the LCoS.

The SLM is placed in the path between the deformable mirror ant the HS wavefront sensor, so that visual stimuli can be projected on the retina of the subject through the different phase patterns (generated with the SLM), while controlling the aberrations of the subject (with the AO Channel). The SLM is conjugated to the pupil by 2 pairs of relay lenses of 125 mm and 250 mm focal lengths (L3 and L4), and 250 mm and 125 mm focal lengths (L5 and L6) (Figure 2.4), so that x1 magnification is achieved from subject's pupil to SLM.

To generate an aberration profile with the SLM, a grey-scaled image containing the wrapped phase map is sent through a computer video port. The software package developed in our lab is capable of presenting Zernike-based phase profiles.

D. The retinal imaging Channel

The double-pass retinal imaging Channel is inserted by means of a 70/30 beam splitter (BS3). Images of the beam spot are projected on a scientific-grade CCD camera (Retiga 1300, CCD Digital Camera, 12-bit, Monochrome, 6.7x6.7 µm pixel size, 1024x1280 pixels; QImaging, Canada) by means of a collimating lens (L9, 63-mm focal length) and a camera lens (L11, 135-mm focal length). This Channel acts as a "one-and-a half pass", with the aerial image being the autocorrelation [188] of the image of the laser spot with a 2-mm entry beam and 1-mm exit beam.

Figure 2.9 illustrates an example of experimental through-focus double-pass retinal images using the artificial eye as optic element, measured at 555 nm in the presence of natural aberrations though different positions of the Badal system to go through all the Sturm interval.

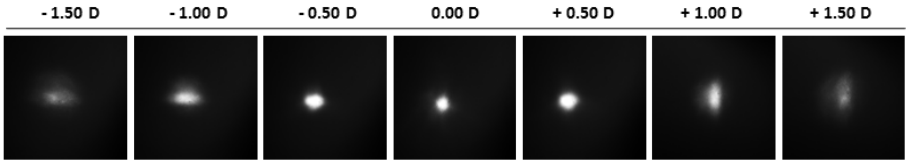

Figure 2.9 Example of experimental through-focus double-pass retinal images for the artificial eye, measured at 555 nm in the presence of natural aberrations.

E. The Badal system

A Badal optometer compensates for spherical error of the subjects. The system is composed of 2 lenses (L1 & L2, focal lengths=125mm) and 2 mirrors (M1 & M2), which are mounted on a motorized stage that allows their displacement to compensate for or to introduce defocus.

Figure 2.10 shows a scheme of the Badal system position for an emmetropic eye (a) and the position for correction of a myopic eye (b). The zero position was achieved when the distance between the lenses is equal to the sum of their focal lengths. When the distance is longer that the sum of their focal lenses, rays converge towards the eye to compensate hyperopic refractive error, when the distance is shorter, rays diverge towards the eye to compensate for myopic refractive error. A displacement of 7.81 mm on the rail was equivalent to a focus shift of 1 D. The system could correct from -8 D to +8 D, with a resolution of 0.125 D.

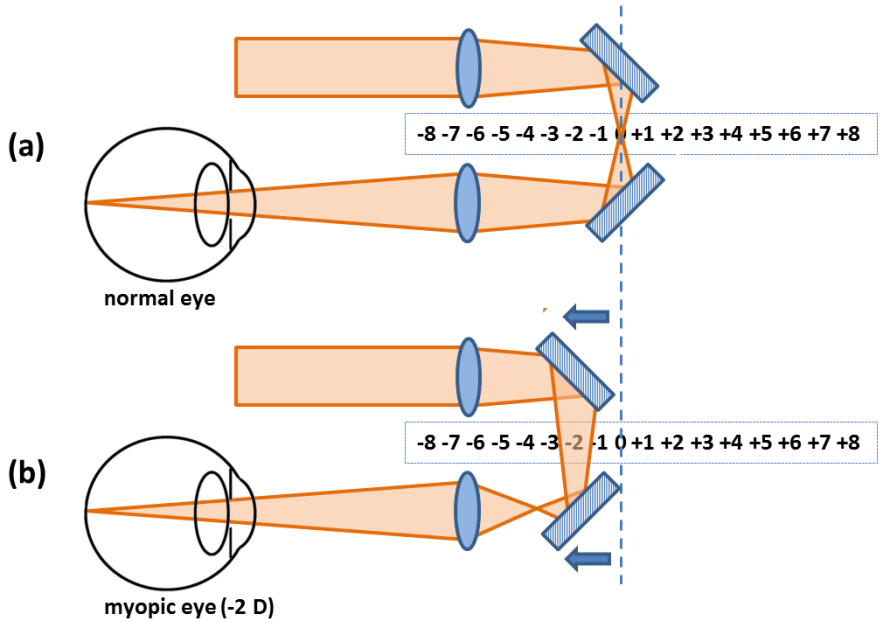

Figure 2.10 Schematic representation of a Badal optometer to correct an emmetropic eye (a) and a myopic eye (-2 D). Adapted from De la Cera (2008) [189].

A calibration of the Badal system was performed for the correcting range by measuring defocus with the HS wavefront sensor for different positions of the Badal system (Figure 2.11), while the deformable mirror was set as to produce a flat wavefront.

An optical calibration element was placed in the pupil of the system (artificial eye consisting of a 50.8-mm focal length achromatic doublet lens and a rotating diffuser as an artificial retina) acting as object for the wavefront sensor.

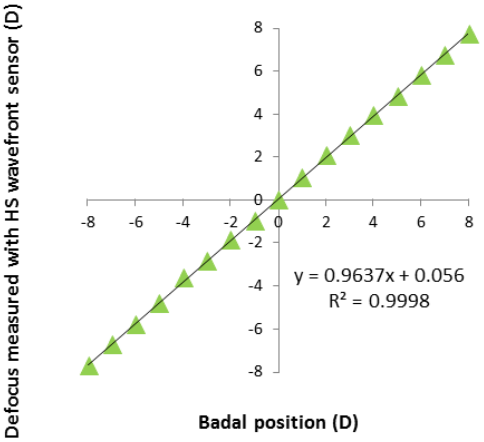

Figure 2.11 Calibration of the Badal system. Defocus measured by the HS, as a function of the estimated dioptric changes produced by the Badal displacement from -8D to 8D in a 1D step.

F. The Pupil monitoring Channel

The natural pupil monitoring system consists of a camera (DCC1545M, High Resolution USB2.0 CMOS Camera, Thorlabs GmbH, Germany) conjugated to the eye's pupil by means of an objective lens with 105-mm focal length (L12). It is inserted in the system using a plate beam-splitter, and is collinear with the optical axis of the imaging Channel.

The camera allows continuous viewing of the pupil and it is used to the eye to the system. In order to correct the position of the eye, an x-y-z stage moving a bite bar is used, taking the line of sight as a reference, while viewing the natural pupil on the monitor. A ring of infrared diodes (λ = 900 nm) placed facing the eye provides the suitable illumination for pupil monitoring. An image of the pupil camera software control is shown in Figure 2.12 for the artificial eye (a) and a subject's eye (b).

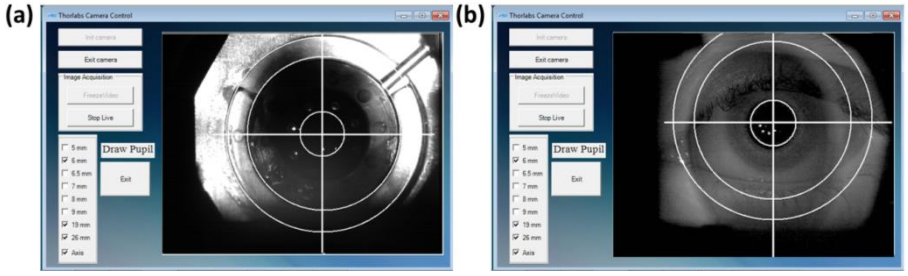

Figure 2.12 Pupil camera software control for the artificial eye (a) and a subject's eye (b).

G. The psychophysical Channel

A visual stimulus Channel is inserted in the deformable mirror path, so that the subject can perform psychophysical tasks under controlled optical aberrations. Two automatized shutters allow simultaneous monochromatic illumination of the eye (S1) and the stimulus (S2) with light coming from the SCLS. A holographic diffuser (HD) placed in the beam path breaks the coherence of the laser providing a uniform illumination of the stimulus. The psychophysical channels were implemented to display visual stimuli during measurement and experiments.

Back-illuminated slide Channel

In a first configuration the psychophysical Channel was composed by a slide with a sunburst chart with spatial frequencies ranging from 3.5 to 150 cycles/degree. It is located in a conjugated retinal plane, inserted in the system by means of a 50/50 beam splitter (BS4) and an objective lens with 50-mm focal length (L10) (Figure 2.3). The visual stimulus subtends 1.62 degrees on the retina, and is monochromatically back illuminated with light coming from the SCLS. The luminance of the stimulus was 20-25 cd/m^2 across the spectral range tested psychophysically (450-700 nm), therefore in the photopic region at all wavelengths [190]. This Channel was used for measurements of Longitudinal chromatic aberration (LCA) shown in *Chapters 5* and *6*, and then replaced by the Digital Micro Mirrors device Channel.

Digital Micro Mirrors device (DMD) Channel

The DMD Channel was specifically developed to allow the presentation of monochromatically illuminated high resolution gray-scale images presented on a Digital Micro-Mirror Device (DMD)(DLP® Discovery™ 4100 0.7 XGA, Texas Instruments Incorporated, USA). It is located in a retinal plane and controlled by a programmable computer graphics system for psychophysical visual stimulus generation (ViSaGe, Cambridge research system).The DMD is a rectangular array of moving micro-mirrors, where the array dimensions are determined by the resolution of the particular DMD.

A scheme of the DMD pixel (mirror) is shown in Figure 2.13. The DMD pixel is an electro-mechanical element composed by two stable micro-mirror states (ON/OFF ±12 degrees) that are determined by geometry and electrostatics of the pixel during operation. The DMD pixel is also an opto-mechanical element, where those two positions determine the direction in which light is deflected. By convention, the positive (+) state is tilted toward the illumination and is referred to as the "on" state. Similarly, the negative (-) state is tilted away from the illumination and is referred to as the "off" state as shown in Figure 2.14, where two pixels are shown one in the ON state and the other in the OFF state.

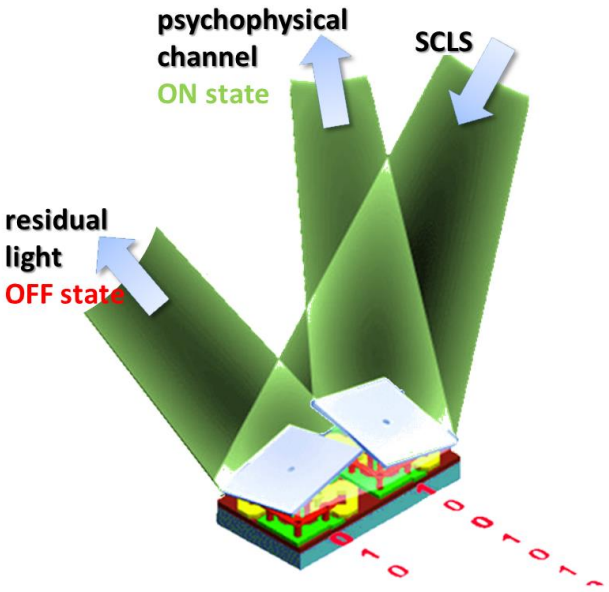

Figure 2.13 Schematic representation of a DMD pixel, composed by 2 micro-mirrors, one in position ON (right) and the other in position OFF (left) (Adapted from Texas Instruments, 2014). The incident beam comes from the SCLS through the holographic diffuser (HD). There are two output beams, one heading to the psychophysical Channel through the objective lens (L10, 50-mm focal length) (ON state), while the other is tilted away (OFF state).

Mechanically, the pixel is comprised of a micro-mirror attached to a hidden torsional hinge, so that the underside of the micro-mirrors makes contact with two spring tips, while two electrodes hold the micro-mirrors in the two operational positions (ON/OFF ±12 degrees). The micro-mirrors can be combined in an array on a chip, and each micro-mirror is associated with the pixel of a projected image. The micro-mirrors can be switched thousands of times per second.

A gray scale image is obtained by varying the amount of time each pixel is ON or OFF, with lighter gray pixels associated with mirrors being ON more than OFF. In this system's configuration a D4100 DVI to DMD (D2D) Interface Board (Digital Light Innovations Incorporated, Texas Instruments Incorporated, USA) was incorporated to the original DLP Discovery 4100 kit to display video on the DMD using a DVI interface and to control the generations of gray scale images.

The DMD Channel is inserted in the system using the elements described in the previous Channel, by means of a 50/50 beam splitter (BS4) placed after the SLM and an objective lens (L10, 50-mm focal length). Its active area is 14 x 10.5 mm and its resolution is 1024 x 768 pixels at 25.6 GB/s. The visual stimulus subtends 1.62 degrees on the retina, and is monochromatically illuminated with light coming from

the SCLS. Figure 2.14 shows an image of a visual stimulus (a) projected on the DMD through the objective lens and (b) seen through the AO system.

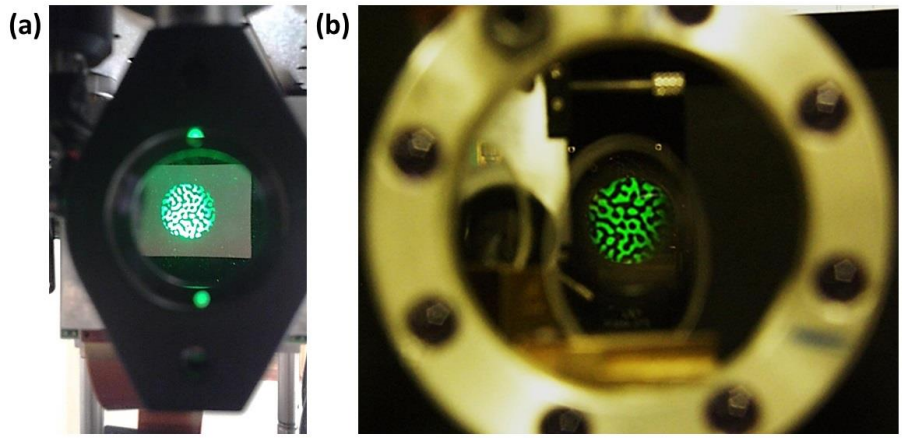

Figure 2.14 Images of a visual stimulus (a) projected on the DMD through the objective lens and (b) seen through the AO system.

The DMD was calibrated to provide linear luminance levels and has an effective luminance of 100 cd/m^2 (calibrated using a ColorCal luminance-meter/colorimeter, Cambridge Research Systems, United kingdom). The calibration of the gamma correction was performed using the ViSaGe platform and the ColorCaL colorimeter of Cambridge Research System using 64 tones, linear fitting and 64 readings per line. It was validated following a procedure similar to that implemented in Psychtoolbox's Visual Gamma Demo) [191, 192] and then applied to the DMD.

H. Pupil and retinal planes

All elements of the system are collinear with the optical axis of the system and are aligned to ensure proper centration of the different devices and accurate location of the conjugate pupil (yellow elements in Figure 2.15) and retinal (pink) planes of the system. Pupil planes of the system are conjugate to the subject's pupil plane.

An artificial pupil (AP-PP) is placed in the first pupil plane of the system with x1 magnification from the subject's pupil, so that a constant pupil diameter is ensured during the measurements and psychophysical experiments regardless the position of the Badal system. Deformable mirror, SLM and HS-wavefront sensor are placed in conjugate pupil planes of the system. Retinal planes are also controlled by means of a pinhole (RP) placed in the first retinal plane of the system in front of the deformable mirror, which allows: to remove the undesired reflections from the cornea, which affect measurements of the HS-wavefront sensor, and to check the projection of the images presented through the psychophysical Channel.

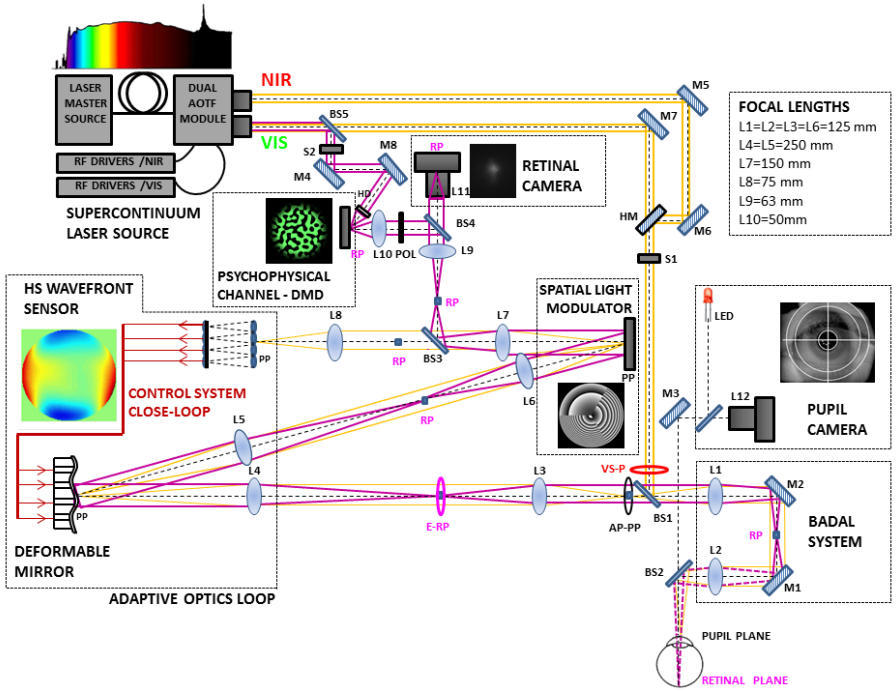

Figure 2.15 Schematic diagram of the location of the pupil (yellow) and retinal (pink) planes of the system, as well as the location of the artificial pupil (AP-PP) and retinal (E-RP) pinhole used for alignment.

2.2.3 Configuration and validation of the polychromatic AO system

The construction of the AO system started once the final design was completed. The first stage of the setting up process involved the setting of the SCLS, the calibration for the different spectral ranges and the laser safety calculations. In a subsequent stage the Badal system was set and aligned. Pupil and retinal planes of the system were validated and the pupil camera was set and calibrated.

The second stage was the implementation of the AO Channel with the deformable mirror and HS wavefront sensor, as well as the first psychophysical Channel with the back illuminated sunburst chart for presentation of visual stimuli. Retinal camera was incorporated as second control Channel. In the last stage, the SLM was set and calibrated to extend the capabilities as visual simulator of the system, and finally the DMD substituted the sunburst chart to project high quality gray scale images.

2.2.3.1 Operation and calibration of the Illumination Channel. Laser safety measurements

The supercontinuum laser source (SCLS) and the dual Acousto-optic Tunable Filter (AOTF) module were the first elements of the system to be set and calibrated. Illumination coming from the two independent fiber-channels of the SCLS enters the system collinearly by means of a hot mirror (HM). The beam is collimated and enters the eye with a diameter of around 2 mm for NIR channel and 3 mm for VIS channel. A variable-size pupil (VS-P) allows modifying the beam size and position of the beam entering the eye. The SCLS power was measured at the corneal plane (subject's pupil plane) for different wavelengths of both fiber-channels (VIS and NIR) for a 2 mm-beam-size (set with the variable-size pupil (VS-P). Power ranges from 1.68 (600 nm) up to 11.9 mW (690 nm) (Table 2.1).

								VIS
λ(nm)	450	488	514	532	600	633	650	690
P(mW)	2.14	1.72	3.94	3.70	7.00	8.50	9.52	11.90
								NIR
λ(nm)	600	670	740	810	880	950	1020	1100
P(mW)	1.68	2.87	4.15	3.73	4.04	2.99	2.84	2.64

Table 2.1 SCLS power at the subject's pupil plane (entering the eye) as a function of light intensity for different wavelengths of both fiber-channels (VIS and NIR).

Retinal damage from light exposure occurs principally from three mechanisms: thermal, thermoacoustic and photochemical damage [184]. Thermal occurs due to protein denaturation induced by temperature increases secondary to light absorption by melanin in the retinal pigment epithelium, while photochemical damage occurs at short visible wavelengths and for exposure duration longer than ~1 s, and thermoacoustic damage occurs for pulses shorter than ~1 ns and is associated with various nonlinear mechanisms (laser-induced breakdown, self-focusing, etc.).

For measurements in the eye, laser safety calculations were performed to find the Maximum Permissible Exposure (MPE) for each wavelength and testing condition. Supercontinuum laser source parameters considered for calculations are: 4.16 W peak power, 40 MHz fixed repetition rate, 400 fs pulse duration and 50nJ of max pulse energy.

Calculations were performed according to level exposures in the ANSI, Z136.1-2007 [185] following calculations methods summarized by Delori et al. (2007)[184]. For this laser, exposure is calculated for repetitive pulses, where a pulse train is described by its pulse repetition frequency ***F***, its total duration ***T***, the number ***n*** of

pulses (*n=FT)*, the duration t_1 and peak radiant power Φ_1 of a single pulse, the energy per pulse

$$Q_1(Q_1 = \Phi_1 t_1) \quad (2.2),$$

and the duty factor

$$\delta = F t_1 \quad (2.3).$$

The average radiant power Φ_{av} is related to Q_1 and Φ_1 by

$$\Phi_{av} = Q_1 F \, \Phi_1 \delta \quad (2.4).$$

The ANSI Standard applies three "rules" that define three separate MP exposures, where the rule that yields the highest protection is used (lowest MP exposure) (Table 2.2).

The first rule tests whether the radiant exposure $H_{c,1}$ of a single pulse (duration: t_1) does not exceed the $MPHc[t_1]$ at pulse duration t_1 (line 1 at Table 2.2). The second rule protects against average-power heat buildup in thermal injury and cumulative injury from the photochemical damage mechanism. It tests the safety of a continuous-wave (CW) equivalent exposure of duration *T* with a constant-power radiant power (equal to the average power of the train).

Both thermal and photochemical limits must be tested separately [line 2 of Table 2.2 (left part)]. The third rule protects against subthreshold pulse cumulative thermal injury and applies only to the thermal limits. Rule 3 essentially tests whether an exposure by a long pulse of duration nt_1 is safe.

The ANSI standard also differentiates 2 cases depending on whether the pulse repetition frequency is higher or lower than the "critical pulse repetition frequency"

$$F_{cr} = 1/t_{min} \quad (2.5).$$

In our case $F \geq F_{cr}$, then, according to the standard, subgroups of more than 1 pulse occur within the time frame of t_{min} and each subgroup is replaced by a "single" pulse. The time between these pulses is also t_{min}, and the pulse train is equivalent to a CW exposure of duration T. The MP level per pulse for rule 3 when $F \geq F_{cr}$ is thus the same as the thermal limit derived in rule 2, and there is thus no need to test rule 3 if $F \geq F_{cr}$. If the pulse train duration $T < t_{min}$, then all pulses occur during t_{min}, and the same reasoning applies ($T = t_{min}$) *[184]*.

ANSI rules

		MP radiant exposure per pulse, $MPH_{c,1}$	MP average power through pupil, $MP\Phi_{av}$
R1	**Single pulse limit**	$MPH_c[t_1]$	$\delta\ MP\Phi[t_1]$
R2	**Average power limit**	$\frac{MPHc[T]}{n}$ (#)	$MP\Phi[T]$
R3	**Multiple pulse limit**	$n^{-0.25}MPH_c[t_1]$ (#)	$n^{-0.25}\ \delta\ MP\Phi\ [t_1]$

Which rules to test?[++]

	$t_1 < 1ns$	$1ns < t_1 < t_{min}$	$t_1 \geq t_{min}$
$F < F_{cr}$	**(a)** R1th R2ph R3*	**(b)** R2ph R3*	**(c)** R2ph R3
$F \geq F_{cr}$	**(d)** R1th R2th R2ph	**(e)** R2th R2ph	

*$t_1=t_{min}$ and $\delta_{min}=Ft_{min}$

[++]Select appropriate cell and test the rules within the cell (th: thermal; ph: photochemical limits). Select lowest as limit for the pulse train. Use rule "2ph" only if 400 ≤λ<600 nm and T>0.7 s

F Pulse repetition frequency (PRF) (Hz)
T Duration of pulse train (s)
(#) If $T > T_2$ then use $T=T_2$ ($MPH_{c,1}$ only)
n Number of pulses: n=FT (round up)
t_1 Duration of single pulse(s)
δ Duty factor: $\delta=Ft_1$
t_{min} 18 μs (400 < λ<1050 nm)
50 μs (1050 < λ<1400 nm)

MPH_c MP radiant exposure at cornea
MPΦ MP radiant power through pupil
F_{cr} Critical PRF = $1/t_{min}$ (55.5 and 20KHz)

Table 2.2 Rationale of the three rules for repetitive pulses (Adapted from Delori et al. (2007)) [184]

Once the rule to be applied for each wavelength and exposure time was applied, the MP radiant power entering the natural or dilated Pupil was calculated for the 3 rules following the procedure explained in Table 3 in Delori et al. (2007)[184]. Results of those calculations are shown in Table 2.3 (a), where the maximum permissible radiant power *MPΦ* (in μW) entering the natural or dilated pupil for different exposure times (1 to 900 s) for the most typical used wavelengths of both channels are shown.

Table 2.3 (b) shows the laser power measured at the corneal plane for a typical exposure time during a typical ocular wave aberration measurement (3-5 s) for the most used wavelengths. Laser power ranges between 0.10 and 10 µW, which is at least one order of magnitude below the ANSI standards safety limits at all tested wavelengths [184-186] for that exposure time.

(a)	Exposure limit *MPΦ* (µW)							(b)
	VIS							
	1 s	5 s	10 s	20 s	60 s	300 s	900 s	3 - 5 s
450	12.5	**2.5**	**1.3**	**0.6**	**0.2**	**0.0**	**0.0**	0.12
488	72.0	14.4	7.2	3.6	**1.2**	**0.2**	**0.1**	0.70
500	125.1	25.0	12.5	6.3	2.1	**0.4**	**0.1**	0.65
532	127.4	85.2	54.6	27.3	9.1	**1.8**	**0.6**	2.85
555	127.4	85.2	71.6	60.2	26.2	5.2	**1.7**	3
570	127.4	85.2	71.6	60.2	45.8	10.5	3.5	4.60
633	221.3	148.0	124.4	104.6	79.5	53.2	13.9	7.65
650	295.6	197.7	166.2	139.8	106.2	71.0	54.0	8.70
	NIR							
	1 s	5 s	10 s	20 s	60 s	300 s	900 s	3 – 5 s
700	696.2	465.6	391.5	329.2	250.1	167.3	127.1	9.40
730	20886.0	13967.3	11745.0	9876.4	7504.4	5018.5	3813.2	0.77
750	34809.9	23278.8	19575.1	16460.6	12507.4	8364.2	6355.4	1.72
810	76581.9	51213.4	43065.1	36213.3	27516.2	18401.2	13981.9	2.30
850	104429.8	69836.4	58725.2	49381.8	37522.1	25092.5	19066.2	2.36
880	125315.8	83803.7	70470.2	59258.2	45026.5	30111.0	22879.4	2.56
950	174049.7	116394.0	97875.3	82303.0	62536.8	41820.9	31777.0	3.25
1020	222783.6	148984.4	125280.4	105347.9	80047.1	53530.7	40674.5	4.85

Table 2.3 (a) Maximum permissible radiant power *MPΦ* (in µW) entering the natural or dilated pupil for different exposure times (1 to 900 s) for the most typical used wavelengths of both channels. Situations highlighted in red are out of the safety limits in the system, thus they never occur. (b) Irradiance (in µW) at the cornea (subject's pupil plane) for a typical measurement time (3-5 s).

2.2.3.2 Validation of the conjugate pupil and retinal planes of the system

After proper alignment of the SCLS and the Badal system, conjugate pupil and retinal planes were set by means of the different relay lenses. In our case, this has to be maintained constant for the different positions of the Badal system. To identify the conjugate pupil planes and to ensure proper magnification in the pupil planes of interest (x1 artificial pupil, x2 deformable mirror, x1 SLM and x0.5 HS wavefront sensor) regardless the Badal position, a CMOS camera (DCC1545M, High Resolution USB2.0 CMOS Camera, Thorlabs GmbH, Germany) was placed in the different tested pupil planes, while a graph paper was placed in the pupil plane (subject's pupil plane) of the system. Images of the graph paper were taken in the different planes while moving the Badal system from ± 6 D in (1 D step).

Results of the validation are shown in Figure 2.16 (a), where images of the graph paper taken in the different conjugated planes are shown for selected positions of the Badal system. The intensity profile of each recorded image was processed to calculate the magnification in each plane, following same procedure than Sawides (2013) [20]. Magnification is fairly constant for all positions of the Badal and the different pupil planes, as shown in Figure 2.16 (b). Magnification between the pupil plane of the system and the artificial pupil plane is 1.005x, ensuring proper magnification between the subject's pupil plane and the artificial pupil plane of the system.

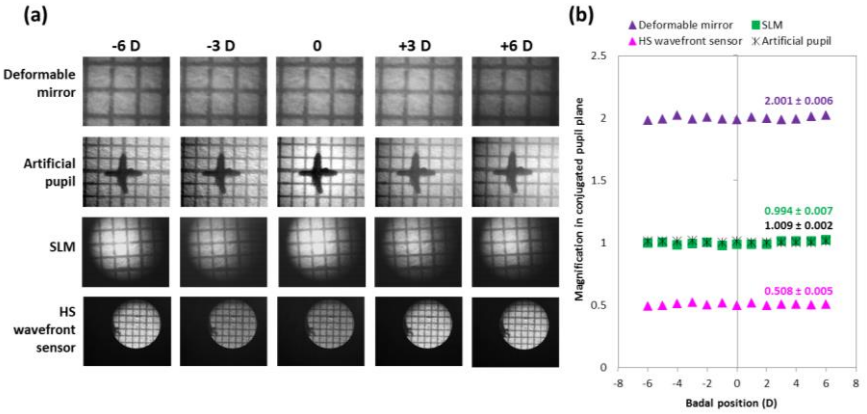

Figure 2.16 (a) Images taken with the CMOS camera of the graph paper (1mm-squared) for the different evaluated conjugated pupil planes: deformable mirror, artificial pupil, SLM and HS wavefront sensor through some of the evaluated Badal positions (b) Corresponding magnification in the different pupil planes for different positions of the Badal for – 6 D to + 6 D in 1 D steps.

Validation of the conjugate pupil planes was also performed with the AO elements. If both AO elements, deformable mirror and HS wavefront sensor, are in conjugate pupil planes, when a deformation is applied on the deformable mirror changes in the shape of the wavefront are introduced but not in the intensity profile. This was achieved by applying a deformation on the deformable mirror and testing the intensity profile, since a deformation on the deformable mirror will introduce changes in the shape of the wavefront but not in the intensity profile. Figure 2.17 shows that when pushing 2 of the central actuators (a) the intensity profile (c) remains constant, while the wavefront is deformed (b).

Conjugate retinal planes of interest (E-RP) were validated using the same procedure. In that case a graph paper was fixed at the retinal plane of the system (subject's retinal plane), while images were taken in the E-RP.

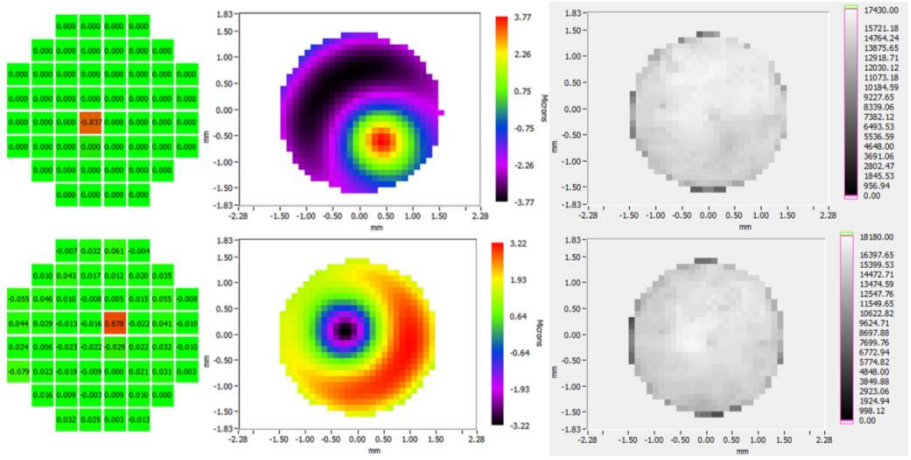

Figure 2.17 Validation of pupil conjugation of the AO elements. (a) The actuator control remote, the representation of the deformable mirror with each actuator and the corresponding voltage applied (b) the wavefront (performed onto a closed-loop) and (c) the corresponding intensity profile.

2.2.3.3 Operation and calibration of the AO Channel

The AO Channel was validated and calibrated first without the presence of the SLM in the path between the deformable mirror and HS-wavefront sensor, where a flat mirror was placed instead of the SLM. Calibration is similar to that in Sawides (2013) [20]. After the incorporation of the SLM a second validation of the SLM and of the complete AO system was performed (explained in section 2.2.3.5).

A. Measurement and correction configurations of the AO Channel

Measurement and close-loop correction of wave aberrations are performed following 4 different steps: Local Slopes Acquisition, Interaction Matrix Acquisition, Command Matrix Construction and finally the Closed-Loop Correction (or induction) of wave aberrations. The four-step process is illustrated in Figure 2.18. To perform this process a calibrated optical element must be placed in the pupil plane of the system, in this case an artificial eye consisting of a 50.8-mm focal length achromatic doublet lens and a rotating diffuser as an artificial retina.

Local Slopes Acquisition

For each acquisition, the HS wavefront sensor automatically detects all calculable subapertures and infers the largest possible pupil, according to the phase reconstruction mode chosen. The slopes are estimated to calculate the wavefront aberrations and expressed as vectors, whose amplitude corresponds to the amplitude of the slope, while the orientation of the vector designates the angle of the largest slope of the wavefront. When measuring the wavefront aberrations, the software interpolates the slope from the adjacent subaperture.

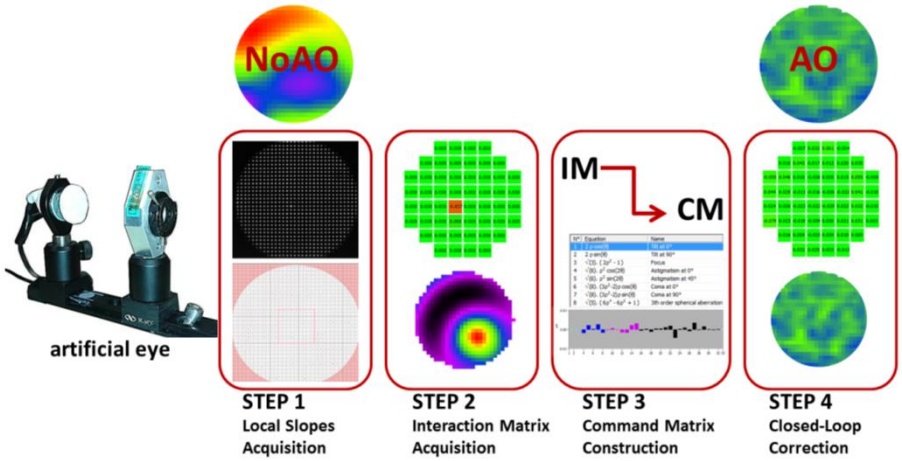

Figure 2.18 The four-step process followed for measurement and close-loop correction of wave aberrations of the artificial eye with the AO system.

Interaction Matrix Acquisition

When a unit voltage is applied to one of the 52 actuators of the deformable mirror the continuous reflective membrane changes its shape. The interaction matrix accounts for the influence of each actuator (actuator's influence function) in the deformation of the entire membrane by pushing and pulling each actuator (± 0.2V). Its effect on the membrane is saved in the Influence Matrix that records all the individual actuators' influence functions. The Interaction matrix (IM) is constructed using the full pupil diameter (7 mm).

Command Matrix Construction

The Command matrix (CM) is constructed from the IM, in fact is the pseudoinverse matrix of the IM, and accounts for the voltage that has to be applied to each actuator to generate different patterns of aberrations. A modal reconstruction algorithm projects the measured slopes onto a polynomial perpendicular base. Forty-eight modes are used and Zernike polynomials up to 7th for circular pupils.

Closed-Loop Correction

A closed-loop (CL) operation consists on the acquisition of the local slopes, calculation of the voltages needed to apply to the actuators of the deformable mirror to change its shape and a subsequent acquisition of the residual slopes. These steps are repeated in N loops, N being the number of iterations required to obtain the desired wavefront pattern. In our system's configuration CL is performed for a 6-mm-pupil, selected by closing the artificial pupil (AR-PP) placed in the first pupil plane after the deformable mirror calibration, while the pupil diameter is estimated by software. The state of the mirror that corrects for the system's aberration is saved and kept as a reference file named "flat mirror", used

when measuring natural subject's aberrations (tilt and defocus are measured but kept free).

This 4-steps-process is performed every time, using the artificial eye as a calibrated optical reference, to measure and correct for the aberrations inherent to the system and to obtain a reference for latter measurements. The four steps of the process are shown in Figure 2.18 for a typical daily calibration, as well as an example of the wave aberrations of the system before and after the closed-loop operation (RMS=0.427 µm for a 7-mm pupil, excluding tilt and defocus; λ=827 nm). For measuring and correction with the artificial eye, we set the SCLS at 827 nm and 1.90 µW as a reference for measurements.

Measurements at this stage are performed at 827 nm for comparison with other setups and for laser safety considerations. We typically used a gain between 0.3 and 0.5, the integration time was set at 45ms (but can be adjusted for each wavefront measurement) and a stable closed-loop correction was obtained in 15 iterations. Typically the residual wavefront error after CL of the system decreases below 0.02 µm and stabilizes after that. A good AO correction in the system reaches 95% of correction.

B. Validation of the AO system for the VIS and NIR

The AO Channel was validated first using an artificial eye with known aberrations (artificial eye, provided by Alcon, Spain). AO-measured values for astigmatisms, defocus, coma and spherical aberration (827 nm, 6-mm pupil) were compared with the values provided by the manufacturer. A good correspondence was found between the nominal and the measured aberrations with the AO system of the different aberrations present in this artificial eye (differences <0.05 µm), except for the defocus term, where higher values were found in the measured values, probably due to the original characterization of the artificial eye with a different wavelength.

A subsequent validation was performed for the most used wavelengths for both channels, where measurements and close-loop corrections of the wave aberrations of the artificial eye were performed across different wavelengths. Figure 2.19 (a) shows astigmatisms, defocus, coma, spherical aberration and the RMS of HOAs of the artificial eye for the most typically used wavelengths, where variability inter-wavelengths is lower than 0.004 µm. Differences in terms of RMS across wavelengths is lower than 0.003 µm. Close-loop correction of wave aberrations of the artificial eye and the system (shown in Figure 2.19 (b)) is similar across wavelengths (Differences inter RMS < 0.001 µm).

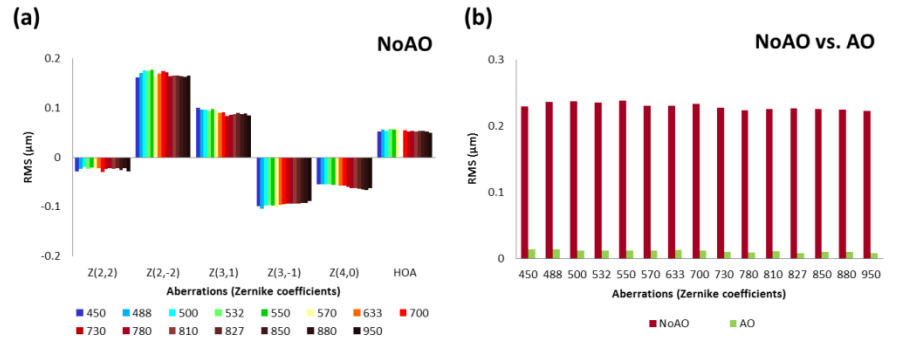

Figure 2.19 (a) Comparison between the measured aberrations (astigmatisms, defocus, coma, spherical aberration and the RMS HOA) at different wavelengths. (b) Comparison in terms of RMS between the measured and AO-corrected aberrations at different wavelengths.

The state of the mirror that compensates for the aberrations (artificial eye or subject's eyes) is found in a closed-loop operation at 827 nm (NIR), and applied in measurements at all wavelengths, as a preliminary experiment showed no benefit of changing the aberration-correcting state of the mirror (measured at each wavelength) for measurements at that given wavelength. For measurements with the artificial eye, differences were lower than 0.005 µm RMS. For example, the state of the mirror that corrects for the aberrations of the system and the subject at 555 nm (VIS) in a subject results in 0.0391 µm RMS residual aberrations. The same state of the mirror applied at 827 nm results in 0.0427 µm RMS.

2.2.3.4 Operation and calibration of the Spatial Light Modulator Channel

The SLM Channel was first calibrated to associate a different level of gray to the different phase shifts generated for each pixel of the device. Afterwards, software was generated to create phase maps in the SLM. Finally the SLM was validated in the environment of the AO system. The SLM is configured by loading different configuration files, which contains the addressing sequence (also called "Bit-plane"), the gamma curve (.csv format), geometric settings and settings of digital potentiometer that can be used to adapt the dynamic range. Gamma curve, geometry and potentiometer can be changed within one configuration file whereas the sequence can only be change by changing the global device configuration.

The used SLM is characterized by its digital addressing scheme were the phase level are created by pulse code modulation. This digital nature enables on one hand a very size and cost effective driver unit, but on the other hand it introduces a certain phase flicker (due to the limited viscosity of the LC molecules what allows them to follow each single pulse at a fraction) with frequencies of multiples of the device refresh rate (60Hz), which can be troublesome. This means that the molecules flicker around an average value what leads to a time dependent phase level, which

affect to the total bit-depth of the SLM. A high bit depth (long sequence) means a high number of different states and a low bit depth (short sequence) vice versa. The limited bandwidth of the used technology allows a shorter sequence to be addressed more often within one frame than a longer one. This directly influences the addressing frequency what therefore influences the flicker. The higher the addressing frequency, the lower the flicker will be. A sequence with lower flicker can create less distinguishable phase level compared to a longer sequence. Also a compromise between flicker amplitude and number of different phase level has to be determined. In this SLM three sequences can be used: 18–6 (default), 5–5 and 0-6 sequence. For our purposes 5-5 sequences is used showing sufficient depth to generate the phase patterns and reduce the phase flicker significantly.

A. Calibration of the SLM

The LCoS active matrix reflective mode phase-only LCD controlled by the SLM needs to be calibrated, in order to associate the different levels of gray to the phase difference created between the different pixels. The calibration process was performed once the SLM was set in the AO system for the most typical wavelengths. The calibration process has two stages, where the phase modulation achieved with the SLM for the SCLS is obtained by measuring the intensity distribution of diffraction orders created by a changeable binary grating. In the first stage of the process an interference pattern is created by means of the auxiliary set up shown in Figure 2.20 (a) (scheme provided by the manufacturer).

An image of the experimental setup for phase modulation measurements and calibration of the SLM is shown in Figure 2.20 (b), where POL1 is the polarizer, A is the analyzer, MO1 is a Microscopic Objective x10/0.25 NA, 16.5 mm, MO2 is a Microscopic Objective x20/0.40 NA, 9 mm, L1 is 125 mm focal-length (L6 in the AO system), L2 is a 150 mm focal-length (L7 in the AO system), MASK is double hole mask (hole diameter approx. 2mm, distance approx. 7mm) and CMOS is a CMOS camera. The laser beam is expanded by the first microscope objective (MO1) and collimated by a lens (L1). A linear polarizer (POL1) in front of the SLM sets the incoming polarization state. The LCoS is illuminated by two coherent and collimated laser beams by using the MASK. Both beams are separately guided to the appropriate half of the display. One half is addressed with a constant gray level whereas the other is addressed with changing gray levels from 0 to 255.

The different phase shifts are generated by applying different voltages to each pixel that changes the refractive index thanks to the properties of the liquid crystal. As a consequence, the optical path changes and generates a phase shift in between one pixel and the others. The two beams are then reflected under a small angle (~6°) and analyzed by the analyzer (A). A lens (L2) behind the display lets both beams interfere with each other and a microscope objective (MO2) images the expanded interference pattern onto a CMOS camera (CMOS). A phase shift as a function of

the addressed gray level appears as a shift in the interference pattern, which is evaluated by software in the second stage of the process.

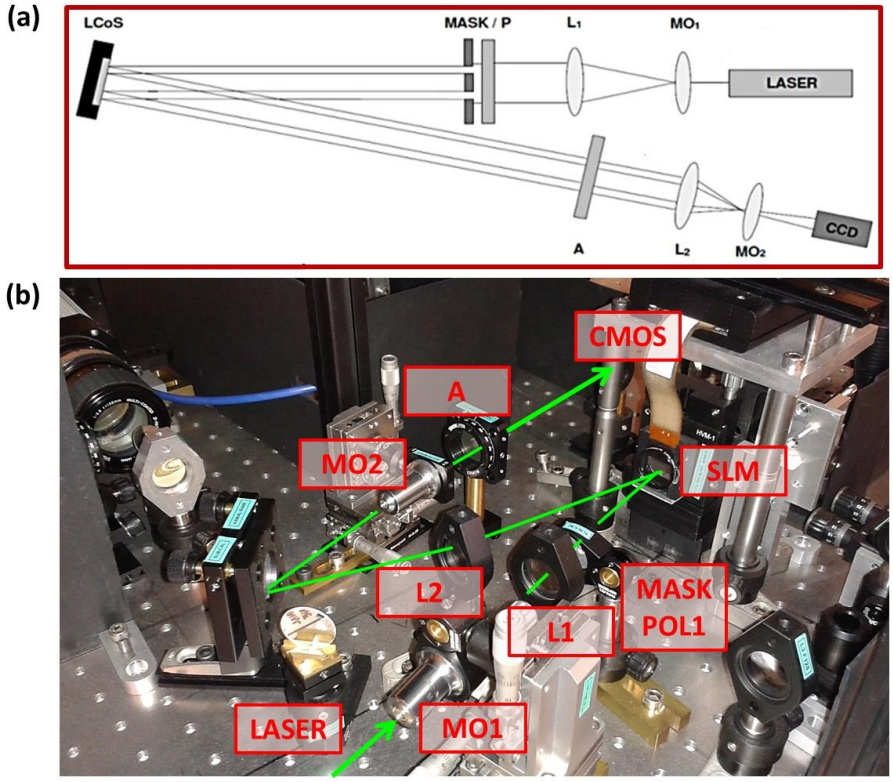

Figure 2.20 (a) Schematic diagram of the setup for phase modulation measurements and calibration of the SLM. (b) Experimental setup for phase modulation measurements and calibration of the SLM, where POL1 is the polarizer, A is the analyzer, MO1 is a Microscopic Objective x10/0.25 NA, 16.5 mm, MO2 is a Microscopic Objective x20/0.40 NA, 9 mm, L1 is 125 mm focal-length (L6 in the AO system), L2 is a 150 mm focal-length (L7 in the AO system), MASK is double hole mask (hole diameter approx. 2mm, distance approx. 7mm) and CMOS is a CMOS camera.

The evaluation of this shift in the interference pattern is performed with the software provided by the manufacturer (PhaseCam, Holoeye Photonics AG, Germany) following 4 different steps: interference pattern image acquisition, phase shift generation, phase shift validation and gamma curve generation and gamma curve validation. The four-step process is illustrated in Figure 2.21, where an intensity minimum of the interference pattern (defined by the user) is the starting point of the measurement. This minimum is detected by the software and its movement, as a function of the addressed gray level, is a measure of the phase shift.

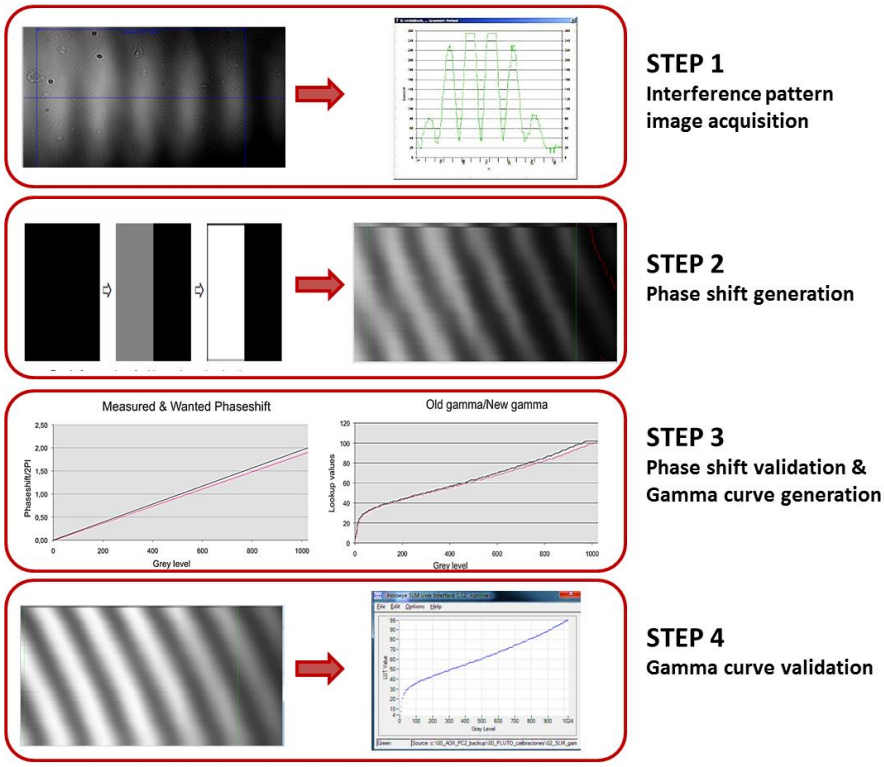

Figure 2.21 The four-step process followed for calibration of the SLM using the software provided by the manufacturer.

Interference pattern image acquisition

A stable image of the interference pattern, containing at least 4-6 fringes, is recorded by the CMOS camera, which is used for selecting the measurement line (Figure 2.21, Step1).

Phase shift generation

The display is divided in two halfs, where the 2 separately guided beams impact. One half is addressed with a constant gray level (as a reference) whereas the other is with changing 256 phase shifts from 0 up to 2π, each of them associated to a different level of gray from 0 to 255 (Figure 2.21, Step2).

For each phase shift, the interference pattern changes, and, as a consequence, the fringes appear curved on the image. To understand the progressive introduction of phase shift process, a vertical line is imagined at the beginning of the image. Certain intensity is shown, when constructive interference. The intensity decays, when the interference is partial, due to the small phase shift between the 2 waves.

Also, in the middle point of that vertical line, waves are in phase opposition, interference is destructive, and a minimum in the intensity is found. At the end of the image and assuming a maximum phase shift of 2π, the interference is constructive and a new maximum in the intensity is found. The software records the measurement line previously selected and stacks all the images in different rows, creating an image where the interference fringe are curved as a consequence of the introduced phase shift (Figure 2.21, Step2).

Phase shift validation & Gamma curve generation

The position of the minimum of intensity, displaced in each row due to the introduction of the different phase shifts, is stored. These values are compared with the theoretical phase shift computed previously. Figure 2.21 (Step3) shows the relationship between the computed and the measured total phase shift. The measured phase shift values are used to obtain the gamma curve of the device for that wavelength, which guarantees a lineal relationship between the level of gray and the phase shift from 0 to 2π. These 2 graphs are generated with 1024 gray levels, although the SLM can reproduce only 256. The reason for this is the unambiguous relationship between the phase shifts and the 1024 initial gray levels: the same phase shift is assigned to consecutive levels of gray, so that the gray levels can be adjusted to obtain a lineal relationship with the phase shift.

In our configuration of the system, the 633 nm-gamma-curve provided for the manufacturer and a linear configuration are used to generate the new gamma curve (gamma curve: *5_5_lin2,0pi_633.csv;* linear configuration 5_5_linear_2pi_633nm.hex) to ensure a maximum phase shift of 2π and a linear relationship between the phase shift and gray levels. Finally, the SLM can recognize 256 phase shifts, identified with the 256 level of gray that result from the grouping of those that share the same phase shift. The new generated gamma curve (Figure 2.21, Step3) is stored and it is applied everytime the SLM is connected. A different gamma curve is generated for each wavelength.

Gamma curve validation

Once the gamma curve is generated and applied in the SLM, the measurement of the interference pattern is performed again. If the gamma correction is correct, the fringes appear straight but bended, instead of the curved fringes that appeared previously (Figure 2.21, Step4). The results for the calibration, in terms of phase shift, and gamma curve generation for the most used wavelengths in the visible range is shown in Figure 2.22 (a) and (b) respectively. Once the gamma curve is obtained and stored in the SLM, the configuration of the device has to be applied.

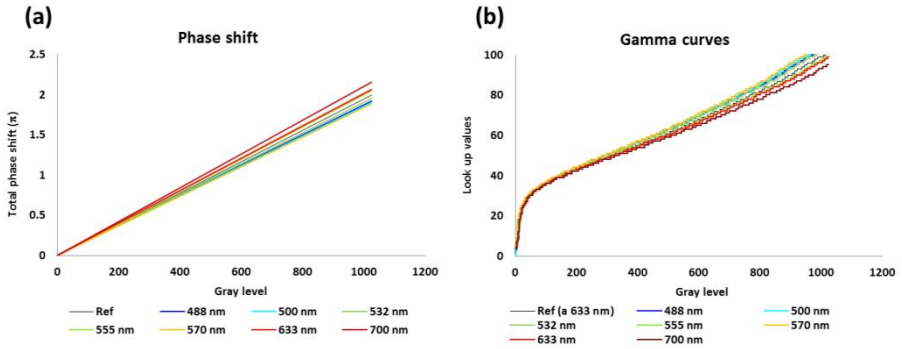

Figure 2.22 (a) Measured phase shifts for the most used wavelengths in the visible range. (b) Generated gamma curves for the most used wavelengths in the visible range.

B. Phase pattern generation using the SLM

The SLM internally converts the intensity images sent from the computer into spatially modulated optical phase, where the different gray levels of the projected images correspond to different optical paths introduced locally over the incoming wavefront. The SLM addresses the different configurations in the LCoS device by the software provided by the manufacturer. Once the channel and port are chosen (green channel and correct COM port), proper gamma curve upload and most suitable configuration chosen (5:5 sequence, linear, 633 nm reference), the SLM can be handled with the commercial software or our custom made software.

Matlab routines are used to numerically simulate complex phase maps, that are converted into .jpg files and later on are generated by means of the LCoS active matrix reflective mode phase-only LCD controlled by the SLM. Phase maps are created using wavefront maps generated using Fourier Optics but SLM can achieve only a fixed range of phase modulations, corresponding to approximately one wave of compensation. The excess phase must be remapped to a phase between 0 to 2π. This is done by a simple modular operation called phase wrapping [36, 180] used to obtain a maximum phase difference of 2π. For that, the phase of the wavefront is obtained, by multiplying each point of the wavefront by the corresponding wave number,

$$k = \frac{2\pi}{\lambda} \qquad (2.6).$$

Then angles are wrapped in lambdas, in radians, to the interval [0 to 2π], such that 0 maps to 0 and 2π maps to π] [193, 194]. The wavefront is now represented according to its phase and limited between 0 and 2π. The generated pattern is then a grey-scale image, where each level of grey corresponds to a certain phase difference between 0 and 2π. Examples of this process are shown in Figure 2.23. A wave aberration map with defocus Zernike term only ($Z_2^0 = 1\ \mu m$) generated for

ʎ=555 nm is shown and so is its phase (a). The same wavefront is shown in terms of phase, after a wrapping process (b). Finally, the same process for ʎ=700 nm, where differences with previous situation are shown, since this is a ʎ-dependent process. Wrapped phase maps are displayed onto the SLM as images generated for a 6mm pupil in the pupil plane where the SLM is placed (x1 magnification; scale of 0.0080 mm/pixel).

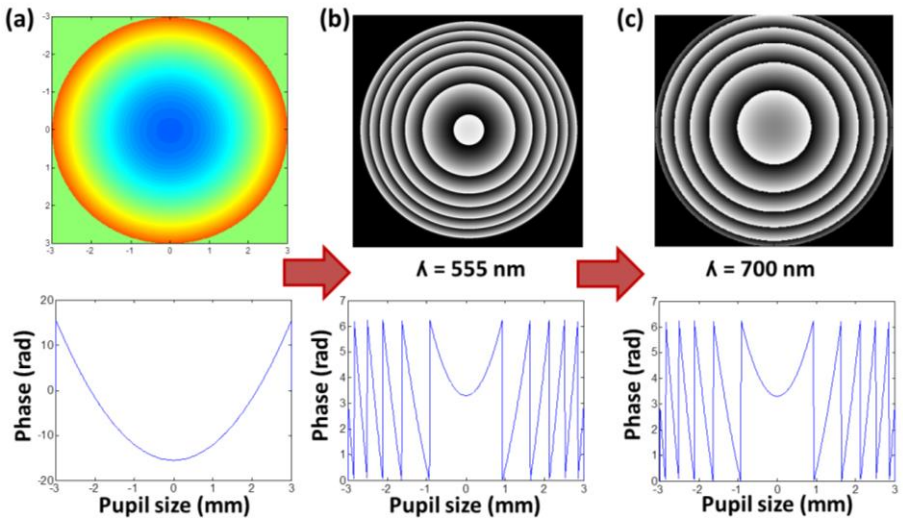

Figure 2.23 (a) Wavefront generated using Fourier Optics ($Z_2^0 = 1\ \mu m$) and its corresponding phase for 555 nm. (b) Result after applying the corresponding wrapping process (c) Similar wavefront ($Z_2^0 = 1\ \mu m$) generated for 700 nm and the corresponding wrapping process.

C. Validation of the SLM

A calibration of the SLM system was performed for the working range by measuring defocus with the HS wavefront sensor for different amounts of defocus (Z_2^0) generated with the SLM (Figure 2.24), while the deformable mirror was set as to produce a flat wavefront and the artificial eye was placed in the pupil plane of the system.

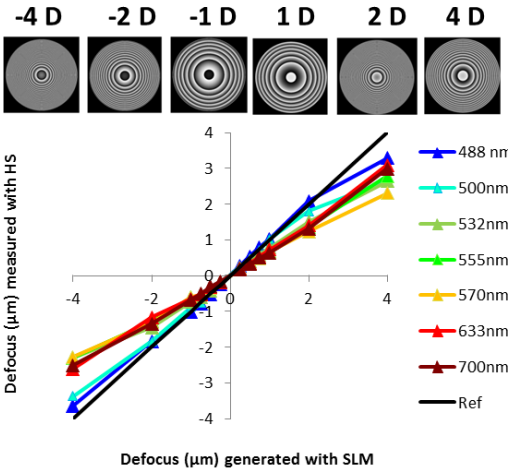

Figure 2.24 Calibration of the SLM system. Defocus measured by the HS wavefront sensor, as a function of the defocus (Z_2^0) induced with the SLM (-4D to 4D).

Measurements were performed for the most typical wavelengths in the VIS range. Black line shows the theoretical response of the system. Shorter wavelengths curves fit better the reference curve than longer, although in general a lineal response is found for all tested wavelengths. From the slopes of the calibration curves, a correction factor is calculated to modify the generated phase maps to obtain proper values of defocus measured with the HS wavefront sensor. Correction factor obtained for the measured wavelengths in the ± 2 D range is shown in Table 2.4.

	R^2	m	Correction factor
488	0.99763	0.994	1.006
500	0.99823	0.924	1.076
532	0.99877	0.752	1.249
555	0.99863	0.662	1.338
570	0.99838	0.642	1.358
633	0.99441	0.657	1.343
700	0.99445	0.663	1.337

Table 2.4 Correction factor for the different wavelengths and defocus obtained from the slopes of the calibration curves.

2.2.3.5 Validation of the system using different elements of calibration

A. Calibration of the different active optic elements

The performance of the different devices of the system was achieved by inducing different amounts of defocus with the active elements of the system (SLM, Deformable mirror and Badal system) and with a calibrated element (trial lenses),

while measuring that defocus with the HS wavefront sensor. Measurements were performed with the artificial eye placed in the pupil plane of the system and for 555 nm. As shown in Figure 2.25, there was a good correspondence between the defocus induced with the different devices, thus all the devices of the system are properly aligned and calibrated.

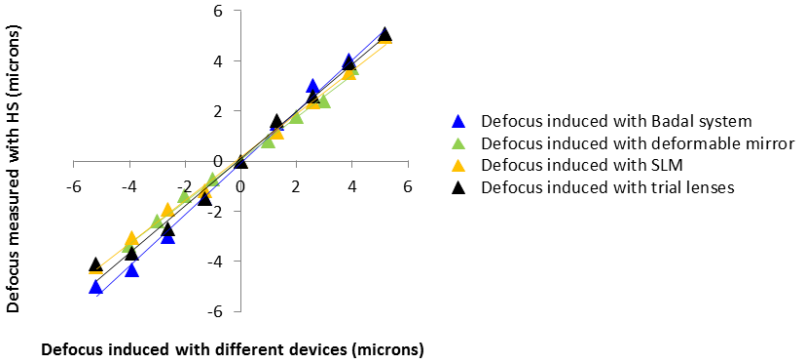

Figure 2.25 Calibration of the AO system. Defocus measured by the HS, as a function of the defocus induced with the different devices (Badal, blue; Deformable mirror, green; SLM, yellow; Trial lenses, black) for 555 nm.

B. Chromatic calibration of the AO system

A chromatic calibration of the setup was performed by measuring the system's aberrations, and estimating the chromatic difference of focus from the defocus Zernike coefficient (Z_2^0) at all wavelengths (450-1020 nm). For calibration, the beam coming from the SCLS was directed (using mirrors but not lenses) to a concave mirror at far distance (1 m from the pupil plane of the system) that created a virtual point source, the same at all wavelengths. Using mirrors instead of lenses has some advantages: they have no chromatic aberration, have no back reflections, and provide the flexibility to make the optical system more compact (by folding the beam) [36]. The light reflected from the concave mirror traversed the system in one-pass and was collected by the HS wavefront sensor, while the electromagnetic deformable mirror corrected for the aberrations of the system. These measurements were compared with those obtained using the artificial eye in place of the patient's eye.

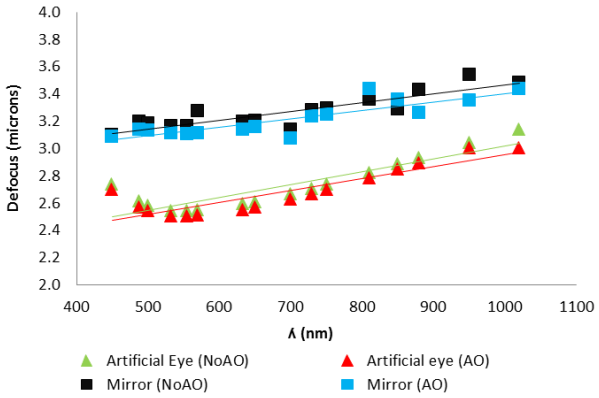

Figure 2.26 Chromatic calibration of the polychromatic AO system. Results in term of measured Zernike defocus term (in µm) for different wavelengths in the VIS and NIR range (450 to 1020 nm) with the concave mirror (squares) and the artificial eye (triangles), with and without correction of the aberrations of the system

The results of the calibration, in term of measured Zernike Defocus term (µm) for all wavelengths (450 to 1020 nm) with the concave mirror and the artificial eye, with and without correction of the aberrations of the system, are shown in Figure 2.26. Both methods provided similar setup's LCA values (within 4%). In the visible range, from 450 to 700 nm, the measured setup's LCA was negligible ~0.00 D. This was expected, as all lenses in the system are achromatic doublets for visible light. In the range from 700 to 1020 nm it was 0.29 D.

2.2.3.6 Daily calibration of the AO system

A series of calibration tasks are performed daily with the artificial eye before each experimental session to ensure proper performance of the AO system.

SCLS is tested spectrally and in terms of power to ensure safety levels. First the different λ-channels are checked with the spectrometer. Second the power for the used wavelengths is measured with a power meter placed in the pupil plane of the system to ensure laser safety power levels.

Pupil planes-Pupil camera alignment is checked daily. A graph paper (6 mm side squared) is placed in the pupil plane of the system and it is back-illuminated with a white light lamp. Proper size and centration in the different pupil planes is checked (AP-PP, deformable mirror and HS wavefront sensor). Figure 2.27 shows the appearance of the graph paper through the system in the HS wavefront sensor, allowing checking the magnification and centration with precision of µm. Once the pupil planes are checked, alignment of the pupil camera is checked by imaging the same graph paper, and displacing the camera if needed.

Psychophysical Channel-Retinal planes alignment is also revised daily by projecting some image on the DMD and testing the size and position on the E-RP, by means of a white light lamp and a graph paper.

The AO Channel is calibrated daily. The 4 steps described in *Section 2.2.3.3* – wavefront measurement, Interaction Matrix acquisition, Command Matrix construction, Closed-Loop Correction of the system aberration – are performed daily with the artificial eye before each experimental session. The interaction matrix is constructed for the full pupil diameter, and the correction performed for a given pupil diameter (depending on the psychophysical experiment, typically 5 or 6mm pupil diameter are used). The corrected state of the mirror named "flat mirror" is saved for a future use in order to ensure an adequate measurement of natural aberrations. This 4 steps-process is performed at 827 nm.

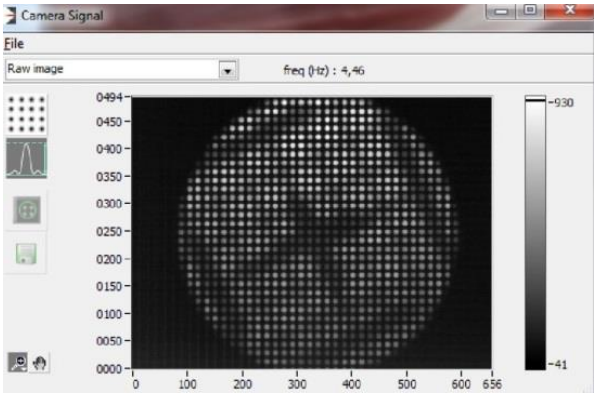

Figure 2.27 Image of a graph paper (6 mm size) placed in the pupil plane of the system seen through the system and image in the HS wavefront sensor to verify centration and magnification in the pupil planes.

2.2.4 Automatic control interface

The AO system is controlled using custom routines written in Visual C++ (with the use of DLL libraries), C# and Matlab. Two different synchronized computers are used for the task, as shown in Figure 2.28. The first computer controls the Illumination Channel (the SCLS and 2 shutters), the AO Channel (Deformable mirror and HS wavefront sensor), the pupil camera and the motorized Badal system, while the second computer controls the Spatial Light Modulator Channel (SLM), the Retinal imaging Channel (scientific-grade CCD camera), and the psychophysical Channel (Digital micro mirrors device and ViSaGe psychophysical platform).

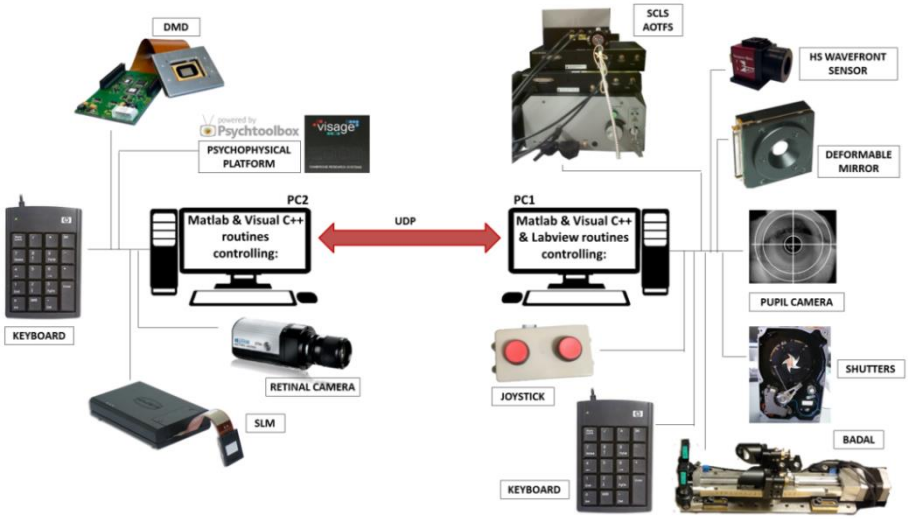

Figure 2.28 Schematic diagram showing the organization and control of the main devices of the AO system using the 2 different synchronized computers. UDP: user datagram protocol.

The two computers are synchronized using the User Datagram Protocol (UDP) for (1) a rapid presentation of visual stimuli under controlled aberrations (AO correction/ aberrations induction) and best spherical error correction (Badal System) of the subject when needed, and (2) fast synchronization of the retinal camera and the Badal system to obtain retinal aerial images, while the Badal system was moved to perform a through focus movement.

The Interface program of the AO system allows control of the SCLS and the AOTFs to modify power and wavelength, measurement, correction induction of ocular aberrations, monitoring the pupil, and automatized displacement with the motorized Badal system. A secondary program allows synchronization between the retinal camera (PC2) and the Badal system (PC1).

2.2.4.1 AO system control software

A custom-made platform was developed to control the main components of the system in both computers, with programs written in Visual C++, C# and Matlab. The platform comprises different modules to control the different Channels and it is shown in Figure 2.29.

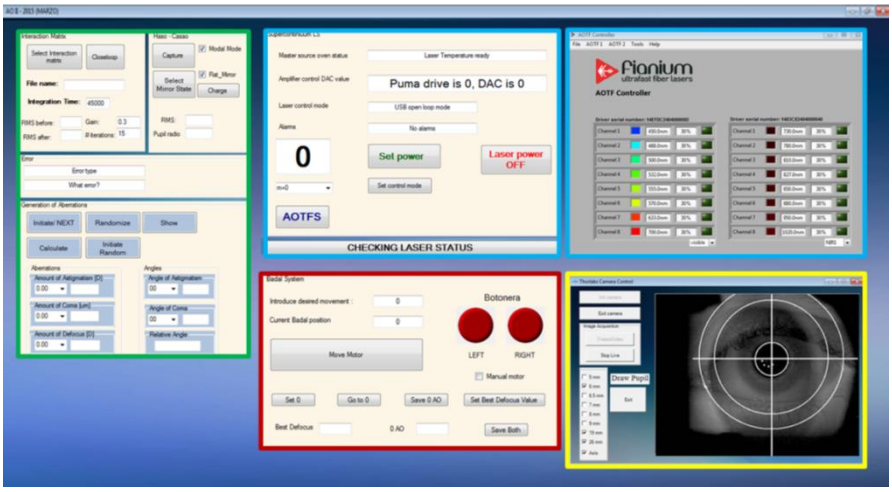

Figure 2.29 Visual C++ interface for the control of the AO system: Badal system module (red box), AO Channel module (green box), SCLS and AOTFs module (blue box) and pupil camera module (yellow).

Badal system module

This module (Visual C++, red box) allows moving the motorized Badal system (in D or mm) and, therefore correcting for the refractive error of the subject or modifying the amount of induced defocus for other purposes. If the "manual motor" box is checked the subject controls the displacement of the Badal, while viewing a stimulus through the system using a keyboard (2/8 numeric button) or a joystick (2 buttons) (shown in Figure 2.29). The module displays the current Badal position and allows saving the different Badal positions.

Pupil monitoring

The "pupil camera" button (yellow box) calls for a C# module, which controls the CMOS camera. The pupil camera allows continuous viewing of the pupil and is used to center the eye during the measurements. A ring of LEDs is used to illuminate the pupil. The interface allows the user to draw circles of different pupil diameters and an axis to assist centration, to save snapshot of the pupil or to capture a pupil video.

Illumination Channel

The SCLS module (Visual C++, blue box) allows controlling the power, mode control, and the status of the main source of the system. The "AOTFS" button calls for the AOTF module control provided by the manufacturer, which allows charging the different calibration curves (VIS or NIR) and selecting the desired wavelength.

AO Channel

This module allows the control of the deformable mirror and HS wavefront sensor and was built with used libraries available in Visual C++ (Software Development Kit,

Imagine Eyes). This module comprises three subsections: interaction matrix, Haso-Casao and generation of aberrations.

➔Interaction matrix section
This section sets the parameters used in the program: Integration Time for the HS acquisition (displayed in micro seconds) and set by default at 45ms; the Gain (0.3 by default) and the number of iterations used in the Closed-loop Correction and Aberrations induction modules (15 iterations by default). The default values can be modified by the user. This section, by the "Select interaction matrix" button, also allows selecting or acquiring the interaction matrix necessary for the closed-loop correction of aberrations. An interaction matrix is obtained prior to a daily experimental calibration session. The corresponding interaction matrix can be selected from a list of saved files. This interaction matrix is necessary to perform a closed-loop correction or induction of aberrations in the corresponding modules. Finally, the "close-loop" button allows the correction of the subject's aberrations. This section allows performing a closed-loop correction in N iterations – N being the number of iterations displayed in the Parameters module. An excel file saved all the Zernike coefficients, along with pupil diameter. The state of the mirror at the end of the closed-loop is saved for a future use and will be available in the "Select Mirror State" of the aberrations.

➔Haso-Casao section
This section allows measurement of the subject's aberrations. The "Capture" button is clicked to perform the measurement. The estimated Zernike polynomials from a HS measurement are written in an Excel file along with the pupil diameter. The RMS value of the last measurement is calculated and automatically displayed in the dialogue box "RMS". This is particularly useful when measuring aberrations under AO-corrected state of the mirror. Modal Mode is used along with a Zernike reconstruction under a round pupil (always checked by default). The "Select Mirror State" button allows selecting from different states of the deformable mirror (for example a closed-loop correction or particular aberrations induction states). The "Flat mirror" – obtained during the daily calibration - corresponds to the system aberrations correction state and allows performing measurements under the natural aberrations of the subject's.

➔Generation of aberrations section
This module controls the induction of individual selected aberrations required in several experiments (astigmatism, coma and/or defocus) by creating a specific state of the mirror. The button "Calculate" performs the closed-loop induction in N iterations and saves the deformable mirror state for future use (and made available in the "Select Mirror State" of the Aberrations Measurement module). Along with the mirror state, the data (Zernike coefficient and pupil diameter) is saved in an excel file in each iteration.

2.2.4.2 Psychophysical Channel software

Dedicated routines in Matlab were developed to control the ViSaGe psychophysical platform, the DMD and the SLM to allow the presentation of different visual stimuli under manipulated optics conditions, while controlling the aberrations with the AO Channel.

2.2.4.3 Retinal imaging Channel interface

A dedicated interface was programmed in C# to simultaneously allow the control of the retinal camera (PC2) and the motorized Badal system (PC1). For these 2 devices, the two computers are synchronized using an Ethernet connection. The interface in PC2 (Figure 2.30 (a)) sets the parameters of the image capture (exposure time, gain, offset), launches the capture of the images after activating the interface in PC1. The interface in PC1 (Figure 2.30 (b)) is activated from PC2 and moves the motorized Badal system every time that the retinal camera captures an image through a defined range in the Badal.

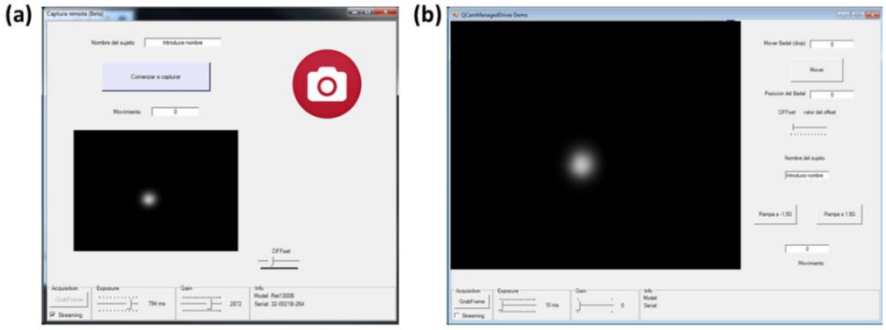

Figure 2.30 Visual C++ interface for Retinal imaging Channel control in (a) PC2, where the image parameters are modified (exposure time, gain, offset), and (b) PC1, which controls the position of the motorized Badal system.

2.3. Different measurement procedures with the AO systems

2.3.1 General protocols with human subjects

Ethics Statement

A total of 45 subjects, with different refractive profiles according with each study, participated in the different experiments described in this thesis. All of them were acquainted with the nature and possible consequences of the study and provided written informed consent before enrolment in the study. All protocols met the tenets of the Declaration of Helsinki and had been previously approved by the Spanish National Research Council (CSIC) Bioethical Committee.

Refraction measurements
Subjects participating in the different experiments followed an exhaustive optometric evaluation at the School of Optometry Clinic of the University Complutense of Madrid (UCM), in which they were classified according to their visual profile. Subjects implanted with IOLs (Chapter 6) received a complete ophthalmic evaluation prior to enrollment in the study and surgery at the Instituto de Oftalmología Avanzada (Madrid, Spain). Finally, prior to the experiments, the subject's refraction was measured, which allowed an initial setting for defocus correction in the Badal system. Measurements were performed using the Automatic Refractor Model 597, Humphrey-Zeiss.

Alignment of the eye and pupil monitoring
Subjects are fixed to the system by means of a dental impression mounted on a xyz linear stage, while looking at a Maltese cross projected on the DMD. Their pupil is monitored on the pupil monitoring system, focused, and its center aligned with respect to the optical axis of the system. In some studies (Chapter 3) the measurements were performed under natural viewing conditions. Most experiments (*Chapters 4, 5, 6* and *7*), were performed under mydriasis (Tropicamide 1%, 2 drops 30 minutes prior to the beginning of the study, and 1 drop every 1 hour).

Refractive error correction with the Badal System
The subject is asked to adjust the best subjective focus (starting from a myopic defocus) by controlling the Badal system with a keyboard while looking at fixation stimuli (Maltese cross projected on the DMD), under his/her natural aberrations. The Badal system is used to correct the defocus of the subject instead of the deformable mirror, due to the chromatic difference of focus between the infrared aberration-measurement Channel and the visible psychophysical Channel. Best subjective focus is obtained for the different states of aberrations under test.

2.3.2 Measurement, correction and induction of aberrations of the human eye

Once the subject is properly aligned, a first wavefront measurement is performed (flat mirror; 827 nm) to obtain the natural aberrations of the subject. Afterwards, a close-loop correction of the natural aberrations of the subject is performed, and the state of the deformable mirror is saved and applied accordingly to the type of the performed experiment. In normal subjects, an AO-correction is considered satisfactory if the residual aberration is lower than 0.2 µm (in most cases the residual is around 0.1 µm). A close-loop correction (at a rate of 13 Hz) is typically achieved in 15 iterations.

To check the validity and stability of the AO-correction, a measurement of the wave aberrations with the newly generated mirror state is performed and the residual RMS is checked. The experiments are performed under static corrections of aberrations. Pupil monitoring and aberration measurements are performed immediately before and after each experiment, to ensure proper centration and AO-correction.

2.3.3 Measurement of the longitudinal chromatic aberration of the human eye

For measurements of the LCA of the human eye, once the subject is properly aligned the best subjective focus is initially searched with the stimulus illuminated at reference wavelength of 555 nm. All settings are referred to the best subjective focus at this wavelength obtained with either natural or AO-corrected aberrations.

A wavefront measurement is performed (flat mirror) to obtain the natural aberrations of the subject and the state of the mirror that compensates for the ocular aberrations of each eye is found in a closed-loop operation at 827 nm (NIR), and applied in measurements at all wavelengths. Aberrations are monitored throughout the experiment to ensure that each measurement is performed under the desired state of aberration corrections. Experiments are performed first under natural aberrations and then under AO-correction. The following measurements of the LCA are performed, in this order:

Psychophysical best focus. Subjects adjust their best subjective focus using the Badal system while looking at the stimulus illuminated with a series of wavelengths in visible light.

Through-focus double pass retinal aerial images at different wavelengths. Retinal aerial images are obtained while the Badal system is moved in a through focus around the best subjective focus at 555 nm). These measurements are obtained both in visible light and near IR light.

Hartmann-Shack wave aberrations at different wavelengths. Wave aberrations are measured in visible light and near IR light, while the Badal system corrects the subject's subjective defocus at 555 nm.

2.4. Psychophysical experiments

2.4.1 Visual stimuli and retinal blur manipulation

Different stimuli were used in the experiments (shown in Figure 2.31), depending on the performed psychophysical tasks. Perlin noise texture (a) and E Snellen chart at 8 orientations (b) were used in the astigmatism experiments (*Chapter 3* and *4* respectively) performed in the VioBio lab AO system. The sunburst chart (c) monochromatically back-illuminated was used in the chromatic aberration experiments (*Chapters 5* and *6*), while the binary noise pattern (d) was used in the multifocal designs experiment (*Chapter 7*), both performed in the Viobio Lab AOII system.

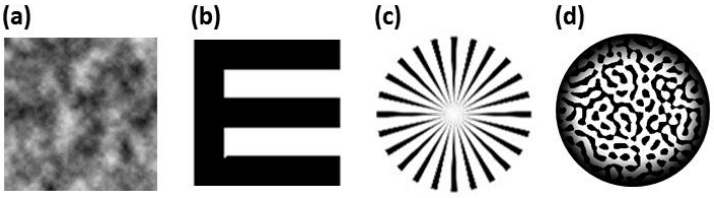

Figure 2.31 Stimuli used in different experiments. (a) Perlin noise texture (b) E Snellen (8 orientations) (c) Sunburst chart (d) Binary noise pattern with sharp edges at random orientations.

The texture and the tumbling E letter were presented on the CRT monitor of the Viobio lab AOI system, whereas the noise pattern was presented on the DMD of the Viobio Lab AOII system. The sunburst chart was a back-illuminated slide with light coming from the SCLS. In the AOI stimuli subtended 1.98 degrees, while in the AOII stimuli subtended 1.62 degrees.

Adaptive Optics allow to cancel the natural aberrations of all subjects, exposing observers to identical aberration patterns and ensuring that any difference across subjects would arise from their own neural processing and their prior neural adaptation. In the experiment presented in *Chapter 3* natural aberrations of the subjects were AO corrected with the deformable mirror, while the retinal blur was manipulated by projecting stimuli (Perlin noise texture) blurred by convolution with known aberrations. The PSF was scaled to match the pixel size of the original image. All computations were performed for a constant pupil diameter (6mm pupil). The Stiles - Crawford effect was not considered, as for typical ρ values ($\rho < 0.10$) [20, 195] its effect was negligible for the purposes of the study. Simulations revealed that the effect on the final contrast of convolved E targets with similar levels of blur to those used on the experiment was less than 10% with respect to the contrast obtained without including these two factors [20].

Standard Fourier optics techniques (Goodman, 1996), including the Fast Fourier Transform (FFT) programmed in Matlab, were used to generate the convolved images. In experiments presented in *Chapter 4* and *7*, induction of aberrations and subsequent manipulation of retinal blur, was performed by means of the deformable mirror (E Snellen) and the SLM (binary noise).

2.4.2 Visual psychophysical techniques used under AO-controlled aberrations

Different psychophysical experiments have been developed throughout the thesis for testing visual performance or neural adaptation to ocular aberrations and/or manipulated optics and to measure chromatic aberration. Subject's responses were recorded (using a keyboard or a specific 2-response joystick).

Astigmatism: visual perception
The experiment was designed to test potential shifts of the perceived neutral point before and after adaptation to different conditions, by using a psychophysical test. A series of artificially blurred images (Perlin noise), with constant blur strength, but orientation tuned to the axis of natural astigmatism of the subjects, were used to estimate deviations from the isotropically blurred image.

Subjects performed a single stimulus detection task, in which the observer sets his /her own internal criteria for response (in this case, their perceived neutral point) [196]. The psychophysical paradigm consisted of a single interval orientation identification task [144, 197], used to detect the threshold for astigmatism orientation, while using a QUEST (Quick Estimation by Sequential Testing) algorithm (maximum likelihood estimator, from the Psychtoolbox package)[191] to calculate the sequence of presented stimulus (level of astigmatic blur in the image) in the test, following the subject's response. The subject had to report the perceived orientation (between two different axes) from a series of images in order to estimate the threshold/ perceived isotropic point (the image that appears non-oriented to the observer). The QUEST routine usually converged after less than 40 trials, where the threshold criterion was set to 75%. The threshold was estimated as the average of the 10 last stimulus values, which oscillated around the threshold with standard deviation below 0.03 µm.

Astigmatism: visual performance
VA was measured using an 8-Alternative Forced Choice (8AFC) procedure [196] with tumbling E letters and a QUEST (Quick Estimation by Sequential Testing) algorithm programmed with the Psychtoolbox package [191, 192], to calculate the sequence of the presented stimulus (letter size and orientation) in the test, following the subject's response. Subjects had to determine the orientation of the letter E (8 orientations; pointing up, down, left, right, oblique up-right, oblique-up-

left, oblique-down-right, oblique down-left), while aberrations were controlled with the deformable mirror.

The QUEST routine for each VA measurement consisted in 50 trials, each one presented during 0.5 s, where the threshold criterion was set to 75%. The threshold, VA measurement, was estimated as the average of the 10 last stimulus values. VA was expressed in terms of decimal acuity (logMAR= - log10(decimal acuity)) [198].

LCA: psychophysical best focus
Subjects adjusted their best subjective focus using the Badal system while looking at the visual stimuli back-illuminated with a series of wavelengths in visible light.

Presbyopic multifocal designs: visual perception
In a psychophysical paradigm, 2AFC weighted response, the subject saw the stimuli (binary noise) through different pairs of multifocal patterns (a total of 210 pairs, randomly presented, each condition and testing distance), and judged the better perceived pattern (first or second) providing a weighted response (±10, ±5 & ±1). The relative perceived visual quality is the sum of all, positive and negative, weighted responses of the different subjects for each phase pattern and all conditions.

3

Perceptual Adaptation to the Correction of Natural Astigmatism

The visual system adjusts to changes in the environment, as well as to changes within the observer, adapting continuously to maintain a match between visual coding and visual environment. In the current Chapter we evaluate whether the perception of oriented blur is biased by the native astigmatism, and studied the time course of the after-effects following spectacle correction of astigmatism in habitually non-corrected astigmats.

This Chapter is based on the paper by *Vinas et al. "Perceptual adaptation to the correction of natural astigmatism" in PLoS ONE (2012)*. The co-authors of the study are Lucie Sawides, Pablo de Gracia and Susana Marcos.

The author of this thesis (1) implemented the experimental procedure, (2) performed the measurement on human eye's, (3) collected the data, (4) analyzed the data (in collaboration with Lucie Sawides and Susana Marcos) and (5) prepared the manuscript (in collaboration with Susana Marcos). This work was also presented as an oral contribution at the Association for Research in Vision and Ophthalmology (ARVO) annual meeting (2012) in Fort Lauderdale (Florida, USA); Parts of this work were also presented as an oral contribution at the 8th Workshop on Adaptive Optics for industry and medicine (2012) in Murcia (Spain); and as a poster contribution at the III Engineering the eye (2011) in Benasque (Spain) and at the IONS 2012 in Paris (France).

3.1 Introduction

Adaptation to astigmatism, and in particular, to a newly prescribed correction of astigmatism, is particularly relevant clinically, where the optometrist or the surgeon faces the decision of astigmatism correction by spectacles, contact lenses, intraocular lenses or corneal surgery. In a recent study Sawides et al. showed strong after-effects after brief periods of adaptation to images blurred with astigmatism (while keeping the blur strength constant), indicating that adaptation can be selective to the orientation of astigmatism [75]. Ohlendorf et al. reported an increase of visual acuity in normal subjects viewing dynamic astigmatic images (either simulated, or through +3 D cylindrical lenses) after 10 min of adaptation, with a significant meridional bias [199]. Potential common mechanisms underlying adaptation and perceptual learning have also been explored using induced astigmatism as a probe. Yehezkel et al. (2010) pointed that the process of adaptation to astigmatic lenses (2 and 4 hrs) might exhibit forms of learning. The course of this adaptation, presence of after-effects, and accumulative effects over sessions (consistent with perceptual learning) differed in two groups of subjects, treated monocularly with the contralateral eye covered or uncovered (dichoptic group), indicating a binocular cortical site of adaptation [130].

The previous studies investigated the pattern of adaptation to astigmatism in non-astigmatic eyes. In the current *Chapter* we will investigate the adaptation process to an astigmatic correction in astigmatic subjects. A previous study suggested that habitually non-corrected astigmats were adapted to their astigmatism, as their measured visual acuity was less impaired by the induction of astigmatism than in non-astigmatic subjects with the same amount of induced astigmatism[94]. This may be also the result of a form of perceptual learning. A similar finding has been described in keratoconic patients (with highly optically degraded corneas), who showed a better performance than normal subjects with simulated identically degraded optics [120, 143]. However, to our knowledge the course of neural adaptation to an astigmatic correction has not been investigated.

This *Chapter* investigates neural adaptation to astigmatism by measuring the astigmatic stimulus level which appears neutral (non-oriented) in corrected-astigmats, and in the latter-corrected astigmats, and subsequently, after an astigmatic prescription was given to the astigmats (2 hours to 6 months). We expect that the level of astigmatism that appears neutral (non-oriented) to the subjects corresponds to a perceptual norm, which reflects a balance in the underlying neural response. To what extent this perceptual norm changes after adaptation to a refractive correction, and the time course for this adaptation has not been, to our knowledge, investigated before.

Alternatively, these experiments will allow exploring whether there may be learned properties in astigmats, which may persist despite the presence of an adapting

stimulus. A previous study [130] actually pointed out to the learned ability of storing multiple transformations of the visual world, allowing observers to switch between two different optical corrections that induced different visual distortions.

3.2 Methods

The experiment was designed to test potential shifts of the perceived neutral point of the astigmatic subjects before and after adaptation to a new astigmatic spectacle correction in comparison with non-astigmats and habitually-corrected astigmats, by using a psychophysical test. A series of artificially blurred images, with constant blur strength, but orientation tuned to the axis of natural astigmatism of the subjects, were used to estimate deviations from the isotropically blurred image.

3.2.1 Subjects

The sample consisted of 21 subjects (ages ranging from 23 to 51 years (31.77 ± 7.99)). Subjects were selected *a priori*, and classified according to their natural astigmatism and whether this was habitually corrected or not.

The subjects were classified in three groups (n=7 per group): G1 (control group of subjects with no clinical astigmatism); G2 (astigmatic subjects, habitually corrected, wearing an astigmatic correction since childhood); G3 (astigmatic subjects, habitually-non-corrected). The inclusion criterion for G1 was that astigmatism was lower than 0.25 D. Inclusion criteria for G2 and G3 were: (1) natural astigmatism ≥ 0.75 D; (2) Myopic astigmatism. Tests were performed only on one eye per subject (less myopic eye in G1; and less myopic eye with ≥ 0.75 D of astigmatism in G2 and G3). All subjects in G3 were provided with astigmatic spectacle correction of their natural astigmatism after an initial test.

Table 3.1 shows the profile and refraction state of all subjects of the study (the measured eye indicated in bold). For G2, spherical error ranged from -5.25 to 0.25 D (mean -2.56 ± 1.87 D), while for G3 spherical error ranged from -1.50 to 0.25 D (mean -0.39 ± 0.64 D). Refractive errors were measured using standard clinical optometric procedures.

	Subject's profile							
	OD			OD				
ID	Sph	Cyl	Axis	Sph	Cyl	Axis	Blur axis (degree)	Age (year)
G1_A	**0.50**	--	--	0.50	--	--	--	29
G1_B	**0.00**	--	--	0.00	--	--	--	33
G1_C	**0.00**	--	--	0.00	--	--	--	31
G1_D	**0.00**	--	--	0.00	--	--	--	30
G1_E	**-0.25**	**-0.25**	**80**	-0.25	--	--	170	30
G1_F	**0.25**	**-0.25**	**90**	0.25	-0.25	80	90	34
G1_G	**0.00**	--	--	0.00	--	--	--	23
G2_A	**-3.50**	**-1.00**	**10**	-4.00	-1.25	170	100	33
G2_B	**-5.25**	**-1.25**	**105**	-6.00	-1.50	90	15	27
G2_C	**-4.00**	**-1.00**	**75**	-3.75	-0.50	115	165	34
G2_D	**-0.75**	**-1.25**	**90**	-1.25	-0.75	85	0	30
G2_E	**-2.25**	**-0.75**	**90**	-2.00	-0.75	90	0	51
G2_F	-4.50	-0.50	30	**-1.75**	**-1.00**	**170**	80	31
G2_G	0.25	-1.00	175	**0.25**	**-1.25**	**175**	85	23
G3_A	**-1.50**	**-0.75**	**10**	-1.50	-0.75	155	100	27
G3_B	0.25	-1.75	95	**0.00**	**-1.25**	**80**	170	29
G3_C	**-0.75**	**-0.75**	**120**	-1.00	-0.50	40	30	27
G3_D	**0.50**	**-0.75**	**170**	2.00	-5.00	175	170	27
G3_E	-0.75	-0.75	130	**-0.75**	**-0.75**	**175**	85	48
G3_F	-1.25	-0.50	90	**-1.00**	**-0.75**	**90**	0	45
G3_G	**0.00**	**-1.00**	**90**	0.25	-1.00	75	0	26

Table 3.1 Subjects' profile. Optometric subjective refractions (spherical error, cylinder, axis), orientation of the retinal blur, and ages. The measured eye is shown in bold. G1 non-astigmats, G2 habitually-corrected astigmats and G3 habitually-non-corrected astigmats. Cyl, cylinder; Sph, spherical error.

3.2.2 Generation of the test images

A Perlin noise image was used as a stimulus test (480 x 480 pixels, 1.98 deg angular subtend). Perlin noise is a procedural texture based on lattice gradient noise [200], which is easily modulated using two computational parameters, the base frequency and persistence [201]. This type of noise produces a repeatable pseudo-random value for each input position, has a known range and band-limited spatial frequency, does not show obvious repeating patterns, and its spatial frequency is invariant under translation [202], which makes it especially suitable for studying astigmatic images. The Perlin noise image was generated with a Perlin Noise Generator Software [203], with the following inputs: persistence 0.7; octaves 8; zoom 16; random seed; normalized noise. The root-mean-square (RMS) contrast of the stimuli was 0.69 calculated following Peli et. al (1990) [204]. Images were blurred using custom algorithms to simulate optical blur by convolving the images with the point spread functions (PSF) corresponding to different levels of astigmatism and defocus, but constant blur strength.

Blur strength (B) is typically defined as

$$B^2 = M^2 + J_0^2 + J_{45}^2 \qquad (3.\ 1),$$

where **M**, $\mathbf{J_0}$, and $\mathbf{J_{45}}$, in diopters, represent equivalent defocus, vertical/horizontal astigmatism, and oblique astigmatism, respectively [38]. *Equation (3. 1)* expressed in microns is as follows:

$$K^2 = 2(C_2^0)^2 + (C_2^{+2})^2 + (C_2^{-2})^2 \qquad (3.\ 2),$$

where $\boldsymbol{C_2^0}$, $\boldsymbol{C_2^{+2}}$ and $\boldsymbol{C_2^{-2}}$ are the Zernike terms for defocus, vertical and oblique astigmatism respectively, and

$$K^2 = (r^4 * B^2)/24 \qquad (3.3)$$

(with $\boldsymbol{r}$ = pupil radius in meters). Each combination of astigmatism and defocus produced the same amount of blur strength (B = 1.5 D in diopters, or K = 2.75 µm in microns). For example, to generate a set of images varying from astigmatism at 0 to 90deg, $\boldsymbol{C_2^{-2}}$ was set to 0, and $\boldsymbol{C_2^{+2}}$ was varied from -2 to +2 µm in 0.02 µm steps (or equivalently from -1.09 to 1.09 D in 0.01 D steps).

Simultaneously, the defocus term was varied to keep the blur strength constant between 1.34 µm (or -1.03 D) when astigmatism was ±2 µm, and 1.95 µm (or -1.5 D) when astigmatism was set to 0, using similar procedures to those described by Sawides et al. 2010 [75].

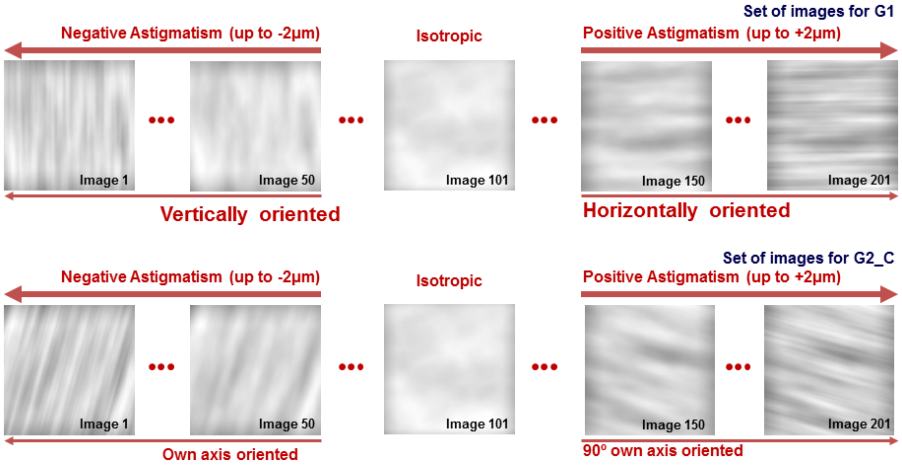

Figure 3.1 Examples of test images series. Astigmatic blur was generated by varying astigmatism (from -2 µm to +2 µm), and defocus to maintain constant blur strength (B=1.5 D). Image 101 was isotropically blurred. Top panel: image series presented to all subjects from G1, with vertically oriented blur (images 1-100) to horizontally oriented blur (images 102 to 201). Bottom panel: an example of image series presented to G2/G3 (the example corresponds to G2_C in particular, with images blurred along the axis of natural astigmatism of the eye (75 deg) to a 90 deg rotated axis (165 deg).

In G1 the axis of astigmatic blur varied from 0deg to 90deg (vertically to horizontally oriented astigmatic blur). In G2 and G3 the axis of astigmatic blur was matched to the subject's axis of natural astigmatism, varying the orientation of astigmatic blur following the natural axis of astigmatism to a 90 deg rotated axis.

A total of 201 images were generated for each test, with constant blur and varying relative contribution of defocus and astigmatism (ranging from negative to positive). Figure 3.1 shows a typical example of sets of test images for G1 subjects (upper panel) and for one of the astigmatic subjects (lower panel), G2_C (Astigmatism: -1.00 x 75 deg).

3.2.3 Experimental protocol and psychophysical paradigm

The Viobio Lab AO I custom-made Adaptive Optics system [83, 84, 89] was used to characterize and correct the aberrations of the subject, therefore controlling the blur of the images projected on the retina. In this experiment, visual stimuli were presented on a CRT monitor (Mitsubishi Diamond Pro 2070) through the Badal and AO mirror correction. The stimulus display was controlled by the psychophysical platform ViSaGe, (Cambridge Research System, UK). The average luminance (after losses in the system) was around ~30cd/m^2 in an otherwise dark environment.

Measurements were performed monocularly, for 6-mm pupils (limited by an artificial pupil), under natural viewing conditions and naked eyes in a darkened room. Measurements were performed always in the same eye of the subject. The eye's pupil was aligned to the optical axis of the instrument, and the subject's was stabilized using a dental impression. Astigmatism and high order aberrations were measured and corrected in a closed loop adaptive optics operation. The subject was then asked to adjust the Badal system position to achieve best subjective focus. The state of the mirror that achieved the correction was saved and applied during the measurements. Psychophysical measurements were performed under full static AO-corrected aberrations and best spherical refraction error correction.

Subjects performed a single stimulus detection task, in which the observer sets his /her own internal criteria for response (in this case, their perceived neutral point) [196]. The psychophysical paradigm consisted of a single interval orientation identification task [144, 197], used to detect the threshold for astigmatism orientation, while using a QUEST (Quick Estimation by Sequential Testing) algorithm (maximum likelihood estimator, from the Psychtoolbox package) [191] to calculate the sequence of presented stimulus (level of astigmatic blur in the image) in the test, following the subject's response.

The subject had to report the perceived orientation (between two different axes) from a series of images in order to estimate the threshold/ perceived isotropic point (the image that appears non-oriented to the observer). The QUEST routine

usually converged after less than 40 trials, where the threshold criterion was set to 75%. The threshold was estimated as the average of the 10 last stimulus values, which oscillated around the threshold with standard deviation below 0.03 μm.

Before the measurement, subjects were instructed on the required responses according to their perceived image orientation. Non-astigmatic subjects and astigmatic subjects with natural astigmatism, which were presented with images oriented vertically or horizontally had to respond up or down respectively. Astigmatic subjects with astigmatism different form 0 deg or 90 deg were presented with images oriented at the axis of their natural astigmatism or at the perpendicular axis, and had to respond right or left respectively. Subjects used a response box from Cambridge Research Systems. The experiments were performed after the subject adapted for 5 s to gray field, and then the test images were presented for 1.5 s. The gray field was presented again between images, for 1 s, during which the subject had to respond.

Subjects performed the same astigmatic blur judgments in 4 different sessions for G1 and G2: first session (S0A), and after 1 week (S1), 1 month (S2), and 6 months (S3). G3 subjects were prescribed with spectacle refractive correction, which compensated their uncorrected astigmatism. Measurements in G3 were performed in a first session, before correction wear (S0A), on the same first day, after 2-hours of correction wear (S0B), and after 1 week (S1), 1 month (S2), and 6 months (S3) of astigmatic correction wear. Subjects G3_A and G3_B did not perform session S1. In each session, the test was repeated 4 times for each subject.

3.2.4 Control experiment: the oblique effect

It is well known that, even in the absence of astigmatism, oblique gratings are less visible than gratings oriented at 0/90 deg [75], and that orientation sensitivity is lower at oblique axes that at the cardinal axes [205]. Unlike for visual performance tasks [206, 207], previous studies have shown that both oblique and 0/90 targets are equally effective in an adaptation experiment [208].

Nevertheless, we conducted a control experiment to ensure that results on non-astigmatic subjects (where the adaptation test was performed using targets blurred along the cardinal axes) were not affected by the selected orientation. The experiment was performed on two non-astigmatic subjects (G0_A and G0_B; ages: 26 and 32; spherical error ≤ 0.25 D), with astigmatic blur imposed at 0/90 deg and at 45/135 deg.

3.2.5 Data analysis

The perceived isotropic image (which did not appear oriented to the subject) was measured for each subject and session, and the corresponding astigmatic blur and axis were estimated. Data were obtained from the image chosen as isotropic by each subject (4 repeated times per trial), converted into amount of astigmatism, and averaged to obtain the average perceived neutral point (in terms of microns of astigmatism) for each measurement session.

Shifts of the isotropic point from the first session (S0A) were analyzed to test potential longitudinal variations of the perceived isotropic point (and after correction of astigmatism in G3). Also, the total shift of the isotropic point (from S0A to S3) was analyzed as a function of the amount of natural astigmatism of the subjects. Statistical analysis with SPSS software (IBM SPSS Statistic Software) was performed to test differences in perception of neutral point across sessions (paired-samples t-test), and also to test the relationship between natural astigmatism and longitudinal variations, as well as the differences between groups and variables of the study (*one-way ANOVA*).

3.3 Results

Adaptation to astigmatism was measured with a series of psychophysical tests (under full-adaptive optics correction) in order to measure the perceived isotropic point (astigmatism level for which the image did not appear oriented to the subject) from images artificially blurred with constant blur strength but orientation tuned to the axis of natural astigmatism of the subjects.

3.3.1 Subjects' natural aberrations

Figure 3.2 shows the average ocular Root-Mean Square wavefront error (RMS) for high order aberrations (HOA) (RMS_{HOA}, blue bars), for HOA and natural astigmatism ($RMS_{HOA+ast}$, yellow bars), and for residual aberrations after AO-correction of all natural aberrations (RMS_{AO}, green bars), in each group. As expected, $RMS_{HOA+ast}$ was significantly higher for G2 and G3 than for G1 (*one-way ANOVA*; $F(2,18) = 6.881$, $p = 0.006$).

RMS_{HOA} was similar across the 3 groups (*one-way ANOVA*; $F(2,18) = 0.403$, $p = 0.674$), although the contribution of HOA to the $RMS_{HOA+ast}$ differs across groups: HOA contributes on average with 85% in G1, 36% in G2, and 33% in G3. The experiments were performed under correction of both HOA and astigmatism. RMS_{AO} was similar across the different groups.

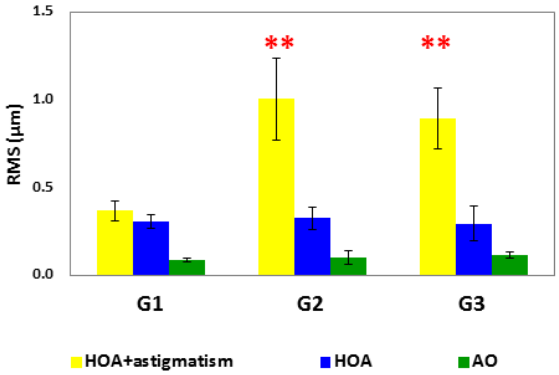

Figure 3.2 RMS wavefront error for natural aberrations for HOAs and astigmatism (yellow bars), HOAs (blue bars), and, residual aberrations after AO correction (green bars), averaged across subjects, groups and measurement sessions. G1 non-astigmats, G2 habitually-corrected astigmats and G3 habitually-non-corrected astigmats. Error bars indicate inter-subject variability. ** indicates a significantly larger RMS ($p < 0.01$) for HOA + astigmatism for G2 and G3 than for G1.

3.3.2 Shifts of the perceived neutral point

Potential changes in the perception of the neutral point of the subjects were studied. In the control experiment in two non-astigmatic subjects, the shift in the perceived neutral point for the two tested orientations was similar (G0_A: 0.13 µm for 0/90 deg and 0.14 µm for 45/135 deg; G0_B: 0.11 µm for 0/90 deg and 0.11 µm for 45/135 deg). Also, the perceived neutral point was not statistically significantly different from the isotropic point (*paired samples t-test*; $t(3) = 0.002$; $p > 0.6$).

Figure 3.3 shows the average deviations from the isotropic point (in terms of amount of astigmatism), obtained from the image chosen as isotropic by each subject (data averaged from the 4 repeated measurements in each session) in the QUEST procedure. For representation purposes we refer to positive perceived neutral point to that oriented vertically (G1) or to the axis of natural astigmatism (G2 and G3). Also, negative perceived neutral point is that oriented horizontally (G1) or that oriented perpendicularly to the axis of natural astigmatism (G2 and G3). The error bars represent the standard deviation for 4 repeated measurements in each subject.

Non-astigmats (G1, Figure 3.3 (a)) judged as isotropic images predominantly blurred by symmetric blur. On average, deviation from the isotropic point (absolute values) at S0A for G1 was 0.12 µm. Only G1_F and G1_G showed some bias towards horizontal and vertical astigmatism, respectively. Also, the perceived neutral point remained constant across sessions for all subjects in G1.

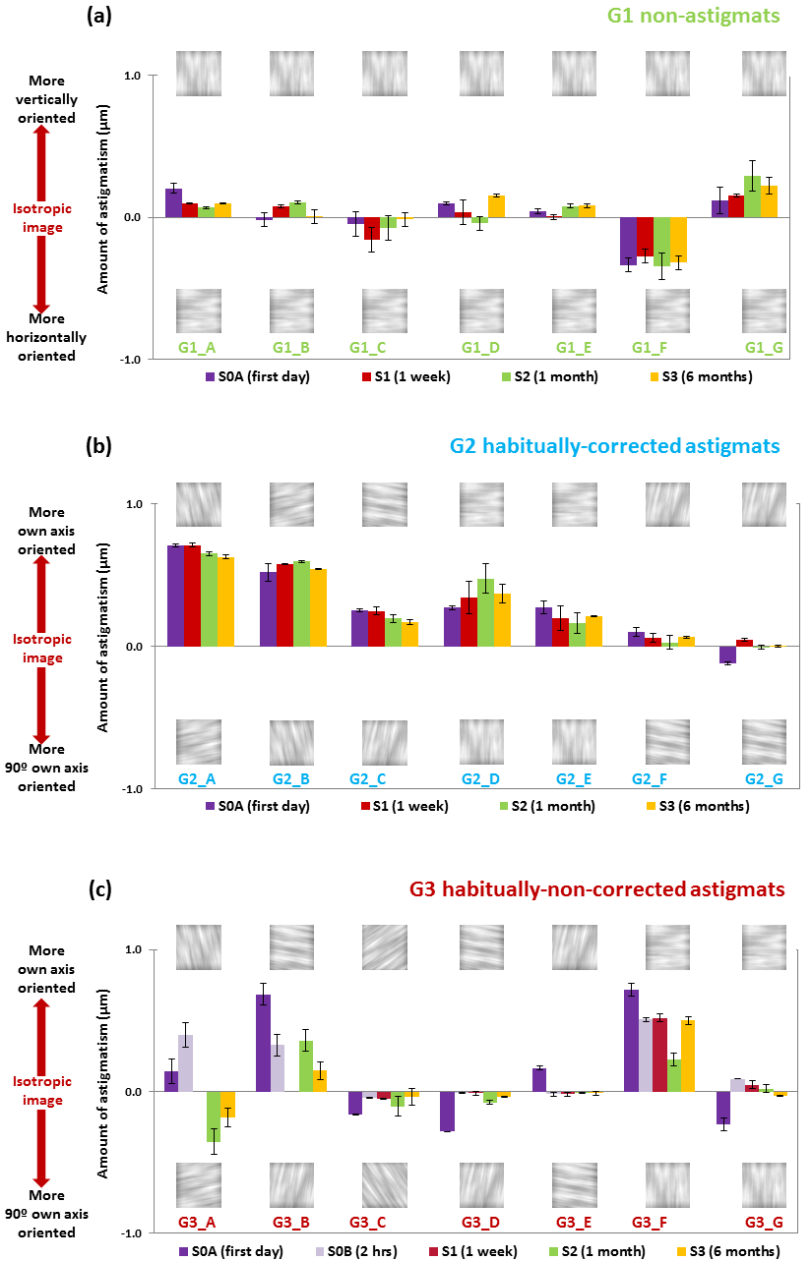

Figure 3.3 Perceived neutral point (µm of astigmatism) for all subjects and in all sessions (First session: purple bars; 2-hrs: violet bars; 1-week: red bars; 1-month: green bars; 6-months: yellow bars). A: G1, non-astigmats. B: G2, habitually-corrected astigmats. C: G3, habitually-non-corrected astigmats. For illustration purposes, the first and last images of the series are shown (-2 µm to + 2 µm of astigmatism). G1: 0deg/90 deg; G2 and G3: tuned to the axis of natural astigmatism/90 deg. Error bars stand for intra-subject variability (standard deviation) for repeated measurements (4 times/test).

Most of the habitually corrected astigmats (G2, Fig 3.3 (b)) showed a bias in the perceived neutral point towards their axis of natural astigmatism (Figure 3.3 (b)). On average, deviation from the isotropic point (absolute values) at S0A for G2 was 0.32 µm. Only the perceived neutral point in G2_F and G2_G showed little astigmatic bias. In general, the perceived neutral point remained constant across sessions for all subjects of G2.

All habitually-non corrected astigmats (G3, Fig 3.3 (c)) showed some bias for astigmatism before astigmatic correction (S0A). The perceived neutral point was biased towards images blurred along their axis of natural astigmatism in the majority (4/7) of the cases (G3_A, G3_B, G3_E and G3_F), although in three cases (G3_C, G3_D and G3_G) the bias was orthogonal to the orientation of the natural astigmatism. Despite this difference, all subjects from G3 did show a bias towards astigmatism in the first session, which was statistically significantly different from zero (one-sample t-test; $p<0.05$), and shifted towards more isotropic points in later sessions. On the other hand, most subjects in G1 (except for G1_F and G1_G; one-sample t-test; $p<0.04$) did not show a significant shift from the isotropic point. On average, the shift for G1 (0.13 µm) was not statistically significantly different from 0, but the shift for G3 (0.34 µm) was statistically significantly different from zero (one-sample t-test; $p=0.03$).

3.3.3 Time-course of the adaptation effect

Figure 3.4 (a) shows the averaged absolute shift from isotropy as a function of session, for each group. The perceived neutral point did not change statistically across sessions for G1 and G2. However, there was a significant shift in the perceived neutral point in astigmats (G3) upon correction of astigmatism (Figure 3.4 (b)). Very consistently, wear of the astigmatic correction shifted the perceived neutral point from the initial values. Two hours of astigmatic correction wear produced a significant shift (paired-samples t-test; $t(6)=5.494$, $p=0.003$) of the perceived neutral point, and a reduction of the astigmatic bias. This adaptation effect stabilized after 1 week of correction wear, and remained constant after 1 and 6 months of astigmatic correction wear, where shift was also statistically significant (*one-way ANOVA* $F(2, 18) = 6.227$, $p=0.009$). On average, the perceived neutral point (absolute values) was 0.20 µm at S0B (2hrs) and 0.14 µm at S3 (6 months).

Since perception of neutral point in G3 subjects is biased in two different ways (4 subjects biased along their axis of natural astigmatism, and 3 subjects in the perpendicular axis) in the initial session (S0A), we have also analyzed the longitudinal variations in these two subgroups independently, following the original bias towards their astigmatism (positive, G3_A, G3_B, G3_E and G3_F) or the perpendicular direction (negative, G3_C, G3_D and G3_G) (Figure 4 (b)). The shifts of the perceived neutral point at S0A were respectively 0.43 µm ± 0.16 and -0.23

µm ± 0.03 on average. Regardless the initial bias all subjects (except G3_A) shifted rapidly and consistently their perceived neutral point towards the isotropic point. Subjects with an initial bias perpendicular to the orientation of the natural astigmatism reached perceived neutral points closer to 0 (-0.04 µm ± 0.002 on average, at 6 months) than those with an initial bias parallel to the orientation of their natural astigmatism, which showed an average residual bias towards their natural astigmatism (0.21 µm ± 0.10 on average at 6 months). However, despite these differences, both sub-groups showed statistically significant longitudinal variations at 6 months (paired-samples t-test: G3 axis t (3) = 2.4999 p=0.04; G3 perpendicular axis t (2) = 1.1999 p=0.01).

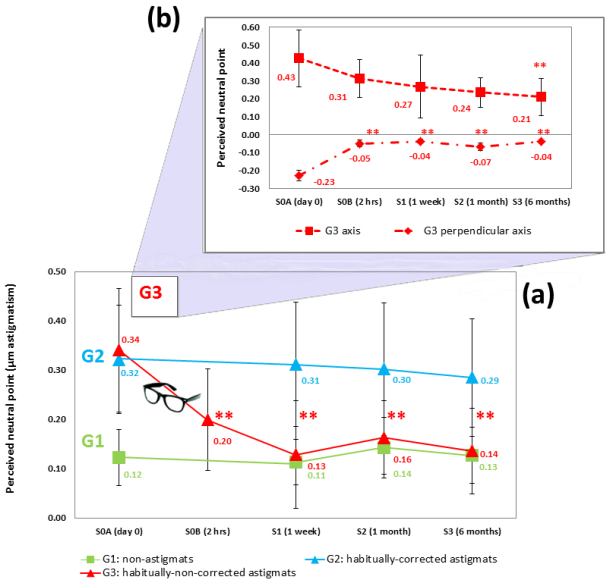

Figure 3.4 Perceived Longitudinal variations in the perception of neutral point. (a) Longitudinal variation of the perceived neutral point (µm astigmatism, absolute value), averaged across subjects in each group (G1: green squares; G2: blue triangles; G3: red triangles). (b) Longitudinal variations of the perceived neutral point (µm astigmatism) averaged across subjects of the 2 subgroups of G3: G3 axis (4/7 subjects) and G3 perpendicular axis (3/7 subjects). ** indicates statistically significant shifts ($p < 0.01$), from the first session to other measurement sessions (2hrs, 1 week, 1 month and 6 months) for G3 . Error bars stand for inter-subject variability (standard deviation).

3.3.4 Adaptation and amount of natural astigmatism

The shift of the perceived neutral point was analyzed as a function of the amount of natural astigmatism (Figure 3.5). The astigmatism was estimated from the second order Zernike terms (RMS in microns), obtained from wavefront measurements on naked eyes, without AO correction, and averaged across sessions. The shift of the perceived neutral point was estimated for S3 (6-month) session, with respect to S0A (First session). While there was no shift in the

perceived neutral point in G1 and G2, the shift of perceived neutral point was statistically correlated with the amount of natural astigmatism in G3 ($p < 0.01$). The amount of natural astigmatism of the G3 subjects was a significant factor in the shift of the perceived neutral point across sessions (*one-way ANOVA* F (2, 18) = 12.936, p=0.001).

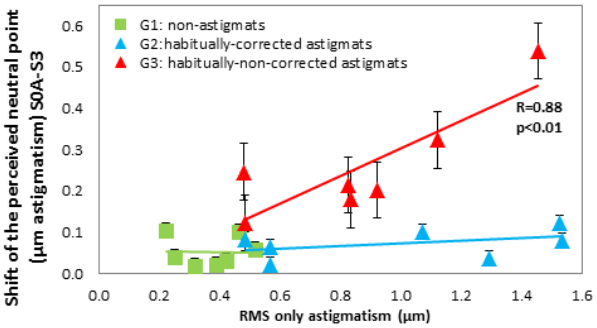

Figure 3.5 Correlation between the shift of the perceived neutral point and natural astigmatism of the subjects. Correlation between the shift of the perceived neutral point (difference between the perceived neutral point measured in the first session, S0A, and the 6-month session, S3) and the natural astigmatism for subjects. Astigmatism is represented in terms of RMS, in µm (G1: green squares; G2: blue triangles; G3: red triangles). Error bars stand for inter-subject variability (standard deviation).

3.4 Discussion

Perception of blur depends on the subject's previous visual experience. Some studies have reported changes in the perceived best focus after brief exposures to sharpened or degraded images, indicating that the visual coding can very rapidly recalibrate to a changing environment. Recently, Sawides et al. showed that the adaptation is also selective to orientation, thus the perceived neutral point shifts after a brief exposure to images blurred by horizontal or vertical astigmatism [75]. Also, longer exposures to blur have been reported to induce changes in visual acuity [120, 123, 141].

Adaptation to astigmatism has been previously reported. However, neural adaptation of uncorrected astigmats to an astigmatic refractive correction, and the time course for this adaptation, had not been explored before. The current study shows differences in the perception of the neutral point under natural adaptation across subjects with different refractive (and corrective profiles). The measurements were conducted under full correction of both low and high order aberrations, allowing identical image quality in all subjects. The observed differences in the perception of neutral point must therefore arise from differences in the internal norm for perception of oriented blur, which is highly dependent on prior visual experience. The change of this norm after compensation of astigmatism

(in a group of previously non-corrected astigmats) reveals rapid adaptability to a new astigmatic prescription.

As expected, for non-astigmats (G1) the perceived neutral point was close to isotropic, and remained stable with time (Figure 3.3 (a), Figure 3.4). As per our control experiment, the effect is similar regardless the orientation of astigmatic blur (cardinal or oblique axis), indicating that the oblique effect [209] does not influence the internal code for blur orientation. This finding goes along with a previous report, which showed that oblique gratings were at least as powerful as horizontal gratings as adapting stimuli [208]. Interestingly, a previous study suggested that the oblique effect anisotropy in fact does not occur when viewing complex visual stimuli with broadband spatial content (such as natural scenes, or likely the noise stimulus used in our study [205].

All habitually-non-corrected astigmats (G3) showed a perceived neutral point shifted from isotropy before astigmatic correction wear (S0A), and in 4 out of 7 subjects, the shift occurred towards the orientation of their uncorrected astigmatism (Figure 3.3 (c), Figure 3.4). The largest shifts toward the orientation of the natural astigmatism occurred in the highest astigmats (G3_B and G3_A). Unexpectedly, in three cases (G3_C, G3_D and G3_G) the shift occurred in a perpendicular orientation. This behavior might be explained by a combination of different factors: (1) a large interocular difference in the amount astigmatism (as it is the case for G3_D with an interocular difference of 4.25 D in astigmatism magnitude, see Table 3.1); (2) interocular difference in the astigmatic axis (as it is the case of G3_C, with a relative angle of 80deg in the astigmatism axis, see Table 3.1); (3) a slightly hyperopic astigmatism (G3_D and G3_G, see Table 3.1). Interocular transfer of after-effects has been recently reported both for the amount of blur and axis of astigmatism [210]. In slightly hyperopic astigmats accommodation can shift the orientation of the blurred image. In a previous study non-corrected hyperopic astigmats showed higher performance (visual acuity) than non-astigmats in the presence of astigmatism, regardless the axis of the induced astigmatism [94]. Also, it has been shown (for large amounts of astigmatism) that meridional amblyopia is more prevalent in astigmats with both meridians myopic than in hyperopic astigmats, consistent with a more constant exposure to oriented blur in myopic than hyperopic astigmats.

Also, our study showed that wear of a newly prescribed astigmatic correction lens for a period of time shifted very systematically the perceived neutral towards isotropy, regardless of the orientation of the shift previous to the astigmatic correction. Interestingly, the shift occurred (although not in full) after two hours of lens wear, and appeared constant after one week of lens wear (and at least up to six months). Some differences in the time-scale effect between subjects of G3 were noticed. Adaptation effect was faster and almost complete after 2 hours for subjects with original bias perpendicular to their natural astigmatism, whereas

subjects with original bias towards their astigmatism showed a slower and decreased adaptation effect.

The habitually corrected astigmatic group (G2), who maintained the same refractive correction throughout the study, did not show longitudinal changes in the perceived neutral point, as expected. However, interestingly, the perceived neutral point was very consistently shifted towards images blurred along the axis of their natural astigmatism (Figure 3.3 (b), Figure 3.4), suggesting (unlike most subjects of G3 at the end of the study) a lack of adaptation to their astigmatic correction. We can only speculate on the reasons of this difference between G2 and G3 at the end of the study. The amount of astigmatism in the subjects of G2 was on average higher than that of G3 (G2: -2.56 ± 1.87 D; G3: -0.39 ± 0.64 D). In fact, G3 subjects with highest astigmatism (G3_B and G3_F), even if they experienced the largest shift in their perceived neutral point, only showed partial adaptation at the end of the study. This suggests that there may be a threshold in the amount of natural astigmatism above which adaptation may not be complete. Although we do not have evidence of clinical meridional amblyopia in the subjects of G2, numerous studies have reported orientation-specific visual performance deficits in late corrected high astigmats, which persisted despite optical correction [94, 135, 136]. Interestingly, most subjects in G2 (G2_A-F) were optically corrected after the age of 7. Another interesting element is the presence of spherical error. Most subjects of G2 had significant amounts of myopic error (corrected years back, typically simultaneously with the correction of astigmatism). The presence of defocus might have influenced the perception of blur orientation, and therefore the adaptation pattern and visual norm in those subjects. In fact G3_A (with similar amount of spherical error than the average of G2) only showed a partial adaptation. The potential impact of spherical error on the adaptation to astigmatism is consistent with differences in the perceptual responses to dioptric blur between refractive groups reported in previous studies [160, 211, 212].

Finally, long-term effects (6 months) of astigmatic correction wear in the perceived neutral point have been measured in G3 (Figure 3.4). Whether, if the subjects keep their correction, the adaptation to an isotropic point persists, or alternatively, a bias towards the natural astigmatism re-appears, could only be tested by monitoring the subjects of G3 after years. It has been suggested that adaptation processes can actually operate at long time-scales, show persistent after-effects, and in fact exhibit some forms of learning [111]. Vul et. al (2008) also pointed the intriguing possibility that the functional form of adaptation might change at different timescales [213]. Yehezkel et. al (2010) pointed out to the possibility of storing multiple transformations of the visual world and applying them when the need arises [130]. Alternatively to our previous hypotheses, the bias for astigmatism in the subjects of G2 might be a manifestation of one of the multiple adaptation stages in corrected astigmatic patients.

3.5 Conclusions

The capability for recalibration shown by subjects just given a new astigmatic prescription is of practical interest in the clinical practice. Astigmatism is routinely under-corrected on the basis that patients usually do not tolerate a full correction, and this needs to be progressively introduced [114]. An open question is whether a period of astigmatic correction wear would alter not only the perceptual bias, but also visual performance in the presence/absence of astigmatism. We had previously shown that habitually-non-corrected astigmats performed better in the presence of astigmatism, than non-astigmats with a similarly induced astigmatism [94]. If a change in visual performance is observed, it is likely the time-scale of those changes is longer than that for perceptual judgment, and involves some type of perceptual learning.

In summary, we have shown that refractive (astigmats vs. non-astigmats) and corrective (habitually-corrected or habitually-non-corrected) profiles in subjects have a large impact on their perception of oriented blur. Uncorrected astigmats appear to be naturally adapted to astigmatism, thus their perception of neutral point is shifted towards astigmatism. The observed differences in the perception of neutral point must therefore arise from differences in the internal norm for perception of oriented blur, which is highly dependent on prior visual experience. Furthermore, astigmatic correction changes significantly the perception of the neutral point in astigmatic subjects, even after a brief period of adaptation, and remains constant once stabilized. An interesting question, which is addressed in the following *Chapter*, is whether the perceptual aftereffects following neural adaptation to natural astigmatism have a related impact on visual performance.

4

Astigmatism Impact on Visual Performance: Meridional and Adaptational Effects

As shown in the previous Chapter, astigmatic subjects are adapted to their astigmatism, and perceptually recalibrate upon its correction. However, the extent to what prior adaptation to astigmatism affects visual performance is not fully understood.

In this Chapter we investigate the extent to what prior adaptation to astigmatism affects visual performance, whether this effect is axis-dependent, and the time-scale of potential changes in visual performance following astigmatism correction. Moreover we investigate the effect of possible positive interactions of aberrations (astigmatism and coma) might be altered after recalibration to correction of astigmatism

This Chapter is based on the paper by *Vinas et al. "Astigmatism impact on visual performance: meridional & adaptational effects" in Optometry and Vision Science (2013)*. The co-authors of the study are Pablo de Gracia, Carlos Dorronsoro, Lucie Sawides, Gildas Marin, Martha Hernandez and Susana Marcos. The research leading to these results has received funding from a collaborative research project funded by Essilor International.

The author of this thesis (1) implemented the experimental procedure, (2) performed the measurement on human eye's, (3) collected the data, (4) analyzed

the data (in collaboration with Carlos Dorronsoro and Susana Marcos), (5) discussed the results (in collaboration with Lucie Sawides, Carlos Dorronsoro, Gildas Marin, Martha Hernandez and Susana Marcos) and (6) prepared the manuscript (in collaboration with Susana Marcos).

This work was also presented as an oral contribution at the Association for Research in Vision and Ophthalmology (ARVO) annual meeting (May 2013) in Seattle (Washington, USA), and at the IONS 2013 in Zurich (Switzerland).

4.1 Introduction

In clinical practice astigmatic correction is often provided gradually, as it is assumed that subjects are adapted to the distortion produced by their natural astigmatism. However, the extent to which astigmatic subjects are adapted to their own astigmatism, and recalibrate upon correction of their astigmatism has only been recently investigated [214], and the extent to what these perceptual changes affect visual performance is not well known [94].

There is increasing evidence that subjects are adapted to the blur produced by their own HOA (magnitude and to some extent also orientation) [114], and that spatial vision is calibrated for the specific blur levels present in each individual's retinal image [74]. Moreover, as shown in the previous Chapter, the perceived neutral point in habitually non-corrected astigmats is shifted towards oriented images (generally toward their own axis of astigmatism, particularly in myopic astigmats), and very interestingly, it shifts towards more isotropic images after correction of their astigmatism, partly after two hours of astigmatic correction wear, and fully after one week [214]. Strong after-effects were also found after brief periods of adaptation to simulated images blurred with horizontal/vertical astigmatism (while keeping the blur strength constant), indicating that adaptation can be selective to the orientation of astigmatism [75]. Direct tests of the best-perceived focus therefore indicate that blur judgments are largely influenced by the subject's previous experience, and that changes in the environment can rapidly result in a shift of perceived blur (or the orientation of this blur) [75, 214].

Furthermore, it is well known that uncorrected astigmatism may limit neural sensitivity [131, 132, 215, 216]. Numerous studies have shown that large amounts of astigmatism left uncorrected in childhood may lead to meridional visual deficits, so called meridional amblyopia, although those are not found in all visual tasks [135, 136]. Also, longer exposures to spherical blur have been reported to induce changes in visual acuity [120, 123, 141]. Adaptation to blur has also been suggested to produce improvements in visual performance, however it is likely that those changes, usually occurring after a longer-term exposure to the adapting stimulus, also entail some form of perceptual learning [130]. Perceptual learning is often described as a training for specific visual tasks leading to long-term improvement in performing the task [217].

In that sense, Fogt (2000) studied the directional aftereffects associated to the prismatic effects of spectacle lenses after being trained to point accurately through a spectacle lens. Subjects were made myopic using a contact lens and then the myopia was corrected with a spectacle lens, while pointing behavior was used to assess directional localization. They found that the ability of the observer to switch between two different optical corrections (spectacle and contact lenses), that induced different visual distortions, was correlated with the presence of after-

effect in localizing objects (a shift in the perceived direction occurring after removal of the optical device used to induce adaptation): those who learned did not show an after-effect, whereas those who did not learn did show an after-effect [218]. Yehezkel et al. (2010) suggested that, after a long experience, adaptation is transferred to a long-term memory that can be instantly engaged when blur is re-applied, or disengaged when blur is removed, thus leaving no aftereffects in shape perception [130]. This pointed out to the possibility of storing multiple transformations of the visual world and applying them when the need arises.

Some studies have reported relatively fast improvements in visual performance upon adaptation of blur. Mon-Williams et al. reported an increase in visual acuity (VA) in subjects after exposure to spherical blur [123]. Pesudovs observed that patients with increased aberrations following refractive surgery, progressively improved VA in the course of 10 weeks after the procedure [124]. Also, the fact that keratoconic patients show a higher VA than normal subjects with simulated identical aberrations [120] suggests that visual performance is possibly improved after prolonged exposure to optical degradation [120, 123, 219]. Similar effects have been observed upon astigmatism induction. Ohlendorf et al. reported an increase of VA in normal subjects viewing dynamic astigmatic images (either simulated, or through +3.00 D cylindrical lenses) after 10 min of adaptation, with a significant meridional bias [199].

A previous study suggested that habitually non-corrected astigmats were adapted to their astigmatism, as their measured VA was less impaired by the induction of astigmatism than in non-astigmatic subjects with the same amount of induced astigmatism [94]. The fact that subjects with identical optical properties exhibit very different relative responses is suggestive of adaptation/perceptual learning effects, to astigmatic blur in particular. However, in the previous study astigmatism was systematically induced at 45 deg (blur in the oblique meridian, OBL), regardless the orientation of the natural astigmatism, and the sample included hyperopic subjects (who may shift their plane of focus along the Sturm interval by accommodating). The increased performance upon induction of astigmatism (with respect to emmetropes or corrected astigmats) could then be the result of adaptation to overall blur. Moreover, the orientation of the astigmatic axis may play an essential role in visual performance in astigmats. Wolffsohn et al. showed that uncorrected astigmatic blur at 45-degree or at 180-degree (blur in the horizontal meridian) resulted in worse distance- and near-VA, as well as worse subjective-rated clarity, than astigmatic blur at 90-degree (blur in the vertical meridian) [131]. Similar trends have been shown in visual performance, where oblique astigmatism has a more deleterious effect on visual performance than WTR or ATR astigmatism, probably due to a higher visual deprivation associated to uncorrected astigmatism [220].

In this *Chapter*, we present the results of experiments to test the effect of prior adaptation to astigmatism in subjects with different refractive (astigmats and non-astigmats) and corrective (habitually-corrected and habitually-non-corrected astigmats) profile in visual performance. In particular, we have measured the impact of astigmatism induction on VA at different axes of astigmatism, including the natural axis of astigmatism, while controlling the natural aberrations of the eye, in each subject. Furthermore, to test the effect of astigmatic correction on visual performance in the presence of astigmatism, measurements were performed in astigmatic patients prior to correction of their astigmatism and at various times, up to 6 months, after astigmatic correction wear. We also tested the effect of interactions between astigmatism and coma on VA, as previous reports showed a lack of agreement between optical predictions and visual performance in the presence of a combination of those aberrations (which is axis-dependent)[95] in non-corrected astigmatic patients, which suggest a role of adaptation to prior astigmatism [94].

4.2 Methods

4.2.1 Subjects

The sample consisted of 25 subjects (ages ranging from 23 to 51 years (31.96 ± 8.15)). Subjects were selected *a priori* and followed an exhaustive optometric evaluation at the School of Optometry Clinic of the University Complutense de Madrid (UCM), in which they were classified according to their natural astigmatism and whether this was habitually corrected or not. The subjects were classified in three groups: G1 (control group of subjects with no clinical astigmatism; n=9); G2 (astigmatic subjects, habitually-corrected, wearing an astigmatic-correction since childhood; n=7); G3 (astigmatic subjects, habitually-non-corrected; n=9). The inclusion criterion for the different groups was, for G1, emmetropic subjects with astigmatism lower than 0.25 D, and for G2 and G3, subjects with myopic astigmatism ≥ 0.75D [221]. Only myopic astigmats were included in the study, since non-corrected hyperopic astigmats could shift their best focus by means of accommodation and, therefore, may experience images blurred along different orientations throughout the Sturm interval for distance vision [222] , which might interfere in the study of the astigmatism orientation effect on visual performance. Some of the subjects also participated in a previous study in which the perceived neutral point was measured from series of images degraded with astigmatism and defocus [214]. Table 4.1 shows the refractive and corrective profile of all subjects of the study, which were measured using standard clinical optometric procedures.

After an initial test, all subjects in G3 were provided with proper astigmatic spectacle correction of their natural astigmatism (in the School of Optometry Clinic of the University Complutense de Madrid (UCM)) and were asked to wear them continuously during six months. Tests were performed only on one (naked) eye per

subject (less myopic eye in G1; and less myopic eye with ≥ 0.75D of astigmatism in G2 and G3).

Optometric measurements of VA (2000 Series Revised ETDRS Translucent Chart "1", Chart "2"; Cat. 2121 & 2122; Precision Vision) were performed in habitually-non-corrected astigmats to measure the improvement in VA with astigmatic correction spectacles with respect to non-correction.

Subject's profile

ID	Measured eye	Refraction			Type of astigmatism	Blur axis (degree)	Age (year)
		Sph	Cyl	Axis			
G1_A	right	0.50	--	--	--	--	29
G1_B	right	0.00	--	--	--	--	33
G1_C	right	0.00	--	--	--	--	31
G1_D	right	0.00	--	--	--	--	30
G1_E	right	-0.25	-0.25	80	ATR	170	30
G1_F	right	0.25	-0.25	90	ATR	90	34
G1_G	right	0.00	--	--	--	--	23
G1_H	right	0.00	--	--	--	--	32
G1_I	right	0.00	--	--	--	--	50
		Avg. Sph: 0.06 ±0.10		**Avg. Cyl: -0.06±0.06**			
G2_A	right	-3.50	-1.00	10	WTR	100	33
G2_B	right	-5.25	-1.25	105	ATR	15	27
G2_C	right	-4.00	-1.00	75	ATR	165	34
G2_D	right	-0.75	-1.25	90	ATR	0	30
G2_E	right	-2.25	-0.75	90	ATR	0	51
G2_F	left	-1.75	-1.00	170	WTR	80	31
G2_G	left	0.25	-1.25	175	WTR	85	24
		Avg. Sph: -2.46±1.92		**Avg. Cyl: -1.07±0.19**			
G3_A	right	-1.50	-0.75	10	WTR	100	27
G3_B	left	0.00	-1.25	80	ATR	170	29
G3_C	right	-0.75	-0.75	120	ATR	30	27
G3_D	right	0.50	-0.75	170	WTR	170	27
G3_E	left	-0.75	-0.75	175	WTR	85	48
G3_F	left	-1.00	-0.75	90	ATR	0	45
G3_G	right	0.00	-1.00	90	ATR	0	26
G3_H	left	0.00	-1.25	175	WTR	85	23
G3_I	right	0.00	-1.25	10	WTR	100	33
		Avg. Sph: -0.39 ± 0.64		**Avg. Cyl: -0.94 ± 0.24**			

Table 4.1 Optometric subjective refractions (spherical error, cylinder, axis), orientation of the retinal blur (most myopic meridian) on measured eye and ages. Averaged spherical error and natural astigmatism are shown for every group. Cyl, cylinder; Sph, spherical error.

4.2.2 Experimental protocol

Measurements were conducted in the Viobio Lab AO I custom-made Adaptive Optics system, described in detail in previous publications [83, 84, 89], which was

used to measure and correct the aberrations of the subject, as well as to induce the different patterns of aberrations, astigmatism and coma. The state of the mirror that compensates the aberrations of the subject was found in a closed-loop operation, and measurements of the subjects' aberrations throughout the test ensured proper correction. The same operation was used to generate and induce the different combinations of astigmatism and coma. Measurements were performed for 6-mm pupils (limited by an artificial pupil of 6 mm placed in a plane conjugate to the natural pupil). Visual stimuli were presented on a CRT monitor (Mitsubishi Diamond Pro 2070) through the Badal system and AO mirror correction. The stimulus display was controlled by the psychophysical platform ViSaGe, (Cambridge Research System, UK). The average luminance (after losses in the system) was ~50cd/m^2 in an otherwise dark environment.

Following dilation, the eye's pupil was aligned to the optical axis of the instrument, and the subject's head was stabilized using a dental impression on a bite bar. The subject's spherical refractive error was corrected with a Badal system. All the measurements were performed after the pupils of the subjects were dilated (by tropicamide 1%, Alcon Cusi, Barcelona, Spain) to normalize the pupil size with an artificial pupil of 6 mm placed in a plane conjugate to the natural pupil. In addition, measurements were performed with naked eye (without spectacles). Best subjective focus was selected by the subject him/herself using a remote control to move the motorized stage while viewing a Maltese cross as fixation target.

Natural astigmatism and HOA were fully corrected and/or selectively induced (astigmatism and coma) with the deformable mirror. The mirror states were measured just before and after each VA measurement. The accuracy of the achieved aberrations (combination of mirror and eye) with respect to the attempted pattern (i.e. astigmatism at a given meridian) was tested before and after VA measurements (a maximum discrepancy of 0.10 μm in the astigmatism or coma terms was allowed). Further details on the mirror control and validations of the achieved mirror states can be found in previous publications [94, 95, 214].

In the current study, we set the orientation of induced astigmatism to the orientation of the retinal blur of the most myopic meridian due to the native astigmatism of each subject, as obtained from the optometric data. Since all astigmatic subjects were myopic and measurements were performed for distance vision, we replicated the oriented blur of the focal line closer to the retina, the most myopic meridian, by inducing ±0.50 D of defocus. For example, when the most myopic meridian of the subject was at 0deg, C_2^2 = 0.92 μm and C_2^{-2} = 0.00 μm were induced with the mirror, and +0.50 D defocus with the Badal system, so that a horizontally blurred image on the subject's retina was achieved. In other words, the vertical meridian was in focus, and the horizontal meridian was made artificially myopic by 1.00 D. The AO mirror was used so that the subject was exposed to 1.00

D of astigmatism (at different orientations), regardless the magnitude of the subject's natural astigmatism. The difference between the attempted and achieved astigmatism was small (<2.1% in G1 and <5.5% in astigmatic groups).

Astigmatism and HOA were measured and corrected in a closed-loop AO operation. The subject was then asked to adjust the Badal system position to obtain again the best subjective focus for the AO-correction condition. The state of the mirror that achieved the correction was saved and applied during the measurements. VA measurements were performed under full static AO-corrected aberrations and best spherical refraction error correction. The steps of an experimental session were, sequentially: (1) focus setting; (2) measurement of ocular aberrations with the Hartmann–Shack sensor; (3) closed loop for natural aberration correction; (4) set of mirror status for the different conditions (aberration correction + specific astigmatism/ coma combination); (5) measurement of ocular aberrations; (6) measurement of VA; (7) measurement of eye + mirror aberrations. The sequence was repeated for each condition tested. The order in which the different conditions were tested was randomized. A training trial, under induced astigmatism, was performed in the first session to familiarize the subject with the procedure.

Measurements were performed in 4 different sessions for all groups: first day (S0A), 1 week (S1), 1 month (S2) and 6 months after (S3). An additional measurement session was performed for the habitually-non-corrected astigmats (G3), after 2 hrs. of spectacle correction wearing, provided right after the initial session.

4.2.3 Tested conditions

A total of 14 different conditions were tested, summarized in Figure 4.1. First, as a baseline, VA measurements with and without AO correction were performed (Conditions #1 and 2, respectively). Then VA was measured under induction of 1.00 D (0.92 µm for 6 mm-pupil size) of astigmatism at 3 different orientations with (Conditions #3, 4 and 5) and without (Conditions #6, 7 and 8) correction of HOAs. For non-astigmatic subjects (G1) the orientations tested were 0deg (horizontal retinal blur) (#3), 90deg (vertical retinal blur) (# 4) and 45deg (oblique retinal blur) (#5). For astigmatic subjects (G2 and G3) the orientations tested were the natural axis of astigmatism (i.e. axis of retinal blur of the most myopic meridian due to the native astigmatism, according to the optometric readings) to replicate the astigmatic orientation of retinal blur of the most myopic meridian (#3), the perpendicular orientation (#4), and at 45deg fixed (oblique retinal blur) (#5). The oblique astigmatism (45deg) was used for comparison across groups and with previous work where only astigmatism induced at 45deg was tested [94].

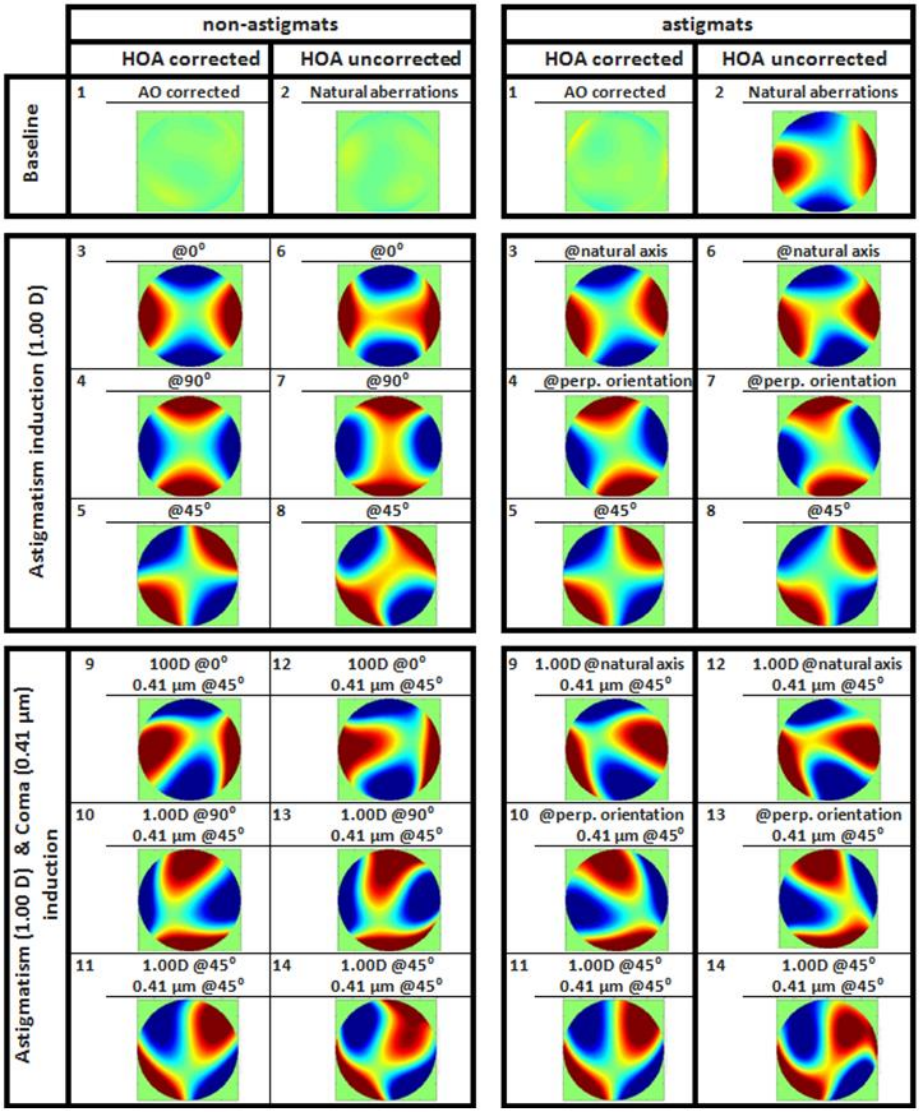

Figure 4.1 Summary of tested conditions. VA was measured under 14 different conditions, numbered in the table for future reference. Baseline conditions (#1-2): VA measurements with and without AO correction. To test whether the effect of astigmatism depends on prior adaptation to astigmatism with and without AO correction (#3 and #6). To test the axis-dependency of astigmatism with and without AO correction (#3-8). To test the benefit of adding coma to astigmatism with and without AO correction (#9-14). Scale of wavefront maps is ± 1.00 µm.

Furthermore, the influence of prior adaptation to astigmatism on potential interactive effects between astigmatism and coma was tested following previous work by De Gracia et al. (2010)[95]. Optical simulations had shown that optical interactions between astigmatism and coma could result in an improvement in optical quality: adding amounts of coma between 0.15 and 0.35 µm to 0.5 µm could lead to an increase in peak Strehl ratio values, in the absence of other HOAs [95]. However, psychophysical measurements showed that the visual improvement produced by adding coma to astigmatism seem to be highly dependent on the presence of natural astigmatism and whether this was habitually corrected or not [94]. For comparison with the previous study [94], combinations of 1.00 D (0.92 µm for 6 mm-pupil size) of astigmatism (at 3 orientations) and 0.41 µm of coma at a relative angle of 45 deg were also tested, since this relative angle between astigmatism and coma provided the best results in the previous study (Conditions #9, 10 and 11). All tested conditions were also performed in the presence of the natural aberrations of the subjects (Conditions #12, 13 and 14). In addition, measurements of VA with full correction of aberrations and astigmatism, and under natural aberrations were also performed as control conditions.

In summary, to further explore the effect of prior adaptation to astigmatism on visual performance in the presence of astigmatism, and possible interaction between astigmatism and coma, a total of 14 conditions were tested. All tests were performed monocularly, always in the same eye, (less myopic eye in G1; and less myopic eye with ≥ 0.75D of astigmatism in G2 and G3).

4.2.4 Visual acuity measurements

VA was measured using an 8-Alternative Forced Choice (8AFC) [196] procedure with tumbling E letters and a QUEST (Quick Estimation by Sequential Testing) algorithm programmed with the Psychtoolbox package [191], to calculate the sequence of the presented stimulus (letter size and orientation) in the test, following the subject's response. Subjects had to determine the orientation of the letter E (8 orientations; pointing up, down, left, right, oblique up-right, oblique-up-left, oblique-down-right, oblique down-left), while aberrations were controlled with the deformable mirror: correction of natural aberrations and/or induction of astigmatism and combination of astigmatism and coma with and without natural aberrations correction, following the different tested conditions.

This 8-orientation test avoided potential convergence problems in the response of the subjects associated to the traditional 0deg/90deg preferential orientation test. The QUEST routine for each VA measurement consisted in 50 trials, each one presented during 0.5 s, where the threshold criterion was set to 75%. The threshold, VA measurement, was estimated as the average of the 10 last stimulus values. VA was expressed in terms of decimal acuity (logMAR= - log10 (decimal acuity)) [198].

4.2.5 Data analysis

Wave aberrations were fitted by 7th-order Zernike polynomials, and OSA convention was used for ordering and normalization of Zernike coefficients. VA was expressed in decimal units and reported in terms of absolute and relative values. Relative values refer to the AO-correction benefit (Ratio VA (AO) / VA (no AO)), sensitivity to astigmatism induction (Ratio VA (astigmatism + AO) / VA (AO)), and visual benefit of adding coma to induced astigmatism (Ratio VA (astigmatism + coma + AO) / VA (astigmatism + AO)).

Statistical analysis was performed with SPSS software (IBM) to test differences across groups, sessions and conditions. More precisely, differences across groups and sessions were analyzed performing *One-Way ANOVA Post hoc tests*, while specific differences between relative data (ratios) were established by performing *Paired sample t-test*s.

4.3 Results

4.3.1 Subjects' natural aberrations

The subject's natural aberrations are shown in Figure 4.2 in terms of average ocular Root-Mean Square wavefront error (RMS, μm) for HOAs and astigmatism (black bars), only astigmatism (oblique line bars), only coma (grey bars) and residual aberrations after AO correction of all natural aberrations (white bars), in each group. The RMS for HOA (RMS_{HOA}) ranged between 0.38 to 0.29 μm across subjects, with no statistical significant differences across groups.

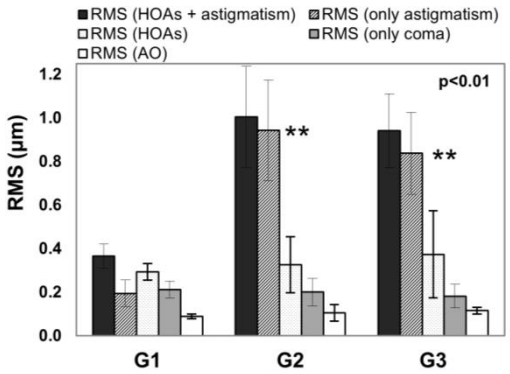

Figure 4.2 RMS wavefront error (excluding defocus) for HOAs and astigmatism (black bars), only astigmatism (oblique line bars), only HOAs (black dots), only coma (grey bars) and residual aberrations after AO correction (white bars), averaged across subjects, groups and measurement sessions. Error bars indicate inter-subject variability. **indicates a significantly larger RMS for HOA + astigmatism for G2 and G3 than for G1.

On the contrary, the astigmatism contribution to the global amount of aberrations of the subjects differed across groups. As expected, $RMS_{HOA+ast}$ was significantly higher for G2 and G3 than for G1 (*One-way ANOVA*; p=0.006) and, astigmatism contribution (RMS_{ast}) to the total amount of aberrations ($RMS_{HOA+ast}$) was 47% for G1, 93% or G2 and 88% for G3, respectively. Natural aberrations of the subjects were properly AO-corrected and the achieved optical correction was similar across groups and measurement sessions (*One-way ANOVA*; p>0.05).

The residual RMS after AO-correction of HOA and astigmatism was similar for all groups, and lower than 0.11 µm in all cases (mean higher-order RMS for 6 mm pupils is approximately 0.3 µm. on average across groups). AO correction was similar throughout the study (6 months).

4.3.2 Visual benefit of Adaptive Optics correction

VA improved significantly with AO-correction for all groups, following previous results [83] and along all measurement sessions (*paired samples t-test*; p< 0.05). Figure 4.3 shows VA with natural aberrations and after AO-correction (HOA + Astigmatism) (best subjective focus in each condition), in all individual subjects of the study (each panel showing data for each group) at day 0.

As expected, VA under natural aberrations was higher for G1, than for G3 and, especially than G2, as a result of the higher amount of natural astigmatism of G2 vs. G3 and G1 (on average, G2 has 0.11 µm of astigmatism more than G3 and 0.65 µm more than G1). VA upon correction of aberrations (HOA and astigmatism) was not statistically significantly different across groups *One-way ANOVA*; p=0.395).

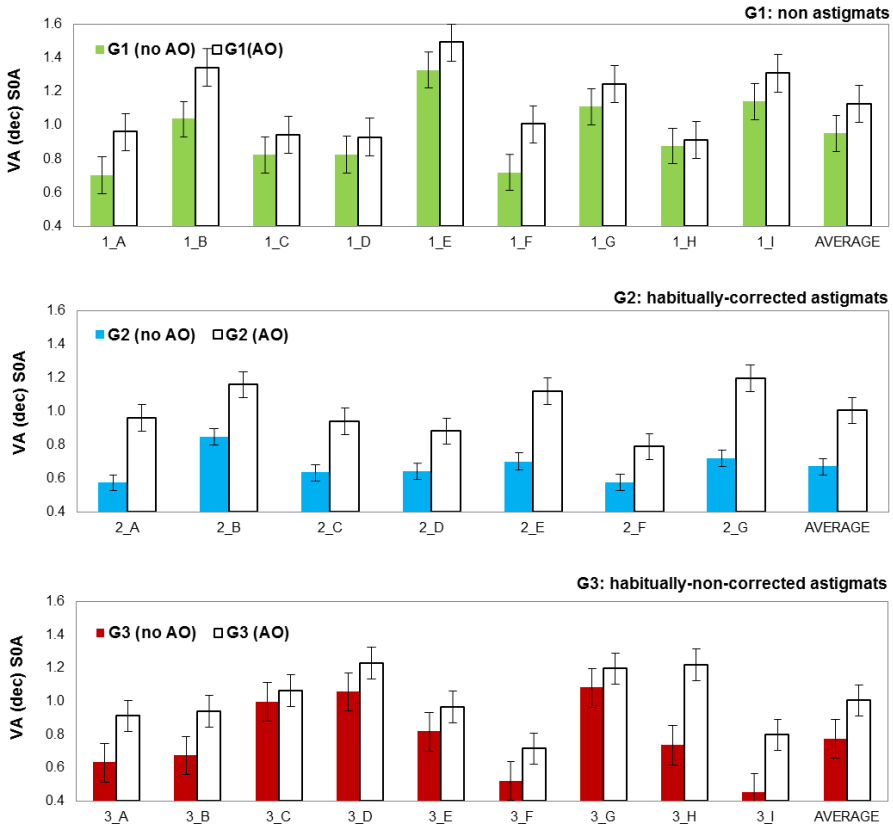

Figure 4.3 Baseline VA measurements. VA for natural aberrations (colored bars) and AO-corrected aberrations (white bars) for the first session (S0A) for the three groups for all individual subjects (divided by group), and average. Error bars represent intra-subject measurement variability (standard deviation).

Figure 4.4 shows the visual benefit (Ratio VA (AO) / VA (noAO)) for the 3 groups for the different sessions (first session, up to 6 months). The larger benefit of the AO correction in G2 (1.47, as opposed to 1.16 and 1.26 in G1 and G3 respectively, on average across subjects and sessions) is due to the larger amount of astigmatism under natural conditions in this group (shown in Figure 4.2). We found a slight but consistent trend towards VA improvement with time, both for natural aberration and AO-corrected conditions in all groups. However, the AO correction benefit did not change significantly across sessions (*One-way ANOVA*; $p>0.05$).

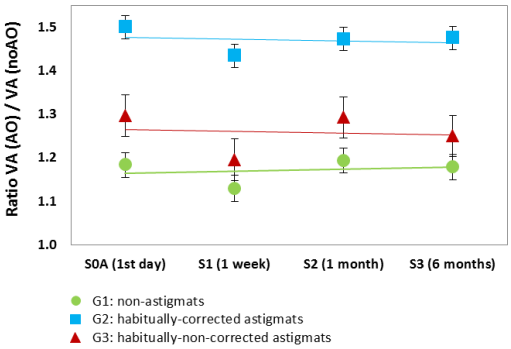

Figure 4.4 AO correction benefit. Ratio VA (AO) / VA (no AO) as a function of session, averaged across subjects, for the three groups. Error bars represent inter-subject variability (standard deviation). G1 (non-astigmats) is represented with circles, G2 (habitually corrected astigmats) with squares, and G3 (habitually non-corrected astigmats) with triangles. Lines represent linear regression.

4.3.3 Visual performance under astigmatism induction at different angles

For G1, VA was measured after induction of 1.00 D (0.92 µm) of astigmatism at three different angles: 0 deg (horizontal retinal blur), 90 deg (vertical retinal blur), and 45 deg (oblique retinal blur. For G2 and G3, VA was measured after induction of 1.00 D of astigmatism at three different angles; axis of natural astigmatism, 90 deg from the natural axis of astigmatism and 45 deg. Figure 4.5 shows VA averaged across subjects, tested at the different angles, as a function of session (left panels, a, c and e, under full AO-correction of aberrations, except for the induced astigmatism; and right panel, b, d and f, under natural aberrations). The corresponding control conditions are shown for reference in black line: VA under full correction of aberrations and no astigmatism, and VA under natural correction of aberrations and natural astigmatism.

VA becomes worse in the presence of induced astigmatism in all groups, conditions and sessions, although the magnitude of that decrease depended on the orientation of the induced astigmatism. For G1, inducing astigmatic blur at 90deg produced a statistically lower reduction in VA (29%) than when astigmatic blur was induced at 0deg (40%) (*paired samples t-test*; p=0.004) or 45 deg (41%) (*paired samples t-test*; t(8)=3.465; p= 0.009) (Figure 4.5, a). The same effect was found in the presence of natural HOA (Figure 4.5, panel b).

For G2, VA decreased significantly less when astigmatism was induced at their axis of natural astigmatism (with AO correction), than for other angles, i.e. at a perpendicular axis (*paired samples t-test*; t(6)=2.896; p=0.027) and at 45 deg (*paired samples t-test*; p=0.003) (Figure 4.5, panel c). VA was only reduced by 23% when astigmatism was induced at the axis of natural astigmatism, in contrast to

36% for a perpendicular axis and 38% for 45 deg. Without AO-correction, differences across angles were not significant (Figure 4.5, panel d).

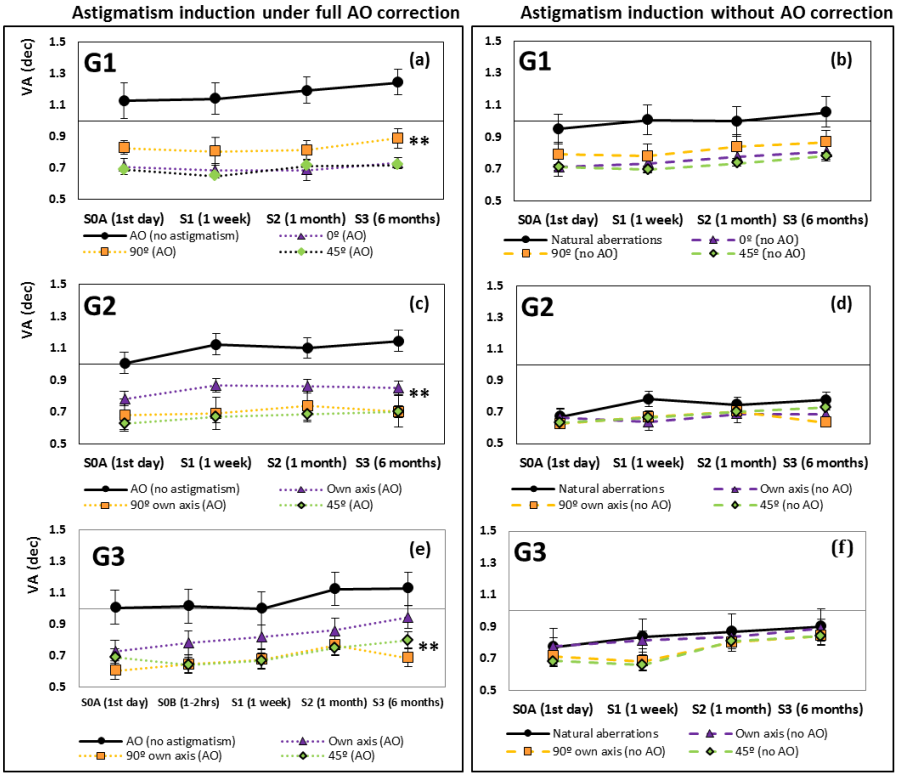

Figure 4.5 Induction of astigmatism. Decimal VA under induced astigmatism at different angles, averaged across subjects in each group, for different sessions. Left panels (A, C, E) show data under full correction of HOA, and right panels (B, D, F) data under natural aberrations. Top panels (A, B) are data for G1 (non-astigmats), middle panels (C, D) are data for G2 and lower panels (E, F) are data for G3. For G1 1.00 D (0.92 µm) of astigmatism was induced at 0deg (triangles), 90deg (squares) and 45 deg (diamonds). For G2 and G3 1.00D of astigmatism was induced at their own axes of natural astigmatism (triangles), at a perpendicular axes (squares) and at 45 deg fixed (diamonds). Decimal VAs under full AO correction and under natural aberrations (including astigmatism) are shown for reference in the left and right panels respectively (black line, circles). ** indicates highly significant differences in G1 between VA at 90 deg vs. the others and in G2 between VA at the natural axis and the others. In G3 ** indicates highly significant differences for data of S3 respect from S0A for G3 when astigmatism is induced at axis of natural astigmatism. In S3 indicates highly significant differences between VA at the natural axis and the others. Error bars represent inter-subject variability (standard deviation).

For G3, VA also decreased significantly less (by 28% in the first session and 16% in the last session) when astigmatism was induced at the axis of natural astigmatism (with AO correction, Figure 4.5, panel e) than for other angles, i.e. 36% for the perpendicular axis (*paired samples t-test* p=0.010), and 31% for 45 deg (*paired*

samples t-test; p=0.034). In fact, VA did not experience any reduction when astigmatism was induced at the axis of natural astigmatism in the presence of natural aberrations (Figure 4.5, panel f).

In the first session, the highest decrease in VA under induced astigmatism (using the best condition in each group, for comparison) was experienced by G3 subjects, followed by G2 and G1 (Figure 4.5, panels a-c-e). VA tended to become slightly better, but not significantly, across sessions for all groups, consistent with some training effect [212]. However only G3 changed significantly after the 6-months-of-astigmatic-correction-wearing (*paired samples t-test*; p=0.001). After 6-months of astigmatic correction wearing, G3 subjects were significantly less sensitive to the induction of astigmatism and reached VA under astigmatism induction values similar to those of non-astigmats (in fact, higher VA values) (Figure 4.5 left panels).

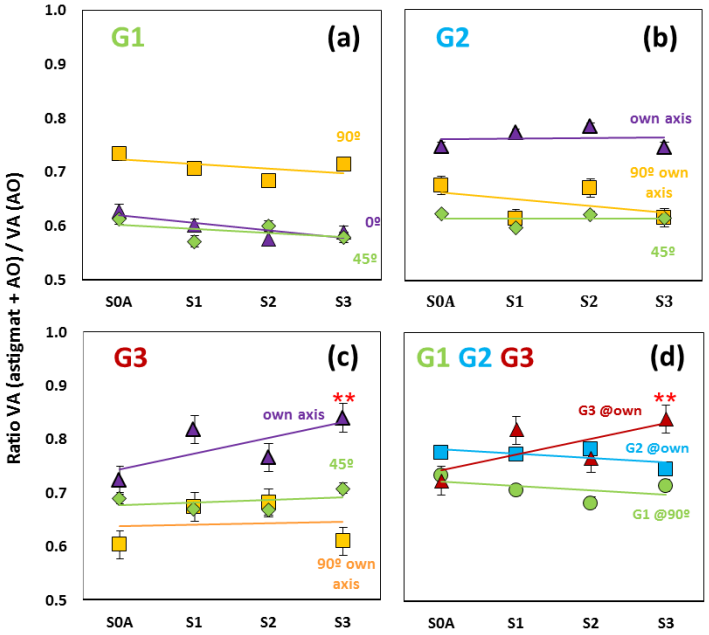

Figure 4.6 Sensitivity to astigmatism induction. Ratio VA (Astigmatism AO)/VA (AO), averaged across subjects in each group, for the different sessions for G1 (non-astigmats, panel A), G2 (Habitually corrected astigmats, panel B) and G3 (habitually-non corrected astigmatism, panel C). For G1 1.00 D (0.92 µm) of astigmatism was induced at 0 deg (triangles), 90 deg (squares) and 45 deg (diamonds). For G2 and G3 1.00D of astigmatism was induced at their own axes of natural astigmatism (triangles), at a perpendicular axes (squares) and at 45 deg fixed (diamonds). Panel D shows a summary of the best condition for each group (G1 at 90deg, circles; G2, squares, and G3, triangles, at own axis). Data are for full AO-correction of natural aberrations.** indicates highly significant differences for data of S3 respect from S0A for G3 when astigmatism is induced at axis of natural astigmatism. Error bars represent inter-subject variability (standard deviation).

We further analyzed this orientation-dependence effect in terms of the relative decrease in VA upon induction of astigmatism. Figure 4.6 shows the relative sensitivity to induction of astigmatism, as the Ratio VA (astigmatism + AO) / VA (AO), for the different orientations of astigmatism. Non-astigmats showed a significantly lower degradation in VA when astigmatism was induced at 90 deg (vertical retinal blur) than at the other orientations (*One-way ANOVA*; p=0.024). Conversely, subjects from either astigmatic group appeared significantly less sensitive to the induction of astigmatism at the subject's natural axis of astigmatism (Figure 4.6, panel a). For G2, the relative sensitivity to induction of astigmatism was significantly lower (*One-way ANOVA*; p=0.011) when astigmatism was induced at the subject's natural axis of astigmatism than at the other orientations (Figure 4.6, panel b). G3 subjects showed, on the very first session, also a slightly lower visual degradation when astigmatism was induced at the own axis of astigmatism than at the other orientations (Figure 4.6, panel c).

After 6 months of astigmatic correction wear of subjects in G3, the better performance under induction of astigmatism at the own axis in comparison with the other orientations (perpendicular orientation and 45deg) was statistically significant (*One-way ANOVA*; p=0.04). In addition, VA changed significantly from the first day to 6 months after correction (*paired samples t-test*; p<0.01) (Figure 4.6, panel d). Clinical measurements of VA, performed on G3 following standard clinical optometric procedures in the first and the last session showed that all G3 subjects (except for G3_B) improved VA after wearing astigmatic correction for 6 months (averaged 19.3% improvement in clinical decimal VA).

4.3.4 Benefit of adding coma to induced astigmatism

Optical simulations showed that certain combinations of astigmatism and coma improve optical performance with respect to astigmatism alone [95]. However, in a prior study we had shown that the predicted improvement occurred in non-astigmats, but failed in habitually non-corrected astigmats, likely as a result of the subject's adaptation to astigmatism [94]. In the referred study, astigmatism was induced systematically at 45 deg, and the optimal relative angle referred to this orientation [94]. Figure 4.7 shows the results from the current study of the relative change in VA when adding coma to astigmatism with respect to VA with astigmatism alone, for different orientations of induced astigmatism (coma at a fixed relative angle of 45 deg with respect to astigmatism).

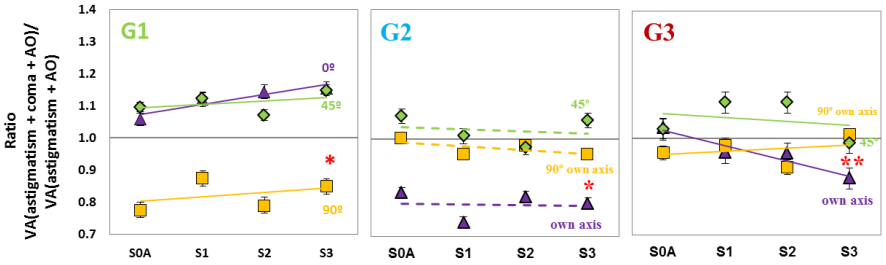

Figure 4.7 Visual degradation under astigmatism and coma induction vs. astigmatism alone. Ratio VA (astigmatism + coma + AO) / VA (astigmatism + AO) for the 3 groups (G1: left panel; G2: middle panel; G3: right panel) at 3 tested conditions (G1 0 deg / G2, G3 own axis: triangles; G1 90deg / G2, G3 90 deg own axis: squares; G1, G2, G3 45 deg: diamonds) and 0.41 µm of coma at a relative angle of 45 deg with full AO correction. *indicates significant differences for data of 90deg respect from 0 deg and 45 deg for G1, and data of axis of natural astigmatism respect from perpendicular orientation and 45 deg for G2. ** indicates highly significant differences for data of S3 respect from S0A for G3 when astigmatism is induced at axis of natural astigmatism. Error bars represent inter-subject variability (standard deviation).

For G1, VA increased significantly when coma was added to astigmatism in comparison with induced astigmatism alone. However, the orientation of the induced astigmatism played an important role. VA increased significantly (*paired samples t-test*; $p<0.01$) for combined coma and astigmatism when astigmatism was induced at 0 deg (horizontal retinal blur) and increased slightly at 45 deg. However VA decreased significantly (*paired samples t-test*; $p=0.02$) when astigmatism was induced at 90 deg (vertical retinal blur). As shown in Figure 4.7 (left panel), in G1 the visual benefit of adding coma to astigmatism over astigmatism alone was therefore statistically different (*One-way ANOVA*; $p<0.01$) when coma was added to astigmatism at 0deg (horizontal retinal blur) or at 45 deg (oblique retinal blur) than when added at 90 deg (vertical retinal blur).

For astigmatic groups, as found for VA in the presence of astigmatism alone, the effect of combined astigmatism and coma in VA was greatly influenced by the prior astigmatism and its orientation. For G2, VA improved slightly when coma was added to astigmatism at 45 deg or at the perpendicular orientation, but decreased significantly when coma was combined with astigmatism induced at the natural axis (*One-way ANOVA*; $p=0.02$) (Figure 4.7, central panel). For G3, prior to the correction of astigmatism, adding coma to astigmatism did not result in an improvement of VA, regardless the axis of the induced astigmatism. However, astigmatic correction wearing produced a statistically significant progressive decrease in performance when coma was combined with astigmatism at the natural axis of astigmatism. After 6-month of astigmatism correction wear, VA under a combination of astigmatism (at the natural axis) and coma was statistically worse than astigmatism alone (*paired samples t-test*; $p=0.012$), similarly to what occurs in G2.

4.4 Discussion

We studied the impact of astigmatism induction (at different axes) on non-astigmats and astigmats, and found that the visual degradation produced by astigmatism was greatly dependent on the axis of the induced astigmatism. As expected from previous studies [94], induction of astigmatism was more deleterious to vision in non-astigmats (compared to non-corrected astigmats, and even habitually corrected astigmats) (Figure 4.4, right panel). Furthermore, even in non-astigmats (and for full correction of HOA), significant differences were found in VA for astigmatism induced at different orientations, but otherwise similar optical degradation (with astigmatism induced at 90deg degrading vision less than at other orientations), indicating a neural basis for the differences. Previous studies differ in their conclusions on the impact of the angle of induced astigmatism on vision, although most reports show that letter target acuity varies with the angle of induced astigmatism [223]. Miller et al. found that subjects tended to be less dissatisfied with induced astigmatism of +0.50 D x 180 deg (vertical retinal blur, following their notation) than with the same astigmatism induced at 90 deg (horizontal retinal blur) or 45 deg (oblique retinal blur) [134], in agreement with our results. Moreover, Atchison et al. (2009) showed, for high contrast letters acuity charts, that the blur limits for induced crossed-cylinder astigmatism were 10% lower than for induced defocus, with considerable meridional influences, with astigmatism at 0 deg (vertical retinal blur in their notation) showing ~30% larger limits than those at 90 deg (horizontal retinal blur) [125]. In subsequent work, they observed that the larger spreading in the horizontal direction than in the vertical spacing produced by horizontal retinal blur had a greater impact on text legibility than other orientations [224]. Also, Schwendeman et al. found that added positive cylinders reduced VA with increasing effect for the cylinder axes 180 deg, 90 deg and 45 deg [225, 226]. In contrast, Remon et al. concluded little effect of the axis of a given astigmatism on VA, although they actually found that that for some eye-charts VA was best for cylinder axis induced at 90deg than at other axes) [227].

For astigmatic subjects, prior experience to astigmatism definitely has an impact on visual performance in the presence of astigmatism. Our results are consistent to a prior study [94] of the effect of induction of astigmatism (and combined astigmatism and coma) on visual performance, in a different population of non-astigmats, habitually corrected astigmats and habitually non-corrected astigmats (which included hyperopic astigmats). While the prior study only considered induction of astigmatism at 45deg, we have investigated and found important meridional differences. In the current study, for both astigmatic groups, G2 and G3, the reduction of VA under induced astigmatism was lower than for non-astigmats (G1), very significantly when astigmatism was induced along the axis of their natural astigmatism. This is indicative of a persistent adaptation to astigmatism, even after its correction (in subjects of G2, and after correction in subjects of G3)

which allows subjects that had a prior exposure to astigmatism to function superiorly with astigmatism induced at their natural axis of astigmatism, even if their astigmatism is normally corrected. This orientation-preference tended to disappear (for G2 and G3) when HOAs were uncorrected (Figure 4.5, panels b, d and f).

A prior study on the influence of astigmatism (and its correction) on perceptual judgment of oriented blur showed that habitually corrected astigmats still tended to identify as isotropic astigmatic images along their axis of astigmatism [214]. Non-corrected astigmats also showed significant shifts of the perceived neutral point away from isotropy prior to correction, which shifted towards isotropy immediately after correction of astigmatism. Those rapid after-effects are not paralleled by a change in the sensitivity to astigmatism on visual performance [141], likely because changes in visual performance require forms of learning and a prolonged exposure to the adapting stimulus. In fact, our results seem to be consistent with the suggested capability of the subject of storing multiple stages of adaptation [130], as corrected astigmats (G2) still appear quite insensitive to astigmatism induction [160, 228] (along their axis of astigmatism), and so do as well previously uncorrected astigmats (G3) after correction of astigmatism. Also the fact that simulated astigmatic defocus may degrade VA more than real astigmatic defocus [199], and, that myopic observers may not benefit to the same extent as emmetropes from AO correction in a VA task [90], could have biased the response of habitually corrected astigmats.

Furthermore, highly statistically significant longitudinal changes were found in G3, who experienced a change in retinal image (from astigmatic to corrected images) during the study following correction of astigmatism, although the exposure to the new correction made the subjects more insensitive to astigmatism (at their natural axis) rather than more susceptible to VA degradation by astigmatism. However, the mechanism and time course for adaptation to induced astigmatism and its impact on visual performance may differ from that associated to the adaptation to an astigmatic correction in astigmatic subjects and their visual response to astigmatism after correction. The astigmatic subjects of our study reached VAs after correction of their astigmatism similar to those of the non-astigmats (G1). Similarly, their clinical visual function was significantly improved with astigmatic correction. However, we found that despite correction of astigmatism, astigmatic subjects appear to keep a certain degree of adaptation (or perhaps learned features) to/of their natural astigmatism which makes them relatively more immune to the induction of astigmatism along their natural axis, and astigmatism correction wear does not eliminate, but rather reinforces this effect.

The same trends were reflected in the effect of adding astigmatism to coma. Beneficial interactions for coma and astigmatism, as predicted from optical theory occurred in non-astigmats (G1, at 0 and at 45 deg) and to some extent in astigmats

(G2 and G3, for astigmatism perpendicular to the natural axis and at 45 deg). However (and despite its optical equivalence) combined astigmatism and coma lowered visual performance at 90 deg for G1, and at the natural axis of astigmatism for G2 and G3, i.e. the same orientations for which astigmatism was less deleterious to vision. Again, the longitudinal measurements in G3 showed a decreasing performance with time under this combination, rather than an improvement, consistent with the decreased sensitivity to the induced astigmatism throughout the same period. The fact that astigmatism affects visual performance differently in the presence or absence of aberrations suggests that aberrations may dilute the measurable adaptational effects to astigmatism. On the other hand, the fact that the effects of combined coma and astigmatism differ across groups suggests that mechanisms do not operate independently, but rather combined effects of aberrations on vision are not only driven by the optics, but are affected by prior adaptation to astigmatism.

4.5 Conclusions

In summary, although astigmatism lowers visual performance, its impact appears to be dependent on the angle of induced astigmatism, both for non-astigmats (for whom inducing astigmatism at 90 deg produced significantly less degradation than at other axes), and astigmats (who experienced less visual degradation when astigmatism was induced at their angle of astigmatism). Both habitually-corrected and initially non-corrected astigmats after correction of astigmatism showed a bias towards better performance with astigmatism induced at their natural axis, which persisted (and actually increased) even after astigmatism correction wear for an extended period of time, suggesting that astigmats may store adaptation states or cues related to their natural astigmatism.

In this and the previous *Chapter*, we have shown the impact on visual function of a specific monochromatic low order wave aberration, astigmatism. However, the retinal image quality is degraded by the presence of both monochromatic and chromatic aberrations in the ocular optics, thus chromatic aberration characterization is of great importance when studying visual function. In the following two *Chapters* we use the polychromatic capacity of the AO system to provide insights on the quantification of the LCA of the eye.

5

Longitudinal Chromatic Aberration of the human eye in the visible and near infrared from wavefront sensing, double-pass and psychophysics

The visual world is polychromatic and the study of the impact of retinal image quality on vision should consider the aberrations in the visible light, as well as the effect of chromatic aberrations. Longitudinal Chromatic Aberration (LCA) influences the optical quality of the eye, however, the reported LCA varies across studies, likely associated to differences in the measurement techniques. In the current Chapter, we present LCA measured in subjects using wavefront sensing, double-pass retinal images, and psychophysical methods with a custom-developed polychromatic Adaptive Optics system in a wide spectral range (450-950 nm), with control of subjects' natural aberrations

This Chapter is based on the paper by *Vinas et al. "*Longitudinal Chromatic Aberration of the human eye in the visible and near infrared from wavefront sensing, double-pass and psychophysics*" in Biomedical Optics Express (2015)*. The co-authors of the study are Carlos Dorronsoro, Daniel Cortes, Daniel Pascual and Susana Marcos.

The author of this thesis (1) implemented the experimental procedure (in collaboration with Daniel Pascual and Daniel Cortes), (2) performed the measurement on human eye's, (3) collected the data, (4) analyzed the data (in collaboration with Carlos Dorronsoro and Susana Marcos) and (5) prepared the manuscript (in collaboration with Susana Marcos). This work was also presented as an oral contribution at the Association for Research in Vision and Ophthalmology (ARVO) annual meeting (May 2014) in Orlando (Florida, USA).

5.1 Introduction

LCA has been measured using different psychophysical techniques (i.e. stigmatoscope [43, 49], Badal optometer [50], Vernier alignment [51], or the spatially resolved refractometry [10]) and across different spectral ranges [7, 229]. Reports of psychophysical LCA span from 3.20 D in a 365-750 nm range [49] to 1.33 D in a 450-650 nm range [10]. Psychophysical data of LCA have been used to derive an average Cornu's expression for the dependence of the index of refraction with wavelength (in the 400-700 nm range). This expression is used in chromatic eye models, i.e. the Indiana chromatic reduced eye model, to predict the chromatic focus shift between two given wavelengths [55].

LCA has also been measured objectively by means of reflectometric techniques, such as double-pass retinal images of a slit [14] or of a point source [18] at different wavelengths. Reports of reflectometric LCA span from 1.40 D (460-700 nm) [14] to 1.00 D (458-632 nm) [18]. More recently, chromatic difference of focus between two wavelengths has been obtained from objective wavefront sensing (Hartmann-Shack and Laser Ray tracing) with a value of 0.72 D (532-787 nm) [17] and 0.40 D in the NIR (700-900 nm) [12, 61]. Only recently, LCA has been measured objectively by means of reflectometric techniques in pseudophakic eyes, with great implications in new designs of intraocular lenses (IOLs). Perez-Merino et al. (2013) have reported the chromatic difference of focus in two groups of pseudophakic eyes implanted with IOLs of different materials, and found statistical differences, consistent with the Abbe number of the IOL materials (0.46 and 0.75 D, respectively), in the 532-787 nm range [230].

Despite the differences in the chromatic ranges and studies, there seems to be a consistent discrepancy between psychophysical and double-pass-based measurements of LCA, with the objective values underestimating the psychophysical values. These differences between objective and psychophysical LCA were observed in measurements on the same subjects where the discrepancies mostly occurred in the shorter wavelength range [14]. A later study compared the objective best focus (from double-pass aerial images) with the subjective best focus of a point source, and showed that objective data were slightly lower that subjective at the fovea and for 6-mm pupil [18]. The lower estimates of LCA from reflectometric double-pass techniques [11, 12] have been hypothesized to arise from the wavelength-dependence of the reflectivity of the different retinal layers [13]. Additionally some authors have speculated that the presence of monochromatic aberrations may affect differently the psychophysical and reflectometric measurements of chromatic aberration [44, 55]. The differences across studies in the measurement techniques and spectral ranges pose uncertainty on the actual magnitude of the differences between psychophysical and reflectometric LCA, and limits the assessment of the different hypotheses.

In this *Chapter*, we present LCA from psychophysical and reflectometric methods performed on the same group of subjects using the same instrument in a wide spectral range. The psychophysical LCA was obtained in the visible range (488-700 nm) and the LCA from reflectometric techniques was obtained both in the visible (488-700 nm) and near-infrared ranges (700-900 nm). Reflectometric techniques included both through-focus double-pass retinal images and wavefront sensing. All measurements were obtained using the new custom-developed Viobio Lab AO II system.

The study therefore provides, to our knowledge, the first evaluation of the change of high order aberrations with wavelength using objective aberration in the visible spectrum. A previous study [10] reporting high order aberrations across visible light used the spatially resolved refractometer, where aberrations were measured through a psychophysical (non-reflectometric) technique. A previous study [12] using Hartmann-Shack aberrometry reported non-significant changes in the high order aberrations with wavelength in the 700-900 nm.

Also, to our knowledge, this is the first time where subjective and objective focus (estimated from Hartman-Shack wavefront measurements) is compared at different wavelengths in visible light. Normally the studies [16, 231] relating subjective and objective best focus have been performed with white and black targets stimulus (for subjective focus) and retinal image quality metrics based on monochromatic aberrations (generally infrared) for estimation of objective best focus, assuming a constant shift produced by LCA. Recent studies have shown that in fact the best focus setting may be substantially biased by blur adaptation, and the perceived best focus not necessarily well predicted by optical model, thus justifying the interest of performing both psychophysical and objective experiments at different wavelengths [74]. Finally, the availability of an adaptive optics system in the same set-up offers a unique opportunity to test a hypothesis stated by previous authors as a potential cause of discrepancy between subjective and reflectometric techniques [44, 55]. If high order aberrations are independent of wavelength (as confirmed in this study) the lack of influence of the high order aberrations on the LCA could have been ruled out, assuming that best focus can be fully predicted by optical models. However, as psychophysical functions are not always well predicted by optical theory [86], performance of the psychophysical testing in the absence of high order aberrations (as corrected by Adaptive Optics) allows to ultimately testing the hypothesis.

5.2 Methods

Longitudinal Chromatic Aberration (LCA) was obtained from reflectometric and psychophysical measurements of best focus at 15 different wavelengths on 5 eyes from 5 normal subjects. The custom-developed polychromatic Viobio Lab AOII system was used for these measurements.

5.2.1 Subjects

Five young subjects (28.60±1.89 years) participated in the experiment. Spherical errors ranged between 0 and -4.50 D (-1.15±0.95 D), and astigmatism was ≤ -0.5 D in all cases. All experiments were conducted under cycloplegia (Tropicamide 1%, 2 drops 30 minutes prior to the beginning of the study, and 1 drop every 1 hour).

5.2.2 Experiments

The polychromatic AO system allowed correction of the aberrations of the subject, while performing psychophysical settings of best focus, acquisition of double-pass retinal images or wavefront aberration measurements at different wavelengths. The Viobio Lab AO II system has been described in detail in Chapter 2. In these experiments the psychophysical Channel contains a slide with a sunburst chart (with spatial frequencies ranging from 3.5 to 150 cycles/deg) located in a conjugated retinal plane. The visual stimulus subtends 1.62 degrees on the retina, and is monochromatically back-illuminated with light coming from the SCLS.

Subjective and objective best focus was obtained for each of the tested wavelengths. All measurements were performed using 6-mm pupil diameters, both for natural aberrations (i.e. correcting the aberrations of the optical system only) and AO-corrected aberrations. The best subjective focus was initially searched with the stimulus back-illuminated at reference wavelength of 555 nm. All settings are referred to the best subjective focus at this wavelength obtained with either natural or AO-corrected aberrations. The state of the mirror that compensates for the ocular aberrations of each eye was found in a closed-loop operation at 827 nm (NIR), and applied in measurements at all wavelengths, as a preliminary experiment showed no benefit of changing the aberration-correcting state of the mirror (measured at each wavelength) for measurements at that given wavelength. For example, the state of the mirror that corrected for the aberrations of the system and the subject at 555 nm (visible light) in a subject resulted in 0.0391 µm RMS residual aberrations. The same state of the mirror applied at 827 nm resulted in 0.0427 µm RMS. The chromatic LCA of the system was measured and measurements were corrected by the calibrated LCA of the optical system, as described in detail in *Chapter 2 Section 2.2.3.5 (B)*.

Aberrations were monitored throughout the experiment to ensure that each state was performed under the desired state of aberration corrections. Experiments were performed first under natural aberrations and then under AO-correction. The following measurements were performed, in this order:

Experiment 1. Psychophysical best focus. Subjects adjusted their best subjective focus using the Badal system while looking at the stimulus back-illuminated with a

series of wavelengths in visible light: 450, 488, 500, 532, 555, 570, 633 & 700 nm. Subjects were instructed to use the keyboard to move the Badal system to find the position where the stimulus appeared sharp. Subjects performed first a trial run to become familiar with the test. Focus search was repeated 3 times for each wavelength.

Experiment 2. Through-focus double pass retinal aerial images at different wavelengths. Retinal aerial images were obtained while the Badal system was moved from -1.50 D to +1.50 D in 0.25-D steps (around the best subjective focus at 555 nm). These measurements were obtained both in visible light (488, 500, 532, 555, 570, 633 & 700 nm) and near IR light (730, 780, 810, 827, 850, 880 & 950 nm).

Experiment 3. Hartmann-Shack wave aberrations at different wavelengths. Wave aberrations were measured in visible light (488, 500, 532, 555, 570, 633 & 700 nm) and near IR light (730, 780, 810, 827, 850, 880 & 950 nm), while the Badal system corrected the subject's subjective defocus at 555 nm.

Experiments 4, 5 and 6**,** were identical to Experiments 1, 2, and 3, but under AO-correction. Psychophysical measurements in *Experiment 4* were performed for the same wavelengths than in Experiment 1. Experiments 5 and 6 were performed for 488, 500, 555 & 700 nm in visible light and 730, 880 & 950 nm in near IR light, to avoid the fatigue of the subjects. The reference for best focus at 555 nm was obtained subjectively first under natural aberrations for Experiments 1, 2 and 3, and under AO-correction for Experiments 4, 5, and 6.

5.2.3 Data analysis

The best subjective foci at each wavelength from Experiment 1 were directly obtained from the automatic readings of the Badal system. The best foci from Experiment 2 were obtained by analysis of the through-focus retinal aerial image series for each wavelength [232]. The best focus image from the series was obtained from the focus position corresponding to the image with minimum spread (lower width at half-height). The wave aberrations measured in Experiment 3 were fitted by 7th order Zernike polynomials. The OSA convention was used for ordering and normalization of Zernike coefficients [15].

For each wavelength, defocus in diopters, *D,* was obtained from the 2nd order Zernike defocus coefficient (C_2^0) in microns, using

$$D = -4.C_2^0.\sqrt{3}/r^2 \qquad (5.1),$$

where $\boldsymbol{C_2^0}$ is the Zernike defocus and ***r*** is the pupil radius [37].

In an alternative analysis, best focus was obtained from through-focus Strehl Ratio (SR) simulations calculated from the measured wave aberrations, as the maximum

of the Point Spread Function (PSF) relative to the diffraction-limited-PSF, for 6-mm pupils and the corresponding wavelength. The best focus was obtained from the maximum of the peak of the calculated through-focus SR curves for each measured wavelength. A control simulation showed that the best focus obtained from the retinal image quality metrics (minimum spread and Strehl ratio, as well as volume under the MTF in the spatial frequency range of the target stimulus), was within 0.15 D, on average. Chromatic difference of focus curves were obtained from the data of best focus of each experiment. The LCA was obtained from the polynomial fitting of those curves. The curves are shifted in the vertical axis such that they cross zero at 555 nm (the reference wavelength). For the psychophysical data, LCA was computed for the visible range only. For the reflectometric experiments, LCA was computed for visible (488-700 nm, VIS), near IR (700-950 nm, NIR) and total (488-950 nm, TOTAL) ranges. Focus setting reproducibility was obtained from measurements of best focus for one subject and all wavelengths, based on 5 focus settings both for natural and AO-corrected aberrations. Variability in focus setting was < 0.05 D for all wavelengths, except in wavelengths at the end of the spectral ranges (450 and 700 nm), where the variability was 0.1 D.

Statistical analysis was performed with SPSS software (IBM, United States) to test differences in the estimated LCA across experiments. A *non-parametric paired samples t-test* with *post hoc* Wilcoxon Signed Ranks test was performed to analyze specific differences between conditions.

5.3 Results

LCA was obtained from measurements of best focus at different wavelengths from psychophysical (Experiment 1/4) and reflectometric (Experiments 2-3/5-6) experiments, with natural and corrected aberrations.

5.3.1 Wave aberration measurement and correction at different wavelengths

Figure 5.1 shows wave aberration maps for astigmatism and HOA (Fig.5.1 (a)) and their corresponding RMS (Fig. 5.1 (b)) for selected measured wavelengths in one subject, with natural aberrations and AO-correction. Wave aberrations maps are similar, with no systematic variation, across wavelengths. The RMS standard deviation across wavelengths was 0.04 µm for natural aberrations and 0.01 µm for AO-correction, averaged across subjects. Residual RMS upon AO-correction was lower than 0.05 µm.

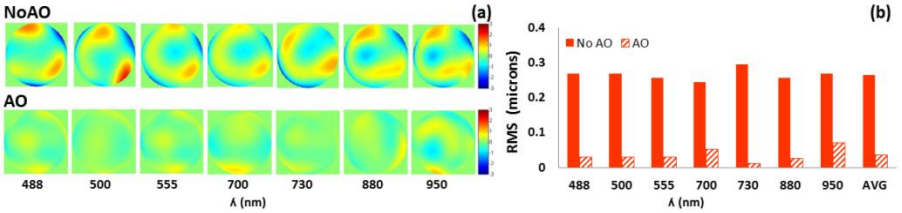

Figure 5.1 (a) Wave aberrations map for astigmatism and HOA for selected wavelengths in Subject #3 with natural aberrations (upper row) and AO-correction (lower row). (b) Corresponding RMS. Data are for 6-mm pupils.

5.3.2 Through-focus image quality at different wavelengths (measurements and simulations)

Through-focus double-pass retinal images (Experiment 2/5) and through-focus SR (calculated from wave aberrations, Experiment 3/6) was used to estimate best focus for each wavelength. Figure 5.2 shows examples of through-focus experimental aerial images (Figure 5.2 (a)), and simulated through-focus Point Spread Functions (PSF), with natural aberrations (Figure 5.2 (b)), and with AO-correction (Figure 5.2 (c)); best focus obtained from series of double-pass images, with natural aberrations and AO correction (Figure 5.2 (d)) and best focus obtained from through-focus SR calculations for natural aberrations (Figure 5.2 (e)) and AO-correction (Figure 5.2 (f)).

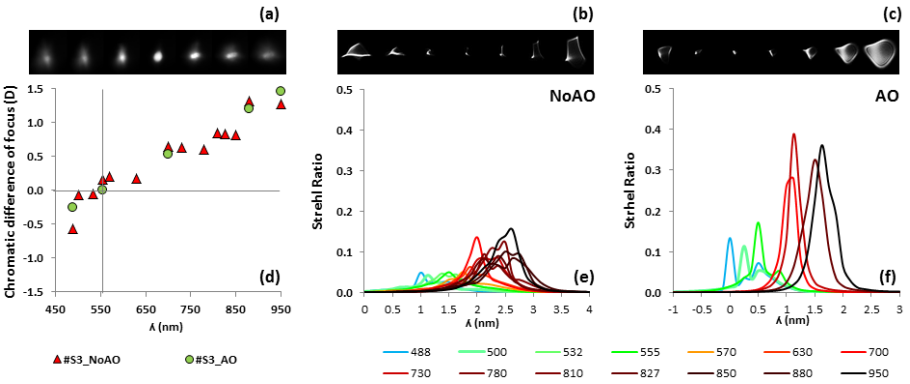

Figure 5.2 (a) Example of experimental through-focus double-pass retinal images for subject #S1 at 555 nm with natural aberrations. (b) Example of simulated through-focus PSF at 555 nm for #S2 under natural aberrations, and (c) under AO-correction. (d) Chromatic difference of focus obtained from series of double-pass images at all measured wavelengths for subject #S3, with natural aberrations (Red triangles), and AO-correction (Green circles). (e) Through-focus Strehl Ratio (SR) calculated from measured wave aberrations at each wavelength for subject #S2 under natural aberrations, and (f) under AO-correction.

5.3.3 Chromatic difference of focus from psychophysical and reflectometric techniques

Figure 5.3 shows the measured chromatic difference of focus from psychophysical measurements [Experiment 1, Figure 5.3 (a)], through focus retinal images [Experiment 2, Figure 5.3 (b)] and defocus Zernike coefficient [Experiment 3, Figure 5.3 (c)] for all 5 subjects and all measured wavelengths, under natural aberrations, [upper row, Figures 5.3 (a)-(c)], and AO-correction, [Figures 5.3 (d)-(f)].

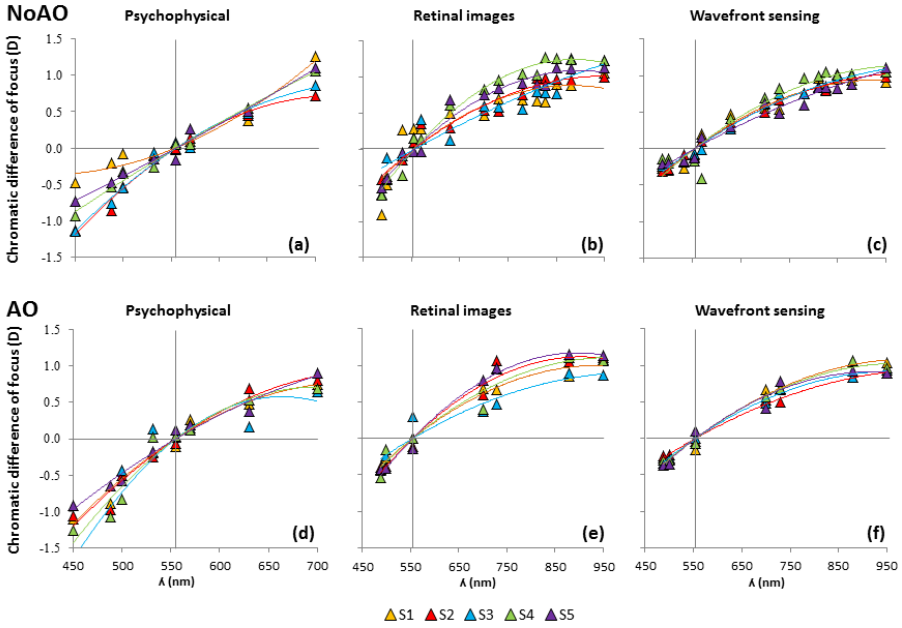

Figure 5.3 Chromatic difference of focus (a) from subjective best focus; (b) from series of double-pass retinal images; (c) from the defocus Zernike coefficient of measured wave aberrations, at different wavelengths. (a-c) Under natural aberrations. (d-e) As in (a-c), but with AO-correction. Data are referred to the best focus at 555 nm for each technique, set as zero defocus.

Figure 5.4 compares chromatic difference of focus curves across the different techniques, averaged across subjects, for natural aberrations [Figure 5.4 (a)] and AO-correction [Figure 5.4 (b)]. The difference between the curve fitting the psychophysical data and that fitting the reflectometric data (0.107 RMS difference for double-pass and 0.769 RMS for wavefront sensing, for natural aberrations and 0.014 RMS difference double-pass and 0.307 RMS for wavefront sensing, for AO-correction) is significantly higher (paired-samples t-test, p=0.004) than the difference between the curves fitting either reflectometric data (0.044 RMS difference for natural aberrations and 0.057 RMS for AO-correction). There is also great similarity between data obtained under natural aberrations and AO-

correction (0.3078, 0.0071, and 0.0032 RMS difference for averaged psychophysical data, wavefront sensing data, and double-pass).

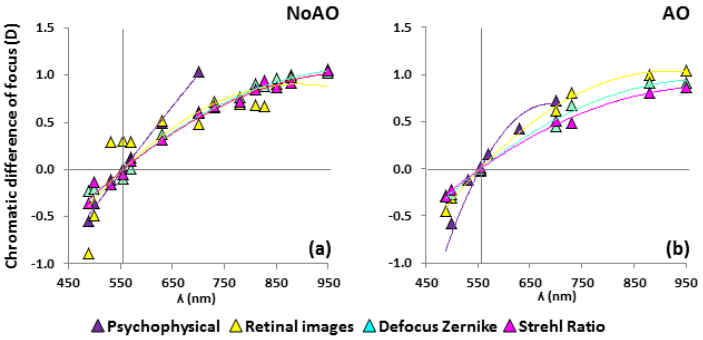

Figure 5.4 (a) Chromatic difference of focus for all 4 techniques: psychophysical, purple; retinal images, yellow; wavefront sensing/defocus Zernike term, green; wavefront sensing/Strehl Ratio, magenta. Data are averaged across subjects; (a) from measurements with natural aberrations. (b) As in (a) but from measurements with AO-correction of natural aberrations. Data are referred to 555 nm by shifting the polynomial regressions of the measured data.

The chromatic difference of focus between green and blue wavelengths was smaller than between and green and red wavelengths in all techniques, although in both ends the chromatic difference of focus was larger for psychophysical than for reflectometric techniques. Table 5.1 shows the chromatic difference of focus for green-blue and green-red for all techniques, both under natural aberrations and AO-correction.

	Green-Blue/555-488 nm		Green-Red/555-700 nm	
	NoAO	AO	NoAO	AO
Psychophysical	0.53 D	0.75 D	0.99 D	0.74 D
Retinal images	0.35 D	0.41 D	0.59 D	0.65 D
Wavefront sensing	0.33 D	0.33 D	0.55 D	0.55 D
Strehl Ratio	0.32 D	0.32 D	0.55 D	0.54 D

Table 5.1 Chromatic difference of focus.

5.3.4 LCA: differences across techniques

Figure 5.5 shows LCA in the visible spectral range common to all techniques (488-700 nm); and LCA in the near IR spectral range (700-950 nm) and total spectral range (450-950 nm) from reflectometric techniques, both with natural aberrations and with AO-correction. The LCA for the largest available spectral range in the visible (450-700 nm was on average 1.84±0.05 D from psychophysical data. The LCA in the 488-700 nm range was 1.52 D from psychophysics, and 0.95 D and 0.88 D from retinal images and wavefront sensing reflectometric techniques, under

natural aberrations. The LCA for the total spectral range was 1.41 D and 1.34 D from for retinal images and wavefront sensing, respectively.

The LCA from psychophysical experiments is statistically significantly higher (*paired-samples t-test, p<0.01*) than that from the reflectometric techniques. There are no statistically significant differences in LCA for neither the visible, NIR or total spectral range from all reflectometric techniques (*paired-samples t-test, p=0.42; p=0.95 and p=0.49, respectively*). Intersubject variability is small for all techniques: psychophysical, ±0.04 D for VIS, retinal images, ±0.07 D, and wavefront sensing, ±0.06 D for the total spectral range, in the presence of natural aberrations.

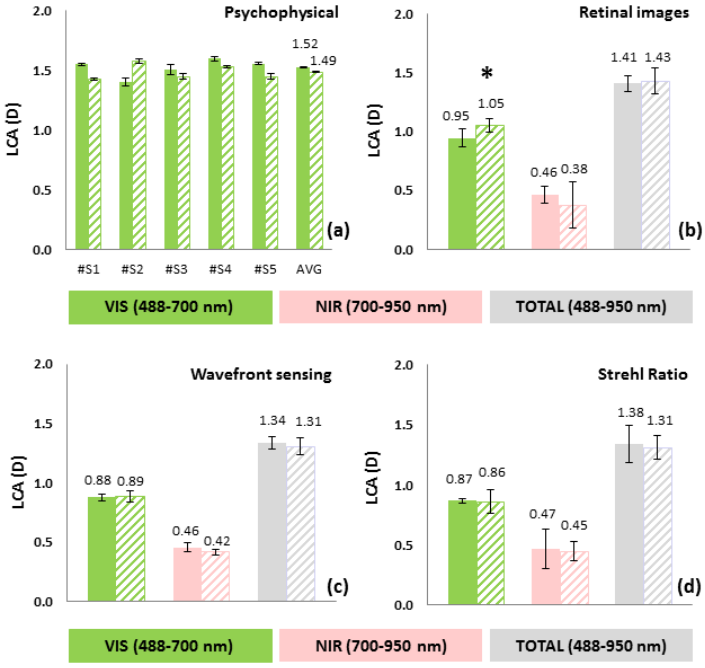

Figure 5.5 LCA averaged across subjects from (a) subjective best focus, (b) retinal images, (c) wavefront sensing and (d) Strehl Ratio for the different spectral ranges: VIS, NIR and TOTAL. Solid bars indicate Natural aberrations, and dashed bars indicate AO-correction; (*) stands for statistically significant differences (p = 0.02) Error bars stand for standard deviations of repeated measurements for subjective LCA and standard deviation across subjects for the other techniques.

5.3.5 LCA: impact of the presence of high order aberrations

Correction of the eye's natural aberrations produces a shift of the best focus, due to interactions between defocus and spherical aberration (and likely other HOA). The average difference in this shift (across subjects and wavelengths) was 0.35±0.12 D for psychophysical measurements, 0.21±0.10 D for double-pass, 0.18±0.05 D for the defocus Zernike coefficient, and 0.27±0.04 D from simulated

SR. In all subjects this shift was constant across wavelengths. This result suggests that the presence of aberrations play a negligible role in the LCA, regardless the technique.

Figure 5.5 shows the LCA obtained from each technique, under natural and AO-corrected aberrations. In general, the presence of natural aberrations does not change LCA significantly, in neither psychophysical or reflectometric techniques, except for in the double-pass LCA in the visible range (*paired-samples t-test, p<0.02*).

5.4 Discussion

5.4.1 Comparison of LCA with previous studies

Our study provides estimates of the LCA measured across a wider spectral range in the visible and IR than that of previous studies. Figure 5.6 shows the chromatic difference of focus found in the current study (psychophysical, purple; reflectometric, yellow), in comparison with the predictions of the Indiana chromatic reduced eye model (black) [55] and the chromatic difference of focus reported in previous studies for different spectral ranges, using psychophysical (blue) and reflectometric (orange) methods. In general, our results are in good agreement with previous studies using psychophysical and reflectometric techniques.

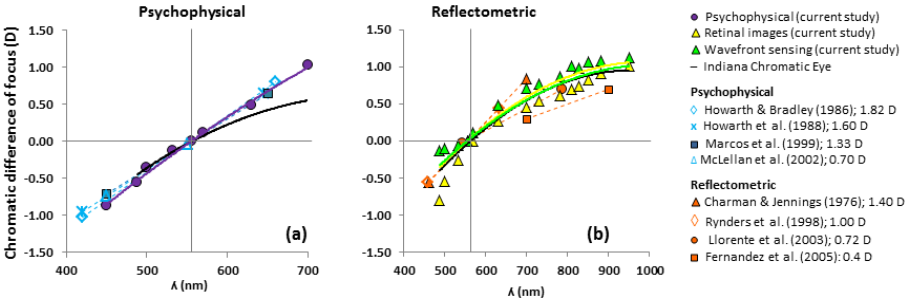

Figure 5.6 (a) Chromatic difference of focus from the psychophysical measurements of the current study (purple), the predictions from the Indiana chromatic reduced eye model (black), and psychophysical data in the literature (blue) in the visible range. (b) Chromatic difference of focus from the reflectometric measurements (yellow, from retinal images; green, from wavefront sensing) of the current study, the predictions from the Indiana chromatic reduced eye model (black), and reflectometric data in the literature (orange) in the visible and NIR range. The measured chromatic range differed across studies, and it is indicated by the symbols in the end of the regression curves. The numbers indicate the corresponding literature reference (see legend). Data are referred to zero defocus at 555 nm.

The Indiana chromatic reduced eye model, built using experimental data [17], predicts a chromatic focus shift of 1.00 D for VIS, 0.44 D for NIR, and 1.45 D for

TOTAL. The chromatic eye model seems to fit well the psychophysical data for shorter wavelengths and the reflectometric data for longer wavelengths. There is a general good agreement with data in shorter ranges from previous studies, both psychophysical and reflectometric.

5.4.2 Impact of natural aberrations: subjective vs. objective focus

The presence of HOA shifts the position of best focus from the best focus in absence of aberrations. Although neural adaptation to astigmatism or HOA may alter the perceived best focus position with respect to that predicted solely by optics [73, 75, 214], several studies indicate that subjective refraction can, in general, be well predicted from objective measurements (wave aberrations or double-pass), particularly when retinal image based metrics are used [10, 48, 231]. Similarly, retinal image quality metrics predict well the best focus shift between natural aberrations and AO-correction [232]. Here, we have shown that the shift in best focus caused by the presence of natural aberrations is constant across wavelengths. This indicates that, while the absolute best focus is affected by the presence of aberrations, this occurs at all wavelengths equally, and therefore LCA remains unaffected by the presence of aberrations (i.e. measurements with a larger or smaller pupil, etc.), ruling out the potential role of HOA in the differences between psychophysical and reflectometric LCA suggested by previous authors [16, 44, 55, 233].

5.4.3 Psychophysical vs. reflectometric LCA: effect of retinal reflection

It has been suggested that most of the light contributing to the core of double-pass aerial images likely comes from the light captured and guided back from the photoreceptors [14, 15]. The halo appearing in the double pass images is likely produced by effects other than aberrations, such as retinal stray light scattered at the choroid [16]. Retinal scattering increases for longer wavelengths due to their deeper penetration within the retina and the choroid [17]. The relative contribution of the directional component coming from the photoreceptors, the diffuse component coming from other retinal layers, choroid and optically turbid media, and a specular component, coming from smooth boundaries of optical media (such as the inner limiting membrane or corneal surface), is wavelength-dependent [18]. Photoreceptor alignment reflectometry demonstrates a high directional component in green light, which is highly reduced in IR [19].

The directional component will be highly concentrated around the central peak of the aerial image, whereas diffuse or (defocused) specular components will yield little contribution to the peak, and lead to potential differences in the plane identified as in focus. Some studies have reported negligible differences between psychophysical and reflectometric focus, concluding that reflection contributing to

the central core of the point-spread function occurred within the photoreceptor layer [16, 17, 234]. However, while this may be true for wavelengths close to the peak of retinal sensitivity (green-red light) it not may be the case for shorter or longer wavelengths.

Assuming that best focus from psychophysical and reflectometric techniques matches at 555 nm, the average data in Figure 5 shows that the deviations occur both at the short and long range of the spectrum. At 488 nm the average difference between psychophysical and reflectometric best focus is 0.25 D, which, from a schematic reduced eye model, corresponds to blue light being reflected 128 µm anteriorly from the photoreceptors inner segments, approximately in the retinal nerve fiber layer in the retina. At 700 nm, the shift is 0.54 D, suggesting that the reflection occurs 370 µm behind the photoreceptors, in the choroid [235-237]. This fact is interesting since in red light the contribution of the choroidal reflections is large compared with that of reflections originating in the inner layers of the retina [238], and might explain the higher shift in red than in blue light.

5.5 Conclusions

We have shown that: (1) ocular LCA shows low intersubject variability; (2) the LCA from a psychophysical method is significantly higher (by 0.50 D in the 488-700 nm range) than the LCA measured using reflectometric techniques, and (3) the LCA (from either psychophysical or reflectometric techniques) is independent of the presence of HOA.

The observed differences between the psychophysical and reflectometric LCA may arise, as previously proposed, from the fact that the retinal reflection may not occur at the plane at which the retinal image must be focused to give the best subjective image at all wavelengths. The hypothesized non-symmetric contribution of red and blue light to chromatic defocus should be considered when calculating the retinal image quality for polychromatic light [77].

An accurate knowledge of the ocular LCA is useful for identifying the focus shifts necessary to convert aberrometric (and refractometric) measurements typically obtained in the IR into visible wavelengths. Knowledge of chromatic aberration is also important for *in vivo* retinal imaging, especially when pursuing multi-wavelength imaging [239] with conventional fundus cameras, Scanning Laser Ophthalmoscopy (SLO), or Optical Coherence Tomography (OCT) [240]. In addition, in multi-wavelength Adaptive Optics SLO, correcting for the eye's chromatic aberrations is necessary in applications that require imaging simultaneously in identical depths with two wavelengths [241]. A better understanding of the interactions between chromatic and polychromatic aberrations is also important in the study of the limits to spatial vision, and more practically for the material selection and design of new intraocular lenses.

As shown in this Chapter, the LCA of the human eye has been extensively measured in phakic eyes. However, most estimates of LCA in pseudophakic eyes come from computations based on the IOL material Abbe number, and very few come from actual measurements on patients. The following Chapter provides estimates of the LCA measured in a wider spectral range in the visible and near infrared than that of previous studies, using both psychophysical and wavefront sensing measurements.

6

In vivo subjective and objective longitudinal chromatic aberration in patients bilaterally implanted with same design hydrophobic and hydrophilic IOLs

The understanding of the mechanisms underlying chromatic aberration and its compensation is of great importance in pseudophakic eyes since the replacement of the lens modifies the chromatic dispersion properties of the eye, as this is affected by the refractive index wavelength-dependency of the IOL material. Therefore, the optical performance of the pseudophakic in polychromatic light will be determined by both the IOL design and the IOL material. However, only a few studies have measured the LCA of pseudophakic eyes *in vivo*. In this Chapter measurements of the LCA *in vivo* using psychophysical and wavefront sensing methods in patients bilaterally implanted with monofocal IOLs of similar aspheric design but different materials are presented.

This Chapter is based on the paper by *Vinas et al. "In vivo subjective and objective longitudinal chromatic aberration in patients bilaterally implanted with same design hydrophobic and hydrophilic IOLs" in Journal of Cataract and Refractive Surgery (2015)*. The co-authors of the study are Carlos Dorronsoro, Nuria Garzón, Francisco Poyales and Susana Marcos. Daniel Pascual and Daniel Cortes provided technical support. The research leading to these results has received funding from a collaborative research project funded by PhysIOL.

The author of this thesis (1) implemented the experimental procedure, (2) performed the measurement on human eye's, (3) collected the data, (4) analyzed the data and (5) prepared the manuscript (in collaboration with Susana Marcos). Selection, and clinical and optometric evaluation of the subjects participating in the study was performed by Nuria Garzón. Surgeries were performed by Francisco Poyales. This work was also presented as an oral contribution at the European Society of Cataract and Refractive Surgery (ESCRS) annual meeting (September 2015) in Barcelona (Spain).

6.1 Introduction

In recent years, monofocal IOL designs have improved not only to restore transparency or to correct refractive errors (sphere and cylinder), but also to reduce the spherical aberration of the eye [97-101]. However the replacement of the lens also modifies the chromatic dispersion properties of the eye, as this is affected by the refractive index wavelength-dependency of the IOL material. Therefore, the optical performance of the pseudophakic in polychromatic light will be determined by both the IOL design and the IOL material.

The impact of the chromatic aberrations in the pseudophakic eye has been acknowledged [163-165]. There are even proposals for IOL (diffractive) designs aiming at correcting the ocular LCA [108, 166]. The dispersion properties of the IOL are defined by the Abbe number (ranging in most of designs from 35 to 60). The higher the Abbe number, the lower the LCA. Most reports of LCA and polychromatic optical quality in pseudophakic eyes are based on computational predictions on eye models and the IOL material Abbe number [163, 166, 167].

There are very few studies reporting *in vivo* measurements of LCA of pseudophakic eyes. Nagata et al. (1999) measured the LCA *in vivo* (500-650 nm) in pseudophakic eyes implanted with PMMA and acrylic IOLs [164], using a modified chromoretinoscopy system [242]. Perez-Merino et al. (2013) reported monochromatic aberrations measured at two wavelengths (532 and 785 nm) in two groups of pseudophakic eyes implanted with two IOLs (Tecnis by Abbott Medical Optics, Santa Ana, California, USA, and Acrysof IQ by Alcon, Alcon Research Labs, Fort Worth, Texas, USA) of different materials, and found statistical differences between the chromatic different of focus with the two IOL types (0.46 and 0.75 D, respectively), consistent with the Abbe number of the IOL materials [230]. Siedlecki et al. (2014) presented the chromatic difference of focus in pseudophakic eyes implanted with two types of AcrySof lenses from Alcon (the IQ SN60WF, spherical asymmetric biconvex lens and the SA60AT, aspheric asymmetric biconvex lens) measured at 470, 525 and 660 nm, using an autorefractometer adapted to monochromatic measurements of refraction [243].

In this Chapter *in vivo* LCA measurements in pseudophakic patients bilaterally implanted with monofocal aspheric hydrophobic and hydrophilic IOLs, by PhysIOL (PhysIOL, Liege, Belgium) are presented. Measurements were performed on patients using psychophysical and wavefront sensing methods, on the custom-developed polychromatic Viobio Lab AO II system described in *Chapter 2*.

The psychophysical LCA was obtained in the visible range (480-700 nm) and the LCA from wavefront sensing was obtained both in the visible (480-700 nm) and near-infrared ranges (700-900 nm). Chromatic difference of focus curves were obtained from best focus data at each wavelength in each experiment, and the LCA was

obtained from the slope of linear regressions to those curves. The measured LCA was compared between eyes of the same patient, with LCA values obtained on young phakic patients using the same experimental system, and with LCA reported on pseudophakic patients in the literature.

6.2 Methods

LCA was obtained from psychophysical and wavefront sensing measurements of best focus at 8 different wavelengths on 18 eyes from 9 subjects, bilaterally implanted with same design but different materials IOLs (Podeye and Poday, by PhysIOL) in each eye. Measurements were performed using the custom-developed polychromatic Viobio Lab AO II system.

6.2.1 Subjects & IOLs

Nine patients (mean age 73.92 ± 4.28 years) participated in the study. Table 6.1 shows the age, refractive and clinical profiles of the participants.

All subjects were bilaterally implanted, one eye with the PhysIOL Podeye double C Loop hydrophobic lens, and the contralateral eye with PhysIOL Poday hydrophilic lens (PhysIOL, Liege, Belgium). Both IOLs are monofocal and aspheric, but they differ in their material. Table 6.2 shows the characteristics of the two IOL types.

Subject's profile

ID	Lens implanted	IOL power	Preoperative data				Follow-up (1 month)			
			Sph	Cyl	Axis	DCVA LogMAR	Sph	Cyl	Axis	DCVA LogMAR
#S1_R_EYE	Podeye	21.50	3	-1	80	0.4	1.5	-1.25	80	0
#S1_L_AY	Poday	22.50	4	-0.5	90	0.3	0	0	0	0
#S2_R_AY	Poday	20.50	-0.75	-1	90	0.15	0	0	0	0
#S2_L_EYE	Podeye	21.00	-1.75	-1.25	95	0.2	0	0	0	0.05
#S3_R_EYE	Podeye	21.00	1.75	-1	55	0.3	0	-0.75	80	0
#S3_L_AY	Poday	19.50	1.25	-1	115	0.2	0	-0.75	100	0
#S4_R_AY	Poday	18.50	1.25	1.25	180	0.1	-1	0	0	0
#S4_L_EYE	Podeye	18.00	0.75	-0.5	12	0.2	0	0	0	0
#S5_R_AY	Poday	21.00	1.75	-1	90	0.2	0	0	0	0
#S5_L_EYE	Podeye	20.50	1.25	-0.5	65	0.25	0	0	0	0
#S6_R_EYE	Podeye	23.00	-2.75	-0.75	120	0.3	0	0	0	0
#S6_L_AY	Poday	22.50	-3.25	-1	110	0.25	0	0	0	0
#S7_R_EYE	Podeye	20.00	-1	-2.25	20	0.5	1	-1	180	0
#S7_L_AY	Poday	21.50	0.5	-0.5	180	0.3	0	0	0	0
#S8_R_EYE	Podeye	18.00	-2.75	-1.5	105	0.2	0.5	-1.5	95	0
#S8_L_AY	Poday	19.50	0	-1	70	0.1	0.5	-1	75	0
#S9_R_AY	Poday	19.00	-1	-0.5	70	0.2	0	-0.75	100	0
#S9_L_EYE	Podeye	18.00	-1	-0.75	100	0.25	0.75	-0.5	70	0

Table 6.1 Optometric subjective refractions (spherical error, cylinder, axis) of the patients of the study, pre-operatively and 1-month post-operatively. #S_EYE stands for eyes implanted with PhysIOL Podeye (hydrophobic) and #S_AY for eyes implanted with PhysIOL Poday (hydrophilic). Cyl, cylinder; Sph, spherical error.

Post-operative clinical evaluations were conducted at 1 day, 1 week and 1 month after surgery, and included uncorrected and best-corrected VA, using the ETDRS test, intraocular pressure (Goldmann) and biomicroscopy. At the 1-month follow-up visit, the visual quality was assessed in the clinic by the objective scatter index (OSI), modulation transfer function (MTF) and Strehl ratio, measured using the Optical Quality Analyzer System (OQAS, Visiometrics S.L., Terrassa, Spain). Night haloes were measured using the software Halo v1.0 (University of Granada, Spain).

Surgical procedures were performed by two surgeons on an outpatient basis under topical anesthesia. For phacoemulsification, the surgeon made a 2.2 mm clear corneal incision. The IOLs were implanted in the capsular bag with a single-use injection system (Microset, PhysIOL). All experiments were conducted under mydriasis (Tropicamide 1%, 2 drops 30 minutes prior to the beginning of the study, and 1 drop every 1 hour).

IOLs profiles

Model	Material	Design*	Asph. aberration-correcting	Hazardous-Light Protection*	RI	Abbe
Podeye [244]	Hydrophobic acrylic GF material	Monofocal, 1-piece, double C-loop	-0.11µ SA	UV/blue	1.52	~41.91
Poday	Hydrophilic acrylic GF material	Monofocal, 1-piece, double C-loop	-0.11µ SA	UV/blue	1.46	~58.00

GF = glistening free; RI = refractive index; UV = ultraviolet;
*Data from the intraocular lens specification

Table 6.2 Specifications of the Podeye and Poday IOLs, provided by the manufacturer.

Patients received a complete ophthalmic evaluation prior to enrollment in the study and surgery at the Instituto de Oftamología Avanzada (Madrid, Spain). The pre-operative examination included uncorrected and best-corrected visual acuity (VA) using the ETDRS test, biomicroscopy, corneal topography (Nidek Co., Ltd), tonometry (Goldmann), and a fundus examination. Axial length, anterior chamber depth and white to white were measured with optical biometry, IOLMaster (Zeiss, Oberkochen, Germany). The IOL power was calculated with the Holladay-2 formula, targeting emmetropia.

The inclusion criterion for the study were good general health, no ocular pathology, no complications during surgery, IOL power between 18.00 and 23.00 D, natural astigmatism <1.50 D, bilateral implant, clear capsule and best corrected post-operatory corrected VA > 0.7. Surgeries in each eye were conducted with a time difference < 7 days, and the IOLs (Podeye or Poday) were randomly assigned to the first or second operated eye.

6.2.2 Experiments

Measurements were conducted in the custom-developed polychromatic Viobio Lab AO II system, described in detail in *Chapter 2 Methods*, which allowed control of the aberrations of the subject, while performing both psychophysical settings of best focus and wavefront aberration measurements at different wavelengths. Experimental setup is similar to the one use in the previous Chapter.

LCA was obtained from psychophysical and objective estimates of best focus for each of the tested wavelengths. The best subjective focus was initially searched with the stimulus back-illuminated at reference wavelength of 550 nm, and set as zero. The following experiments were performed, in this order:

Experiment 1: Psychophysical best focus at different wavelengths. Patients adjusted their best subjective focus using the Badal system while viewing the

stimulus back-illuminated with different wavelengths in visible light (480, 532, 550, 650 & 700 nm). Patients were instructed to use the joystick to move the Badal towards the position where the stimulus, initially blurred by means of defocus induced with the Badal system, appeared sharp for the first time. Patients performed a trial before the experiment to become familiar with the test. The best focus settings were repeated 3 times for each wavelength, presented randomly.

Experiment 2: Hartmann-Shack wave aberrations at different wavelengths. Wave aberrations were obtained in visible light (480, 532, 550, 650 & 700 nm) and near IR light (780, 827 & 950 nm), while the Badal system corrected the subjective defocus of the patient at 550 nm. The reference for best focus at 550 nm was obtained subjectively under natural aberrations for Experiments 1 and 2.

6.2.3 Data analysis

The best subjective foci at each wavelength in Experiment 1 were directly obtained from the automatic readings of the Badal optometer. The best foci at each wavelength in Experiment 2 were obtained from the 2nd order Zernike defocus coefficients (C_2^0) in microns, from the Zernike polynominal expansions fitting the wave aberrations measured at each wavelength. Chromatic difference of focus curves were obtained from the best foci vs. wavelength dataset of each experiment. LCA was obtained from a 2^{nd} order polynomial fitting to those curves. The curves are shifted in the vertical axis such that they cross zero at 550 nm (the reference wavelength) for a unique reference for all techniques.

For the psychophysical data, LCA was computed for the visible range only. For the wavefront sensing experiments, LCA was computed for visible (480-700 nm, VIS), near IR (700-950 nm, NIR) and total spectral ranges (480-950 nm, TOTAL). For comparisons with the literature, the chromatic difference of focus between two specific wavelengths was also calculated.

Statistical analysis was performed with SPSS software (IBM) to test differences in the estimated LCA across experiments and conditions. A *paired samples t-test* was performed to analyze specific differences between conditions.

6.3 Results

6.3.1 Wave aberration measurement at different wavelengths

Wave aberrations were measured for both eyes and all subjects at 8 wavelengths. With wavelength, only the defocus Zernike term shows significant differences, while astigmatism and HOA do not show systematic changes.

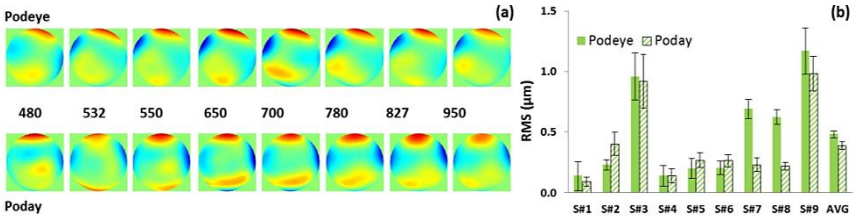

Figure 6.1 (a) Wave aberrations maps for the astigmatism and HOA in Subject #6, for the eye implanted with the Podeye (upper row) and Poday (lower row) IOLs, for all measured wavelengths. (b) Averaged RMS (astigmatism and HOA) for all subjects (eyes implanted with Podeye and Poday IOLs, respectively), and average across each lens type. Data are for 6-mm pupils.

Figure 6.1 (a) shows wave aberrations maps (astigmatism and HOA) in Subject #6 (a) for the eye implanted with PhysIOL Podeye (upper row) and PhysIOL Poday (lower row) IOLs, illustrating little variations in the wave aberrations with wavelength. On average across eyes, the variation of RMS for astigmatism and HOA was less than 4% across wavelengths.

Figure 6.1 (b) shows the average RMS (astigmatism and HOA) across wavelengths for each subject (eyes implanted with Podeye and Poday IOLs, respectively). RMS for astigmatism and HOA was, on average, 0.48±0.03 µm for Podeye and 0.39±0.03 µm for Poday (last bars in Figure 6.1 (b)) IOLs.

6.3.2 Chromatic difference of focus from psychophysical and wavefront sensing

Figure 2 shows the measured chromatic difference of focus from psychophysical measurements (Experiment 1: Figure 6.2 (a) for Podeye IOLs and (b) for Poday IOLs), and from the defocus Zernike coefficients from wavefront sensing (Experiment 2: Figure 6.2 (c) for Podeye IOLs and (d) for Poday IOLs), for all measured wavelengths in each experiment. Lines represent polynomial fitting curves to the data.

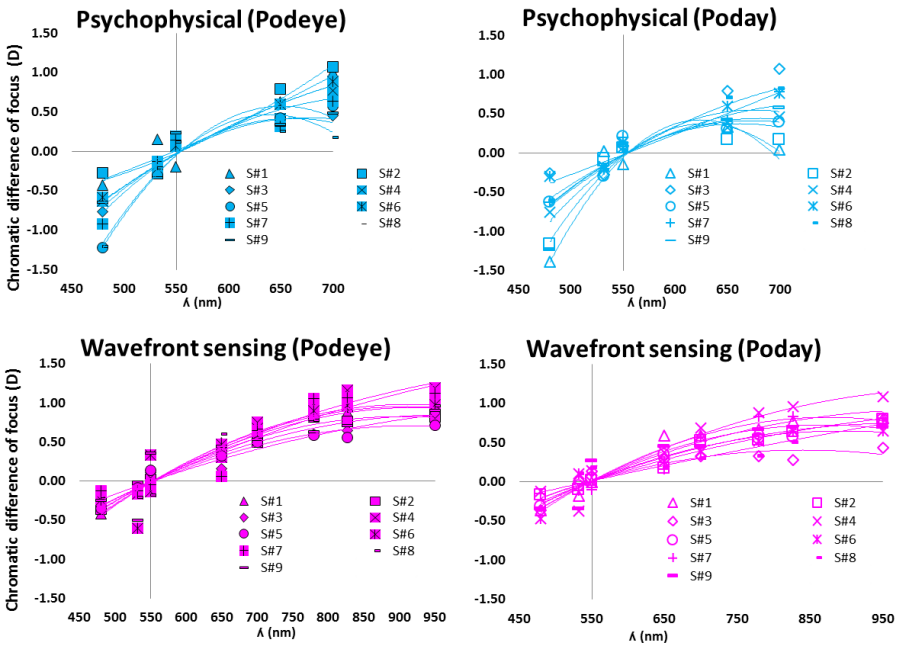

Figure 6.2 Chromatic difference of focus from psychophysical best focus of monochromatic stimuli (a-b) and from defocus Zernike terms from wavefront sensing (c-d) for eyes implanted with PhysIOL Podeye (a-c) and Poday (b-d) IOLs, for all subjects and all measured wavelengths (psychophysical: 480, 532, 550, 650 & 700 nm; wavefront sensing: 480, 532, 550, 650, 700, 780, 827 & 950 nm). Data are referred to the best focus at 550 nm, set as zero defocus.

6.3.3 LCA: differences across eyes and techniques

Figure 6.3 shows LCA from psychophysical measurements (a) in the visible range (480-700 nm) and from wavefront sensing (b) in the visible range (480-700 nm) and (c) in the total spectral range (480-950 nm) for all subjects and all implanted eyes, Podeye (solid bars) and Poday (dashed bars).

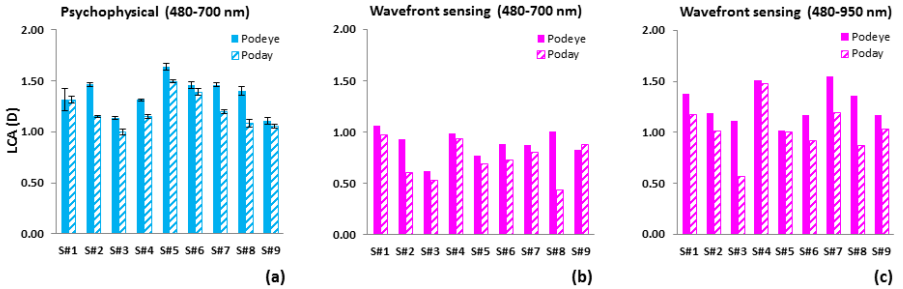

Figure 6.3 Chromatic LCA from (a) subjective best focus and (b) wavefront sensing for the visible (480-700 nm) and (c) Visible + NIR (480-950 nm) spectral range for all subjects and averaged across subjects. Solid bars indicate eyes implanted with Podeye IOL, and dashed bars indicate eyes implanted with Poday IOL. Error bars in the subjective LCA stand for standard deviation of repeated measurements.

Table 6.3 shows the average LCA from psychophysical and wavefront sensing measurements in the different spectral ranges measured for both IOL types. LCA from Podeye is statistically higher than LCA from Poday in both techniques in the visible range as well as in the total spectral range. Intersubject variability is small for both techniques: ±0.008 D for the psychophysical technique (visible range) and ±0.006 D for wavefront sensing (total spectral range).

		Psychophysical			Wavefront sensing		
		Podeye	Poday	p-value	Podeye	Poday	p-value
Visible	480-700 nm	1.37±0.08 D	1.21±0.08 D	p=0.003 (*)	0.88±0.07 D	0.73±0.09 D	p=0.004 (*)
NIR	700-950 nm				0.39±0.07 D	0.29±0.08 D	p=0.184
Visible + NIR	480-950 nm				1.27±0.09 D	1.02±0.13 D	p=0.004 (*)

Table 6.3 Averaged LCA from psychophysical and wavefront sensing measurements in the different spectral ranges measured for both IOL types, and p-values from *paired-samples t-test.*

6.4 Discussion

6.4.1 Differences in LCA between psychophysical and wavefront sensing methods

We found that the LCA from the psychophysical method is consistently higher (p=0.001) for all eyes than the LCA obtained from wavefront sensing, by 0.48 D (35.41%) for the Podeye IOL and 0.48 D (39.43%) in the Poday IOL. Similar differences were also found in a previous study [182] on young phakic eyes using the same experimental system (0.61 D, 40.4%). Lower values of LCA from reflectometric than from psychophysical had been also reported earlier. Some studies [13, 16, 41] had attributed those differences to the presence of high order

aberrations, although our previous study [182] discarded this hypothesis by performing measurements under correction of natural aberrations with adaptive optics, which showed similar discrepancies between psychophysical and reflectometric (wavefront sensing and double-pass based) techniques.

It is likely that the difference arise by wavelength-dependent reflectivity of the different retinal layers. In our previous study [182], we showed that deviations in the best focus from psychophysical and reflectometric techniques, occurred both at the short and long range of the spectrum, with higher shift in red than in bue light. We hypothesized that blue light was reflected anteriorly from the photoreceptors inner segments, approximately in the retinal nerve fiber layer in the retina, and that red light was reflected behind the photoreceptors, in the choroid.

This fact is interesting since in red light the contribution of the choroidal reflections is large compared with that of reflections originating in the inner layers of the retina [238], and might explain the higher shift in red than in blue light. In any case, the relative difference in LCA in eyes implanted with different IOLs remains constant regardless the measurement technique.

6.4.2 Differences in LCA from phakic eyes

The LCA measured in the pseudophakic eyes of the current study can be compared with the LCA measured in our previous study on young phakic, using the same methods, and for similar wavelength ranges (see Figure 6.4).

For both techniques we found that the LCA in phakic eyes is higher than in the pseudophakic eyes. These differences were statistically significant with both techniques for the Poday IOL, but only for the wavefront sensing technique for the Podeye IOL (*independent samples t-test; Psychophysical: Poday-Phakic, p=0.002; Wavefront sensing: (1) Visible, Podeye-Phakic, p=0.041, Poday-Phakic, p=0.009; (2) NIR, Poday-Phakic, p=0.008; (3) Visible+NIR, Podeye-Phakic, p=0.018, Poday-Phakic, p=0.02*). The LCA in these pseudophakic eyes is, on average, similar than the LCA in normal phakic eyes, whether measured with the psychophysical or reflectometric technique, in the same spectral ranges.

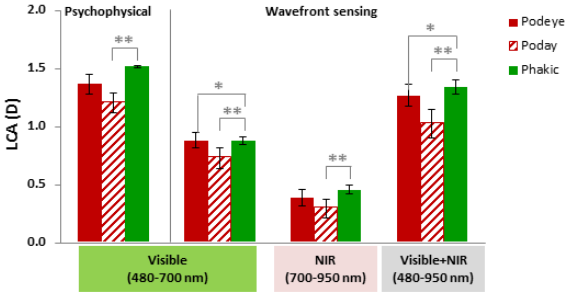

Figure 6.4 LCA averaged across subjects for Podeye IOL (red solid bars), Poday IOL (red dashed bars) and phakic eyes (green solid bars) for spectral ranges in the visible, near infrared and total spectral ranges, from subjective best focus and wavefront sensing. (* and **) stands for statistically significant ($p<0.05$) and highly statistically significant ($p<0.01$) differences, respectively, between pseudophakic and phakic eyes. Error bars stand for measurement error for subjective LCA and intersubject variability in wavefront sensing.

6.4.3 Differences in LCA from other studies in pseudophakic eyes

Chromatic aberrations play a major role on the quality of vision [41, 76, 108, 245], however only a few studies have addressed the chromatic properties of the IOLs and the chromatic aberration of the pseudophakic eyes *in vivo*. Our study provides estimates of the LCA measured in a wider spectral range in the visible and near infrared than that of previous studies, using psychophysical and wavefront sensing measurements.

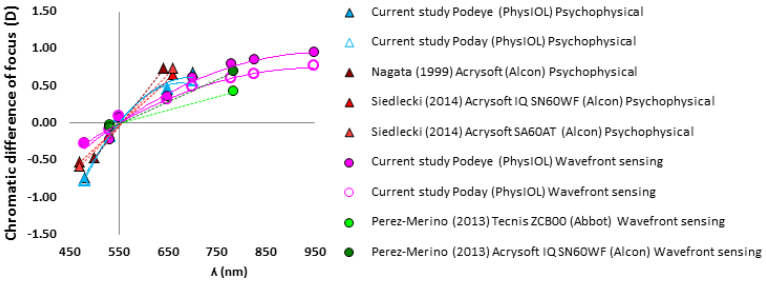

Figure 6.5 Chromatic difference of focus from the psychophysical (blue triangles) and wavefront sensing (pink circles) measurements of the current study, and other psychophysical (red triangles) and reflectometric (green circles) data in the literature. The measured chromatic range differed across studies, and it is indicated by the symbols in the end of the regression lines. Data are referred to zero defocus at 550 nm.

Figure 6.5 shows the chromatic difference of focus found in the current study (psychophysical data in blue; wavefront sensing, in pink), in comparison with *in vivo* chromatic difference of focus (in the corresponding spectral range) from previous studies from psychophysical (red triangles) and reflectometric (green circles) techniques with different types of IOLs [164, 230, 243]. In general, our results fall

within values reported by previous studies using both psychophysical and reflectometric techniques, with the data from psychophysical techniques showing consistently higher LCAs than those from reflectometric techniques.

6.5 Conclusions

We have measured LCA in a wide range of wavelengths, using a psychophysical method and wavefront sensing at multiple wavelengths –both implemented in the same polychromatic AO system– on pseudophakic eyes bilaterally implanted, one eye with the PhysIOL Podeye hydrophobic and the contralateral eye with Poday hydrophilic IOLs. The study design minimizes potential patient-bias, particularly in psychophysical measurements (same subject perform the subjective best focus settings with either IOL), as well as a direct comparison of both low and high order aberrations across groups.

We have found that the eyes implanted with the hydrophobic (Podeye) IOL exhibit a small but consistently higher LCA than the eyes implanted with the hydrophilic (Poday) IOL (a difference of 0.16 and 0.15 D from psychophysical and wavefront sensing methods, respectively, in the visible 480-700 nm range). The difference is consistent with the lower Abbe number of the hydrophobic material. IOL material potentially has relevance on visual performance, as the IOL material affects the chromatic aberration of the eye.

In this and previous *Chapter*, the polychromatic capacity of the AO system was used. In the next *Chapter* the combine performance of the deformable mirror and spatial light modulator is used to explore vision with new multifocal designs for Presbyopia.

7

Testing vision with radial and angularly segmented multifocal patterns using Adaptive Optics

Current available solutions aim to optically correct for Presbyopia, the age-related loss of the accommodative amplitude of the human eye [148], and restore some near-vision functionality, although none of them is able to restore the full dynamic capability of the young eye. However there are multiple treatments that attempt to provide functionality for both near and far vision. Current techniques for the correction of Presbyopia are based on one of four principles: alternating vision [151, 152], monovision [153], simultaneous vision [154, 155], and accommodating IOLs.. In this Chapter we evaluate the effect of new multi-zone multifocal designs on vision, in the presence and absence of natural aberrations.

This Chapter is based on the paper by *Vinas et al. "Testing vision with radial and angularly segmented multifocal patterns using Adaptive Optics" currently in preparation.* The coauthors of the study are Carlos Dorronsoro, Veronica González, Daniel Cortes, Ayswariah Radhakrishnan and Susana Marcos. A follow-up of this study was developed at the Ophthalmic Optics Laboratory from the College of Optical Sciences at the University of Arizona, Arizona (USA) under the supervision of Prof. Jim Schwiegerling (Associate Professor, Ophthalmology & Vision Sciences).

The author of this thesis (1) implemented the experimental procedure (in collaboration with Veronica González, Daniel Cortes and Ayswariah Radhakrishnan), (2) performed the measurement on human eye's, (3) collected the

data, and (4) analyzed the data (in collaboration with Carlos Dorronsoro and Susana Marcos). Part of the work was also presented as a poster contribution at the Frontiers in Optics (FIO) 2014 in Tucson (Arizona, Spain), where it was awarded in the Emil Wolf Outstanding Student Paper Competition. This work was also presented as an oral contribution at the Association for Research in Vision and Ophthalmology (ARVO) (May 2015) in Denver (Colorado, USA), where it was awarded with an ARVO International Travel Grant.

7.1 Introduction

Restoring near-vision functionality in Presbyopia [148], requires providing some near-vision functionality to patients that have lost the ability to accommodate. Multifocal vision corrections are increasingly used solutions to correct for Presbyopia. Multifocal corrections work by the principle of simultaneous vision, projecting simultaneously on the retina focused and defocused images on the retina, providing multifocality at the expense of reducing optical quality at all distances. There are multiple multifocal designs, attempting to produce different foci [154, 155, 246-251], working on diffractive or refractive principles.

Diffractive IOLs use diffractive optics whereby constructive and destructive interferences produce near and far foci [252]. Diffractive IOLs are not pupil-diameter dependent [150], and multifocality is achieved at any pupil diameter. However, they are subject to diffractive effects by multiple orders as well as chromatic effects, as the inferences are wavelength-dependent. Diffractive efficiency can be reduced for the peripheral zones of the lens, so that they contribute relatively more light to the far image, by progressively reducing the height of the diffractive phase steps on the lens surface as the zonal radius increases (apodization), as in the RESTOR diffractive bifocal IOL (Alcon UK surgical, United Kingdom) [150]. Moreover, good binocular acuity at far, intermediate and near distances has been found by splitting the light between the distance and near foci by adjusting the height of the diffractive phase steps across the entire lens [250]. Diffractive bifocal IOLs fail to enhance vision at intermediate distances, thus some of the most recent diffractive designs are trifocal, providing an intermediate focus [253]. An example of trifocal diffractive design is the FineVision lens (Physiol, Belgium), in which the diffractive surface profile is designed to concentrate light into near (+ 3.5 D), intermediate (+1.75 D) and distant foci [253] and the AT LISA tri (Zeiss, Germany), where the diffractive profile provides + 3.33 D and + 1.66 D for near and intermediate foci respectively.

Some multifocal refractive contact and IOL lens aim at expanding depth of focus (DoF) using different strategies, most frequently using aspheric profiles (i.e. Tecnis Z9000/2/3 IOL, AMO, USA; AcrySof IQ IOL, Alcon, USA; SofPort AO IOL, Bausch & Lomb, USA) that modify spherical aberration [254] or other symmetric terms. In this approach, it has been realized that the specific amount aberration to be introduced is critical and may be subject-specific. Recently, using an optical design multiconfiguration approach, IOLs with surface optimized to enhance retinal image quality over a certain range of focus have been presented [255].

Several studies have used Adaptive Optics (AO) to simulate the effects of inducing different levels of spherical aberration in an experimental setting [158, 256, 257]. Piers et al. used an AO simulator to assess visual acuity and contrast sensitivity for two different values of spherical aberration, and concluded that completely

correcting ocular spherical aberration improves spatial vision in the best-focus position without compromising the subjective tolerance to defocus [158]. In fact, the use of AO visual simulators has allowed exploring different combinations of high order aberrations (HOAs) to expand DoF (i.e. primary and secondary spherical aberration [254] or astigmatism and coma [95]. From these studies, it is concluded that not only the specific design, but also the native aberrations of the subjects play a role in the multifocal performance with those lenses.

Multizonal refractive designs, in which certain pupillary regions are devoted for far, and others for near are also common. Multizonal lenses come most frequently in concentric areas, that typically alternate near and far zones [258]. There is at least a refractive bifocal design with an asymmetric distribution of near and far, the Lentis Mplus (Oculentis, Germany), where the design approximates to a 2 segment bifocal with the rear surface add (+ 3.00 D) occupying almost half the lens (a sector enclosing an angle of ~160 deg) [150]. The optimal pupillary distribution for far and near, and the extent to what a particular design interacts with the aberration pattern of the eye has been little addressed.

A given optical design does not produce the same optical through-focus energy distributions in all eyes [249]. Among other parameters in bifocal lenses, the amount of near add largely determines visual quality both in terms of visual acuity [259] and perceived image quality [260]. Besides, neural adaption to simultaneous vision image has also been shown to shift perceived visual quality [150].

Multifocal corrections (both intraocular and contact lenses) increase depth of focus at the expense of decreasing optical quality at all distances. While some studies have measured through-focus retinal image quality, generally using double-pass imaging techniques [161, 261, 262] or visual quality [247, 248, 250, 263], these are generally restricted to patients implanted or fitted with commercial lenses, and therefore limited to specific conditions. Most of the systematic evaluations of many of the available lenses are limited to optical computer simulations and on bench experiments, therefore lacking from the optical and the neural complexity of a patient [249].

Computer simulations allow a first approximation to understand the optical performance of multifocal lens designs. In a recent study in our laboratory, we studied computationally the through focus optical performance in diffraction-limited eyes with multi-zonal phase patterns, with 2-50 zones of varying power with maximum addition of +3 D distributed either angularly or radially [259]. Only some of these patterns represent designs commercially available to date. Multifocality was evaluated in terms of two metrics, which considered the volume under the Visual Strehl through-focus curves in a certain dioptric range and the dioptric range for which through-focus Strehl exceeded a certain threshold. The study revealed clear differences in the predicted multifocality across lens designs,

with 3- and 4-zone angular designs outperforming radial designs, or designs with more zones. Interestingly, the 50-zone radial designed provided almost identical performance to a spherical aberration pattern, lower than most multi-zonal configurations of fewer zones.

Visual simulators allow testing experimentally different designs. Dorronsoro et al. evaluated experimentally visual perception with 14 different bifocal zonal corrections, using a custom-developed simultaneous vision simulator provided with a transmission Spatial Light Modulator [264, 265]. All corrections had a 50% far-50% near energy balance and +3 D near add, with different angular and radial distributions. Subjects showed significant perceptual preferences across patterns. The same 2-zone angularly segmented pattern in different orientations produced significant differences in perception in the same subject, suggesting an influence of the interactions of the eye's aberration pattern and the multifocal pattern design.

AO simulators provide the possibility of testing the influence of the eye's HOAs on the performance of multifocal corrections. To test visual performance with different multi-zone segmented patterns, we specifically developed a two-active-element adaptive optics system, provided with a deformable mirror that could compensate for the eye's aberrations, and a phase spatial light modulators, which simulated multifocal (2, 3 and 4 zone) angular and zonal patterns. This study will help gain a better understanding of optical and visual interactions in multifocal simultaneous vision corrections, and whether these are driven by optical and neural effects, which is critical to improve intraocular lens design and select the optimal design for a patient.

7.2 Methods

Visual quality with six radial and angularly segmented multiple zone multifocal phase patterns was evaluated optically and psychophysically, by means of simulations of Visual Strehl-based-metrics and measurements of the relative perceived visual quality, respectively.

7.2.1 Subjects

Six young subjects (ages ranging from 22 to 31 years, 29 ± 3.5 years) participated in the study. Spherical errors ranged between 0 and 0.50 D 0.10 ± 0.22 D), and astigmatism was ≤ -0.5 D in all cases. All experiments were conducted with dilated eyes (Tropicamide 1%, 2 drops 30 minutes prior to the beginning of the study, and 1 drop every 1 hour).

All participants were acquainted with the nature and possible consequences of the study and provided written informed consent. All protocols met the tenets of the Declaration of Helsinki and had been previously approved by the Spanish National Research Council (CSIC) Ethical Committee.

7.2.2 Experimental protocol

Perceived visual quality measurements were conducted in the custom-developed polychromatic Viobio Lab Adaptive Optics (AO) II system, described in detail in *Chapter 2 Methods* and partially in previous publications [182] which allowed control and correction of the aberrations of the subject, while performing the psychophysical experiments.

7.2.2.1 Optical Quality

Fourier Optics was used to compute the through-focus optical quality for the different multi-zone multifocal phase designs. Natural aberrations of the 6 subjects measured with the AO system were incorporated to the optical simulations, as well as the residual aberrations after AO-correction, to study the impact of the natural aberrations of the subjects in the optical simulations.

Segmented multiple zone multifocal phase patterns

We evaluated six different multi-zone multifocal phase designs consisting of segmented pupils (2 zones up to 4) of progressive power (0 to + 3.0 D) in different radial and angular pattern configurations described in a previous work from the lab [259]. Defocus (in a Zernike expansion) varied sequentially and linearly across zones between 0 and -3.89 µm in a 6 mm pupil, equivalent to a dioptric power change from +0 D for far distance correction to +3.0 D for near (i.e., near addition). The area of each zone was constant in all cases. Natural aberrations of the 6 subjects measured with the AO system were incorporated to the optical simulations, as well as the residual aberrations after AO-correction, to study the impact of the natural aberrations of the subjects in the optical simulations.

Optical quality metrics

Through-focus Visual Strehl (VS) curves, obtained as the volume between the OTF and a general neural transfer function to emphasize the spatial frequency range most relevant to visual function, were used as optical quality metric [64, 65] and computed through-focus. The following parameters were computed from the through-focus VS curves: (1) Area under VS curves in a 6.0 D dioptric range; (2) Dioptric range above a certain threshold (0.06); (3) VS at far, intermediate and near distance (0 D, 1.5 D and 3.0 D, respectively) were obtained from the through-focus curves.

The response of an “ideal observer” purely responding based on optical grounds to the psychophysical test performed on subjects was calculated for all patients with the 6 multifocal patterns in two conditions (presence of their natural aberrations and residual aberrations after AO correction). A weighted response on pairs of VS values with different patterns, for each subject and distance. A given pattern was deemed as producing better of optical quality with weighting factors of ±10, ±5 and

±1, if VS was 80%, 50% or 25% higher, respectively, than the corresponding pattern. A score for each pattern was calculated from the sum of the weighted responses, from a total of 210 comparisons. This estimation was based on the corresponding psychophysical paradigm (see section 2.4.2).

7.2.2.2 Perceived Visual Quality

A psychophysical experiment was designed to test the impact of the 6 different multi-zone multifocal patterns on vision, in patients with and without their natural aberrations. The aberrations were measured and manipulated, and the multifocal corrections generated, using an AO system.

A. Phase pattern generation

Matlab routines were used to numerically simulate the multi-zone multifocal phase maps, which were later programmed in a reflective LCoS (phase-only) Spatial Light Modulator. Figure 2 shows the multifocal phase designs and orientations tested in this study. Each phase pattern is defined by the wavefront in each zone and a mask (radial or angular, 2, 3 and 4 zones) that equals to 1 in the corresponding zone and 0 elsewhere[259]. A wrapping process [193, 194] was applied to the phase patterns to achieve a maximum phase difference of 2π defined by the calibration of the SLM. The generated pattern was a grey-scale image, where each level of grey corresponds to a certain phase difference between 0 and 2π. Images were generated for a 6mm pupil in the pupil plane where the SLM is placed.

Calibration of the SLM and in between the different active-devices of the system (SLM, Deformable mirror and Badal system) were conducted to assure proper correspondence between them, as explained in Chapter 2 Sections 2.2.3.4 and 2.2.3.5.

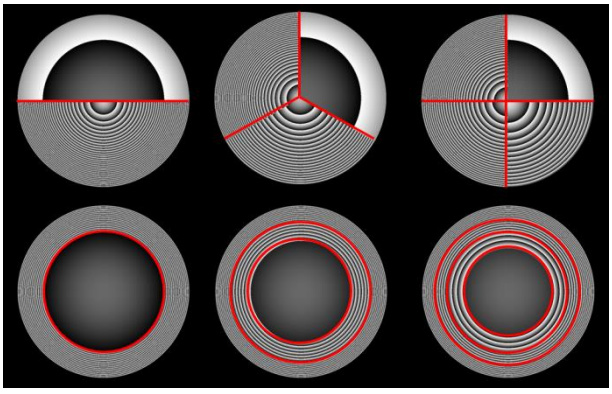

Figure 7.1 Phase designs evaluated in the study: 2, 3 and 4 segmented angular (upper row) and radial (lower row) designs. For clarification, separation between zones has been highlighted.

B. Measurement protocol and psychophysical paradigm

Measurements were performed monocularly, under natural viewing conditions and naked eyes in a darkened room. Astigmatism and high order aberrations were measured and corrected in a closed loop adaptive optics operation. Defocus was corrected subjectively by the subject using a Badal system. The state of the mirror that achieved the correction was saved and applied during the measurements. Psychophysical measurements were performed under full static AO-corrected aberrations and best spherical refraction error correction for far, in each condition (natural and corrected aberrations). Measurements were performed at far, intermediate and near distances simulated with the Badal system (0 D, +1.5 D and +3.0 D respectively), in the presence of natural aberrations and after AO-correction. Before the measurement, subjects were instructed on the nature of the experiment and performed some trial runs. One measurement session lasted about 4 hrs.

Subject viewed the psychophysical stimulus generated by the Digital Micro-Mirror Device, illuminated monochromatically at 555 nm, through the psychophysical channel of the AO system (Figure 1). The stimulus contained a binary noise pattern with sharp edges at random orientations, where the binary noise pattern was produced from a uniform noise distribution spatially filtered with an annular filter in the frequency domain (inner radius: 3 cycles/deg; outer radius: 6 cycles/deg). This gray-level was later transformed to a binary image and then the edge of the field was smooth by means of a Gaussian function(Chen, Singer, Guirao, Porter & Williams, 2005). A different noise pattern was used to generate a new stimulus on each trial so that edges at all orientations were presented over the course of the experiment.

In a psychophysical paradigm consisted on a 2AFC weighted response to images viewed through 2 different multifocal patterns, in a series of 210 pairs of patterns. Patterns and viewing distances were randomly selected. The subject viewed the stimuli and judged whether the first or second had better quality and provided a ranked response according to the certainty of the judgment. Positively judged patterns received a score of +10, +5 and +1, and negatively judged patterns received a rank of -10, -5 and -1. The relative perceived visual quality of a given pattern is the sum of all responses to this pattern weighted by the corresponding scores. This procedure was done for each pattern, condition (natural and AO-corrected aberrations) and distances.

7.2.3 Data analysis

To test differences across multifocal designs, a multifocal benefit metric weighting the contribution of the different tested distances was built from the relative optical and perceived visual quality results. The metric assigned a 60% weight to far distance data, 15% to intermediate distance and 25% to near distance.

To compare the pattern preference at the different conditions (3 different distances, natural aberrations and AO correction) with both methods, optical simulations and experimental measurements, results were ranked according to the results of the different metrics (optical and perceived). The 6 patterns were organized in a ranking from 1 to 6, from the least preferred to the most preferred pattern.

7.3 Results

Visual quality with the 6 different multi-zone multifocal patterns was obtained from optical simulations from wave aberrations measurements and psychophysical measurements, both performed in the AO system.

7.3.1 Wave aberration measurement and correction

Figure 7.2 shows wave aberration maps for astigmatism and HOA and their corresponding RMS for all 6 subjects measured at 827 nm and 6-mm pupil, for astigmatism and HOAs (purple), for astigmatism (yellow), for coma (pink) and residual aberrations after AO-correction (green). Residual RMS upon AO-correction was lower than 0.05 µm.

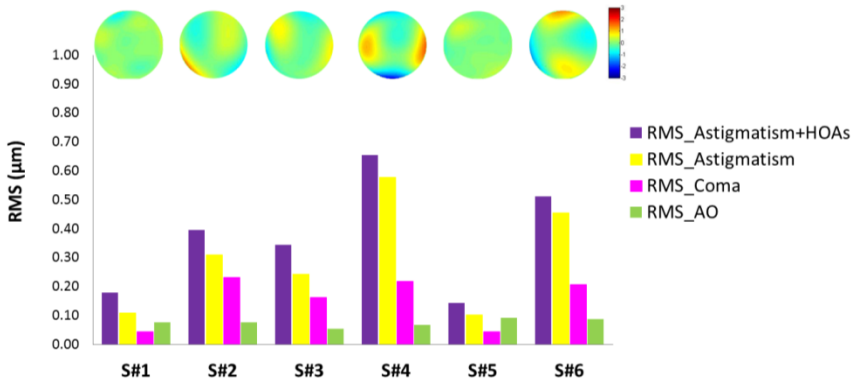

Figure 7.2 Subject's aberrations profile in terms of Root Mean Square (RMS) for astigmatism and HOAs (purple), for astigmatism (yellow), for coma (pink) and residual aberrations after AO-correction (green). Data are for 6-mm pupils.

7.3.2 Optical Quality

The optical quality was computed from the combination of the multifocal aberration and the subject's aberrations (natural or residual after AO-correction. Figure 4 shows an example of the corresponding wave aberrations for the tested patterns (2, 3 and 4 angular and radial) and the corresponding MTF radial profiles, for natural aberrations (upper row) and residual aberrations after AO-correction (lower row) in subject S#4.

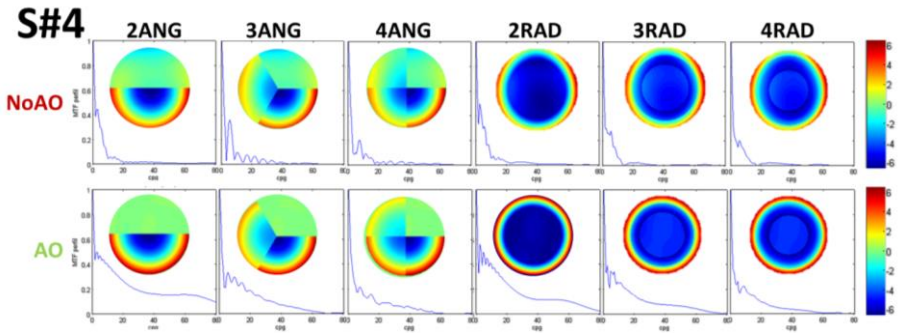

Figure 7.3 Multi-zone multifocal designs evaluated in the study: 2, 3 and 4 segmented angular (left) and radial (right) designs), as well as the corresponding MTF profiles (x-profiles), incorporating natural aberrations (upper row) and residual aberrations after AO-correction (lower row) of one of the subjects of the study.

Figure 7.4 shows the simulated through-focus Visual Strehl (VS) curves for all 6 multifocal patterns for a diffraction limited eye (A) and angular (left column, B-D) and radial (right column, E-G) in the presence of natural aberrations. Each color represents a different subject. A threshold to normalize the area under the VS curves was set at the minimum value at intermediate distance (1.5 D) for 2-segmented designs through-focus curves. Through-focus curves are different across designs, even for similar zone designs and no aberrations (A). The presence of natural aberrations produces variations from the diffraction-limited condition, including minor shifs in the maximum VS values, shifts in the curve peaks and variations in the performance of the same pattern across subjects.

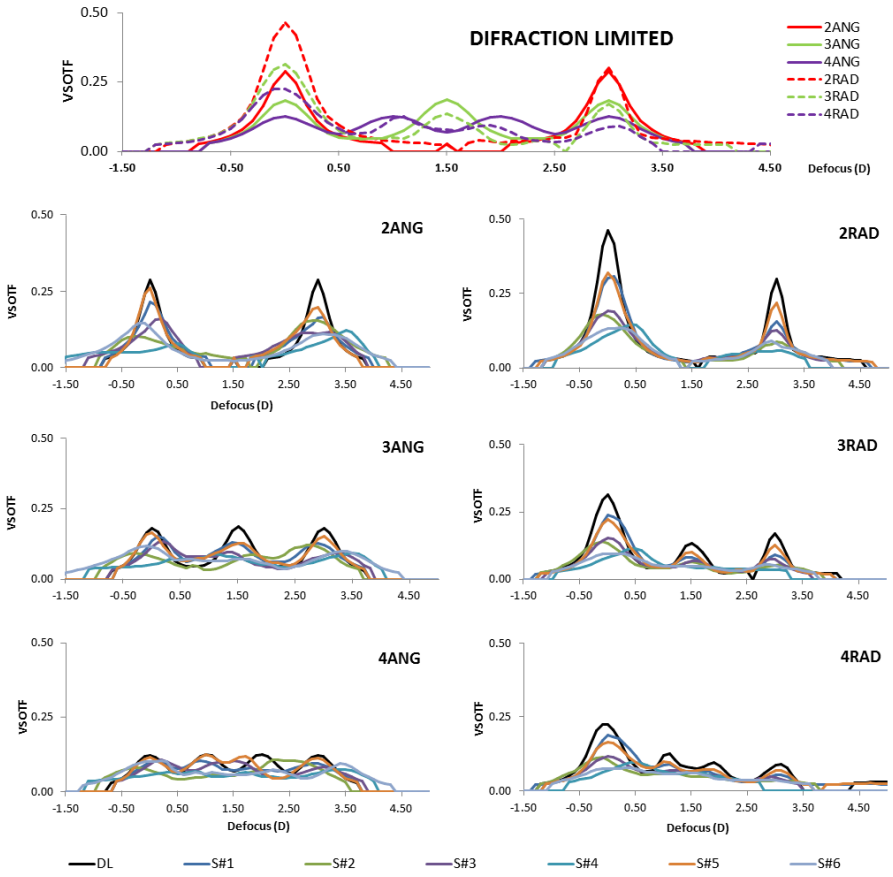

Figure 7.4 Through-focus VSOTF curves for angular (left column) and radial (right column) phase patterns in the presence of natural aberrations for the 6 subjects of the study, and for diffraction limited (black lines).

Figure 7.5 shows shows analysis of two different multifocal metrics (similar to those presented by de Gracia et al. 2013) for the different patterns, in a diffraction limited eye (open green symbols) and average across subjects in the two conditions under test: natural aberrations (closed red symbols) and residual aberrations (closed green symbols). For these particular metrics a better multifocal response is provided by patterns with higher values on both axes. In both conditions, 3 and 4 angular designs produce a better multifocal response than the rest of the tested multifocal designs.

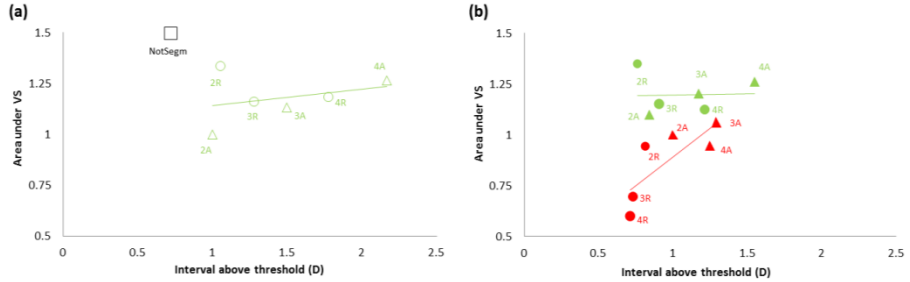

Figure 7.5 Visual Strehl-based optical performance metrics for diffraction limited (a) and for the averaged data of the 6 subjects of the study. Red symbols indicate natural aberrations and green symbols AO-corrected aberrations (open symbols are pure diffraction-limited eyes, and closed symbols are for real eyes with residual aberrations following AO-correction). Triangles stand for angular designs and Circles for radual designs.

Figure 7.6 shows the average (across 6 eyes) relative optical quality calculated from pair comparisons of the corresponding VS data, for three distances (far, intermediate and near). Simulations were performed in three conditions (diffraction limited eye, empty bars; residual aberrations following AO correction; natural aberrations, filled bars). For far and near distance, 2-segmented designs (angular and radial) provided the better performance (Far: 2RAD 0.6, 2ANG 0.19; Near: 2ANG 0.61, 2RAD 0.44), while for intermediate vision, 3- and 4-segmented designs provided the better results with angular designs performing better than radial designs (Intermediate: 3ANG 0.65, 4ANG 0.59, 3RAD 0.40). AO-correction of natural aberrations has reduced impact in these trends.

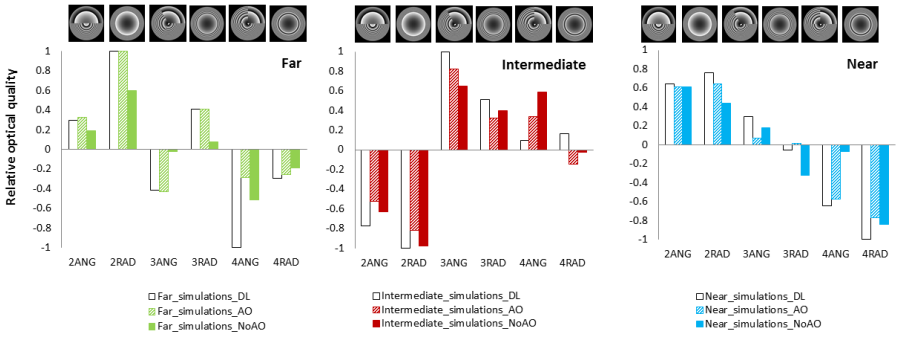

Figure 7.6 Averaged responses of the 6 Ideal observers for far (green bars), intermediate (red bars) and near (blue bars) distance in the presence of natural aberrations (solid bars) and after AO-correction (dashed bars). Black empty bars are for diffraction-limited ideal observer for the 3 distances.

7.3.3 Perceived Visual Quality

Figure 7.7 shows the average (across 6 eyes) perceived visual quality obtained from pair comparisons of the corresponding psychophysical experiment, in the presence of natural aberrations (dashed bars) and after AO-correction (solid bars) for far

(green bars), intermediate (red bars) and near (blue bars) vision. In 78.93 % of the psychophysical pattern evaluations, a positive or negative statistically significant preference was found ($p<0.05$; not compatible with chance), in pair comparisons with other patterns. For far vision, 2-segmented designs (angular and radial) provided the better performance (Far: 2RAD 0.56, 2ANG 0.65), while for intermediate vision angular 3- and 4-segmented designs provided the better results (Intermediate: 4ANG 0.29, 3ANG 0.21). For near vision, 2-segmented designs and 3-segmented angular are preferred over the others (Near: 3ANG 0.30, 2ANG 0.14, 2RAD 0.14). AO-correction of natural aberrations has reduced impact in these trends. The presence of natural aberrations slightly increases the inter subjects variability (Far: 0.15; Intermediate: 0.27; Near: 0.25) in comparison with results with AO-correction (Far: 0.10; Intermediate: 0.20; Near: 0.17) Intersubject varibaility is lower for far distance and higher for intermediate distance.

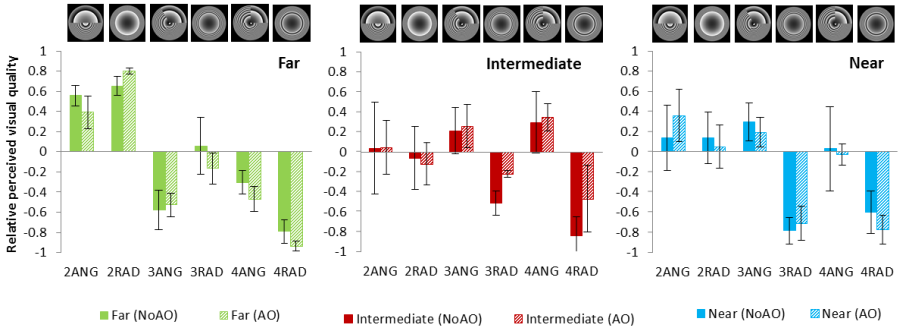

Figure 7.7 Averaged relative perceived visual quality for the 6 different multi-zone multifocal patterns in the presence of natural aberrations (solid bars) and after AO-correction (dashed bars) for far (green bars), intermediate (red bars) and near (blue bars) distance. Error bars stand for standard deviations across subjects.

7.3.4 Optical vs. Perceived Visual Quality

For comparison between optical and perceived visual quality, the 6 patterns were organized in a ranking from 1 to 6, from the least preferred to the most preferred pattern. The ranking was done using the preference results of the different metrics (optical and perceived) at the different conditions (3 different distances, natural aberrations and AO correction) with both methods. Figure 9 shows the results of these rankings for the 3 testing distances (far: green, intermediate: red and near: blue) from the optical quality "ideal observer" calculations (squares, dashed lines) and perceived visual quality metric (triangles, solid lines) in the presence of natural aberrations (upper row) and after AO-correction (lower row). In general there is a

good agreement between both metrics particularly for far and intermediate vision.

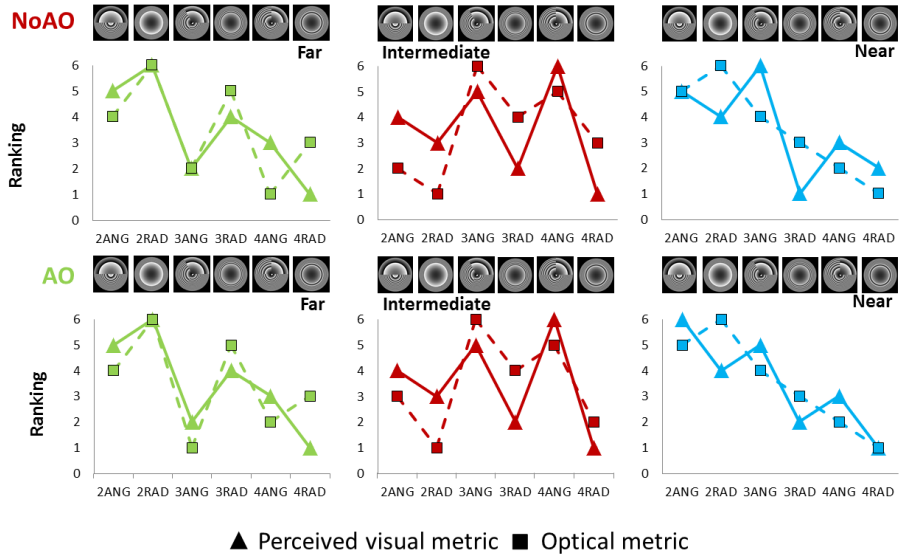

Figure 7.8 Averaged rankings for the 3 testing distances (far: green, intermediate: red and near: blue) from optical metric (squares, dotted lines) and perceived visual quality metric (triangles, straight lines) in the presence of natural aberrations (upper row) and after AO-correction (lower row).

Figure 7.9 shows average results of the multifocal benefit metric weighting the contribution of the different tested distances (60% weight to far distance data, 15% to intermediate distance and 25% to near distance) are Multifocal benefit metric was obtained from the relative optical quality results (red bars) and the relative visual quality results (green bars) in the presence of natural aberrations (dashed bars) and after AO-correction (solid bars).

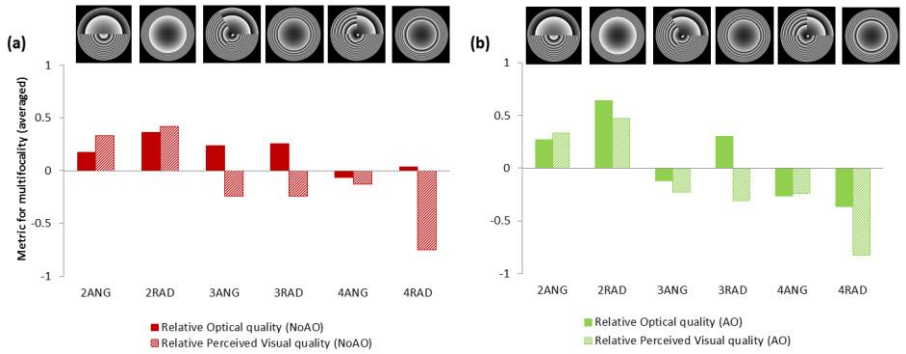

Figure 7.9 Averaged multifocal benefit metric obtained from the relative optical quality results (solid bars) and the relative visual quality results (dashed bars), with (a) natural aberrations; (b) AO-correction (dashed bars) for the 6 different multifocal patterns. Data are averaged across 6 patients.

7.4 Conclusions

Multifocal optical corrections are becoming popular solutions for compensation of Presbyopia, aiming at providing the patient with a range of focus for functional vision at near without compromising far vision (Cochener, Lafuma, Khoshnood, Courouve & Berdeaux, 2011, Kim, Zheleznyak, Macrae, Tchah & Yoon, 2011, Lichtinger & Rootman, 2012). In the current study we have evaluated, optically and psychophysically, the quality provided by six radial and angularly segmented multiple zone multifocal phase patterns. Optical quality was evaluated by means of Visual Strehl-based-metrics and relative visual quality was obtained by means of a psychophysical paradigm in which images viewed through 210 pairs of patterns were perceptually judged. For that purpose we have developed a two-active-element AO system provided with a deformable mirror that could compensate for the eye's aberrations, and a phase SLM, which simulated multifocal (2, 3 and 4 zone) angular and zonal patterns. The study improved understanding of optical and visual interactions in multifocal simultaneous vision corrections, and whether these are driven by optical and neural effects.

In a recent study in our laboratory (de Gracia et al., 2013a), computer simulations of optical performance in diffraction-limited eyes with different multifocal designs allowed a first approximation to understand the effect of the multifocal design on multifocality. Multifocality was evaluated in terms of two metrics, which considered the volume under the Visual Strehl through-focus curves in a certain dioptric range and the dioptric range for which through-focus Strehl exceeded a certain threshold. The study revealed clear differences in the predicted multifocality across lens designs, with 3- and 4-zone angular designs outperforming radial designs, or designs with more zones. In the current study, we have replicated those metrics for multifocality incorporating in the simulations the natural aberrations of the subjects. We have shown that the predicted multifocality across lens designs showed, in general, similar trends to those from the diffraction-limited simulations (Figure 6). As found in the earlier study, 3- and 4-zone angular designs predicted the best multifocal responses also in the presence of natural aberrations of the subjects, as well as after AO-correction of those aberrations. In fact, a simple optical observer whose responses are purely based on the optical metric comparing VS across patterns using similar paradigms as those of the psychophysical study predicted very closely the findings from the perceptual experiment (Figure 7).

The pattern-comparison tests (both optical and psychophysical), showed that while 2-segmented designs (angular and radial) provided better performance for far and near vision, 3- and 4-zone angular designs performed better for intermediate vision (Figure 7), and over performed the same-zone radial designs. AO-correction of natural aberrations of the subjects modified the response for the different subjects but general trends remained. A comparison of these findings with the multifocality

metrics based on dioptric range above threshold and area under the VS curves indicate that these metrics favor designs with intermediate powers. Using a metric that integrated the relative perceived quality at near, intermediate and far distances, predicted multifocal benefit trends for optical and perceived visual quality are coincident when natural aberrations of the subjects are AO-corrected. Presence of natural aberrations of the subjects raised some differences between optical and perceived multifocal predictions, especially for 3-zone designs and 4-zone radial design.

This study will help to a better understanding of optical and visual interactions in multifocal simultaneous vision corrections, which is critical to improve lens design.

8

Conclusions

In this thesis, a custom developed polychromatic Adaptive Optics system was designed, built and validated, and combined with a psychophysical Channel. We performed a series of studies aiming at understanding the impact of mono- and chromatic aberrations on visual function, as well as to explore new optical solutions for Presbyopia.

The results give new insights on the impact of astigmatism on visual function, the amount of LCA in normal and pseudophakic eyes and the impact on vision of new multifocal designs for Presbyopia. These results are crucial in the development of new vision correction alternatives.

In this thesis we have accomplished the following achievements:

- Evidence of the impact of natural astigmatism and its correction in both visual perception and performance. In particular, we have tested whether the perception of oriented blur is biased by the native astigmatism of the subject and the time course of the after-effects following spectacle correction of astigmatism in habitually non-corrected astigmats. In addition we have tested whether the impact of astigmatism on VA is greatly dependent on the orientation of the induced astigmatism, even in non-astigmats, and whether prior experience to astigmatism plays a role on VA.

- Development of a polychromatic Adaptive Optics system, combined with a psychophysical Channel to measure, correct/ induce mono- and chromatic aberrations, and to simulate sophisticated optical correction.

- Implementation of psychophysical paradigms to study visual performance and visual perception under controlled ocular aberrations – judgment of perceived blur, 8 alternative forced choice procedures, sequential images pairs comparisons and rating scale tasks.

- Measurement of the Longitudinal Chromatic Aberration of the human eye in visible and near infrared with objective and subjective techniques in the same subjects in a wider spectral range than previously. We have provided, to our knowledge, the first evaluation of the change of high order aberrations with wavelength using objective aberration in both the visible and near infrared spectral ranges. In addition, we have provided insights of the reasons for the different magnitudes of the LCA obtained with objective and subjective techniques.

- Measurement of the LCA *in vivo* using psychophysical and wavefront sensing methods in patients bilaterally implanted with monofocal IOLs of similar aspheric design but different materials in the same subjects in a wider spectral range than previously.

- Experimental simulation of new multiple multifocal designs, using a Spatial Light Modulator, with control of the natural aberrations of the subjects, using Adaptive Optics elements. We have studied the effect of multifocal simultaneous vision corrections on vision, in the presence and absence of natural aberrations.

The development of the polychromatic Adaptive Optics (AO) system combined with a psychophysical Channel and the experiment results allow us to conclude that:

1 Perception of astigmatic blur depends on the refractive (astigmats vs. non-astigmats) and corrective (habitually-corrected or habitually-non-corrected) profiles of the subjects. Uncorrected astigmats appear to be naturally adapted to astigmatism, thus their perception of isotropic blur is shifted towards astigmatism. The observed differences in the perception of the neutral point must therefore arise from differences in the internal norm for perception of oriented blur, which is highly dependent on prior visual experience. Furthermore, astigmatic correction changes significantly the perception of the neutral point in astigmatic subjects, even after a brief period of adaptation, and remains constant once stabilized.

2 Visual degradation produced by astigmatism induction is greatly dependent on the axis of the induced astigmatism, both for non-astigmats (for whom inducing astigmatism at 90 deg produced significantly less degradation than at other axes), and astigmats (who experienced less visual degradation when astigmatism was induced at their angle of astigmatism). Both habitually-corrected and initially non-corrected astigmats after correction of astigmatism showed a bias towards better performance with astigmatism induced at their natural axis, which persisted even after astigmatism correction wear for 6 months, suggesting that astigmats may store adaptation states or cues related to their natural astigmatism.

3 Beneficial interactions for coma and astigmatism, as predicted from optical theory, occurred in non-astigmats and to some extent in astigmats, but differed across groups. This suggests that mechanisms underlying adaptation to astigmatism do not operate independently, but rather combined effects of aberrations on vision are not only driven by the optics, but are affected by prior adaptation to astigmatism.

4 Longitudinal Chromatic Aberration (LCA) of the human eye measured with psychophysical methods is significantly higher (by 0.50 D in the 488-700 nm range) than the LCA measured using reflectometric techniques. The observed differences between the psychophysical and reflectometric LCA are independent of the presence of high order aberrations and may arise from the fact that the retinal reflection may not occur at the plane at which the retinal image must be focused to give the best subjective image at all wavelengths.

5 Longitudinal Chromatic Aberration (LCA) of pseudophakic eyes is, on average, similar than the LCA in phakic eyes, with LCA in phakic eyes being slightly higher than in the pseudophakic eyes. Psychophysical LCA is consistently higher than objective LCA in pseudophakic eyes, similarly to phakic eyes.

6 Eyes implanted with the hydrophobic (Podeye) IOL exhibit a small but consistently higher LCA than the eyes implanted with the hydrophilic (Poday) IOL. The difference is consistent with the lower Abbe number of the hydrophobic material.

7 Multi-zone multifocal simultaneous vision solutions impact on vision depends on their design. Experimentally, angular designs provide better multifocal benefit than radial designs. The presence of high order aberrations plays a role in perceived visual quality across the different multifocal patterns, however this is secondary.

Future work

A direct follow-up of the study presented here includes the implementation of several improvements in the design of the polychromatic Adaptive Optics (AO) system, the design of new experiments on the current AO system to study the impact of vision of new multifocal designs and the new experimental protocols to study impact of chromatic aberration on polychromatic retinal quality.

1. Improvements on the design of the polychromatic AO system

The studies presented here show the extensive capabilities of the system both to measure subjective/objective chromatic aberrations as well as to simulate a wide variety of multifocal corrections. Further synchronization of the devices will improve the automatization of the instrument could enhance the capabilities of the system. The resolution of the retinal imaging Channel can be increased by filtering the laser beam coming from the 2 fiber optics channels. This would result in higher quality through focus retinal images.

2. Visual performance and adaptation to multifocal corrections

In this thesis we have evaluated vision with simulated new multifocal designs for Presbyopia, using the extended capabilities as visual simulator of the AO system. A direct follow-up of this project, performed in collaboration with the University of Arizona, has been already designed. The multifocal designs evaluated in this project have been manufactured, so that they can be incorporated to the AO system and therefore vision tested with them. Visual performance experiments with Adaptive Optics manipulated wave aberrations will allow to test the suitability of novel multifocal corrections and evaluate the effect of natural aberrations on their performance.

Scientific activities during this thesis 2011-2015

1. Scientific articles associated with this thesis

5. M. Vinas, C. Dorronsoro, V. Gonzalez, D. Cortes, A. Radhakrishnan, S. Marcos. *Testing vision with angular and radial multifocal phase patterns using adaptive optics* (in preparation)

4. M. Vinas, C. Dorronsoro, N. Garzon, F.Poyales, S. Marcos. *In vivo subjective and objective longitudinal chromatic aberration in patients bilaterally implanted with same design hydrophobic and hydrophilic IOLs*. JCRS (in press, December 2015)

3. M. Vinas, C. Dorronsoro, D. Cortes, D. Pascual, S. Marcos. *Longitudinal chromatic aberration of the human eye in the visible and near infrared from wavefront sensing, double-pass and psychophysics*. BOE Vol. 23, No. 4, February 2015; DOI:10.1364/OE.23.00948

2. M. Vinas, P. de Gracia, C. Dorronsoro, L. Sawides, G. Marin, M. Hernández, S. Marcos. *Astigmatism impact on visual performance: meridional & adaptational effects*. OVS Vol. 90, No. 12, December 2013; DOI:10.1097/OPX.0000000000000063

1. M. Vinas, L. Sawides, P. de Gracia, S. Marcos. *Perceptual adaptation to the correction of natural astigmatism*. PLoS ONE 7(9): e46361; September 2012; DOI:10.1371/journal.pone.0046361

Other co-authored scientific articles

1. L. Sawides, C. Dorronsoro, P. de Gracia, M. Vinas, M. Webster, S. Marcos. *Dependence of subjective image focus on the magnitude and pattern of High Order Aberrations*. J Vis August 7, 2012 12(8): 4; August 2012; DOI:10.1167/12.8.4

Proceedings

2. E. LaVilla, M. Vinas, S. Marcos, and J. Schwiegerling, *Freeform Design of Multifocal Zone Plates* , in *Imaging and Applied Optics 2015*, OSA Technical Digest (Optical Society of America, 2015), paper FW3B.3.

1. M.Vinas, L. Sawides, P. de Gracia, S. Marcos. *Adaptive Optics as a tool to study changes in the perceived neutral point after correction of astigmatism*. 8th Workshop on Adaptive Optics for Industry and Medicine (Murcia, Spain). AOIM Droplets in Murcia, 2011

2. Diffusion of the results

Personally presented

(authors are indicated by signature order, p=poster, t=talk)

[2015 – *t*] M. Vinas, C. Dorronsoro, A. Radhakrishnan, S. Marcos. *Testing vision with angular and radial multi-zone multifocal designs using Adaptive Optics*. RNO 2015. Salamanca (Spain)

[2015 – *t*] M. Vinas, C. Dorronsoro, V. Gonzalez, D. Cortes, S. Marcos. *Testing vision with radial and angularly segmented multifocal patterns using adaptive optics*. Pr. Nr. 1358. Ses. Nr. 216 IOL optics and visual performance. ARVO 2015. Denver (Colorado, USA)

[2014 – *p*] M. Vinas, C. Dorronsoro & S. Marcos. *Optical performance with multi-zone multifocal designs with natural and corrected ocular aberrations*. Abstract ID: JW3A.37. Session Joint Poster Session II. FIO-2014 (Tucson, Arizona, USA).

[2014 – *t*] M. Vinas, C.Dorronsoro, L. Sawides, D. Cortés, D. Pascual, A. Radhakrishnan, S. Marcos. *Longitudinal Chromatic Aberration of the human eye in the visible and near infrared from Hartmann-Shack wavefront sensing, double-pass and psychophysics*. Pr. Nr. 5974. Ses. Nr. 527 Vision with Adaptive Optics. ARVO 2014. Orlando (Florida, USA)

[2013 – *p*] M. Vinas, P. de Gracia, C. Dorronsoro, L. Sawides, S. Marcos. *Testing the effect of astigmatism on vision with Adaptive Optics*. IONS-13. (Zurich, Switzerland)

[2013 – *t*] M. Vinas, P. de Gracia, C. Dorronsoro, L. Sawides, G. Marin, M. Hernández, S. Marcos. *Visual performance under natural, corrected and Adaptive Optics induced astigmatism: meridional and adaptational effects*. Pr. Nr. 1281. Ses. Nr. 218 Aberrations, Image Quality and Visual Performance. ARVO 2013. Seattle (Washington, USA)

[2012 – *p*] M. Vinas, L. Sawides, P. de Gracia, S. Marcos. *Adaptive Optics as a tool to study changes in neural adaptation to astigmatism*. IONS-11. (Paris, France)

[2012 – *t*] M. Vinas, L. Sawides, P. de Garcia, S. Marcos. *Longitudinal Changes in Perceptual Judgment Of Astigmatic Blur*. Pr. Nr. 3656; Ses. Nr. 361 Optical, Neural and Adaptational Limits of Vision. ARVO 2012. Fort Lauderdale (Miami, USA)

[2011 – *p*] M. Vinas, L. Sawides, P. de Gracia, S. Marcos. *Shift of the neutral perceived focus after correction of astigmatism: evidence using adaptive optics*. III Engineering of the eye 2011 (Benasque, Spain)

[2011 – *t*] M.Vinas, L. Sawides, P. de Gracia, S. Marcos. *Adaptive Optics as a tool to study changes in the perceived neutral point after correction of astigmatism*. 8th Workshop on Adaptive Optics for Industry and Medicine 2011 (Murcia, Spain)

Presented by collaborators

(authors are indicated by signature order, p=poster, t=talk)

[2015 – *t*] S. Marcos, M. Vinas, C. Dorronsoro, N. Garzon, F. Poyales. *In vivo chromatic aberration in patients bilaterally implanted with same design hydrophobic and hydrophilic IOLs*. ESCRS 2015. Barcelona (Spain)

[2013 – *t*] S. Marcos, L. Sawides, C. Dorronsoro, M. Vinas, A. Radhakrisnan. *The internal visual coding for blur matches the ocular optics*.

International Myopia Conference. IMC 2013. Asilomar (California, USA)

[2012 – *t*] L. Sawides, C. Dorronsoro, P. de Gracia, M. Vinas, A. Haun, E. Peli, S. Marcos. *Classification Method to Test Natural Adaptation to the High Order Aberrations of the Eye*. Session III: Visual Acuity, Adaptation, and the Stiles-Crawford Effect. EMVPO 2012. Dublin (Ireland)

[2012 – *t*] L. Sawides, C. Dorronsoro, P. de Gracia, M. Vinas, M. Webster, A. Haun, E. Peli, S. Marcos. *Natural Adaptation to the Orientation of High Order Aberrations*. Pr. Nr. 3659; Ses. Nr. 361 Optical, Neural and Adaptational Limits of Vision. ARVO 2012. Fort Lauderdale (Miami, USA)

[2012 – *t*] L. Sawides, P. de Gracia, M. Vinas, C. Dorronsoro, M. Webster, S. Marcos. *Adaptive Optics to Test Adaptation to the Eye's Optics*. IONS-11. (Paris, France)

[2011 – *p*] S. Marcos et. al. *Development of biomedical imaging instrumentation for applications in vision and ophthalmology*. Madrid-MIT Vision Consortium. Networking meeting (Madrid, Spain)

[2011 – *t*] S. Marcos, L. Sawides, P. de Gracia, M. Vinas, M. Webster, C. Dorronsoro. *Adaptation to the aberrations and daily tasks*. III Engineering of the eye. (Benasque, Spain)

3. Visits and stays in research institutions

[09/11 2014] Ophthalmic Optics Laboratory from the College of Optical Sciences at the University of Arizona, Arizona (USA). Advisor: Prof. Jim Schwiegerling, Associate Professor, Ophthalmology & Vision Sciences. Short stay funded by the Spanish Government (FPU fellowship).

4. Teaching experience associated to FPU fellowship

[2013 - 2015] Teaching assistant at the Department of Optics in the Faculty of Optics and Optometry of the Complutense University of Madrid (UCM). Program: Graduate in Optics and Optometry. Subject: Physical Optics (80hrs).

5. Grants during this thesis

[2011-2015] FPU-PhD fellowship of the Spanish Goverment (MICINN), to develop the thesis project: Study of the impact of the mono- and poly-chromatic aberrations in the optical and visual quality by using a new custom-made Polychromatic Adaptive Optics system. Advisor: Prof. S. Marcos. Visual Optics and Biophotonics Lab, Spanish National Research Council (CSIC)

[2011-2011] JAE-PhD fellowship of the Spanish National Research Council (CSIC), to develop the thesis project: Study of the impact of the mono- and poly-chromatic aberrations in the optical and visual quality by using a new custom-made Polychromatic Adaptive Optics system. Advisor: Prof. S. Marcos. Visual Optics and Biophotonics Lab, Spanish National Research Council (CSIC)

6. Awards during this thesis

[05/2015] ARVO International Travel Grant. These grants, from the Association for Research in Vision and Ophthalmology (ARVO), are awarded to PhD students attending and presenting their scientific work at the 2015 ARVO Annual Meeting (Denver, Colorado, USA).

[10/2014] Emil Wolf Outstanding Student Paper Competition award at Frontiers in Optics (FIO) 2014. This grant recognizes the innovation and research excellence of students presenting their work during Frontiers in Optics (FiO) and honors Emil Wolf for his many contributions to science and the Optical Society. This program is administered by the OSA Foundation and sponsored by Optics Communications published by Elsevier.

[10/2014] Finalist for the Incubic Milton Chang Travel Grant at FIO2014. Funded by an endowment from Milton and Rosalind Chang and administered by the OSA Foundation, to students presenting papers at Frontiers in Optics (FiO).

[06/2013] Optical Society of America (OSA) Professional Development grant to participate in ARVO 2013, the most important congress in Visual Sciences organized by the Association for Research in Vision and Ophtalmology (ARVO)

7. Other scientific activities

[06/2015] Founding partner of a spin-off company of the Spanish National Research Council (CSIC), 2EyesVision S.L. (CNAE 7211: Research & Experimental development in Biotechnology), whose main goal is to design and to develop biotechnoly focussed on a simultaneous vision device to study the visual function and related optical solutions.

[2011-2015] Journal reviewer for Biomedical Optics Express (BOE) and Journal of the Optical Society of America A (JOSAA).

[2010-2015] Member of the IO-CSIC Student Chapter of the Optical Society of America (IOSA, http://iosastudentchapter.osahost.org). President of the OSA student chapter from October 2011 to January 2013. Treasurer from January 2014 to December 2014. Vice-President from January 2013 to December 2013 and nowadays. We organize internal seminars series of the IOSA student Chapter, as well as invited talks and informal coffees with great researchers. We have also collaborated in the organization of an IONS OSA congress (IONS-Valencia2015). We organize activities in order to promote the scientific knowledge among our local community. All the activities are funded by the OSA.

Bibliography

1. J. Liang, B. Grimm, S. Goelz, and J. F. Bille, "Objective measurement of wave aberrations of the human eye with the use of a Hartmann-Shack wave-front sensor," J Opt Soc Am A Opt Image Sci Vis **11**, 1949-1957 (1994).
2. S. Gaukroger, *Descartes.The World and other writtings* (Cambridge University Press, New York (USA), 1998).
3. J. Kepler, *The Optical Part of Astronomy* (1604).
4. R. Descartes, *Discourse on the Method, Optics, Geometry, and Meteorology.* (Hackett Publishing (2001), Indianapolis, Indiana (USA), 1637).
5. H. L. F. v. Helmholtz, *Popular lectures on scientific sujects* (Appleton, New York (USA), 1885).
6. M. P. Keating, *Geometric, physical, and visual optics* (Butterworth-Heinemann, Philadelphia (USA), 2002).
7. D. A. Atchison, and G. Smith, *Optics of the human eye* (Butterworth Heinemann, Edinburgh (UK), 2000).
8. W. S. Stiles, and B. H. Crawford, "The luminous efficieny of rays entering the eye pupil at different points," Proc Roy Soc, 112:428-450 (1933).
9. J. M. Enoch, and V. Lakshminarayanan, *Retinal fibre optics* (CRC Press, London (UK), 1991).
10. S. Marcos, S. A. Burns, E. Moreno-Barriusop, and R. Navarro, "A new approach to the study of ocular chromatic aberrations," Vision Res. **39**, 4309-4323 (1999).
11. C. Ware, "Human axial chromatic aberration found not to decline with age," Graefes Arch. Clin. Exp. Ophthalmol **218**, 39-41 (1982).
12. E. Fernandez, A. Unterhuber, P. Prieto, B. Hermann, W. Drexler, and P. Artal, "Ocular aberrations as a function of wavelength in the near infrared measured with a femtosecond laser," Opt. Express **13**, 400-409 (2005).

13. X. Zhang, L. N. Thibos, and A. Bradley, "Wavelength-dependent magnification and polychromatic image quality in eyes corrected for longitudinal chromatic aberration," Optom. Vis. Sci **74**, 563-569 (1997).
14. W. N. Charman, and J. A. Jennings, "Objective measurements of the longitudinal chromatic aberration of the human eye," Vision Res. **16**, 999-1005 (1976).
15. L. N. Thibos, R. A. Applegate, J. T. Schwiegerling, and R. Webb, "Standards for reporting the optical aberrations of eyes," J. Refract. Surg. **18**, S652-660 (2002).
16. D. R. Williams, D. H. Brainard, M. J. McMahon, and R. Navarro, "Double-pass and interferometric measures of the optical quality of the eye," J. Opt. Soc. Am. A **11**, 3123-3135 (1994).
17. L. Llorente, L. Diaz-Santana, D. Lara-Saucedo, and S. Marcos, "Aberrations of the human eye in visible and near infrared illumination," Optom. Vis. Sci. **80**, 26-35 (2003).
18. M. C. Rynders, R. Navarro, and M. A. Losada, "Objective measurement of the off-axis longitudinal chromatic aberration in the human eye," Vision Res. **38**, 513-522 (1998).
19. S. Marcos, and S. A. Burns, "Cone spacing and waveguide properties from cone directionality measurements," J. Opt. Soc. Am. A **16**, 995-1004 (1999).
20. L. Sawides, "Correction and control of ocular aberrations with Adaptive Optics: effects on human vision," in *Institute of applied Ophtalmobiology (IOBA)*(University of Valladolid, Valladolid (Spain), 2013).
21. R. W. Hart, and R. A. Farrell, "Light scattering in the cornea," Journal of the Optical Society of America **59**, 766-774 (1969).
22. T. J. van den Berg, and H. Spekreijse, "Light scattering model for donor lenses as a function of depth," Vision research **39**, 1437-1445 (1999).
23. S. Marcos, "Aberrations and visual performance following standard laser vision correction," J Refract Surg **17**, S596-601 (2001).
24. D. A. Atchison, and W. N. Charman, "Thomas Young's contribution to visual optics: the Bakerian Lecture "on the mechanism of the eye"," Journal of vision **10**, 16 (2010).
25. H. L. F. v. Helmholtz, *Treatise on Physiological Optics. Translated from the Third German Edition* (The Optical Society of America (1924), 1885).
26. K. Biedermann, "The eye, Hartmann, Shack, and Scheiner," in *Optical Information Processing: A Tribute to Adolf Lohmann*, H. J. Caulfield, ed. (SPIE PRESS, Bellingham, Washington, USA., , 2002).
27. V. N. Mahajan, *Aberration theory made simple* (SPIE- The international society for optical engineering, Washington (USA), 1991).
28. R. Navarro, and M. A. Losada, "Aberrations and relative efficiency of light pencils in the living human eye," Optometry and vision science : official publication of the American Academy of Optometry **74**, 540-547 (1997).
29. R. H. Webb, C. M. Penney, and K. P. Thompson, "Measurement of ocular local wavefront distortion with a spatially resolved refractometer," Applied optics **31**, 3678-3686 (1992).
30. A. Hartwig, and D. A. Atchison, "Analysis of higher-order aberrations in a large clinical population," Investigative ophthalmology & visual science **53**, 7862-7870 (2012).
31. J. Porter, A. Guirao, I. G. Cox, and D. R. Williams, "Monochromatic aberrations of the human eye in a large population," J Opt Soc Am A Opt Image Sci Vis **18**, 1793-1803 (2001).
32. L. N. Thibos, X. Hong, A. Bradley, and X. Cheng, "Statistical variation of aberration structure and image quality in a normal population of healthy eyes," J Opt Soc Am A Opt Image Sci Vis **19**, 2329-2348 (2002).

33. L. Llorente, "Optical aberrations in ametropic eyes and their change with corneal refractive surgery," in *Department of Optometry and Visual Science*(City University London, London (UK), 2009).
34. W. N. Charman, "Wavefront aberration of the eye: a review," Optometry and vision science : official publication of the American Academy of Optometry **68**, 574-583 (1991).
35. M. Born, and E. Wolf, *Principles of Optics* (Pergamon Press, Oxford (UK), 1993).
36. J. Porter, H. M. Queener, J. E. Lin, K. Thorn, and A. Awwal, *Adaptive Optics for Vision Science. Principles, Practices, Design, and Applications* (Wiley Interscience, Hoboken (USA), 2006).
37. L. N. Thibos, X. Hong, A. Bradley, and R. A. Applegate, "Accuracy and precision of objective refraction from wavefront aberrations," Journal of vision **4**, 329-351 (2004).
38. L. N. Thibos, W. Wheeler, and D. Horner, "Power vectors: an application of Fourier analysis to the description and statistical analysis of refractive error," Optom Vis Sci **74**, 367-375 (1997).
39. A. E. Shapiro, *The Optical papers of Isaac Newton. Volumen I: The optical papers (1670-1672)* (Cambrigde University Press, Cambridge (UK), 2012).
40. K. Graef, and F. Schaeffel, "Control of accommodation by longitudinal chromatic aberration and blue cones," J. Vis. **12**, 14 (2012).
41. L. N. Thibos, A. Bradley, and X. X. Zhang, "Effect of ocular chromatic aberration on monocular visual performance," Optom. Vis. Sci. **68**, 599-607 (1991).
42. W. N. Charman, *Optics of the Human Eye* (CRC Press, 1991).
43. R. E. Bedford, and G. Wyszecki, "Axial chromatic aberration of the human eye," J. Opt. Soc. Am. **47**, 564-565 (1957).
44. L. N. Thibos, A. Bradley, and D. L. Still, "Interferometric measurement of visual acuity and the effect of ocular chromatic aberration," Appl Opt **30**, 2079-2087 (1991).
45. P. A. Howarth, "The lateral chromatic aberration of the eye," Ophthalmic. Physiol. Opt. **4**, 223-226 (1984).
46. M. Rynders, B. Lidkea, W. Chisholm, and L. N. Thibos, "Statistical distribution of foveal transverse chromatic aberration, pupil centration, and angle psi in a population of young adult eyes," J. Opt. Soc. Am. A. **12**, 2348-2357 (1995).
47. L. N. Thibos, A. Bradley, D. L. Still, X. Zhang, and P. A. Howarth, "Theory and measurement of ocular chromatic aberration," Vision Res. **30**, 33-49 (1990).
48. S. Marcos, S. A. Burns, P. M. Prieto, R. Navarro, and B. Baraibar, "Investigating sources of variability of monochromatic and transverse chromatic aberrations across eyes," Vision Res. **41**, 3861-3871 (2001).
49. G. Wald, and D. R. Griffin, "The change in refractive power of the human eye in dim and bright light," J. Opt. Soc. Am. **37**, 321-336 (1947).
50. B. Gilmartin, and R. E. Hogan, "The magnitude of longitudinal chromatic aberration of the human eye between 458 and 633 nm," Vision Res. **25**, 1747-1753 (1985).
51. P. A. Howarth, X. X. Zhang, A. Bradley, D. L. Still, and L. N. Thibos, "Does the chromatic aberration of the eye vary with age?," J. Opt. Soc. Am. A **5**, 2087-2092 (1988).
52. P. A. Howarth, and A. Bradley, "The longitudinal chromatic aberration of the human eye, and its correction," Vision Res. **26**, 361-366 (1986).
53. W. N. Charman, and H. Whitefoot, "Speckle motion in laser refraction. II. Experimental," American journal of optometry and physiological optics **56**, 295-304 (1979).
54. D. A. Atchison, and G. Smith, "Chromatic dispersions of the ocular media of human eyes," J Opt Soc Am A Opt Image Sci Vis **22**, 29-37 (2005).

55. L. N. Thibos, M. Ye, X. Zhang, and A. Bradley, "The chromatic eye: a new reduced-eye model of ocular chromatic aberration in humans," Appl. Opt. **31**, 3594-3600 (1992).
56. M. Nakajima, T. Hiraoka, Y. Hirohara, T. Oshika, and T. Mihashi, "Verification of the lack of correlation between age and longitudinal chromatic aberrations of the human eye from the visible to the infrared," Biomedical optics express **6**, 2676-2694 (2015).
57. M. Millodot, "The influence of age on the chromatic aberration of the eye," Albrecht Von Graefes Arch. Klin. Exp. Ophthalmol. **198**, 235-243 (1976).
58. J. A. Mordi, and W. K. Adrian, "Influence of age on chromatic aberration of the human eye," Am. J. Optom. Physiol. Opt. **62**, 864-869 (1985).
59. B. N. Kishto, "The colour stereoscopic effect," Vision research **5**, 313-329 (1966).
60. P. Simonet, and M. C. Campbell, "The optical transverse chromatic aberration on the fovea of the human eye," Vision research **30**, 187-206 (1990).
61. E. J. Fernandez, A. Unterhuber, B. Povazay, B. Hermann, P. Artal, and W. Drexler, "Chromatic aberration correction of the human eye for retinal imaging in the near infrared," Opt. Express **14**, 6213-6225 (2006).
62. R. A. Applegate, J. D. Marsack, and L. N. Thibos, "Metrics of retinal image quality predict visual performance in eyes with 20/17 or better visual acuity," Optom Vis Sci **83**, 635-640 (2006).
63. K. M. Hampson, "Adaptive optics and vision," J. Mod. Opt. **55**, 3425-3467 (2008).
64. D. R. Iskander, "Computational aspects of the visual Strehl ratio," Optom Vis Sci **83**, 57-59 (2006).
65. J. D. Marsack, L. N. Thibos, and R. A. Applegate, "Metrics of optical quality derived from wave aberrations predict visual performance," J Vis **4**, 322-328 (2004).
66. J. W. Goodman, *Introduction to Fourier Optics* (McGraw-Hill, New York, 1996).
67. G. Westheimer, and F. W. Campbell, "Light distribution in the image formed by the living human eye," Journal of the Optical Society of America **52**, 1040-1045 (1962).
68. G. J. Burton, and N. D. Haig, "Effects of the Seidel aberrations on visual target discrimination," Journal of the Optical Society of America. A, Optics and image science **1**, 373-385 (1984).
69. P. Artal, "Calculations of two-dimensional foveal retinal images in real eyes," Journal of the Optical Society of America. A, Optics and image science **7**, 1374-1381 (1990).
70. L. N. Thibos, and A. Bradley, *Vision Models for Target Detection and Recognition. Modeling off-axis vision II: the effect of spatial filtering and sampling by retinal neurons* (World Scientific Press, Singapore, 1995).
71. R. A. Applegate, J. D. Marsack, R. Ramos, and E. J. Sarver, "Interaction between aberrations to improve or reduce visual performance," J Cataract Refract Surg **29**, 1487-1495 (2003).
72. R. Legras, N. Chateau, and W. N. Charman, "Assessment of just-noticeable differences for refractive errors and spherical aberration using visual simulation," Optometry and vision science : official publication of the American Academy of Optometry **81**, 718-728 (2004).
73. L. Sawides, P. de Gracia, C. Dorronsoro, M. Webster, and S. Marcos, "Adapting to blur produced by ocular high-order aberrations," J. Vis. **11** (2011).
74. L. Sawides, P. de Gracia, C. Dorronsoro, M. A. Webster, and S. Marcos, "Vision is adapted to the natural level of blur present in the retinal image," PLoS ONE **6**, e27031 (2011).
75. L. Sawides, S. Marcos, S. Ravikumar, L. Thibos, A. Bradley, and M. Webster, "Adaptation to astigmatic blur," J. Vis. **10**, 22 (2010).

76. G. Y. Yoon, and D. R. Williams, "Visual performance after correcting the monochromatic and chromatic aberrations of the eye," J Opt Soc Am A Opt Image Sci Vis **19**, 266-275 (2002).
77. S. Ravikumar, L. N. Thibos, and A. Bradley, "Calculation of retinal image quality for polychromatic light," J. Opt. Soc. Am. A **25**, 2395-2407 (2008).
78. A. van Meeteren, "Calculations on the optical modulation transfer function of the human eye for white light," Opt. Acta 395-412 (1974).
79. J. Liang, D. R. Williams, and D. T. Miller, "Supernormal vision and high-resolution retinal imaging through adaptive optics," Journal of the Optical Society of America. A, Optics, image science, and vision **14**, 2884-2892 (1997).
80. D. Williams, G. Y. Yoon, J. Porter, A. Guirao, H. Hofer, and I. Cox, "Visual benefit of correcting higher order aberrations of the eye," Journal of refractive surgery **16**, S554-559 (2000).
81. S. Li, Y. Xiong, J. Li, N. Wang, Y. Dai, L. Xue, H. Zhao, W. Jiang, Y. Zhang, and J. C. He, "Effects of monochromatic aberration on visual acuity using adaptive optics," Optometry and vision science : official publication of the American Academy of Optometry **86**, 868-874 (2009).
82. S. L. Elliott, S. S. Choi, N. Doble, J. L. Hardy, J. W. Evans, and J. S. Werner, "Role of high-order aberrations in senescent changes in spatial vision," Journal of vision **9**, 24 21-16 (2009).
83. S. Marcos, L. Sawides, E. Gambra, and C. Dorronsoro, "Influence of adaptive-optics ocular aberration correction on visual acuity at different luminances and contrast polarities," J Vis **8**, 1 1-12 (2008).
84. L. Sawides, E. Gambra, D. Pascual, C. Dorronsoro, and S. Marcos, "Visual performance with real-life tasks under adaptive-optics ocular aberration correction," J Vis **10**, 19 (2010).
85. L. Lundstrom, S. Manzanera, P. M. Prieto, D. B. Ayala, N. Gorceix, J. Gustafsson, P. Unsbo, and P. Artal, "Effect of optical correction and remaining aberrations on peripheral resolution acuity in the human eye," Optics express **15**, 12654-12661 (2007).
86. P. de Gracia, S. Marcos, A. Mathur, and D. A. Atchison, "Contrast sensitivity benefit of adaptive optics correction of ocular aberrations," Journal of vision **11** (2011).
87. L. Chen, P. B. Kruger, H. Hofer, B. Singer, and D. R. Williams, "Accommodation with higher-order monochromatic aberrations corrected with adaptive optics," Journal of the Optical Society of America. A, Optics, image science, and vision **23**, 1-8 (2006).
88. E. J. Fernandez, and P. Artal, "Study on the effects of monochromatic aberrations in the accommodation response by using adaptive optics," Journal of the Optical Society of America. A, Optics, image science, and vision **22**, 1732-1738 (2005).
89. E. Gambra, L. Sawides, C. Dorronsoro, and S. Marcos, "Accommodative lag and fluctuations when optical aberrations are manipulated," J Vis **9(6)**, 1-15 (2009).
90. E. A. Rossi, P. Weiser, J. Tarrant, and A. Roorda, "Visual performance in emmetropia and low myopia after correction of high-order aberrations," J Vis **7**, 14 (2007).
91. E. Dalimier, and C. Dainty, "Use of a customized vision model to analyze the effects of higher-order ocular aberrations and neural filtering on contrast threshold performance," Journal of the Optical Society of America. A, Optics, image science, and vision **25**, 2078-2087 (2008).
92. D. R. Williams, "Aliasing in human foveal vision," Vision research **25**, 195-205 (1985).
93. J. S. McLellan, P. M. Prieto, S. Marcos, and S. A. Burns, "Effects of interactions among wave aberrations on optical image quality," Vision Res **46**, 3009-3016 (2006).

94. P. de Gracia, C. Dorronsoro, G. Marin, M. Hernandez, and S. Marcos, "Visual acuity under combined astigmatism and coma: optical and neural adaptation effects," Journal of vision **11** (2011).
95. P. de Gracia, C. Dorronsoro, E. Gambra, G. Marin, M. Hernandez, and S. Marcos, "Combining coma with astigmatism can improve retinal image over astigmatism alone," Vision Res **50**, 2008-2014 (2010).
96. R. Legras, and H. Rouger, "Just-noticeable levels of aberration correction," Journal of optometry, 71-77 (2008).
97. J. T. Holladay, P. A. Piers, G. Koranyi, M. van der Mooren, and N. E. Norrby, "A new intraocular lens design to reduce spherical aberration of pseudophakic eyes," J Refract Surg **18**, 683-691 (2002).
98. S. Marcos, S. Barbero, and I. Jimenez-Alfaro, "Optical quality and depth-of-field of eyes implanted with spherical and aspheric intraocular lenses," J Refract Surg **21**, 223-235 (2005).
99. J. Tabernero, P. Piers, A. Benito, M. Redondo, and P. Artal, "Predicting the optical performance of eyes implanted with IOLs to correct spherical aberration," Invest Ophthalmol Vis Sci **47**, 4651-4658 (2006).
100. P. A. Piers, H. A. Weeber, P. Artal, and S. Norrby, "Theoretical comparison of aberration-correcting customized and aspheric intraocular lenses," J Refract Surg **23**, 374-384 (2007).
101. A. Franchini, "Compromise between spherical and chromatic aberration and depth of focus in aspheric intraocular lenses," J Cataract Refract Surg **33**, 497-509 (2007).
102. J. S. McLellan, S. Marcos, P. M. Prieto, and S. A. Burns, "Imperfect optics may be the eye's defence against chromatic blur," Nature **417**, 174-176 (2002).
103. A. C. van Heel, "Correcting the spherical and chromatic aberrations of the eye," Journal of the Optical Society of America **36**, 237-239 (1947).
104. A. Ames, and C. A. Proctor, "Dioptrics of the eye," Journal of the Optical Society of America **5**, 22-84 (1921).
105. A. L. Lewis, M. Katz, and C. Oehrlein, "A modified achromatizing lens," American journal of optometry and physiological optics **59**, 909-911 (1982).
106. I. Powell, "Lenses for correcting chromatic aberration of the eye," Applied optics **20**, 4152-4155 (1981).
107. X. X. Zhang, A. Bradley, and L. N. Thibos, "Achromatizing the human eye: the problem of chromatic parallax," J Opt Soc Am A **8**, 686-691 (1991).
108. P. Artal, S. Manzanera, P. Piers, and H. Weeber, "Visual effect of the combined correction of spherical and longitudinal chromatic aberrations," Opt Express **18**, 1637-1648 (2010).
109. G. M. Stratton, "Some preliminary experiments on vision without inversion of the retinal image," Psychological Review, 611–617 (1896).
110. C. W. Clifford, M. A. Webster, G. B. Stanley, A. A. Stocker, A. Kohn, T. O. Sharpee, and O. Schwartz, "Visual adaptation: neural, psychological and computational aspects," Vision research **47**, 3125-3131 (2007).
111. M. A. Webster, "Adaptation and visual coding," J Vis **11(5)**, 1-23 (2011).
112. A. Kohn, "Visual adaptation: physiology, mechanisms, and functional benefits," J Neurophysiol **97**, 3155-3164 (2007).
113. B. Wark, B. N. Lundstrom, and A. Fairhall, "Sensory adaptation," Curr Opin Neurobiol **17**, 423-429 (2007).
114. P. Artal, L. Chen, E. J. Fernandez, B. Singer, S. Manzanera, and D. R. Williams, "Neural compensation for the eye's optical aberrations," Journal of vision **4**, 281-287 (2004).

115. M. A. Webster, M. A. Georgeson, and S. M. Webster, "Neural adjustments to image blur," Nature neuroscience **5**, 839-840 (2002).
116. M. A. Webster, Y. Mizokami, L. A. Svec, and S. L. Elliott, "Neural adjustments to chromatic blur," Spatial vision **19**, 111-132 (2006).
117. A. C. Bilson, Y. Mizokami, and M. A. Webster, "Visual adjustments to temporal blur," Journal of the Optical Society of America. A, Optics, image science, and vision **22**, 2281-2288 (2005).
118. P. W. Battaglia, R. A. Jacobs, and R. N. Aslin, "Depth-dependent blur adaptation," Vision research **44**, 113-117 (2004).
119. J. S. Werner, and B. E. Schefrin, "Loci of achromatic points throughout the life span," Journal of the Optical Society of America. A, Optics and image science **10**, 1509-1516 (1993).
120. R. Sabesan, and G. Yoon, "Neural compensation for long-term asymmetric optical blur to improve visual performance in keratoconic eyes," Investigative ophthalmology & visual science **51**, 3835-3839 (2010).
121. L. Chen, P. Artal, D. Gutierrez, and D. R. Williams, "Neural compensation for the best aberration correction," Journal of vision **7**, 9 1-9 (2007).
122. L. Sawides, C. Dorronsoro, P. de Gracia, M. Vinas, M. Webster, and S. Marcos, "Dependence of subjective image focus on the magnitude and pattern of high order aberrations," J Vis **12(8)**, 1-12 (2012).
123. M. Mon-Williams, J. R. Tresilian, N. C. Strang, P. Kochhar, and J. P. Wann, "Improving vision: neural compensation for optical defocus," Proc Biol Sci **265**, 71-77 (1998).
124. K. Pesudovs, "Involvement of neural adaptation in the recovery of vision after laser refractive surgery," J Refract Surg **21**, 144-147 (2005).
125. D. A. Atchison, H. Q. Guo, W. N. Charman, and S. W. Fisher, "Blur limits for defocus, astigmatism and trefoil," Vision research **49**, 2393-2403 (2009).
126. Z. L. Lu, T. Hua, C. B. Huang, Y. Zhou, and B. A. Dosher, "Visual perceptual learning," Neurobiology of learning and memory **95**, 145-151 (2011).
127. A. F. Teich, and N. Qian, "Learning and adaptation in a recurrent model of V1 orientation selectivity," J Neurophysiol **89**, 2086-2100 (2003).
128. Z. L. Lu, C. Yu, T. Watanabe, D. Sagi, and D. Levi, "Perceptual learning: functions, mechanisms, and applications," Vision Res **49**, 2531-2534 (2009).
129. Q. Haijiang, J. A. Saunders, R. W. Stone, and B. T. Backus, "Demonstration of cue recruitment: change in visual appearance by means of Pavlovian conditioning," Proc Natl Acad Sci U S A **103**, 483-488 (2006).
130. O. Yehezkel, D. Sagi, A. Sterkin, M. Belkin, and U. Polat, "Learning to adapt: Dynamics of readaptation to geometrical distortions," Vision Res **50**, 1550-1558 (2010).
131. J. S. Wolffsohn, G. Bhogal, and S. Shah, "Effect of uncorrected astigmatism on vision," J Cataract Refract Surg **37**, 454-460 (2011).
132. W. N. Charman, and L. Voisin, "Optical aspects of tolerances to uncorrected ocular astigmatism," Optom Vis Sci **70**, 111-117 (1993).
133. D. E. Mitchell, and F. Wilkinson, "The effect of early astigmatism on the visual resolution of gratings," J Physiol **243**, 739-756 (1974).
134. A. D. Miller, M. J. Kris, and A. C. Griffiths, "Effect of small focal errors on vision," Optom Vis Sci **74**, 521-526 (1997).
135. D. E. Mitchell, R. D. Freeman, M. Millodot, and G. Haegerstrom, "Meridional amblyopia: evidence for modification of the human visual system by early visual experience," Vision research **13**, 535-558 (1973).

136. V. Dobson, J. M. Miller, E. M. Harvey, and K. M. Mohan, "Amblyopia in astigmatic preschool children," Vision Res **43**, 1081-1090 (2003).
137. S. Barbero, S. Marcos, J. Merayo-Lloves, and E. Moreno-Barriuso, "Validation of the estimation of corneal aberrations from videokeratography in keratoconus," J Refract Surg **18**, 263-270 (2002).
138. S. Marcos, P. Rosales, L. Llorente, and I. Jimenez-Alfaro, "Change in corneal aberrations after cataract surgery with 2 types of aspherical intraocular lenses," J Cataract Refract Surg **33**, 217-226 (2007).
139. E. A. Villegas, and P. Artal, "Spatially resolved wavefront aberrations of ophthalmic progressive-power lenses in normal viewing conditions," Optom Vis Sci **80**, 106-114 (2003).
140. M. Vilaseca, F. Díaz-Doutón, S. O. Luque, M. Aldaba, M. Arjona, and J. Pujol, "Optics of Astigmatism and Retinal Image Quality," in *Astigmatism. Optics, Physiology and Management*, M. Goggin, ed. (InTech, 2012).
141. K. Pesudovs, and N. A. Brennan, "Decreased uncorrected vision after a period of distance fixation with spectacle wear," Optom Vis Sci **70**, 528-531 (1993).
142. R. Sabesan, T. M. Jeong, L. Carvalho, I. G. Cox, D. R. Williams, and G. Yoon, "Vision improvement by correcting higher-order aberrations with customized soft contact lenses in keratoconic eyes," Opt Lett **32**, 1000-1002 (2007).
143. R. Sabesan, and G. Yoon, "Visual performance after correcting higher order aberrations in keratoconic eyes," J Vis **9(5)**, 1-10 (2009).
144. D. G. Pelli, and B. Farell, "Psychophysical methods," in *Handbook of Optics*, M. Bass, E. W. Van Stryland, D. R. Williams, and W. L. Wolfe, eds. (McGraw-Hill, New York, 1995).
145. A. B. Watson, and D. G. Pelli, "QUEST: a Bayesian adaptive psychometric method," Percept Psychophys **33**, 113-120 (1983).
146. M. L. Calvo, *Óptica avanzada* (Ariel, Barcelona (Spain), 2002).
147. P. Perez-Merino, "Topography and aberrometry of the anterior segment: clinical applications," in *Institute of applied Ophthalmobiology*(University of Valladolid, Valladolid, 2015).
148. A. Glasser, and M. C. Campbell, "Presbyopia and the optical changes in the human crystalline lens with age," Vision Res **38**, 209-229 (1998).
149. W. N. Charman, "Developments in the correction of presbyopia I: spectacle and contact lenses," Ophthalmic & physiological optics : the journal of the British College of Ophthalmic Opticians **34**, 8-29 (2014).
150. W. N. Charman, "Developments in the correction of presbyopia II: surgical approaches," Ophthalmic & physiological optics : the journal of the British College of Ophthalmic Opticians **34**, 397-426 (2014).
151. S. C. Han, A. D. Graham, and M. C. Lin, "Clinical assessment of a customized free-form progressive add lens spectacle," Optometry and vision science : official publication of the American Academy of Optometry **88**, 234-243 (2011).
152. E. S. Bennett, "Contact lens correction of presbyopia," Clinical & experimental optometry **91**, 265-278 (2008).
153. B. J. Evans, "Monovision: a review," Ophthalmic & physiological optics : the journal of the British College of Ophthalmic Opticians **27**, 417-439 (2007).
154. C. Buznego, and W. B. Trattler, "Presbyopia-correcting intraocular lenses," Current opinion in ophthalmology **20**, 13-18 (2009).
155. A. Bradley, H. Abdul Rahman, P. S. Soni, and X. Zhang, "Effects of target distance and pupil size on letter contrast sensitivity with simultaneous vision bifocal contact lenses,"

Optometry and vision science : official publication of the American Academy of Optometry **70**, 476-481 (1993).
156. P. R. Fernandes, H. I. Neves, D. P. Lopes-Ferreira, J. M. Jorge, and J. M. Gonzalez-Meijome, "Adaptation to multifocal and monovision contact lens correction," Optometry and vision science : official publication of the American Academy of Optometry **90**, 228-235 (2013).
157. M. A. Nanavaty, A. R. Vasavada, A. S. Patel, S. M. Raj, and T. H. Desai, "Analysis of patients with good uncorrected distance and near vision after monofocal intraocular lens implantation," Journal of cataract and refractive surgery **32**, 1091-1097 (2006).
158. P. A. Piers, E. J. Fernandez, S. Manzanera, S. Norrby, and P. Artal, "Adaptive optics simulation of intraocular lenses with modified spherical aberration," Invest Ophthalmol Vis Sci **45**, 4601-4610 (2004).
159. S. Barbero, S. Marcos, and I. Jimenez-Alfaro, "Optical aberrations of intraocular lenses measured in vivo and in vitro," J Opt Soc Am A Opt Image Sci Vis **20**, 1841-1851 (2003).
160. S. George, and M. Rosenfield, "Blur adaptation and myopia," Optom Vis Sci **81**, 543-547 (2004).
161. R. Navarro, M. Ferro, P. Artal, and I. Miranda, "Modulation transfer functions of eyes implanted with intraocular lenses," Appl Opt **32**, 6359-6367 (1993).
162. E. Peli, and A. Lang, "Appearance of images through a multifocal intraocular lens," Journal of the Optical Society of America. A, Optics, image science, and vision **18**, 302-309 (2001).
163. H. Zhao, and M. A. Mainster, "The effect of chromatic dispersion on pseudophakic optical performance," The British journal of ophthalmology **91**, 1225-1229 (2007).
164. T. Nagata, S. Kubota, I. Watanabe, and S. Aoshima, "[Chromatic aberration in pseudophakic eyes]," Nippon Ganka Gakkai zasshi **103**, 237-242 (1999).
165. K. Negishi, K. Ohnuma, N. Hirayama, T. Noda, L. Policy-Based Medical Services Network Study Group for Intraocular, and S. Refractive, "Effect of chromatic aberration on contrast sensitivity in pseudophakic eyes," Arch Ophthalmol **119**, 1154-1158 (2001).
166. H. A. Weeber, and P. A. Piers, "Theoretical performance of intraocular lenses correcting both spherical and chromatic aberration," J Refract Surg **28**, 48-52 (2012).
167. D. Siedlecki, and H. S. Ginis, "On the longitudinal chromatic aberration of the intraocular lenses," Optom Vis Sci **84**, 984-989 (2007).
168. C. Scheiner, *Oculus, hoc est: Fundamentum opticum* (Oeniponti, Innsbruck 1619).
169. J. W. Hardy, J. E. Lefebvre, and C. L. Koliopoulos, "Real-time atmospheric compensation," Journal of the Optical Society of America. A, Optics, image science, and vision, 360-369 (1977).
170. Z. Y. Zhang, Z; Chu, Z;, "Fundamentals of phase-only liquid crystal on silicon (LCOS) devices," Light: Science & Applications (2014).
171. H. Hofer, P. Artal, B. Singer, J. L. Aragon, and D. R. Williams, "Dynamics of the eye's wave aberration," J Opt Soc Am A Opt Image Sci Vis **18**, 497-506 (2001).
172. D. T. Miller, D. R. Williams, G. M. Morris, and J. Liang, "Images of cone photoreceptors in the living human eye," Vision Res **36**, 1067-1079 (1996).
173. R. H. Webb, and G. W. Hughes, "Scanning laser ophthalmoscope," IEEE transactions on bio-medical engineering **28**, 488-492 (1981).
174. F. A. Vera-Díaz, and N. Doble, "The human eye and Adaptive Optics," in *Topics in Adaptive Optics.*, B. Tyson, ed. (2012).
175. D. T. Miller, J. Qu, R. S. Jonnal, and K. E. Thorn, "Coherence gating and adaptive optics in the eye," **Proceedings of SPIE**, 65–72 (2003).

176. R. Sabesan, K. Ahmad, and G. Yoon, "Correcting highly aberrated eyes using large-stroke adaptive optics," Journal of refractive surgery **23**, 947-952 (2007).
177. H. Guo, D. A. Atchison, and B. J. Birt, "Changes in through-focus spatial visual performance with adaptive optics correction of monochromatic aberrations," Vision research **48**, 1804-1811 (2008).
178. K. Baskaran, R. Rosen, P. Lewis, P. Unsbo, and J. Gustafsson, "Benefit of adaptive optics aberration correction at preferred retinal locus," Optometry and vision science : official publication of the American Academy of Optometry **89**, 1417-1423 (2012).
179. E. Dalimier, C. Dainty, and J. Barbur, "Effects of higher-order aberrations on contrast acuity as a function of light level," J. Mod. Opt., 791–803 (2008).
180. P. Prieto, E. Fernandez, S. Manzanera, and P. Artal, "Adaptive optics with a programmable phase modulator: applications in the human eye," Optics express **12**, 4059-4071 (2004).
181. E. J. Fernandez, P. M. Prieto, and P. Artal, "Binocular adaptive optics visual simulator," Optics letters **34**, 2628-2630 (2009).
182. M. Vinas, C. Dorronsoro, D. Cortes, D. Pascual, and S. Marcos, "Longitudinal chromatic aberration of the human eye in the visible and near infrared from wavefront sensing, double-pass and psychophysics," Biomed Opt Express **6**, 948-962 (2015).
183. M. Vinas, C. Dorronsoro, N. Garzon, F. Poyales, and S. Marcos, "*In vivo* subjective and objective longitudinal chromatic aberration in patients bilaterally implanted with same design hydrophobic and hydrophilic IOLs," Journal of Cataract & Refractive Surgery (2015).
184. F. C. Delori, R. H. Webb, D. H. Sliney, and I. American National Standards, "Maximum permissible exposures for ocular safety (ANSI 2000), with emphasis on ophthalmic devices," J. Opt. Soc. Am. A **24**, 1250-1265 (2007).
185. "American National Standar for Safe Use of Lasers, ANSI Z.136.1-2007," (American National Standards Institute (2007)).
186. J. I. Morgan, J. J. Hunter, B. Masella, R. Wolfe, D. C. Gray, W. H. Merigan, F. C. Delori, and D. R. Williams, "Light-induced retinal changes observed with high-resolution autofluorescence imaging of the retinal pigment epithelium," Invest. Ophthalmol. Vis. Sci. **49**, 3715-3729 (2008).
187. E. J. Fernandez, L. Vabre, B. Hermann, A. Unterhuber, B. Povazay, and W. Drexler, "Adaptive optics with a magnetic deformable mirror: applications in the human eye," Opt Express **14**, 8900-8917 (2006).
188. P. Artal, S. Marcos, R. Navarro, and D. R. Williams, "Odd aberrations and double-pass measurements of retinal image quality," J. Opt. Soc. Am. A **12**, 195-201 (1995).
189. E. Garcia de la Cera, "Optical quality and role of the ocular aberrations in animal models of myopia," in *Institute of applied Ophtalmobiology (IOBA)*(University of Valladolid, Valladolid, 2008).
190. J. L. Barbur, and A. Stockman, " Photopic, Mesopic and Scotopic Vision and Changes in Visual Performance," in *Encyclopedia of the Eye*, D. A. Dartt, ed. (Elsevier. Oxford: Academic Press, 2010), pp. 323-331.
191. D. H. Brainard, "The Psychophysics Toolbox," Spat Vis **10**, 433-436 (1997).
192. D. G. Pelli, "The VideoToolbox software for visual psychophysics: transforming numbers into movies," Spat Vis **10**, 437-442 (1997).
193. D. G. Voelz, "Computational fourier optics: a MATLAB tutorial," (SPIE, 2011).
194. H. S. Abdul-Rahman, M. A. Gdeisat, D. R. Burton, M. J. Lalor, F. Lilley, and C. J. Moore, "Fast and robust three-dimensional best path phase unwrapping algorithm," Appl Opt **46**, 6623-6635 (2007).

195. S. Marcos, and S. A. Burns, "On the symmetry between eyes of wavefront aberration and cone directionality," Vision research **40**, 2437-2447 (2000).
196. W. H. Ehrenstein, and A. Ehrenstein, "Psychophysical methods," in *Modern techniques in neuroscience research*, U. Windhorst, and H. Johansson, eds. (Springer, 1999), pp. 1211-1240.
197. J. A. Phipps, A. J. Zele, T. Dang, and A. J. Vingrys, "Fast psychophysical procedures for clinical testing," Clinical & experimental optometry **84**, 264-269 (2001).
198. J. T. Holladay, "Proper method for calculating average visual acuity," J Refract Surg **13**, 388-391 (1997).
199. A. Ohlendorf, J. Tabernero, and F. Schaeffel, "Neuronal adaptation to simulated and optically-induced astigmatic defocus," Vision research **51**, 529-534 (2011).
200. K. Perlin, "An image synthesizer," SIGGRAPH Comput. Graph. **19**, 287-296 (1985).
201. A. Coninx, G. P. Bonneau, G. Thibault, and J. Droulez, "Psychophysical evaluation and modelisation of contrast sensitivity thresholds for Perlin noise," Perception **40**, 114-114 (2011).
202. S. Green, "GPU gems 2 : programming techniques for high-performance graphics and general-purpose computation," in *Part III: High-Quality Rendering. Chapter 26. Implementing Improved Perlin Noise*, M. Pharr, ed. (Library of Congress Cataloging-in-Publication Data, 2005).
203. I. McGarvey, "Perlin noise generator. Version 1.1," (2005), http://infohost.nmt.edu/~imcgarve/ perlin_noise/, Accessed june, 2009.
204. E. Peli, "Contrast in complex images," Journal of the Optical Society of America. A, Optics and image science **7**, 2032-2040 (1990).
205. R. Vogels, and G. A. Orban, "The effect of practice on the oblique effect in line orientation judgments," Vision research **25**, 1679-1687 (1985).
206. T. Borra, I. T. Hooge, and F. A. Verstraten, "A dichoptic study of the oblique effect," Perception **39**, 909-917 (2010).
207. D. W. Heeley, H. M. Buchanan-Smith, J. A. Cromwell, and J. S. Wright, "The oblique effect in orientation acuity," Vision research **37**, 235-242 (1997).
208. M. J. McMahon, and D. I. MacLeod, "The origin of the oblique effect examined with pattern adaptation and masking," J Vis **3**, 230-239 (2003).
209. S. Appelle, "Perception and discrimination as a function of stimulus orientation: the "oblique effect" in man and animals," Psychol Bull **78**, 266-278 (1972).
210. E. Kompaniez, A. Dye, L. Sawides, S. Marcos, and M. Webster, "Adaptation to interocular differences in blur," J Vis **11(11)**, 306 (2011).
211. M. Rosenfield, and J. A. Abraham-Cohen, "Blur sensitivity in myopes," Optometry and vision science : official publication of the American Academy of Optometry **76**, 303-307 (1999).
212. E. A. Rossi, and A. Roorda, "Is visual resolution after adaptive optics correction susceptible to perceptual learning?," J Vis **10(12)**, 1-14 (2010).
213. E. Vul, E. Krizay, and D. I. MacLeod, "The McCollough effect reflects permanent and transient adaptation in early visual cortex," Journal of vision **8(12)**, 1-12 (2008).
214. M. Vinas, L. Sawides, P. de Gracia, and S. Marcos, "Perceptual Adaptation to the Correction of Natural Astigmatism," Plos One **7** (2012).
215. R. D. Freeman, and L. Thibos, "Contrast sensitivity in humans with abnormal visual experience," J. Physiol., 687-710 (1975).
216. R. D. Freeman, "Contrast sensitivity in meridional amblyopia," Invest Ophthalmol **14**, 78-81 (1975).
217. M. Fahle, "Perceptual learning: gain without pain?," Nat Neurosci **5**, 923-924 (2002).

218. N. Fogt, "The negative directional aftereffect associated with adaptation to the prismatic effects of spectacle lenses," Optom Vis Sci **77**, 96-101 (2000).
219. H. Rouger, Y. Benard, D. Gatinel, and R. L., "Visual Tasks Dependence of the Neural Compensation for the Keratoconic Eye's Optical Aberrations," J Optom **3**, 60-65 (2010).
220. H. Kobashi, K. Kamiya, K. Shimizu, T. Kawamorita, and H. Uozato, "Effect of axis orientation on visual performance in astigmatic eyes," J Cataract Refract Surg **38**, 1352-1359 (2012).
221. D. D. Koch, "Revisiting the conoid of sturm," J. Cataract. Refract. Surg. **32** (2006).
222. R. D. Freeman, "Asymmetries in human accomodation and visual experience," Vision Res **15**, 483-492 (1975).
223. A. G. Bennett, and R. B. Rabbetts, *Clinical Visual Optics* (Butterworth-Heinemann, 1998).
224. H. Guo, and D. A. Atchison, "Subjective blur limits for cylinder," Optom Vis Sci **87**, E549-559 (2010).
225. F. J. Schwendeman, B. B. Ogden, D. G. Horner, and L. N. Thibos, "Effect of sphero-cylinder blur on visual acuity," Optom Vis Sci **74(suppl)**, 180 (1997).
226. D. A. Atchison, and A. Mathur, "Visual acuity with astigmatic blur," Optom Vis Sci **88**, E798-805 (2011).
227. L. Remon, M. Tornel, and W. D. Furlan, "Visual acuity in simple myopic astigmatism: influence of cylinder axis," Optom Vis Sci **83**, 311-315 (2006).
228. B. Wang, K. J. Ciuffreda, and B. Vasudevan, "Effect of blur adaptation on blur sensitivity in myopes," Vision Res **46**, 3634-3641 (2006).
229. H. von Helmholtz, *Treatise on Physiological Optics (1866)* (University of Pennsylvania, 2001).
230. P. Perez-Merino, C. Dorronsoro, L. Llorente, S. Duran, I. Jimenez-Alfaro, and S. Marcos, "In vivo chromatic aberration in eyes implanted with intraocular lenses," Invest. Ophthalmol. Vis. Sci. **54**, 2654-2661 (2013).
231. A. Guirao, J. Porter, D. R. Williams, and I. G. Cox, "Calculated impact of higher-order monochromatic aberrations on retinal image quality in a population of human eyes," J. Opt. Soc. Am. A **19**, 620-628 (2002).
232. S. Marcos, E. Moreno, and R. Navarro, "The depth-of-field of the human eye from objective and subjective measurements," Vision Res. **39**, 2039-2049 (1999).
233. T. O. Salmon, L. N. Thibos, and A. Bradley, "Comparison of the eye's wave-front aberration measured psychophysically and with the Shack-Hartmann wave-front sensor," J Opt Soc Am A Opt Image Sci Vis **15**, 2457-2465 (1998).
234. N. Lopez-Gil, and P. Artal, "Comparison of double-pass estimates of the retinal-image quality obtained with green and near-infrared light," J. Opt. Soc. Am. A **14**, 961-971 (1997).
235. A. M. Bagci, M. Shahidi, R. Ansari, M. Blair, N. P. Blair, and R. Zelkha, "Thickness profiles of retinal layers by optical coherence tomography image segmentation," Am. J. Ophthalmol. **146**, 679-687 (2008).
236. M. Karampelas, D. A. Sim, P. A. Keane, V. P. Papastefanou, S. R. Sadda, A. Tufail, and J. Dowler, "Evaluation of retinal pigment epithelium-Bruch's membrane complex thickness in dry age-related macular degeneration using optical coherence tomography," Br. J. Ophthalmol. **97**, 1256-1261 (2013).
237. V. Manjunath, M. Taha, J. G. Fujimoto, and J. S. Duker, "Choroidal thickness in normal eyes measured using Cirrus HD optical coherence tomography," Am. J. Ophthalmol. **150**, 325-329 e321 (2010).

238. F. C. Delori, and K. P. Pflibsen, "Spectral reflectance of the human ocular fundus," Appl. Opt. **28**, 1061-1077 (1989).
239. A. E. Elsner, S. A. Burns, J. J. Weiter, and F. C. Delori, "Infrared imaging of sub-retinal structures in the human ocular fundus," Vision Res. **36**, 191-205 (1996).
240. E. Fernandez, and W. Drexler, "Influence of ocular chromatic aberration and pupil size on transverse resolution in ophthalmic adaptive optics optical coherence tomography," Opt. Express **13**, 8184-8197 (2005).
241. K. Grieve, P. Tiruveedhula, Y. Zhang, and A. Roorda, "Multi-wavelength imaging with the adaptive optics scanning laser Ophthalmoscope," Opt. Express **14**, 12230-12242 (2006).
242. C. W. Bobier, and J. G. Sivak, "Chromoretinoscopy," Vision Res **18**, 247-250 (1978).
243. D. Siedlecki, A. Jozwik, M. Zajac, A. Hill-Bator, and A. Turno-Krecicka, "In vivo longitudinal chromatic aberration of pseudophakic eyes," Optom Vis Sci **91**, 240-246 (2014).
244. D. Bozukova, C. Pagnoulle, and C. Jerome, "Biomechanical and optical properties of 2 new hydrophobic platforms for intraocular lenses," J Cataract Refract Surg **39**, 1404-1414 (2013).
245. F. W. Campbell, and R. W. Gubisch, "The effect of chromatic aberration on visual acuity," The Journal of physiology **192**, 345-358 (1967).
246. A. Zlotnik, S. Ben Yaish, O. Yehezkel, K. Lahav-Yacouel, M. Belkin, and Z. Zalevsky, "Extended depth of focus contact lenses for presbyopia," Opt Lett **34**, 2219-2221 (2009).
247. J. Woods, C. Woods, and D. Fonn, "Visual Performance of a Multifocal Contact Lens versus Monovision in Established Presbyopes," Optom Vis Sci **92**, 175-182 (2015).
248. N. Gupta, S. A. Naroo, and J. S. Wolffsohn, "Visual comparison of multifocal contact lens to monovision," Optom Vis Sci **86**, E98-105 (2009).
249. J. A. Martin, and A. Roorda, "Predicting and assessing visual performance with multizone bifocal contact lenses," Optom Vis Sci **80**, 812-819 (2003).
250. G. Schmidinger, W. Geitzenauer, B. Hahsle, U. M. Klemen, C. Skorpik, and S. Pieh, "Depth of focus in eyes with diffractive bifocal and refractive multifocal intraocular lenses," J Cataract Refract Surg **32**, 1650-1656 (2006).
251. R. Bellucci, "Multifocal intraocular lenses," Current opinion in ophthalmology **16**, 33-37 (2005).
252. J. A. Davison, and M. J. Simpson, "History and development of the apodized diffractive intraocular lens," J Cataract Refract Surg **32**, 849-858 (2006).
253. D. Gatinel, C. Pagnoulle, Y. Houbrechts, and L. Gobin, "Design and qualification of a diffractive trifocal optical profile for intraocular lenses," J Cataract Refract Surg **37**, 2060-2067 (2011).
254. F. Yi, D. R. Iskander, and M. Collins, "Depth of focus and visual acuity with primary and secondary spherical aberration," Vision Res **51**, 1648-1658 (2011).
255. D. Fernandez, S. Barbero, C. Dorronsoro, and S. Marcos, "Multifocal intraocular lens providing optimized through-focus performance," Opt Lett **38**, 5303-5306 (2013).
256. L. Zheleznyak, R. Sabesan, J. S. Oh, S. MacRae, and G. Yoon, "Modified monovision with spherical aberration to improve presbyopic through-focus visual performance," Invest Ophthalmol Vis Sci **54**, 3157-3165 (2013).
257. C. Schwarz, C. Canovas, S. Manzanera, H. Weeber, P. M. Prieto, P. Piers, and P. Artal, "Binocular visual acuity for the correction of spherical aberration in polychromatic and monochromatic light," J Vis **14** (2014).

258. H. N. Sen, A. U. Sarikkola, R. J. Uusitalo, and L. Laatikainen, "Quality of vision after AMO Array multifocal intraocular lens implantation," J Cataract Refract Surg **30**, 2483-2493 (2004).
259. P. de Gracia, C. Dorronsoro, and S. Marcos, "Multiple zone multifocal phase designs," Opt Lett **38**, 3526-3529 (2013).
260. A. Radhakrishnan, C. Dorronsoro, L. Sawides, and S. Marcos, "Short-term neural adaptation to simultaneous bifocal images," PLoS One **9**, e93089 (2014).
261. P. Artal, S. Marcos, R. Navarro, I. Miranda, and M. Ferro, "Through focus image quality of eyes implanted with monofocal and multifocal intraocular lenses," Opt. Eng. **34**, 772-779 (1995).
262. T. Kawamorita, and H. Uozato, "Modulation transfer function and pupil size in multifocal and monofocal intraocular lenses in vitro," J Cataract Refract Surg **31**, 2379-2385 (2005).
263. W. A. Maxwell, S. S. Lane, and F. Zhou, "Performance of presbyopia-correcting intraocular lenses in distance optical bench tests," Journal of cataract and refractive surgery **35**, 166-171 (2009).
264. P. de Gracia, C. Dorronsoro, A. Sanchez-Gonzalez, L. Sawides, and S. Marcos, "Experimental simulation of simultaneous vision," Invest Ophthalmol Vis Sci **54**, 415-422 (2013).
265. C. Dorronsoro, A. Radhakrishnan, P. de Gracia, L. Sawides, J. R. Alonso-Sanz, D. Cortés, and S. Marcos, "Visual testing of segmented bifocal corrections with a compact simultaneous vision simulator," Invest. Ophthalmol. Vis. Sci. **55**, 781-781 (2014).